

Peptide discotics : synthesis, self-assembly and application

Citation for published version (APA):

Hout, van den, K. P. (2008). *Peptide discotics : synthesis, self-assembly and application*. [Phd Thesis 1 (Research TU/e / Graduation TU/e), Biomedical Engineering]. Technische Universiteit Eindhoven.
<https://doi.org/10.6100/IR635208>

DOI:

[10.6100/IR635208](https://doi.org/10.6100/IR635208)

Document status and date:

Published: 01/01/2008

Document Version:

Publisher's PDF, also known as Version of Record (includes final page, issue and volume numbers)

Please check the document version of this publication:

- A submitted manuscript is the version of the article upon submission and before peer-review. There can be important differences between the submitted version and the official published version of record. People interested in the research are advised to contact the author for the final version of the publication, or visit the DOI to the publisher's website.
- The final author version and the galley proof are versions of the publication after peer review.
- The final published version features the final layout of the paper including the volume, issue and page numbers.

[Link to publication](#)

General rights

Copyright and moral rights for the publications made accessible in the public portal are retained by the authors and/or other copyright owners and it is a condition of accessing publications that users recognise and abide by the legal requirements associated with these rights.

- Users may download and print one copy of any publication from the public portal for the purpose of private study or research.
- You may not further distribute the material or use it for any profit-making activity or commercial gain
- You may freely distribute the URL identifying the publication in the public portal.

If the publication is distributed under the terms of Article 25fa of the Dutch Copyright Act, indicated by the "Taverne" license above, please follow below link for the End User Agreement:

www.tue.nl/taverne

Take down policy

If you believe that this document breaches copyright please contact us at:

openaccess@tue.nl

providing details and we will investigate your claim.

Peptide Discotics

Synthesis, self-assembly and application

Peptide Discotics
Synthesis, self-assembly and application

PROEFSCHRIFT

ter verkrijging van de graad van doctor aan de
Technische Universiteit Eindhoven, op gezag van de
Rector Magnificus, prof.dr.ir. C.J. van Duijn, voor een
commissie aangewezen door het College voor
Promoties in het openbaar te verdedigen
op donderdag 26 juni 2008 om 14.00 uur

door

Kelly Petronella Stelwagen-van den Hout

geboren te Drunen

Dit proefschrift is goedgekeurd door de promotor:

prof.dr. E.W. Meijer

Copromotoren:

dr. J.A.J.M. Vekemans

en

dr.ir. M.H.P. van Genderen

The research described in this thesis was financially supported by the Netherlands Organisation for Scientific Research (*NWO*).

Omslagontwerp: Koen Pieterse

Druk: Gildeprint Drukkerijen B.V. te Enschede

A catalogue record is available from the Eindhoven University of Technology Library

ISBN: 978-90-386-1289-8

Voor mijn ouders

Voor Sjoerd

Table of contents

Chapter 1

Self-assembling contrast agents for MRI

1.1	Magnetic resonance imaging and the use of contrast agents.....	2
1.1.1	Applied strategies for contrast-enhancement	
1.1.2	Synthetic approaches: towards more efficient contrast agents	
1.2	Self-assembling paramagnetic amphiphiles for MR imaging.....	5
1.3	Self-assembly behaviour of C_3 -symmetrical discotics.....	9
1.3.1	Self-assembly of discotic molecules in apolar media	
1.3.2	Self-assembly of discotic molecules in water	
1.4	^1H relaxation time measurements: study self-assembly in dilute solutions.....	16
1.4.1	Determining the critical micelle concentration	
1.4.2	Probing the interaction of the biotin–avidin complex	
1.5	Aim and outline of the thesis.....	17
1.6	References and notes.....	19

Chapter 2

Syntheses of peptide discotics with aliphatic solubilizing tails

2.1	Introduction.....	24
2.2	Syntheses of dipeptide discotics with an achiral glycine at the C-terminus.....	26
2.3	Syntheses of dipeptide discotics with a chiral phenylalanine at the C-terminus.....	28
2.4	Syntheses of mono-peptide discotics.....	31
2.5	Conclusions.....	32
2.6	Experimental section.....	33
2.7	References and notes.....	46

Chapter 3

Self-assembly of peptide discotics with aliphatic solubilizing tails

3.1	Introduction.....	48
3.2	Self-assembly behaviour of dipeptide discotics in the neat state.....	50
3.3	Self-assembly behaviour of dipeptide discotics in solution.....	53
3.4	Stability of assemblies of dipeptide discotics.....	58
3.5	Self-assembly behaviour of mono-peptide discotics in the neat state.....	60

3.6	Self-assembly behaviour of mono-peptide discotics in solution.....	61
3.7	Stability of assemblies of mono-peptide discotics.....	63
3.8	Conclusions.....	64
3.9	Experimental section.....	64
3.10	References and notes.....	65

Chapter 4

From apolar media to water: Self-assembly of a peptide-based discotic amphiphile

4.1	Introduction.....	68
4.2	Synthesis.....	69
4.3	Self-assembly in solution.....	70
4.4	Size of the self-assembled structures in water.....	72
4.5	Conclusions.....	76
4.6	Experimental section.....	76
4.7	References and notes.....	80

Chapter 5

Self-assembly of paramagnetic discotic amphiphiles

5.1	Introduction.....	84
5.2	Small Gd ^{III} -DTPA discotics.....	86
	5.2.1 Syntheses	
	5.2.2 Self-assembly in solution	
	5.2.3 Conclusions	
5.3	Medium Gd ^{III} -DTPA discotics.....	90
	5.3.1 Syntheses	
	5.3.2 Self-assembly in solution	
	5.3.3 Conclusions	
5.4	Large Gd ^{III} -DTPA discotics.....	95
	5.4.1 Syntheses	
	5.4.2 Self-assembly in solution	
	5.4.3 Fitting of the T ₁ measurements	
	5.4.4 Evaluation of the aggregation concentration	
	5.4.5 Conclusions	
5.5	Large Gd ^{III} -DOTA discotic.....	108
	5.5.1 Synthesis	
	5.5.2 Longitudinal relaxation time measurements	
	5.5.3 Conclusions	

5.6	Overall conclusions.....	112
5.7	Epilogue.....	112
5.8	Experimental section.....	115
5.9	Appendices.....	125
5.10	References and notes.....	130
	<i>Summary</i>	133
	<i>Samenvatting</i>	137
	<i>Curriculum Vitae</i>	141
	<i>Dankwoord</i>	143

1

Self-assembling contrast agents for MRI

ABSTRACT: *Chemists have designed more efficient contrast agents for magnetic resonance imaging for the past three decades. Several approaches and synthetic strategies are applied to gain contrast-enhancement. Recently it has been shown that self-assembling contrast agents based on paramagnetic amphiphiles allow combining the benefits of both high and low molecular weight contrast agents, namely a high relaxivity and complete excretion from the body, respectively. Thus far, research in this area has focused on the use of classical linear amphiphiles mainly forming spherical objects, such as micelles. Discotic amphiphiles are until now unexplored, but may be attractive candidates for self-assembling contrast agents in view of their unique spatial features. In this chapter, currently reported systems based on classical paramagnetic amphiphiles will be dealt with and the characteristic properties of discotic amphiphiles and of their self-assembly will be highlighted.*

1.1 Magnetic resonance imaging and the use of contrast agents

Magnetic resonance imaging (MRI) is anticipated to become one of the most powerful non-invasive techniques used in the medical world for early disease diagnosis. Its advantages comprise a high spatial resolution with three-dimensional viewing, the use of a non-ionizing radiation source, and the ability to extract simultaneously physiological and anatomical information from soft tissue. A main disadvantage of MRI, however, is its low sensitivity. To overcome the problem of low sensitivity, scientists have developed agents for contrast-enhanced MRI. The first clinically approved contrast agent, Gd^{III} -DTPA (gadolinium-diethylenetriaminepentaacetic acid), has been commercialized in 1988 under the trade name MagnevistTM (Figure 1.1).^[1,2] After that, four other low molecular weight, Gd^{III} -based contrast agents have been approved by the Food and Drug Administration (FDA) among which Gd^{III} -DOTA (gadolinium-1,4,7,10-tetraazacyclododecane-1,4,7,10-tetraacetic acid) or DotaremTM (Figure 1.1).^[1,2]

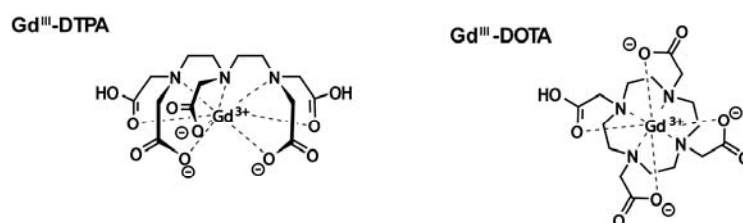


Figure 1.1 Molecular structures of Gd^{III} -DTPA and Gd^{III} -DOTA.

The Gd^{III} -ion is by far the most frequently used metal ion for MRI agents due to its high magnetic moment (seven unpaired f-electrons), its relatively long electronic relaxation time and its ability to form highly stable complexes.^[3] The high stability of gadolinium chelates (association constants usually between 10^{16} to 10^{23} $\text{L}\cdot\text{mol}^{-1}$)^[4] is a requirement to avoid the release of free Gd^{III} -ions, which are very toxic even at low concentrations (LD_{50} values are in the range of 0.20 – 0.30 $\text{mmol}\cdot\text{kg}^{-1}$).^[3,4] Properties that severely limit the utility of these low molecular weight contrast agents are their non-specificity, their low efficiency and their fast renal excretion, which necessitates high dosages.

1.1.1 Applied strategies for contrast-enhancement

One of the strategies applied to increase the contrast, and thereby reduce the required dosage of contrast agent, is to attach multiple MRI labels to one single scaffold in order to obtain higher local concentrations of contrast agent (Figure 2).^[4–6] Theory predicts that slow rotation of the chelates in solution (long τ_{R} values) and fast water exchange between the ion coordination sphere and the bulk water (short τ_{M} values) will lead to higher relaxivities.^[4,7] Thus, an extra gain in contrast may result from a slower rotation of the Gd^{III} -complex due to a loss in local and global mobility caused by coupling to a macromolecule. Another advantage

of attaching low molecular weight Gd^{III} -chelates to macromolecules originates from the increased size of the complete contrast agent guaranteeing a longer circulation time in the blood, and hence reduction of the required dosage. A different strategy to reduce the required dosage of contrast agent is to provide the contrast agent with additional groups for active targeting to increase specificity (Figure 1.2).^[3,5] Specificity of the low molecular weight contrast agents only stems from their preference to reside in the blood stream, due to their hydrophilicity. Active targeting can be introduced by tagging a Gd^{III} -complex to a ligand, which recognizes receptor molecules specific for a certain disease. As a result, the MRI contrast agent accumulates at the region of interest in the body. Scaffolds consisting of multiple ligands and multiple MRI labels combine the benefits of a high relaxivity and a high specificity.

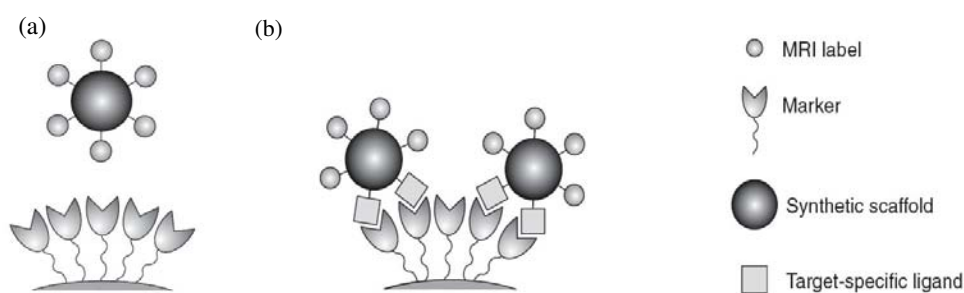


Figure 1.2 (a) Multiple MRI labels attached to a synthetic scaffold will give more contrast. (b) target-specific MRI agents lead to more contrast and to accumulation of contrast agent at regions of interest.^[8]

1.1.2 Synthetic approaches: towards more efficient contrast agents

Several synthetic approaches have been proposed in order to obtain highly efficient contrast agents for MR imaging. The first approach makes use of modified, low molecular weight Gd^{III} -chelates, like MS-325, that reversibly bind to plasma proteins, like albumin.^[9,10] The binding to albumin reduces the extravasation of the contrast agent and leads to a high increase in relaxivity. On the other hand, the reversible nature of the binding makes sure that the low molecular weight Gd^{III} -chelates are released from the albumin and thus can be cleared from the body. A second method takes advantage of gadolinium complexes covalently linked to macromolecules displaying multiple functional endgroups, like polymers^[11–15], dendrimers^[16–19], biological molecules^[20–22] or nanoparticles^[23–25]. These systems can be made target-specific by linking next to MRI labels one or more targeting ligands to the scaffold molecule.^[26] The drawback of most of these covalently linked macromolecular systems is that they often suffer from incomplete excretion from the body (due to their high molecular weight), and hence from a higher toxicity.^[4,27] Furthermore, the relaxivity gain reached by increasing the molecular size of the contrast agent is often disappointing as a result of internal flexibility or non-rigid attachment of the chelate to the macromolecule.^[11,12] A third strategy

employs supramolecular systems like liposomes and micelles. Several studies describe the encapsulation of MRI labels into liposome vesicles^[28] or its immobilization into micelles^[29–32] or the liposome membrane^[33–36]. These systems display easily controlled properties and good pharmacological characteristics. Furthermore, it has been shown that supramolecular contrast agents can be made target-specific by mixing in peptide amphiphiles displaying a certain bioactive peptide sequence.^[37–44] Another advantage of micellar systems is their reversible nature, which allows combining the benefits of both high and low molecular weight contrast agents, namely a high relaxivity and complete excretion from the body, respectively. This unique set of properties has drawn the attention of many researchers. As a consequence, there are many detailed investigations known concerning the use of paramagnetic amphiphiles.

So far, research in the area of self-assembling contrast agents has focused on the use of linear paramagnetic amphiphiles. These amphiphiles consist of a hydrophilic gadolinium containing head group and a hydrophobic alkyl tail and mainly form spherical assemblies, such as micelles and liposomes, in solution. The linear amphiphiles that have been designed by Hartgerink *et al.*^[45–47] are an exception to this rule because these amphiphiles can self-assemble into micellar rods and thus form columnar objects in solution. These amphiphiles, called peptide amphiphiles, contain a hydrophilic peptide head group and a hydrophobic alkyl tail. Gadolinium chelates have been linked to these peptide amphiphiles to create columnar self-assembling contrast agents for MRI.^[48,49]

The use of paramagnetic discotic amphiphiles has not been explored yet. Discotic amphiphiles are a special class of amphiphiles that self-assemble into columnar structures. Columnar self-assembling contrast agents based on discotic amphiphiles have some advantages compared to spherical assemblies based on linear amphiphiles; firstly, they are able to become very long, hence ensuring high local concentrations of gadolinium, and secondly, the discotic amphiphiles making up the columns have a multivalent character, which leads to higher local concentrations of contrast agent and opens possibilities for the use of asymmetric target-specific discotics. Furthermore, the self-assembly of discotic molecules— C_3 -symmetrical (C_3)-discotics in particular—has been well-studied. C_3 -discotics have exerted special attraction, since their symmetry often promotes the formation of helical aggregates, is advantageous in synthesis design and rules out the importance of rotational order within the assemblies. Most of the self-assembly studies currently reported have been performed in apolar media, but the few studies describing the self-assembly of discotic amphiphiles in water show similar characteristics. Synthesizing paramagnetic discotic amphiphiles might, therefore, be an attractive strategy for creating a new class of self-assembling contrast agents. On the other hand, if these self-assembling contrast agents are available, it would also be interesting to investigate whether relaxation time measurements can be used as an extra tool to study the self-assembly process of these discotic amphiphiles.

In the following sections, the relaxivities of currently reported self-assembling contrast agents based on paramagnetic linear amphiphiles will be dealt with, and the fascinating self-assembly behaviour of C_3 -symmetrical discotics in apolar media and in water will be highlighted. Finally, the use of longitudinal relaxation time measurements as a tool to study self-assembly processes will be briefly addressed.

1.2 Self-assembling paramagnetic amphiphiles for MR imaging

Paramagnetic amphiphiles are able to self-assemble into well-defined architectures, which ideally exhibit four valuable properties: i) a high payload of Gd^{III} -chelates, ii) an enhanced ability to increase solvent proton relaxation rates due to a long molecular reorientation time (τ_R), iii) an increased residence time in the blood by retarding the extravasation that is typical for the small-sized Gd^{III} -complexes commonly employed in MRI, and/or iv) a dynamic character to ensure that the low molecular weight amphiphiles will eventually be released and excreted from the body. A variety of Gd^{III} -based micellar and liposomal systems built up from paramagnetic linear amphiphiles has been designed and characterized, and it has been shown that the longitudinal proton relaxivities of the aggregated species are indeed considerably improved owing to the longer tumbling times of the Gd^{III} -complexes.^[29–36]

The longitudinal 1H relaxation rate R_1 is equal to the inverse of the longitudinal relaxation time T_1 (equation (E1)). For systems without a critical concentration (or a very low critical concentration such as liposomes) equation (E2) holds, in which R_1^d is the diamagnetic contribution (the relaxation rate of pure water), r_1 represents the ionic relaxivity of the Gd^{III} -chelate (in $mM^{-1}s^{-1}$), and c_{Gd} is the Gd^{III} -concentration (in mM).

$$R_1 = \frac{1}{T_1} \quad (E1)$$

$$R_1^{obs} - R_1^d = r_1 \times c_{Gd} \quad (E2)$$

$$R_1^{obs} - R_1^d = r_1^{n.a.} \times c_{Gd} \quad (E3)$$

$$R_1^{obs} - R_1^d = r_1^{n.a.} \times cmc + r_1^a (c_{Gd} - cmc) \quad (E4)$$

For micelles, equations (E3) and (E4) can be derived. Equation (E3) describes the water 1H relaxation rate in solutions below the cmc , in which $r_1^{n.a.}$ represents the ionic relaxivity of non-aggregated Gd^{III} -chelate (in $mM^{-1}s^{-1}$). At concentrations greater than the cmc , the measured relaxation rate is the sum of two contributions, one caused by the free monomer chelate

present at a concentration given by the *cmc* and one due to the micellar structures. The water ^1H relaxation rate can then be expressed as in equation (E4), in which r_1^a gives the relaxivity of the aggregated species. It has to be noted that equations (E3) and (E4) can only be applied to self-assembling systems that display a critical concentration as is the case for micelles. A typical graph for contrast agents showing a critical concentration is depicted in Figure 1.3.

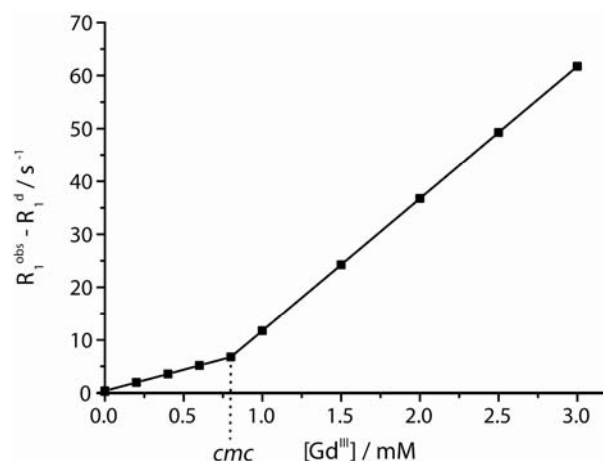


Figure 1.3 A typical graph for a micellar contrast agent; the longitudinal relaxation rate ($R_1^{\text{obs}} - R_1^{\text{d}}$) is plotted against the concentration of Gd^{III} .

That self-assembly processes of linear, paramagnetic amphiphiles are governed by hydrophobic interaction between the hydrocarbon chains has been demonstrated by Nicolle *et al.*^[50] They synthesized four potential MRI contrast agents; three of them were DOTA-like chelates bearing a simple alkyl side chain constituted of 10, 12 and 14 carbon atoms respectively, and the fourth one contained a DOTA chelating unit with a monoamide-octadecyl carbon side chain (Figure 1.4).

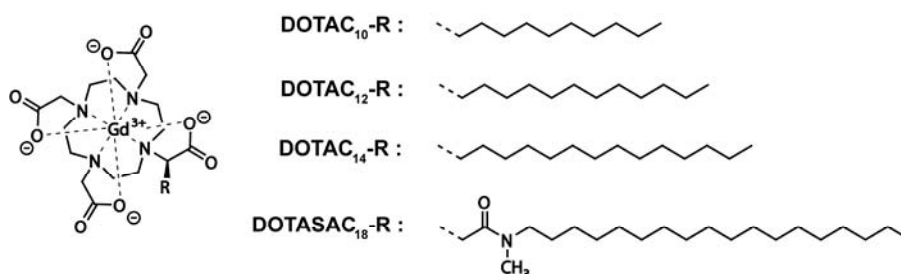


Figure 1.4 Molecular structures of paramagnetic linear amphiphiles designed by Nicolle *et al.*^[50]

It was shown that global rotational correlation times increase with increasing length of the side chain. Local motions, on the other hand, were influenced by the length and chemical structure of the side chain. The importance of the nature of the side chain was demonstrated

by the fact that despite its 30% longer global rotational correlation time, $\text{Gd}^{\text{III}}(\text{DOTASAC}_{18})(\text{H}_2\text{O})$ did not display a higher relaxivity than $\text{Gd}^{\text{III}}(\text{DOTAC}_{14})(\text{H}_2\text{O})$ owing to its much shorter local rotational correlation time. As a reference, the ionic relaxivity of micellar systems consisting of $\text{Gd}^{\text{III}}\text{-DOTAC}_{14}$ was $22.0 \text{ mM}^{-1}\text{s}^{-1}$ (1.5 T, 25 °C).

Despite their promising features, (mixed) micelles containing gadolinium complexes bearing only one aliphatic tail could not be used as contrast agent because they had a strong haemolytic effect and were quickly eliminated from the blood stream.^[32] These drawbacks were completely circumvented using gadolinium complexes bearing two aliphatic tails. Once recognized, research mainly focused on physically stable mixed micelle formulations that contained phospholipids, surfactants and paramagnetic amphiphiles with two alkyl tails (Figure 1.5). One of the parameters studied in more detail was the influence of alkyl chain length on the proton relaxivity. Kimpe *et al.*^[51] described the synthesis of neutral amphiphilic bisamide derivatives of DTPA with two alkyl tails constituted of 14, 16 and 18 carbon atoms, respectively. The gadolinium complexes were mixed into micelles containing phospholipids (DPPC) and a surfactant (Tween 80). The proton relaxivities of $\text{Gd}^{\text{III}}\text{-DTPA-BC}_{14}$ and $\text{Gd}^{\text{III}}\text{-DTPA-BC}_{16}$ were quite similar ($r_1^a = 13 \text{ mM}^{-1}\text{s}^{-1}$; 0.5 T, 37 °C) and larger than for micellar $\text{Gd}^{\text{III}}\text{-DTPA-BC}_{18}$ ($r_1^a = 9.8 \text{ mM}^{-1}\text{s}^{-1}$; 0.5 T, 37 °C). This was attributed to the less effective immobilization of $\text{Gd}^{\text{III}}\text{-DTPA-BC}_{18}$ inside the micellar structure, probably because the alkyl chains were longer than the alkyl chains of the major component of the micelles, DPPC, in which it was inserted. This ensured an increased mobility of the polar head and hence a lower relaxivity.

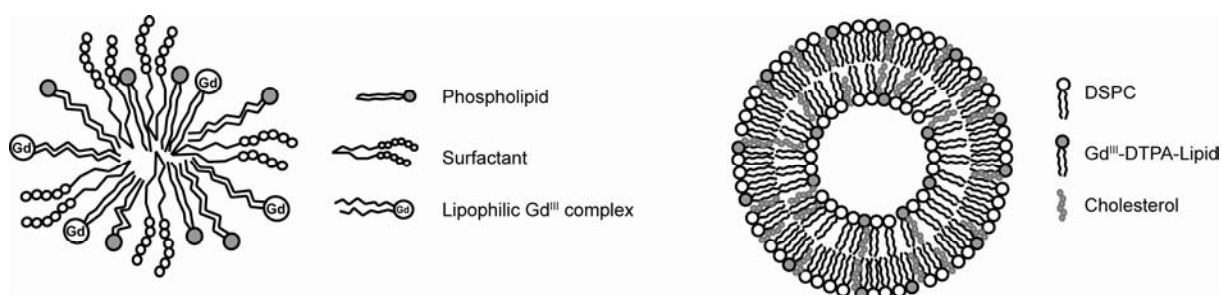


Figure 1.5 Schematic representations of paramagnetic mixed micelles and liposomes.

Parac-Vogt *et al.*^[35] studied very similar $\text{Gd}^{\text{III}}\text{-DTPA}$ bisamide derivatives containing long chain phenylalanine esters with 14, 16, 18 carbon atoms in the alkyl tails. The presence of the bulky phenylalanine units resulted in inefficient packing into micelles. Nevertheless, all complexes were efficiently incorporated into DPPC-based liposomes. As observed before, the $\text{Gd}^{\text{III}}\text{-DTPA}$ bisamide complexes with tails of 14 carbon atoms long showed the highest relaxivity, $r_1 = 12 \text{ mM}^{-1}\text{s}^{-1}$ (0.5 T, 37 °C).

In the case of liposomes, the proton relaxivity could also be limited by a slow water exchange rate between the liposome interior and exterior as was illustrated by Strijkers *et al.*^[36] They showed that unsaturated DOPC-based liposomes displayed a higher relaxivity compared to saturated DSPC-based liposomes, and they attributed this effect to a less rigid DOPC membrane that was more permeable to water. They also demonstrated that cholesterol was needed in their system to obtain monodisperse unilamellar liposomes (Figure 1.5). The highest relaxivity per Gd^{III}-ion of 11.3 mM⁻¹s⁻¹ (0.625 T, 37 °C) was obtained for DOPC based liposomes containing cholesterol. Gløgard *et al.*^[33] also showed that DMPC-based liposomes, which were in the liquid crystalline state, showed a higher relaxivity compared to DSPC-based membranes that were in the solid gel state, which indicated that the relaxivity was again exchange limited. They used fractional factorial design to find the liposome composition with the highest relaxivity. The highest relaxivity, $r_1 = 52.0 \text{ mM}^{-1}\text{s}^{-1}$, was obtained in the region with no cholesterol and low content of Gd^{III}-chelate. However, it is questionable whether liposomes without any cholesterol are stable monodisperse unilamellar liposomes. The same authors also reported NMRD-profiles for DMPC/DMPG liposomes containing 5.5% Gd^{III}-HHD-DO3A and 20% cholesterol, which possessed an observed relaxivity of 43 mM⁻¹s⁻¹ (0.5 T, 39 °C).

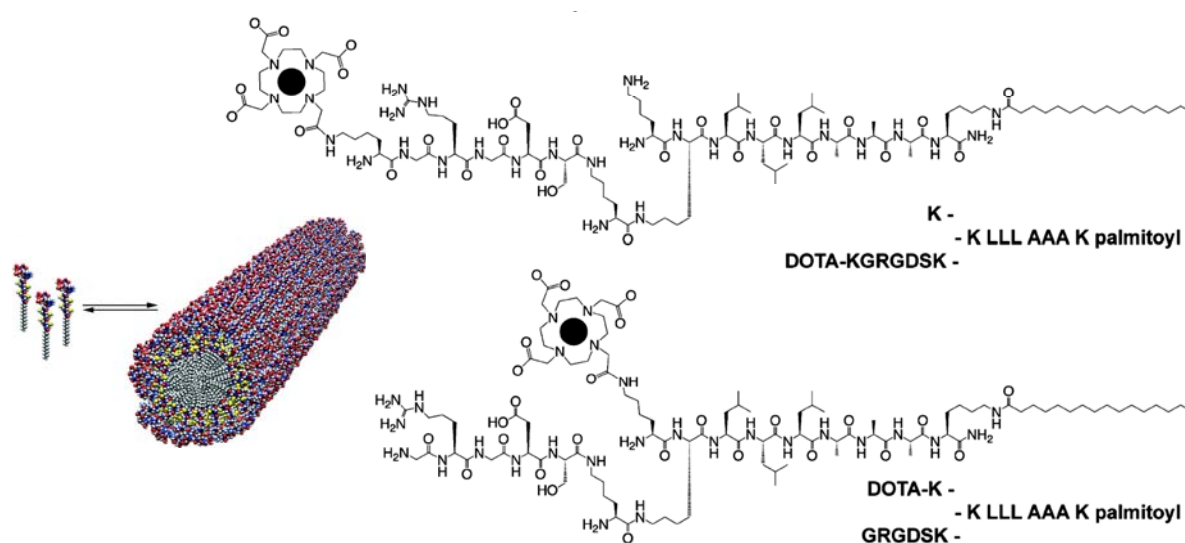


Figure 1.6 Schematic representations and molecular structures of two paramagnetic peptide amphiphiles forming peptide nanofibers.

Bull *et al.* reported the synthesis and *in vitro* MR images of two self-assembled paramagnetic linear peptide amphiphiles. These paramagnetic peptide amphiphiles together with their analogues lacking the Gd^{III}-chelates were self-assembled into mixed micellar rods called peptide nanofibers (Figure 1.6).^[48,49] The only difference between the two paramagnetic amphiphiles investigated was the position of Gd^{III}-chelate. It was shown that positioning of

the Gd^{III}-chelate close to the hydrophobic tail of the molecule resulted in a higher relaxivity. The ionic relaxivity of self-assembled amphiphiles displaying the chelator at the end of the peptide fragment was 14.7 mM⁻¹s⁻¹ (1.5 T, 37 °C), while the ionic relaxivity of the self-assembled amphiphiles having the chelator close to the alkyl tail equalled 21.5 mM⁻¹s⁻¹.

So far, the highest relaxivity per Gd^{III}-ion was obtained by using liposomes (highest relaxivity reported 43 mM⁻¹s⁻¹)^[33] rather than mixed micelles (highest relaxivity reported 29 mM⁻¹s⁻¹)^[31] or peptide nanofibers (highest relaxivity reported 21.5 mM⁻¹s⁻¹)^[48]. However, it should be noted that the range of reported relaxivities was rather broad (liposomes $r_1 \approx 5\text{--}43$ mM⁻¹s⁻¹ and (mixed) micelles $r_1^a \approx 12\text{--}29$ mM⁻¹s⁻¹)^[25]. The field strengths and temperatures at which these measurements have been performed are not identical so it is not quite possible to compare these systems, but it gives a first indication. To judge whether the observed proton relaxivities of self-assembling paramagnetic discotic amphiphiles are promising, the proton relaxivities for self-assembled paramagnetic linear amphiphiles will be used as a reference.

1.3 Self-assembly behaviour of C₃-symmetrical discotics

The self-assembly of discotic molecules is studied in detail in the liquid crystalline state, in the gel state and in solution. In general, C₃-discotics are more thoroughly studied compared to asymmetric discotics, since their symmetry offers some advantages; it is compatible with chirality, it is advantageous in the synthetic design and, in many cases, it rules out the importance of rotational order within the column. Most of the studies dealing with the self-assembly of C₃-discotics have been performed in apolar media, but the few studies describing the self-assembly of discotic amphiphiles in water show similar characteristics, which suggest that paramagnetic discotic amphiphiles may be applicable as self-assembling contrast agents for MRI.

1.3.1 Self-assembly of discotic molecules in apolar media

In the 1990s, C₃-symmetrical discotics based on *cis-cis*-1,3,5-cyclohexanetricarboxamide or 1,3,5-benzenetricarboxamide cores started to play an important role in the area of nanoscience, because these molecules displayed a strong tendency to adopt appealing conformations, like helices or propellers, as was demonstrated by their crystal structures.^[52,53] An important goal in this developing field was the identification of molecular subunits that allow controlled formation of one-dimensional supramolecular constructs. New discotic molecules were developed with the aim to investigate the effect of steric hindrance, pre-orientation and the balance between secondary interactions on the stability of the aggregates.

Our laboratory started to investigate disc-like molecules that were built up by linking three lipophilic, *N*-monoacetylated 2,2'-bipyridine-3,3'-diamine wedges to a central 1,3,5-

benzenetricarboxamide unit (Figure 1.7 large).^[54,55] These large discs adopted a propeller-like structure in which the bipyridine units were tilted with respect to the central core (Figure 1.8). Self-assembly of these molecules gave one-dimensional, helical columns. Equal amounts of *P* and *M* helices were present in solutions of the achiral disc. When chiral discs were used in the self-assembly, only one (*P* or *M*) type of helix is formed due to the diastereomeric selection of the *P* and *M* helix. One chiral disc (sergeant) could dictate the helical sense of as many as 80 achiral discs (soldiers) as was studied by means of circular dichroism (CD) spectroscopy.^[56] The addition of a small amount of chiral disc to a solution of achiral discs instantaneously resulted in a CD-effect, which suggested fast exchange between molecules of different stacks. Majority rule experiments carried out on mixtures of the enantiomers also showed a non-linear response of the CD-effect on the enantiomeric excess, which confirmed the strong tendency for chiral amplification.^[57]

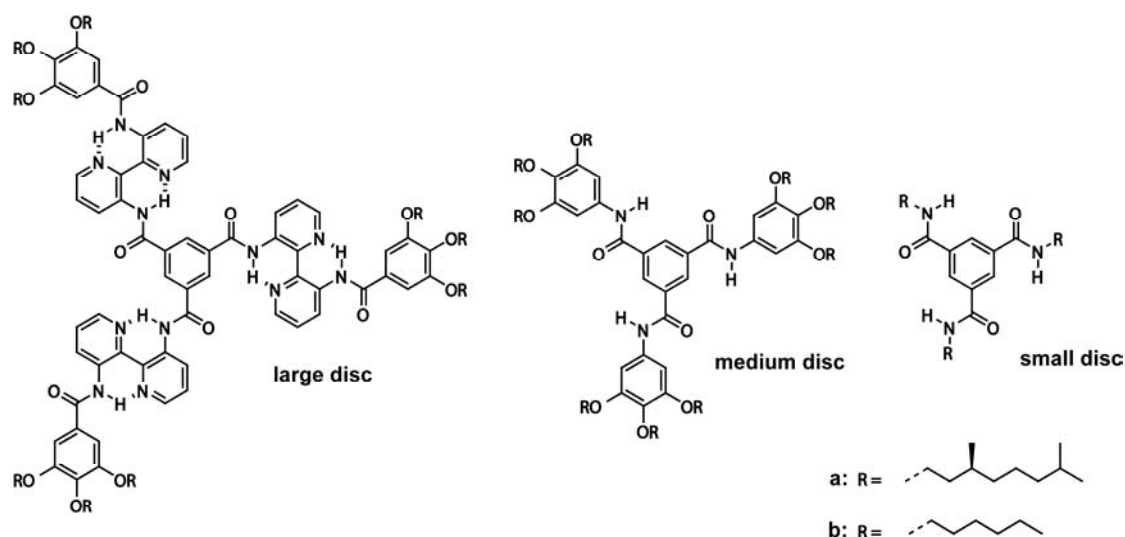


Figure 1.7 Molecular structures of the large, medium and small 1,3,5-benzenetricarboxamide discs.^[60]

Small structural modifications in different parts of the disc strongly influenced the stability and dynamics of and order within the stacks. Bipyridine discs provided with additional methoxy substituents displayed stronger aggregation due to stronger π - π interaction, but lacked any expression of chirality.^[58] The same held for discs containing diphenylpyrazine moieties instead of bipyridines.^[58] The importance of the peripheral mesogenic groups was illustrated when the bipyridine units were functionalized with chiral OPV side chains.^[59] Stable aggregates with little chiral ordering were formed, which was explained by competing types of π - π interaction that differ in strength and orientation. Changes in the interior of the discs were also studied by replacing the three central amide groups by three central urea groups.^[60] Also in this case, columnar stacks were formed but they were not able to express the chiral information embedded in the structure of the

molecule. Remarkably, in all of the modified systems evaluated, the ability for chiral amplification was completely suppressed. This confirmed that careful matching of the different types of interactions is the key to create dynamic systems that enable amplification of chirality.

In 2002, the bipyridine series was enlarged with two amide (Figure 1.7: medium and small) and two corresponding urea discs to elucidate the contribution of the different secondary interactions to the self-assembly of the discs.^[60] In the 'medium' discs the bipyridine unit was omitted and the gallic acid moiety was directly reacted with the central core. It was shown that the medium trisamide did not form columnar structures in apolar solutions, while the medium trisurea compound did. On the other hand, small N,N',N'' -trialkylbenzene-1,3,5-tricarboxamides and triureas did show chiral amplification. In the case of the triurea 75% of chiral compound was needed to give the Cotton effect of the pure chiral compound, while for the tricarboxamide 0.5% of chiral compound was already sufficient. The differences in behaviour of these discs demonstrated that changing the balance between secondary interactions drastically affected the properties of the supramolecular aggregates.

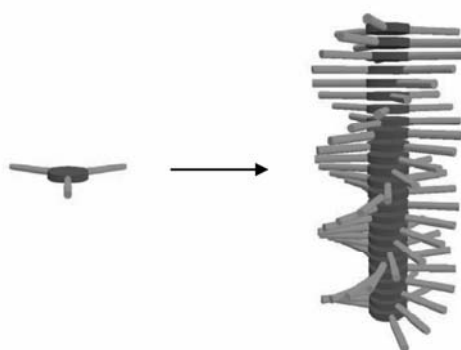


Figure 1.8 A cartoon of the helical columns formed by 1,3,5-benzenetricarboxamide based discs.^[61]

The introduction of small structural changes without a rigorous modification of the overall structure could be facilitated by using amino acids as structuring elements as was shown by De Loos *et al.*^[62] They synthesized several C_3 -symmetrical molecules based on cyclohexane cores as well as benzene cores (Figure 1.9) to judge whether their discotics might act as efficient organogelators. It was shown that benzene-based compounds display disappointing aggregation behaviour. Substitution of the benzene core by the cyclohexane core resulted in a dramatic increase in the gelation and aggregation properties of the compounds. The increased gelation ability was related to a more favourable orientation of the hydrogen bonding units with respect to the main plane of the core. Furthermore, it was demonstrated that the type and number of hydrogen bonding interactions and the nature of

the R-group of the amino acid significantly influence the gelation and hence the aggregation ability.

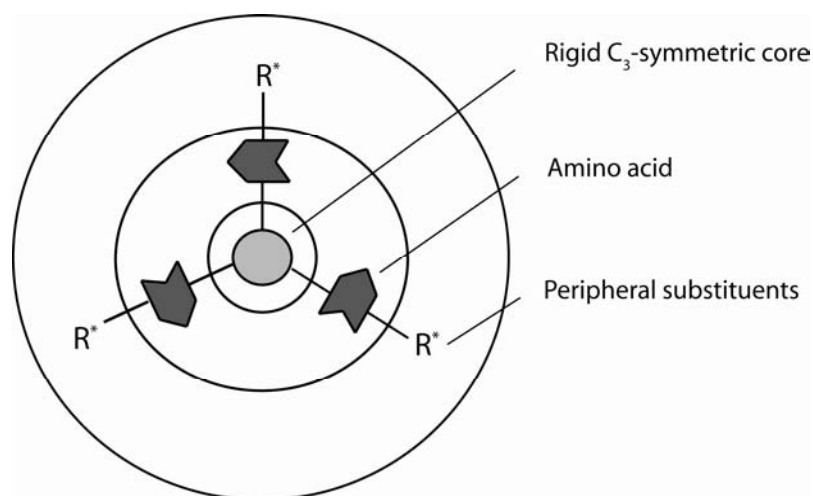


Figure 1.9 Schematic representation of the *cis,cis*-1,3,5-cyclohexanetricarboxamide and 1,3,5-benzene tricarboxamide based amino acid containing discotics.^[62]

Hanabusa *et al.* also investigated the viscoelastic behaviour of supramolecular organogels involving gelators with threefold symmetry, N, N', N''-tris(3,7-dimethyloctyl)-benzene-1,3,5-tricarboxamide (DO₃B)^[63–65] and tris-3,7-dimethyloctyl-*cis*-1,3,5-cyclohexanetricarboxamide (DO₃CH)^[66–68], in organic solvents, at varying gelator concentrations. Both C₃-symmetrical discotics formed enormously long supramolecular polymers that exhibited remarkable viscoelastic properties due to entanglements between the supramolecular polymers. The cyclohexane-based molecules formed straight columnar structures, while the benzene-based compounds formed helical columnar structures with equal amounts of left- and right-handed helicities. It was demonstrated that the addition of (*S*)DO₃B to this racemic mixture resulted in one helicity in excess, due to the majority rule effect.^[69]

Recent studies by Nuckolls and coworkers explored hexasubstituted benzene rings in which the presence of alkoxy or alkyne substituents in the 2,4,6-positions resulted in “crowded” aromatics (Figure 1.10).^[70–75]

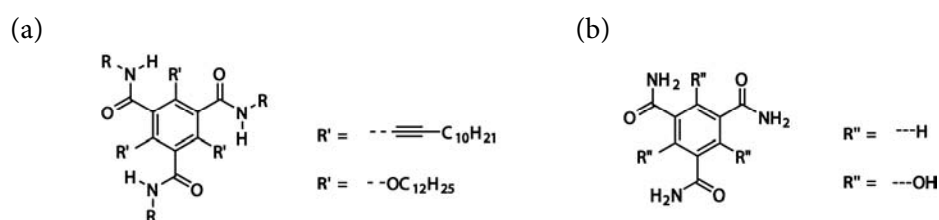


Figure 1.10 Molecular structure of crowded aromatics designed by (a) Nuckolls *et al.*^[70–75] and (b) Hadj-Messaoud *et al.*^[76].

The introduction of chiral amide side chains provided evidence that helicity was also present in these columnar stacks, even in solution. Hadj-Messaoud and coworkers demonstrated the influence of intramolecular versus intermolecular hydrogen bonding interactions in these kinds of systems on the creation of strongly organized assemblies and their physical properties.^[76] It was shown that the presence of substituents in the 2,4,6-position with the opportunity to participate in intramolecular hydrogen bonds (Figure 1.10) hindered twisting of the amides, made the molecule flatter, the ring–ring separation shorter and the cohesive energy smaller. In contrast, the presence of substituents that preferably form intermolecular hydrogen bonds were predicted to increase the ring–ring separation, induce twisting of the amides out of the plane of the aromatic core, improve the overall dipole moment, and improve the stability of the self-assembly. Consequently, physical properties—like charge transport through the columns—were tuneable by balancing the intra- and intermolecular hydrogen bonds by selecting the proper functional groups.

These examples illustrate that (hierarchical) self-assembly of C_3 -symmetrical discotics offers a powerful strategy for producing nano-architectures. But, although widely used, the mechanistic details of self-assembly are not completely understood. Recently, it has been shown that accurate temperature-dependent spectroscopic measurements allow studying self-assembly mechanisms of π -conjugated molecules into helical fibers in great detail.^[77] In general, two mechanisms can be discerned: an isodesmic^[78,79] or a nucleation-elongation mechanism^[77,79,61]. The first C_3 -symmetrical discotics investigated by means of accurate temperature-dependent measurements are the small N,N',N'' -trialkylbenzene-1,3,5-tricarboxamides.^[61] It is shown that these molecules self-assemble via a nucleation-growth mechanism. Later on, the large bipyridine discs have also been investigated and these discotics self-assemble via an isodesmic mechanism.^[80] At the moment it is not understood why some systems self-assemble via an isodesmic model and others via a cooperative model.

1.3.2 Self-assembly of discotic molecules in water

There exists a vast body of experimental and theoretical work on self-assembly of amphiphilic molecules in water. Almost all of this research concerns linear amphiphiles^[81–84] with hydrophilic heads and hydrophobic tails. These amphiphiles exhibit a complex phase behaviour, as a consequence of the variety of self-assembled structures that can be formed (Figure 1.11a: A) micellar rod; B) micelle; C) bilayer; D) vesicle and E) inversed micelle).^[85–88]

Discotic amphiphiles belong to a class of amphiphiles with a different shape. They possess a rigid hydrophobic core surrounded by a hydrophilic rim. The rim must be sufficiently hydrophilic to enable the molecule to dissolve and the core must be sufficiently hydrophobic to generate a tendency for the discs to stack on top of each other in order to shield the cores from the solvent. In contrast to linear amphiphiles, their aggregation only generates columnar aggregates, a so called linear self-assembly (Figure 1.11b). Due to the

quasi-one-dimensional nature of the aggregates, the length distribution is often polydisperse. The number of discotic amphiphiles currently reported is very limited.

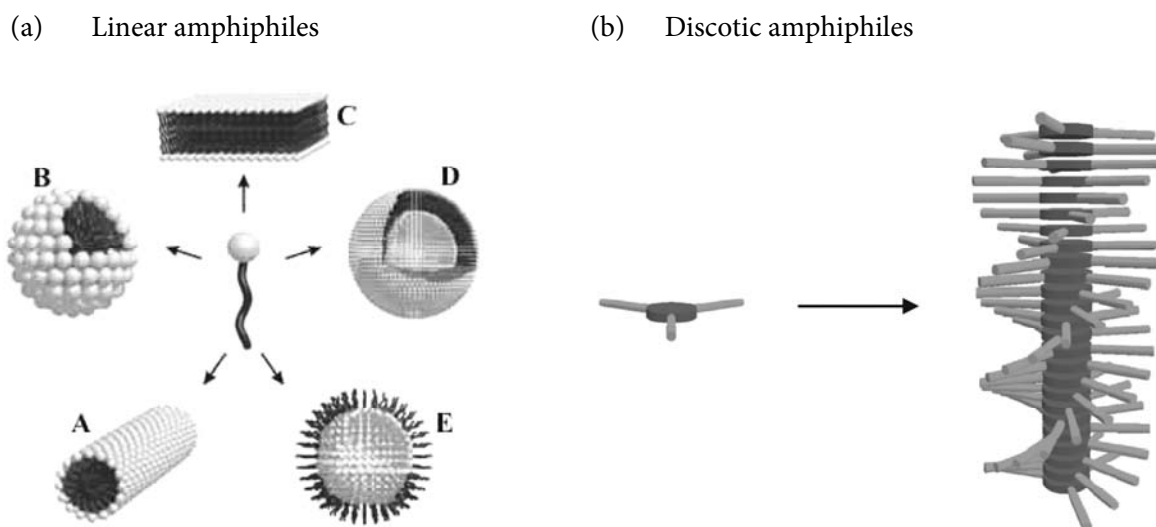
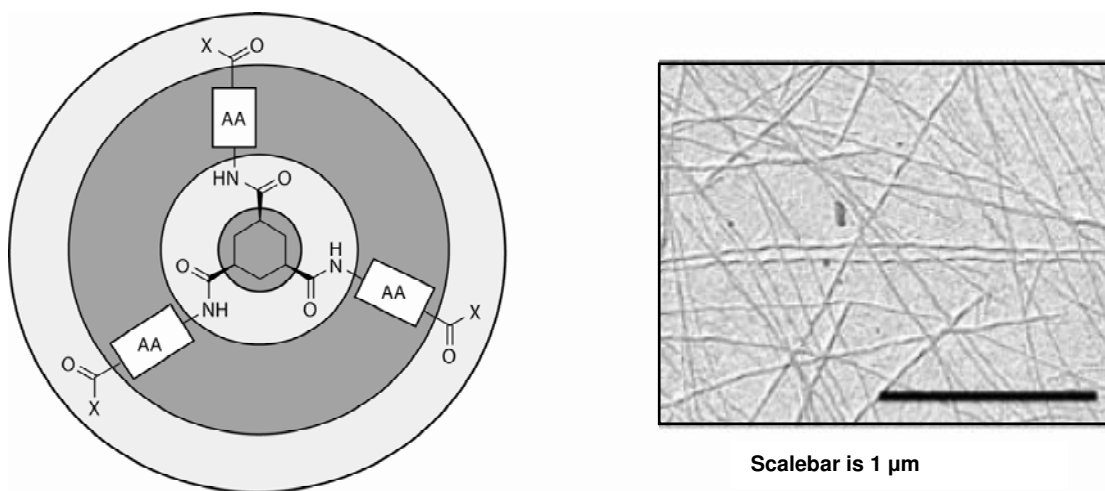


Figure 1.11 Linear amphiphiles may give rise to a variety of self-assembled structures, while discotic amphiphiles only generate linear self-assembly^[61].

The first discotic amphiphiles reported were 2,3,6,7,10,11-hexa(polyethyleneoxy) derivatives of triphenylene.^[89] It was shown that these discotic molecules form lyotropic discotic nematic and hexagonal mesophases by dissolution in water, which indicated they gave rise to ordered arrays of aggregates.

Discotic amphiphiles that can function as low molecular weight hydrogelators were investigated by Van Esch *et al.*^[90-92] Their general architecture was based on a *cis,cis*-1,3,5-cyclohexanetricarboxamide core linked to various amino acid based substituents, which provided additional driving forces for gelation (i.e. hydrogen bonding and hydrophobic interactions) (Figure 1.12). Their work showed that the properties of the gels could be easily tuned by changing the nature of the amino acid and/or the number of hydrogen bonding moieties.^[90,91] They also demonstrated that chirality of the amino acids and/or peripheral functionalization played important roles in controlling the gelation properties.^[92] To obtain well-defined architectures the appropriate balance between forces, such as hydrophobic interactions and hydrogen bonding, had to be found. The self-assembly of peptide containing discotic amphiphiles was also investigated by Bose *et al.*^[93] They demonstrated that the helical nanofibers could further self-assemble into triple-helical nanofibers.



Light grey regions = hydrophilic ; Dark grey regions = hydrophobic ; AA = amino acid (s) ; X = hydrophilic substituent

Figure 1.12 Schematic representation of the *cis,cis*-1,3,5-cyclohexanetricarboxamide based peptide discotics. Transmission electron microscopy (TEM) images of such gels show a network of thin, unbranched fibre bundles with diameters of 20 nm.^[92]

In our laboratory, a discotic amphiphile that formed helical columns with a preferred handedness in protic media was synthesized. The molecule contained a 1,3,5-benzenetricarboxamide core extended with 3,3'-diamino-2,2'-bipyridine units bearing gallic moieties with chiral oligo(ethylene oxide) peripheral tails. Self-assembly of this molecule in dilute solutions in *n*-butanol and in water was studied with spectroscopic techniques like UV/Vis, CD and NMR. The measurements demonstrated that self-assembly in *n*-butanol occurred in a hierarchical fashion. In a stepwise growth first achiral small aggregates were generated by hydrophobic interactions between the aromatic cores, and in the next step, expression of the hydrogen bonds gave rise to large chiral self-assembled structures (Figure 1.13).^[94,95] In water, it was impossible to monitor the entire self-assembly process of this bipyridine disc, due to the LCST behaviour of the oligo(ethylene oxide) tails.^[96] Dilute solutions in water became turbid around 70 °C, what was ascribed to the formation of clusters of columns. “Sergeant and Soldiers” experiments in water revealed that one chiral molecule was able to induce chirality into 12 achiral molecules at 5 °C.^[97] The fact that exchange between the discs took place, illustrated that the system, despite the extremely ordered and stable packing, was still dynamic in nature. In *n*-butanol, amplification of chirality was even stronger and it was possible to transfer the chirality of one chiral seed molecule to 400 achiral molecules within a helical stack.^[98]

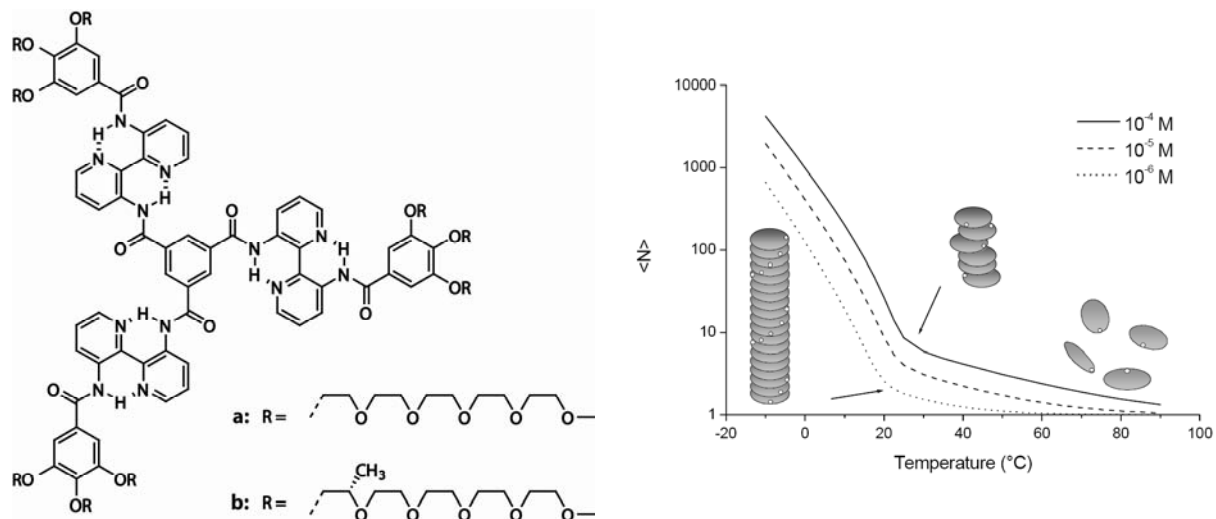


Figure 1.13 Molecular structures of the large bipyridine discs decorated with chiral oligo(ethylene oxide) tails and their hierarchical self-assembly.^[94,95]

1.4 ¹H relaxation time measurements: study self-assembly in dilute solutions

1.4.1 Determining the critical micelle concentration

¹H longitudinal relaxation time measurements have already been applied to study the self-assembly processes of paramagnetic linear amphiphiles.^[29,50] The ¹H relaxation time measurements by Nicolle *et al.*^[50] demonstrate that the critical micelle concentrations of the linear paramagnetic amphiphiles investigated (for molecular structures see Figure 1.4) decrease with increasing alkyl chain length (Figure 1.14). This indicates that the self-assembly processes are governed by the hydrophobic interactions between the hydrocarbon tails. They state that the *cmc*s of these compounds are rather high since *in vivo* concentrations would be expected at or below 1 mM. These compounds may, therefore, lose their high relaxivity benefit of aggregation *in vivo*.

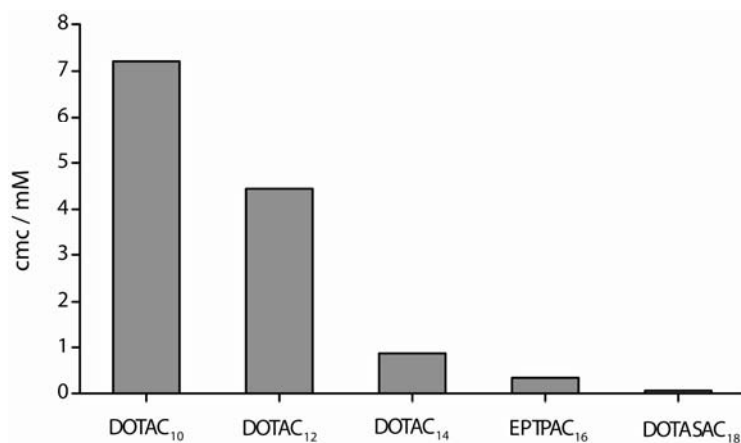


Figure 1.14 The critical micelle concentrations for five linear paramagnetic amphiphiles.^[29,50]

1.4.2 Probing the interaction of the biotin-avidin complex

The binding between biotin and avidin has also been studied by means of ^1H longitudinal relaxation time measurements.^[99,100] Avidin, a tetrameric protein, is capable of binding four equivalents of biotin in a strong, non-cooperative fashion ($K_{\text{ass}} \approx 1.7 \times 10^{15} \text{ M}^{-1}$).

Biotinylated Gd^{III} -DTPA analogues have been synthesized in order to study the biotin-avidin binding using the longitudinal relaxivity of the MRI label. MRI titration experiments with avidin and biotinylated Gd^{III} -DTPA (Figure 1.15) show a linear increase in the longitudinal ionic relaxivity, which is indicative for strong binding between the two components.^[99] After the addition of 0.25 equivalents of avidin, a plateau value of the ionic relaxivity is reached. This illustrates that ^1H longitudinal relaxation time measurements allow determining the binding stoichiometry between avidin and the biotinylated complex.

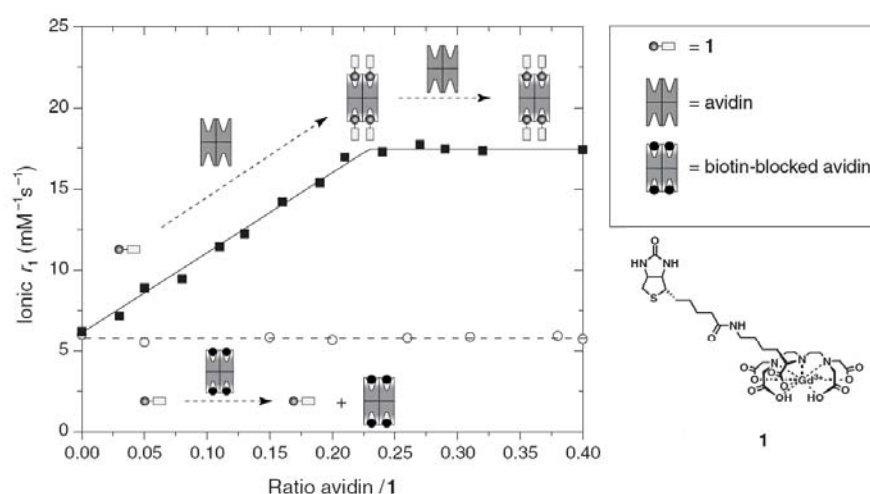


Figure 1.15 Variation of the longitudinal ionic relaxivity r_1 versus the ratio avidin/1 at 1.5 T and 25 °C for biotinylated Gd^{III} -DTPA compound **1**.^[99]

Since relaxation time measurements allow studying the formation of supramolecular assemblies in water, it might be rewarding to employ this method to investigate the self-assembly process of paramagnetic discotic amphiphiles.

1.5 Aim and outline of the thesis

The beauty of C_3 -discotic amphiphiles relies on their unique aggregation behaviour in combination with their C_3 -symmetry. Their shape ensures that aggregation only generates columnar aggregates, a so called linear self-assembly. Their C_3 -symmetry gives a multivalent character to the single discotics and supports the formation of ordered assemblies, which are often dynamic in nature. The aim of this research is to develop self-assembling systems based

on C_3 -symmetrical discotics, which in the end should find their application in biomedical fields, in particular focusing on magnetic resonance imaging. For this a C_3 -symmetrical core fragment that self-assembles and allows functionalization and fine-tuning of the secondary interactions in an easily accessible manner, should be designed. Peptide fragments are selected as structuring elements—in combination with the 1,3,5-benzenetricarboxamide core—for their biocompatibility, hydrogen bonding properties and versatile nature.

In **Chapter 2**, the synthesis of a new class of peptide discotics is described. These model compounds consist of a 1,3,5-benzenetricarboxamide core extended with peptide fragments decorated with peripheral mesogenic groups incorporating hydrophobic tails. Several mono- or dipeptide fragments were incorporated into the discs to create a library. The disc-like molecules have been synthesized using a convergent strategy in combination with consecutive coupling of the desired amino acids to avoid solubility problems and to minimize racemization.

The self-assembly characteristics of these mono- and dipeptide discotics in apolar media are described in **Chapter 3**. Two important properties of the assemblies investigated are their order and their stability. These properties have been studied in the neat state as well as in solutions in chloroform and in heptane, firstly, to determine whether the self-assembly of these peptide discotics is tuneable by modifying the peptide, and secondly, to judge whether these peptide discotics are potential building blocks for self-assembled structures in water.

In **Chapter 4** the synthesis and self-assembly behaviour of a water-soluble peptide discotic is described. The molecule consists of a 1,3,5-benzenetricarboxamide core extended with phenylalanine moieties bearing mesogenic groups containing oligo(ethylene oxide) tails. Self-assembly of this discotic amphiphile is studied in solutions in chloroform and in water. Extra attention has been paid to the size of the assemblies in water using different techniques like ^1H -DOSY NMR and *cryo*TEM.

Going towards an application in MRI, in **Chapter 5**, the syntheses are described of three Gd^{III} -DTPA bearing peptide discotics, which differ in their opportunities for hydrogen bonding and/or π - π interaction and one Gd^{III} -DOTA disc. The Gd^{III} -chelates function as MRI labels and as solubilizing ‘tails’. The self-assembly behaviour of these paramagnetic discotics has been studied in buffered aqueous solutions using a combination of spectroscopic techniques. Longitudinal relaxation time measurements have been performed for three reasons: i) to determine the efficiency of these new contrast agents, ii) to judge whether it is feasible to tune the aggregation concentration by the introduction of small structural changes, and (iii) to investigate whether these measurements can probe the self-assembly process of paramagnetic discotics. The size of the assemblies is determined with *cryo*TEM and ^1H -DOSY NMR. For this last purpose, Y^{III} -variants of the three DTPA discotics have been synthesized, since the Gd^{III} -versions are paramagnetic and hence not compatible with NMR.

1.6 References and notes

- [1] S-P. Lin, J.J. Brown, *J. Magn. Res. Imaging* **2007**, *25*, 884–899.
- [2] S. Laurent, L. vander Elst, R.N. Muller, *Contrast Med. Mol. Imaging*, **2006**, *1* 128–137.
- [3] R.B. Lauffer, *Chem. Rev.* **1987**, *87*, 901–927.
- [4] P. Caravan, J.J. Ellison, T.J. McMurry, R.B. Lauffer, *Chem. Rev.* **1999**, *99*, 2293–2352.
- [5] V. Jacques, J.F. Desreux, *Top. Curr. Chem.* **2002**, *221*, 123–164.
- [6] T. Barrett, H. Kobayashi, M. Brechbiel, P.L. Choyke, *Eur. J. Radiol.* **2006**, *60*, 353–366.
- [7] É. Tóth, L. Helm, A.E. Merbach, *Top. Curr. Chem.* **2002**, *221*, 61–101.
- [8] S. Langereis, Thesis: *Dendritic MRI contrast agents: Synthetic strategies for targeting and multivalency*; Eindhoven University of Technology: Eindhoven (The Netherlands), **2005**.
- [9] R.B. Lauffer, D.J. Parmelee, S. Ouellet, R.P. Dolan, H. Sajiki, M. Scott, P.J. Bernard, E.M. Buchanan, K. Y. Ong, Z. Tyeklár, K.S. Midelfort, T.J. McMurry, R.C. Walovitch, *Acad. Radiol.* **1996**, *3*, 356–358.
- [10] P. Caravan, N.J. Cloutier, M.T. Greenfield, S.A. McDermid, S.U. Dunham, J.W.M. Bulte, J.D. Amedio Jr., R.J. Looby, R.M. Supkowski, W. DeW. Horrocks Jr., T.J. McMurry, R.B. Lauffer, *J. Am. Chem. Soc.* **2002**, *124*, 3152–3162.
- [11] V.S. Vexler, O. Clement, H. Schmitt-Willich, R.C. Brasch, *J. Magn. Res. Imaging* **1994**, *4*, 381–388.
- [12] T.S. Desser, L.D. Rubin, H.H. Muller, F. Qing, S. Khodor, G. Zanazzi, S.W. Young, D.L. Ladd, J.A. Wellons, K.E. Kellar, *J. Magn. Res. Imaging* **1994**, *4*, 467–472.
- [13] F. Kiessling, M. Heilmann, T. Lammers, K. Ulbrich, V. Subr, P. Peschke, B. Waengler, W. Mier, H-H. Schrenk, M. Bock, L. Schad, W. Semmler, *Bioconjugate Chem.* **2006**, *17*, 42–51.
- [14] M. Spanoghe, D. Lanens, R. Dommissse, A. van der Linden, F. Alderweireldt, *Magn. Res. Imaging* **1992**, *10*, 913–917.
- [15] P. Rongved, J. Klaveness, *Carbohydr. Res.* **1991**, *214*, 315–323.
- [16] E.C. Wiener, M.W. Brechbiel, H. Brothers, R.L. Magin, O.A. Gansow, A.D. Tomalia, P.C. Lauterbur, *Magn. Reson. Med.* **1994**, *31*, 1–8.
- [17] S. Langereis, Q.G. de Lussanet, M.H.P. van Genderen, W.H. Backes, E.W. Meijer, *Macromolecules* **2004**, *37*, 3084–3091.
- [18] B. Misselwitz, H. Schmitt-Willich, W. Ebert, T. Frenzel, H-J. Weinmann, *Magn. Reson. Mater. Phys., Biol. Med.* **2001**, *12*, 128–134.
- [19] D.A. Fulton, E.M. Elemento, S. Aime, L. Chaabane, M. Botta, D. Parker, *Chem. Commun.* **2006**, 1064–1066.
- [20] J.M. Hooker, A. Datta, M. Botta, K.N. Raymond, M.B. Francis, *Nano Lett.* **2007**, *7*, 2207–2210.
- [21] D.J. Hnatowich, W.W. Layne, R.L. Childs, D. Lanteigne, M.A. Davis, T.W. Griffin, P.W. Doherty, *Science* **1983**, *220*, 613–615.
- [22] R.B. Lauffer, T.J. Bardy, *Magn. Res. Imaging* **1985**, *3*, 11–16.
- [23] P-J. Debouttière, S. Roux, F. Vocanson, C. Billotey, O. Beuf, A. Favre-Réguillon, S. Pellet-Rostaing, R. Lamartine, P. Perriat, O. Tillement, *Adv. Funct. Mater.* **2006**, *16*, 2330–2339.
- [24] W.J. Rieter, J.S. Kim, M.L. Taylor, H. An, W. Lin, T. Tarrant, W. Lin, *Angew. Chem.* **2007**, *119*, 3754–3756; *Angew. Chem. Int. Ed.* **2007**, *46*, 3680–3682.
- [25] W.J.M. Mulder, G.J. Strijkers, G.A.F. van Tilborg, A.W. Griffioen, K. Nicolay, *NMR Biomed.* **2006**, *19*, 142–164.
- [26] S. Langereis, A. Dirksen, T.M. Hackeng, M.H.P. van Genderen, E.W. Meijer, *New J. Chem.* **2007**, *31*, 1152–1160.
- [27] R.B. Clarkson, *Top. Curr. Chem.* **2002**, *221*, 201–235.

- [28] S. Aime, L. Frullano, S. Geninatti Crich, *Angew. Chem.* **2002**, *114*, 1059–1061; *Angew. Chem., Int. Ed.* **2002**, *41*, 1017–1019.
- [29] S. Torres, J.A. Martins, J.P. André, C.F.G.C. Geraldes, A.E. Merbach, E. Tóth, *Chem. Eur. J.* **2006**, *12*, 940–948.
- [30] J.P. André, É. Tóth, H. Fisher, A. Seelig, H.R. Mäcke, A.E. Merbach, *Chem. Eur. J.* **1999**, *5*, 2977–2983.
- [31] H. Tournier, R. Hyacinthe, M. Schneider, *Acad. Radiol.* **2002**, *9*, S20–S28.
- [32] P.L. Anelli, L. Lattuada, V. Lorusso, M. Schneider, H. Tournier, F. Uggeri, *Magma* **2001**, *12*, 114–120.
- [33] C. Gløgaard, G. Stensrud, R. Hovland, S.L. Fossheim, J. Klaveness, *Int. J. Pharm.* **2002**, *233*, 131–140.
- [34] M. Vaccaro, A. Accardo, D. Tesauero, G. Mangiapia, D. Löf, K. Schillén, O. Södermann, G. Morelli, L. Paduano, *Langmuir* **2006**, *22*, 6635–6643.
- [35] T.N. Parac-Vogt, K. Kimpe, S. Laurent, C. Piérart, L. vander Elst, R.N. Muller, K. Binnemans, *Eur. Biophys. J.* **2006**, *35*, 136–144.
- [36] G.J. Strijkers, W.J.M. Mulder, R.B. van Heeswijk, P.M. Frederik, P. Bomans, P.C.M.M. Magusin, K. Nicolay, *Magma* **2005**, *18*, 186–192.
- [37] G.A.F. van Tilborg, W.J.M. Mulder, N. Deckers, G. Storm, C.P.M. Reutelingsperger, G.J. Strijkers, K. Nicolay, *Bioconjugate Chem.* **2006**, *17*, 741–749.
- [38] W.J.M. Mulder, G.J. Strijkers, A.W. Griffioen, L. van Bloois, G. Molema, G. Storm, G.A. Koning, K. Nicolay, *Bioconjugate Chem.* **2004**, *15*, 799–806.
- [39] D.A. Sipkins, K. Gijbels, F.D. Tropper, M. Bednarski, K.C.P. Li, L. Steinman, *J. Neuroimmunology* **2000**, *104*, 1–9.
- [40] A. Accardo, D. Tesauero, G. Morelli, E. Gianolio, S. Aime, M. Vaccaro, G. Mangiapia, L. Paduano, K. Schillén, *J. Biol. Inorg. Chem.* **2007**, *12*, 267–276.
- [41] F. Alhaique, I. Bertini, M. Fragai, M. Carafa, C. Luchinat, G. Parigi, *Inorg. Chim. Acta* **2002**, *331*, 151–157.
- [42] D. Tesauero, A. Accardo, E. Gianolio, L. Paduano, J. Teixeira, K. Schillén, S. Aime, G. Morelli, *ChemBioChem.* **2007**, *8*, 950–955.
- [43] F. Leclercq, M. Cohen-Ohana, N. Mignet, A. Sbarbati, J. Herscovici, D. Scherman, G. Byk, *Bioconjugate Chem.* **2003**, *14*, 112–119.
- [44] S.W.A. Reulen, W.W.T. Brusselaars, S. Langereis, W.J.M. Mulder, M. Breurken, M. Merckx, *Bioconjugate Chem.* **2007**, *18*, 590–596.
- [45] J.D. Hartgerink, E. Beniash, S.I. Stupp, *Proc. Natl. Acad. Sci. U. S. A.* **2002**, *99*, 5133–5138.
- [46] J.D. Hartgerink, E. Beniash, S.I. Stupp, *Science* **2001**, *294*, 1684–1688.
- [47] S.E. Paramonov, H.-W. Jun, J.D. Hartgerink, *J. Am. Chem. Soc.* **2006**, *128*, 7291–7298.
- [48] S.R. Bull, M.O. Guler, R.E. Bras, T.J. Meade, S.I. Stupp, *Nano Lett.* **2005**, *5*, 1–4.
- [49] S.R. Bull, M.O. Guler, R.E. Bras, P.N. Venkatasubramanian, S.I. Stupp, T.J. Meade, *Bioconjugate Chem.* **2005**, *16*, 1343–1348.
- [50] G.M. Nicolle, E. Tóth, K-P. Eiseniener, H.R. Mäcke, A.E. Merbach, *J. Biol. Inorg. Chem.* **2002**, *7*, 757–769.
- [51] K. Kimpe, T.N. Parac-Vogt, S. Laurent, C. Piérart, L. vander Elst, R. N. Muller, K. Binnemans, *Eur. J. Inorg. Chem.* **2003**, *16*, 3021–3027.
- [52] E. Fan, J. Yang, S.J. Geib, T.C. Stoner, M.D. Hopkins, A.D. Hamilton, *J. Chem. Soc., Chem. Commun.* **1995**, 1251–1252.
- [53] M.P. Lightfoot, F.S. Mair, R.G. Pritchard, J.E. Warren, *Chem. Commun.* **1999**, 1945–1946.
- [54] A.R.A. Palmans, J.A.J.M. Vekemans, R.A. Hikmet, H. Fischer, E.W. Meijer, *Chem. Eur. J.* **1997**, *3*, 300–307.

- [55] A.R.A. Palmans, J.A.J.M. Vekemans, R.A. Hikmet, H. Fischer, E.W. Meijer, *Adv. Mater.* **1998**, *10*, 873–876.
- [56] A.R.A. Palmans, J.A.J.M. Vekemans, E.E. Havinga, E.W. Meijer, *Angew. Chem.* **1997**, *109*, 2763–2765; *Angew. Chem., Int. Ed.* **1997**, *36*, 2648–2651.
- [57] J. van Gestel, A.R.A. Palmans, B. Titulaer, J.A.J.M. Vekemans, E.W. Meijer, *J. Am. Chem. Soc.* **2005**, *127*, 5490–5494.
- [58] E.W. Meijer, J.A.J.M. Vekemans, A.R.A. Palmans, P. Breure, J. de Kraker, L. Brunsveld, *Polym. Prepr.* **2000**, *41*, 902–903.
- [59] J. van Herrikhuyzen, P. Jonkheijm, A.P.H.J. Schenning, E.W. Meijer, *Org. Biomol. Chem.* **2006**, *4*, 1539–1545.
- [60] J.J. van Gorp, J.A.J.M. Vekemans, E.W. Meijer, *J. Am. Chem. Soc.* **2002**, *124*, 14759–14769.
- [61] M.M.J. Smulders, A.P.H.J. Schenning, E.W. Meijer, *J. Am. Chem. Soc.* **2007**, *130*, 606–611.
- [62] M. de Loos, Thesis: *Hydrogen-bonded low molecular weight gelators*; University of Groningen: Groningen (The Netherlands), **2005**.
- [63] K. Hanabusa, C. Kato, M. Kimura, H. Shirai, A. Kakehi, *Chem. Lett.* **1997**, 429–430.
- [64] A. Sakamoto, D. Ogata, T. Shikata, O. Urakawa, K. Hanabusa, *Polymer* **2006**, *47*, 956–960.
- [65] T. Shikata, D. Ogata, K. Hanabusa, *J. Phys. Chem. B* **2004**, *108*, 508–514.
- [66] K. Hanabusa, A. Kawakami, M. Kimura, H. Shirai, *Chem. Lett.* **1997**, 191–192.
- [67] A. Sakamoto, D. Ogata, T. Shikata, K. Hanabusa, *Macromolecules* **2005**, *38*, 8983–8986.
- [68] T. Shikata, D. Ogata, K. Hanabusa, *J. Soc. Reol. Jpn* **2003**, *31*, 229–236.
- [69] D. Ogata, T. Shikata, K. Hanabusa, *J. Phys. Chem. B* **2004**, *108*, 15503–15510.
- [70] T.-Q. Nguyen, R. Martel, P. Avouris, M.L. Bushey, L. Brus, C. Nuckolls, *J. Am. Chem. Soc.* **2004**, *126*, 5234–5242.
- [71] M.L. Bushey, T.-Q. Nguyen, W. Zhang, D. Horoszewski, C. Nuckolls, *Angew. Chem.* **2004**, *116*, 5562–5570; *Angew. Chem., Int. Ed.* **2004**, *43*, 5446–5453.
- [72] G.S. Tulevski, M.L. Bushey, J.L. Kosky, S.J.T. Ruter, C. Nuckolls, *Angew. Chem.* **2004**, *116*, 1872–1875; *Angew. Chem., Int. Ed.* **2004**, *43*, 1836–1839.
- [73] M.L. Bushey, A. Hwang, P.W. Stephens, C. Nuckolls, *J. Am. Chem. Soc.* **2001**, *123*, 8157–8158.
- [74] M.L. Bushey, A. Hwang, P.W. Stephens, C. Nuckolls, *Angew. Chem.* **2002**, *114*, 2952–2955; *Angew. Chem., Int. Ed.* **2002**, *41*, 2828–2831.
- [75] M.L. Bushey, T.-Q. Nguyen, C. Nuckolls, *J. Am. Chem. Soc.* **2003**, *125*, 8264–8269.
- [76] A. Rochefort, E. Bayard, S. Hadj-Messaoud, *Adv. Mater.* **2007**, *19*, 1992–1995.
- [77] P. Jonkheijm, P. van der Schoot, A.P.H.J. Schenning, E.W. Meijer, *Science* **2006**, *313*, 80–83.
- [78] R.B. Martin, *Chem. Rev.* **1996**, *96*, 3043–3064.
- [79] P. van der Schoot, In *Supramolecular polymers*, 2nd ed.; A. Ciferri, Ed.; Taylor & Francis: London **2005**.
- [80] Manuscript in preparation.
- [81] J.C.M. van Hest, D.A.P. Delnoye, M.W.P.L. Baars, M.H.P. van Genderen, E.W. Meijer, *Science* **1995**, *268*, 1592–1595.
- [82] J.T. Kunjappu, P. Somasundaran, *Colloid Surf. A: Physicochem. Eng. Aspects* **1996**, *117*, 1–5.
- [83] Y. Chevalier, *Curr. Opin. Colloid Interface Sci.* **2002**, *7*, 3–11.
- [84] K. Matsuoka, Y. Moroi, *Curr. Opin. Colloid Interface Sci.* **2003**, *8*, 227–235.
- [85] J.N. Israelachvili, D.J. Mitchell, B.W. Ninham, *J. Chem. Soc. Faraday Trans. II* **1976**, *72*, 1525–1568.
- [86] J.N. Israelachvili, D.J. Mitchell, B.W. Ninham, *Biochim. Biophys. Acta* **1977**, *470*, 185–201.
- [87] F. Cavagnetto, A. Relini, Z. Mirghani, A. Gliozzi, D. Bertoia, A. Gambacorta, *Biochim. Biophys. Acta* **1992**, *1106*, 273–281.

- [88] S. Svenson, *J. Disp. Sci. Technol.* **2004**, *25*, 101–118.
- [89] N. Boden, R.J. Bushby, C. Hardy, *J. Physique Lett.* **1985**, *46*, L-325–L-328.
- [90] A. Heeres, C. van der Pol, M. Stuart, A. Friggeri, B.L. Feringa, J. van Esch, *J. Am. Chem. Soc.* **2003**, *125*, 14252–14253.
- [91] K.J.C. van Bommel, C. van der Pol, I. Muizebelt, A. Friggeri, A. Heeres, A. Meetsma, B.L. Feringa, J. van Esch, *Angew. Chem.* **2004**, *116*, 1695–1699; *Angew. Chem., Int. Ed.* **2004**, *43*, 1663–1667.
- [92] A. Friggeri, C. van der Pol, K.J.C. van Bommel, A. Heeres, M. Stuart, B.L. Feringa, J. van Esch, *Chem. Eur. J.* **2005**, *11*, 5353–5361.
- [93] P.P. Bose, M.G.B. Drew, A.K. Das, A. Banerjee, *Chem. Commun.* **2006**, 3196–3198.
- [94] L. Brunsveld, H. Zhang, M. Glasbeek, J.A.J.M. Vekemans, E.W. Meijer, *J. Am. Chem. Soc.* **2000**, *122*, 6175–6182.
- [95] P. van der Schoot, M.A.J. Michels, L. Brunsveld, R.P. Sijbesma, A. Ramzi, *Langmuir*, **2000**, *16*, 10076–10083.
- [96] L. Brunsveld, Thesis: *Supramolecular chirality: From molecules to helical assemblies in polar media*, Eindhoven University of Technology, Eindhoven (The Netherlands), **2001**.
- [97] L. Brunsveld, B.G.G. Lohmeijer, J.A.J.M. Vekemans, E.W. Meijer, *Chem. Commun.* **2000**, 2305–2306.
- [98] L. Brunsveld, B.G.G. Lohmeijer, J.A.J.M. Vekemans, E.W. Meijer, *J. Incl. Phenom. Macrocycl. Chem.* **2001**, *41*, 61–64.
- [99] S. Langereis, H-A.T. Kooistra, M.H.P. van Genderen, E.W. Meijer, *Org. Biomol. Chem.* **2004**, *2*, 1271–1273.
- [100] A. Dirksen, S. Langereis, B.F.M. de Waal, M.H.P. van Genderen, T.M. Hackeng, E.W. Meijer, *Chem. Commun.* **2005**, 2811–2813.

2

Syntheses of peptide discotics with aliphatic solubilizing tails

ABSTRACT: *The syntheses of C₃-symmetrical molecules are described that consist of a 1,3,5-benzenetricarboxamide core extended with peptide fragments bearing peripheral mesogenic groups incorporating aliphatic solubilizing tails. Seven dipeptide discs with combinations of glycine and L- and/or D-phenylalanine are synthesized. It is shown that two synthetic strategies, direct coupling of the dipeptide and consecutive coupling of the desired amino acids, are needed in order to obtain all target discotics in high chemical and optical purities. Secondly, two mono-peptide discotics are manufactured. The amino acids incorporated are L-alanine and L-phenylalanine. All compounds have been characterized with a combination of analytical techniques including matrix assisted laser desorption/ionization time of flight mass spectrometry (MALDI-TOF MS), ¹H- and ¹³C-NMR spectroscopy, IR spectroscopy and elemental analysis. The chemical purity of the final discotics has also been demonstrated with gel permeation chromatography (GPC).*

* Part of this work has been published: K. P. van den Hout, R. Martín-Rapún, J. A. J. M. Vekemans, E. W. Meijer, *Chem. Eur. J.* **2007**, *13*, 8111–8123; X. Lou, K. P. van den Hout, M. H. C. J. van Houtem, J. L. J. van Dongen, J. A. J. M. Vekemans, E. W. Meijer, *J. Mass Spectrom.* **2006**, *41*, 659–669.

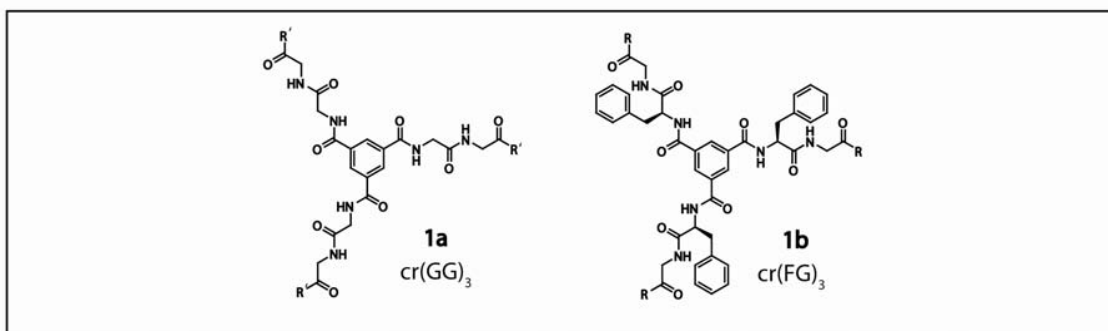
2.1 Introduction

In chemistry, C_3 -symmetrical molecules have attracted considerable attention in the fields of asymmetric catalysis and molecular recognition.^[1-3] Since the late 1980s, C_3 -symmetrical (C_3 -)discotics, based on *cis-cis*-1,3,5-cyclohexanetricarboxamide or 1,3,5-benzenetricarboxamide cores, have also started to play an important role in the area of nanoscience, because these molecules display a strong tendency to adopt appealing conformations, like helices or propellers, as has been demonstrated by their crystal structures.^[4,5] An important goal in this developing field has been the identification of molecular subunits that allow controlled formation of one-dimensional, supramolecular constructs.^[6-11] New C_3 -discotics are developed with the aim to investigate the effect of steric hindrance, pre-orientation and the balance between secondary interactions on the stability of the aggregates^[11-14]. A better understanding of how to alter the aggregate stability—and hence the dynamics—in a controlled way may lead to new applications in many fields, such as electronics, biology, material science, etc.

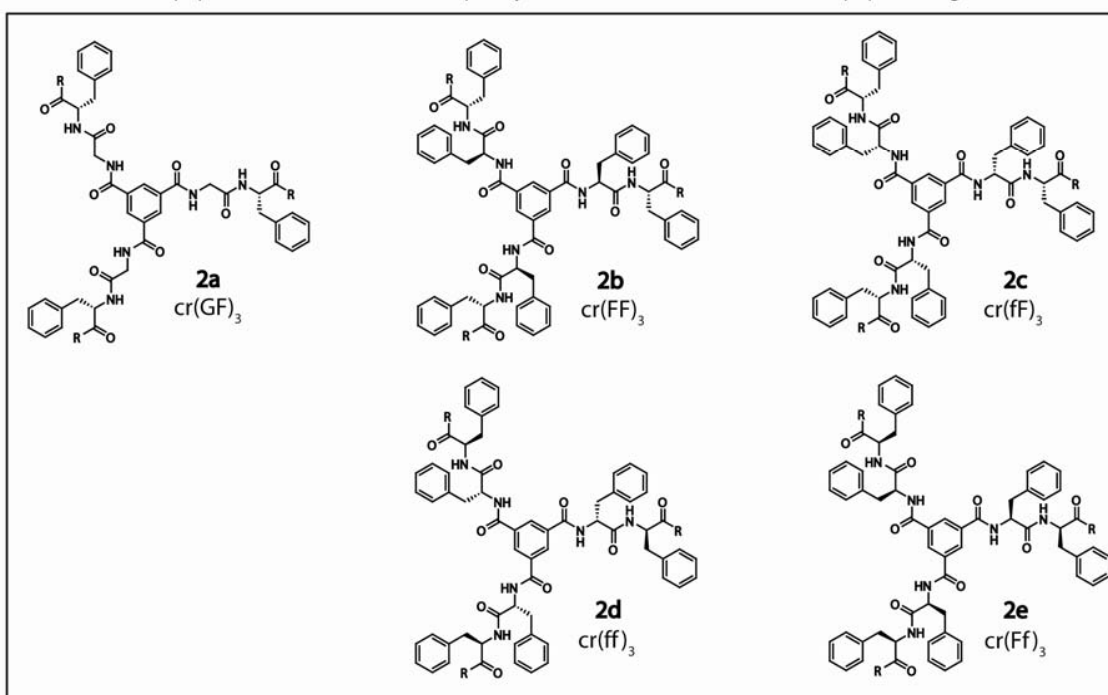
One of the first C_3 -discotics synthesized in our group contained a 1,3,5-benzenetricarboxamide core extended with bipyridine units bearing apolar mesogenic groups.^[15,16] The importance of steric hindrance and careful matching of secondary interactions that played a role in the self-assembly process was illustrated by studying the self-assembly behaviour of analogous discs provided with additional methoxy groups on the bipyridine units or with diphenylpyrazine moieties.^[17] The importance of the periphery of the disc-shaped molecules was highlighted when the bipyridine unit was functionalized with peripheral, chiral OPVs.^[18] A few years ago, a complete library of twelve C_3 -symmetrical molecules with various π - π interacting groups and hydrogen bonding units was synthesized in order to clarify the features governing self-assembly in apolar media.^[19] The remaining challenge is to develop discotic molecules that self-assemble and allow functionalization and fine-tuning of the secondary interactions in an easily accessible manner. For this reason, C_3 -symmetrical molecules that consist of a 1,3,5-benzenetricarboxamide centre extended with peptide fragments bearing mesogenic groups with apolar tails, called peptide discotics, have been designed (Figure 2.1). Peptide fragments are used as structuring elements because of their biocompatibility, hydrogen bonding properties and versatile nature. Firstly, seven dipeptide discotics with different combinations of glycine and L-and/or D-phenylalanine are considered. Glycine has been selected because it is achiral and phenylalanine since it is chiral and it carries a large hydrophobic substituent, which in principle can facilitate additional π - π interaction to strengthen the self-assembly. Secondly, two mono-peptide discotics are evaluated. The amino acids incorporated are L-alanine and L-phenylalanine. L-Phenylalanine is used since it is the general building block incorporated in the dipeptide discotics. L-Alanine is incorporated to determine the effect of the phenyl group of phenylalanine on the stacking properties.

Library of discs

Dipeptide discotics with an achiral glycine at the C-terminus of the dipeptide fragment



Dipeptide discotics with a chiral phenylalanine at the C-terminus of the peptide fragment



Monopeptide discotics

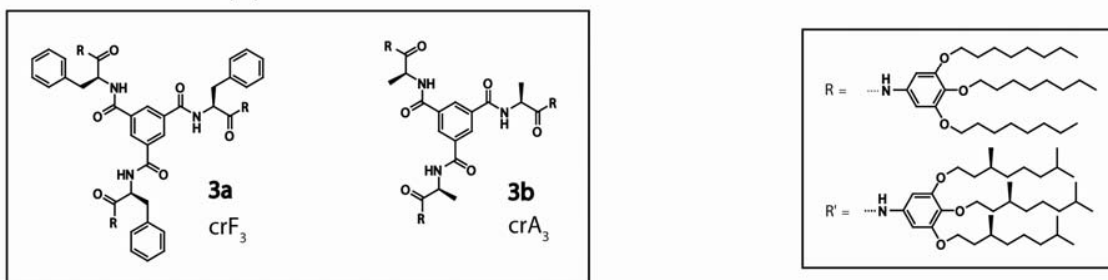
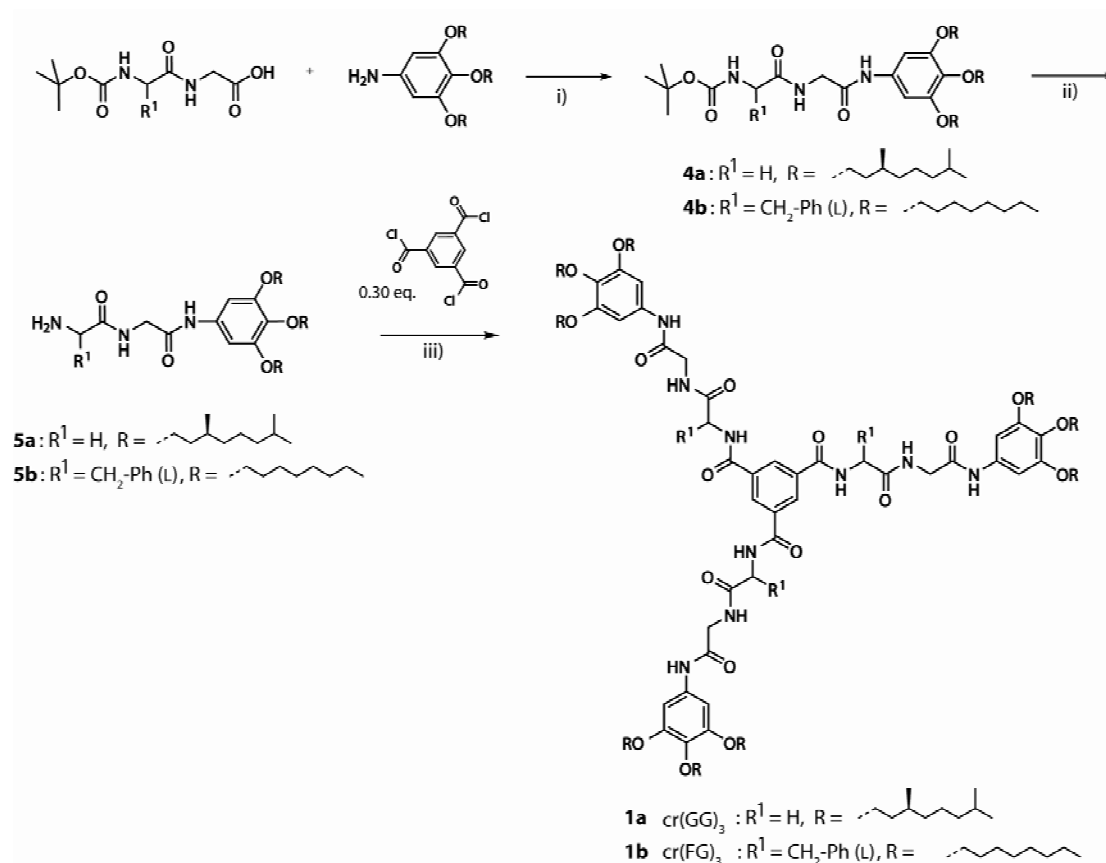


Figure 2.1 Library of peptide discotics; G = glycine, F = L-phenylalanine, f = D-phenylalanine, A = alanine, cr = 1,3,5-benzenetricarbonyl core.

In this Chapter, the syntheses of nine C_3 -symmetrical peptide discotics are presented. The self-assembly behaviour of these discs, both in the solid state and in solution, will be dealt with in Chapter 3.

2.2 Syntheses of dipeptide discotics with an achiral glycine at the C-terminus

Dipeptide discotics $cr(xG)_3$ (**1a,b**) containing a glycine at the C-terminus of the dipeptide fragment were prepared as depicted in Scheme 2.1.



Scheme 2.1 Synthetic route towards discotics $cr(xG)_3$ (**1a,b**): i) HBTU, DiPEA, DMF, RT, overnight, ~63%; ii) 1) TFA, RT, 1 h, 2) basic work-up, ~90% ; iii) Et_3N , DCM, RT, overnight, ~65%.

3,4,5-Trioctyloxyaniline^[20] and 3,4,5-tri((S)-3,7-dimethyloctyloxy)aniline^[21] were synthesized according to literature procedures. Direct coupling of the desired Boc-protected dipeptides with the anilines was accomplished using HBTU as a coupling reagent and DiPEA as a base and yielded pure compounds **4a,b**. In these two cases, racemization could be excluded due to the presence of an achiral glycine at the C-terminus of the peptide fragments. Deprotection of **4a,b** with trifluoroacetic acid, followed by a basic work up, gave **5a,b**. Finally, discotics **1a,b** were obtained after coupling of compounds **5a,b** with 0.30 molar equivalents of trimesic chloride in the presence of triethylamine as a base. The MALDI-TOF MS spectra of compounds **4a**, **5a** and **1a** are shown in Figure 2.2.

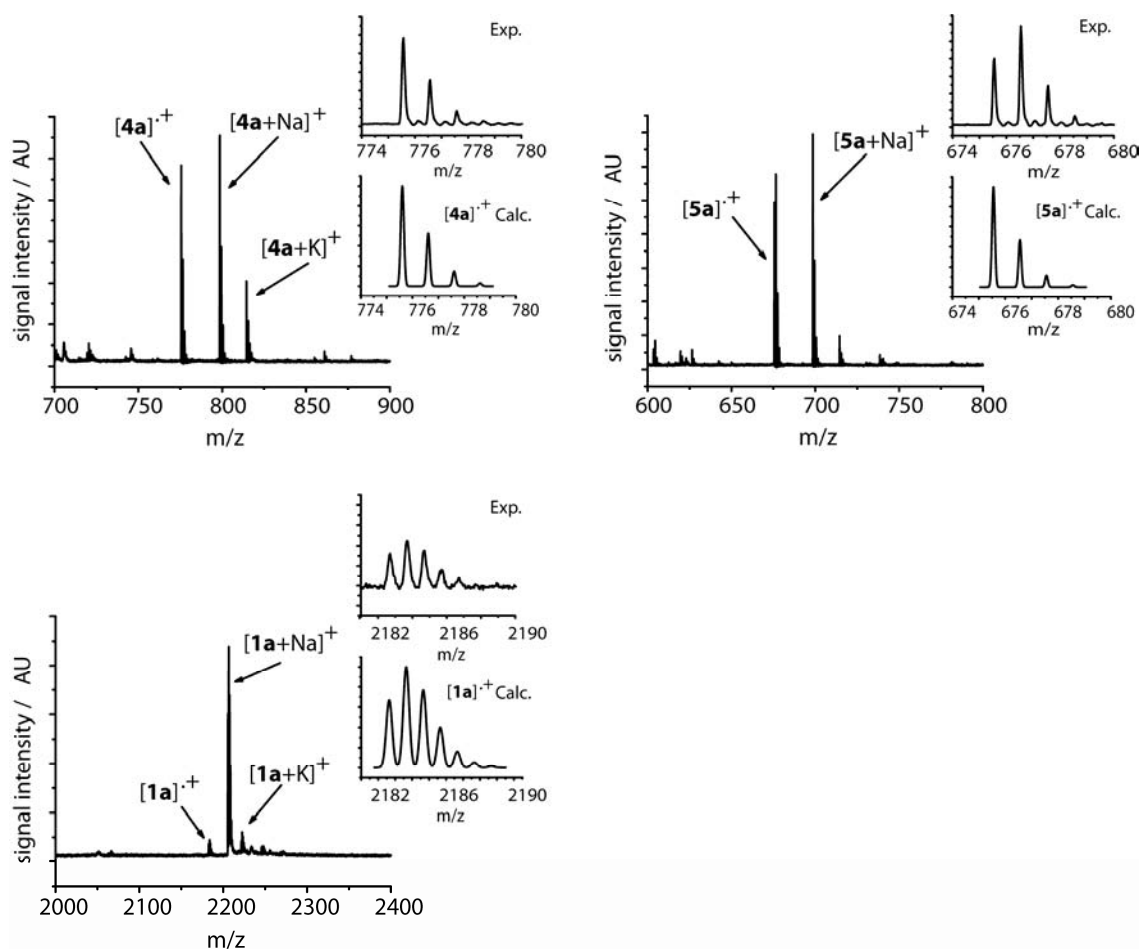
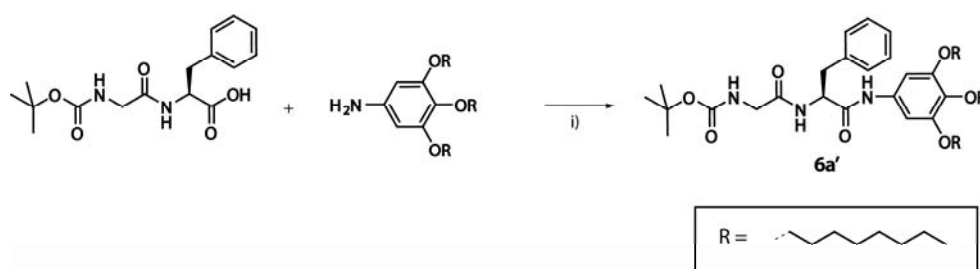


Figure 2.2 MALDI-TOF MS spectra for compounds **4a**, **5a** and **1a**.

It is remarkable that besides protonated and cationized pseudomolecular ion signals strong radical ion signals were observed for all compounds, including amino-terminated compounds **5a,b** that were expected to be protonated prior to laser irradiation using acidic MALDI matrices. The radical ion peaks $[M]^{•+}$ of compounds **4a**, **5a** and **1a** could be observed at $m/z = 775.5$, $m/z = 675.5$ and $m/z = 2183.7$, respectively. Possible mechanisms for radical ion formation were investigated with the employment of radical scavengers, with various matrices and with direct laser desorption/ionization (LDI). Most likely the radicals were formed by losing one electron from the aniline nitrogens, whereby the radicals were stabilized by conjugation through the phenyl rings. It appeared that direct photo/thermal ionization of analytes was an important route for the radical ion formation of compounds with trialkoxy aniline/anilide groups.^[22]

2.3 Syntheses of dipeptide discotics with a chiral phenylalanine at the C-terminus

Discs $cr(xF)_3/cr(xf)_3$ (**2a–e**), which contain a chiral phenylalanine moiety at the C-terminus of the dipeptide fragment were synthesized to complete the series of dipeptide discotics. At first, the direct coupling strategy previously described was explored, but it was demonstrated by chiral HPLC that direct coupling of Boc-protected glycyl-L-phenylalanine with 3,4,5-trioctyloxyaniline induced racemization at the C-terminus of the dipeptide fragment (Scheme 2.2, Figure 2.3). Consequently, the enantiomeric excess of compound **6a'** was 0%.



Scheme 2.2 Direct coupling of glycyl-L-phenylalanine with 3,4,5-trioctyloxyaniline: i) HBTU, DiPEA, DMF, RT, overnight.

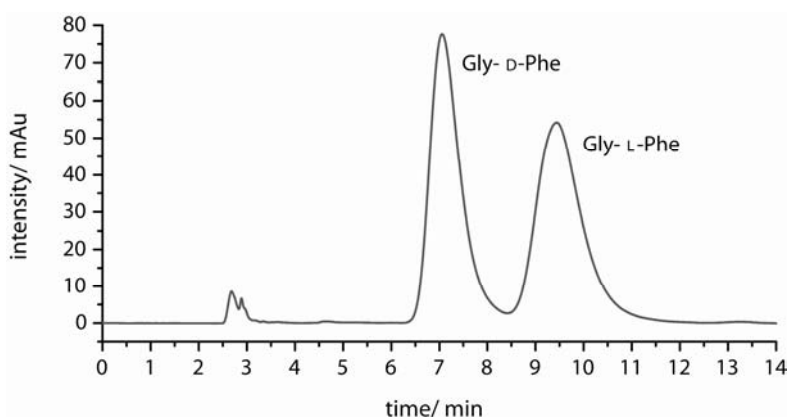
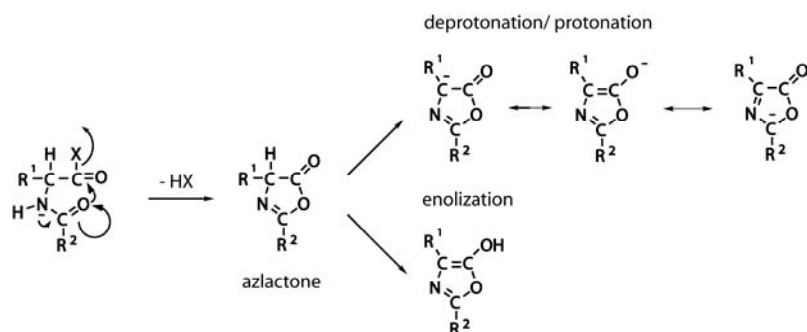
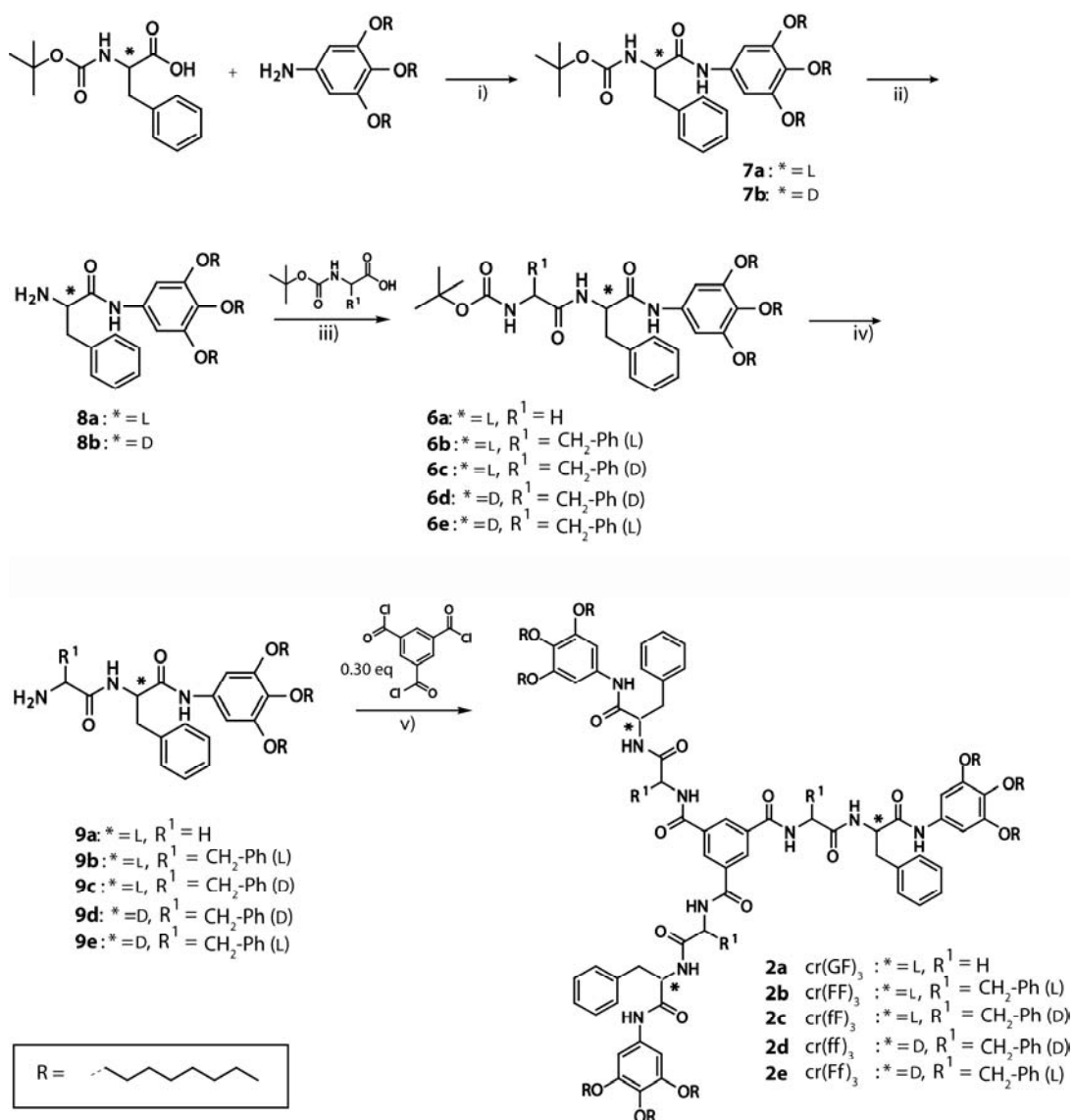


Figure 2.3 Chiral HPLC trace of compound **6a'** obtained via direct coupling method.

Racemization of a phenylalanine can take place via direct abstraction of the α -proton by a strong base.^[23] However, a proton abstraction mechanism can be prevented by employing suitable reaction conditions, especially by controlling the use of base.^[23] In the applied direct coupling reactions, 2 molar equivalents of DiPEA (compared to 1 molar equivalent of acid) have been used as base to minimize racemization. Racemization can also take place through azlactone formation followed by deprotonation/protonation^[24] or by enolization^[25] (Figure 2.3).



Scheme 2.3 Mechanism of racemization via azlactone formation.



Scheme 2.4 Synthetic route towards discotics $cr(xF)_3/cr(xf)_3$ (**2a-e**): i) HBTU, DiPEA, DMF, RT, overnight; ii) 1) TFA, RT, 1 h, 2) basic work-up, ~85% over first two reaction steps; iii) HBTU, DiPEA, DMF, RT, overnight, ~75%; iv) 1) TFA, RT, 1 h, 2) basic work-up, ~90%; v) Et₃N, DCM, RT, overnight, 32–71%.

It is known that the azlactone that is formed is less sensitive towards racemization when R^2 is an alkoxy (F-moc or Boc). Therefore, discotics $cr(xF)_3/cr(xf)_3$ (**2a–e**) have been synthesized via consecutive coupling of the desired amino acids. The synthetic route towards these discotics is depicted in Scheme 2.4. First, a single Boc-protected phenylalanine was reacted with 3,4,5-trioctyloxyaniline using HBTU as a coupling reagent and *Di*PEA as a base. Removal of the Boc-group with trifluoroacetic acid, followed by a basic work-up gave free amines **8a,b**. Repetition of these consecutive steps with the desired amino acids and compounds **8a,b** as starting materials, gave dipeptide anilines **9a–e**. Finally, discotics **2a–e** were obtained after coupling compounds **9a–e** with 0.30 molar equivalents of trimesic chloride in the presence of triethylamine as a base.

Figure 2.4 shows the HPLC trace of Boc-protected glycyl-L-phenylalanine **6a** synthesized via the consecutive coupling strategy. The enantiomeric excess of intermediate **6a** is above 99.5%. The enantiomeric excesses of all other intermediates (**6b–e**) are all very similar and also above 99.5%. Efforts to determine the optical purity of the final discotics with chiral HPLC unfortunately failed due to the strong tendency of the discs to stick to the stationary phase. For this reason, and the fact that no critical reaction steps are involved after the coupling of the Boc-protected amino acids to the gallic amines, it is assumed that the discs also have comparably high optical purities.

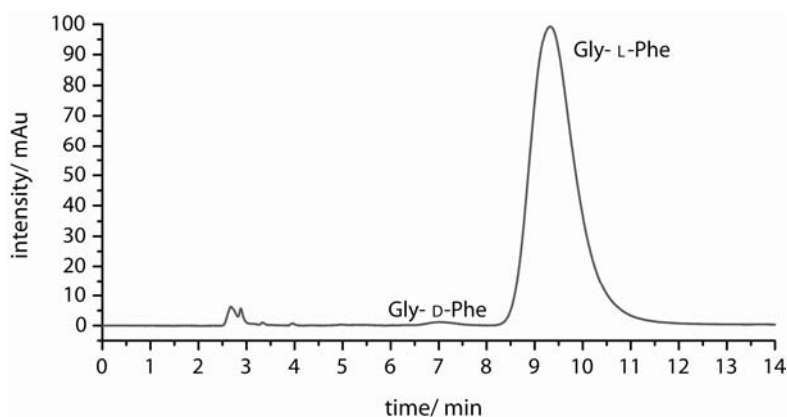
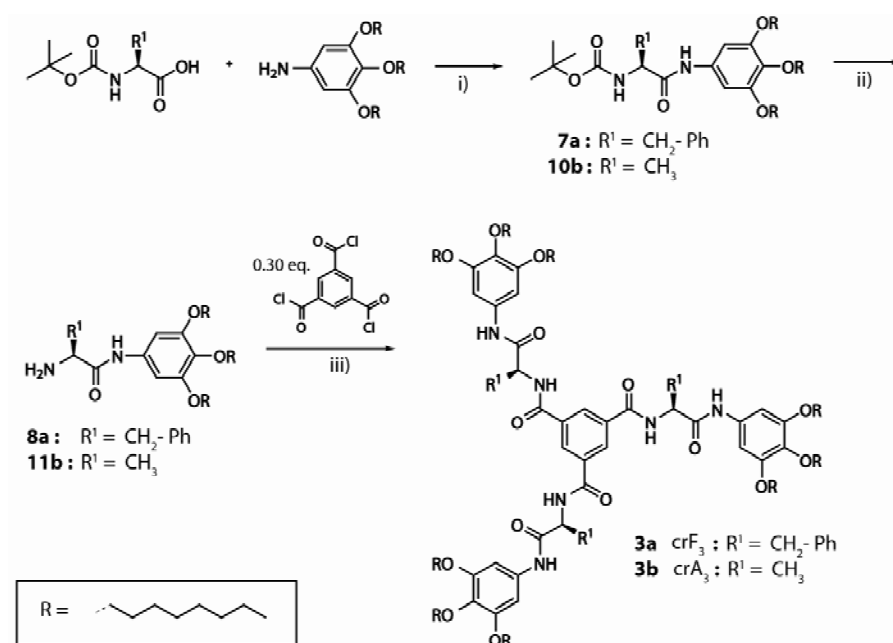


Figure 2.4 Chiral HPLC trace of compound **6a** obtained after consecutive coupling of the desired Boc-protected amino acids with 3,4,5-trioctyloxyaniline.

2.4 Syntheses of mono-peptide discotics

In order to simplify and shorten the syntheses of the C_3 -symmetrical discs, mono-peptide discotics based on one single amino acid have been synthesized. The amino acids incorporated are L-alanine and L-phenylalanine. L-phenylalanine is used because it is the general building block incorporated in the dipeptide discotics. L-alanine is incorporated to determine the effect of the phenyl group of phenylalanine on the stacking properties.

C_3 -symmetrical mono-peptide discotics crx_3 (**3a,b**) were prepared as depicted in Scheme 2.5.



Scheme 2.5 Synthetic route towards mono-peptide discotics crx_3 (**3a,b**): i) HBTU, DiPEA, DMF, RT, overnight; ii) 1] TFA, RT, 1 h, 2] basic work-up, 85% and 67% (over two reaction step, respectively); iii) Et₃N, DCM, RT, overnight, ~70%.

Direct coupling of the desired Boc-protected amino acids with the 3,4,5-trioctyloxyaniline was accomplished with HBTU as coupling reagent and DiPEA as base and yielded pure compounds **7a** and **10b**, respectively. The enantiomeric excess of intermediate compound **10b** was above 99% according to chiral HPLC. Deprotection with trifluoroacetic acid, followed by a basic work up, gave **8a** and **11b** in yields of 85% and 67% (over first two reaction steps), respectively. Finally, discotics **3a,b** were obtained after coupling of compounds **8a** and **11b** with 0.30 molar equivalents of trimesic chloride in the presence of triethylamine as a base.

As an example, the GPC traces of disc **3b** after the first and second recrystallization from a mixture of tetrahydrofuran/methanol are depicted in Figure 2.5.

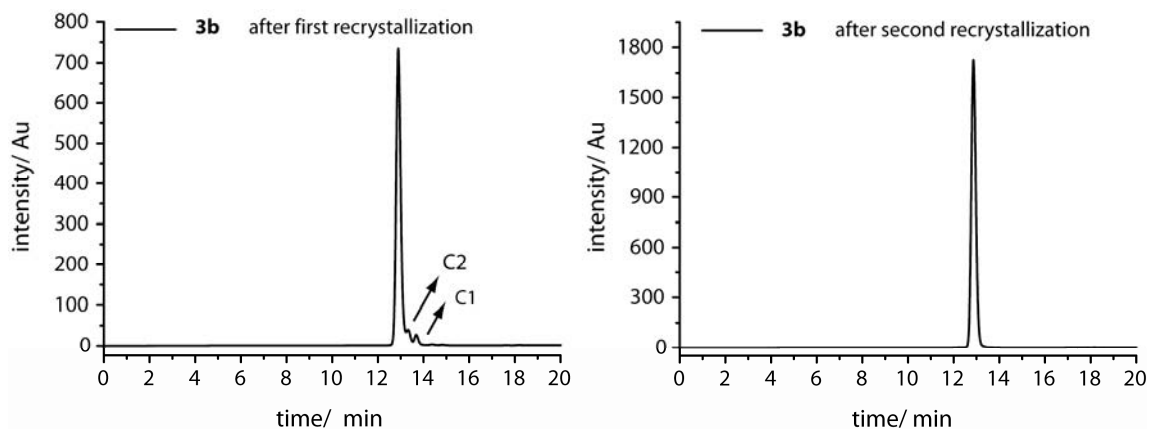


Figure 2.5 GPC traces of disc **3b** after first (left) and after second (right) recrystallization of the product from a mixture of tetrahydrofuran/methanol.

The most common impurities are benzene derivatives of which just one (C1) or two (C2) acid chlorides reacted with the desired amino-compound. The GPC traces in Figure 2.5 prove that it is possible to separately detect those impurities from the reaction product using GPC, which makes it an excellent technique to determine the chemical purity of the final discotics.

2.5 Conclusions

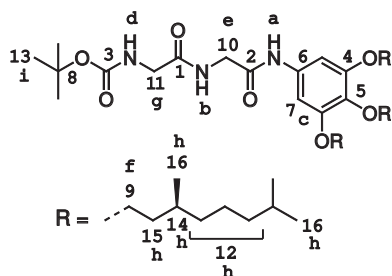
Nine peptide discotics that consist of a 1,3,5-benzenetricarboxamide core extended with peptide fragments bearing peripheral mesogenic groups containing aliphatic solubilizing tails were successfully synthesized. All discs were synthesized via a convergent synthetic approach whereby, already in the first reaction step, the solubilizing mesogenic group (a gallic amine) was linked to the desired peptide fragment in order to avoid solubility problems. Dipeptides with an achiral glycine at the C-terminus were directly reacted with the mesogenic groups and yielded discotics **1a,b** in high optical purities. As expected, racemization was not an issue in these cases. On the other hand, it was shown that a dipeptide with a chiral phenylalanine at the C-terminus did racemize if directly coupled. Direct coupling of glycyl-L-phenylalanine to a gallic amine gave an intermediate with an enantiomeric excess of 0%. It was demonstrated that racemization could be limited by consecutive coupling of the desired Boc-protected amino acids as was illustrated by the enantiomeric excesses of discotics **2a–e** which generally exceeded 99%. This indirectly indicated that azlactone formation was the main cause for racemization. As a consequence, mono-peptide discotics **3a,b** could also be synthesized in high optical purities because also in these cases (chiral) Boc-protected amino acids were coupled.

2.6 Experimental section

General

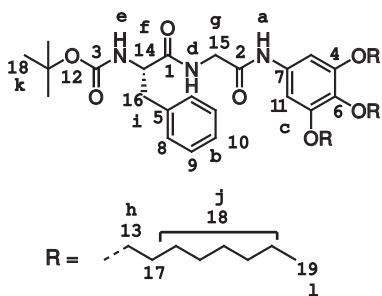
Unless stated otherwise, all reagents and chemicals were obtained from commercial sources and used without further purification. 3,4,5-Trioctyloxyaniline^[20] and 3,4,5-tri((S)-3,7-dimethyloctyloxy)aniline^[21] were synthesized according to procedures described in the thesis of K. Pieterse (TU/e, 2001). Water was demineralised prior to use. Dichloromethane and tetrahydrofuran were obtained by distillation over Merck molecular sieves (4 Å). ¹H-NMR, ¹H-¹H COSY and ¹⁹F-NMR spectra were recorded on a Varian Gemini 300 spectrometer, a Varian Mercury Vx 400 spectrometer or a Varian Unity Inova 500 spectrometer at 298 K. Chemical shifts are given in ppm (δ) values relative to tetramethylsilane (TMS). Splitting patterns are designated as s, singlet; d, doublet; dd, double doublet; t, triplet; q, quartet; m, multiplet and br stands for broad. Neat state IR spectra were measured at 298 K on a Perkin-Elmer 1605 FT-IR spectrophotometer. Matrix assisted laser desorption/ionization mass spectra were obtained on a PerSeptive Biosystems Voyager DE-PRO spectrometer using α-cyano-4-hydroxycinnamic acid (CHCA) and 2-[(2E)-3-(4-tert-butylphenyl)-2-methylprop-2-enylidene]malononitrile (DCTB) as matrices. Elemental analyses were carried out using a Perkin Elmer 2400. GPC measurements were performed on a Shimadzu system with a mixed column (2 × PL gel 3 μm, 100 Å), with a flow of 1 mL·min⁻¹, and tetrahydrofuran as eluting solvent. The injection volume was 50 μL and photodiode array detection (260 nm) was applied. Chiral HPLC was performed on a Shimadzu system consisting of a Shimadzu LC-10 ADvp pump, a Spark Midas autosampler and a Shimadzu SPD-10ADvp UV-Vis detector. Two columns were used, a Daicel Chiralcel OD (0.46 × 25 cm) and a DNBPG (covalent 5 μm; 0.46 × 25 cm) both with a 9/1 (v/v) hexane/isopropanol mixture as the eluent.

N^α-(*tert*-Butyloxycarbonyl)-N^ω-[3,4,5-tri((S)-3,7-dimethyloctyloxy)phenyl]glycylglycinamide (4a)



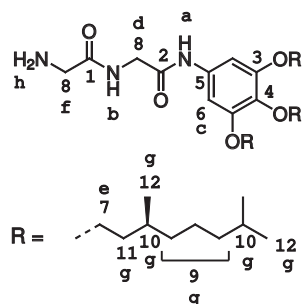
To a magnetically stirred solution of HBTU (0.28 g, 0.75 mmol) in dry dimethylformamide (1.5 mL), DiPEA (0.4 mL, 1.49 mmol) and Boc-PheGlyOH (0.16 g, 0.67 mmol) were added consecutively. This mixture was stirred for 5 min after which 3,4,5-tri((S)-3,7-dimethyloctyl)aniline (0.21 g, 0.37 mmol) was added. Stirring was continued overnight at room temperature. The reaction mixture was slowly added to a mixture of diethyl ether (25 mL), acidic water (pH < 3, 25 mL) and ice. The organic layer was washed with sat. KCl (15 mL), 1 N NaOH (3 × 15 mL)

and 10 mM NaHCO₃ (3 × 15 mL) and dried over MgSO₄. After evaporation, the crude product was purified by column chromatography (silica, 4% methanol in dichloromethane) to yield the pure compound as a transparent, sticky oil (0.19 g, 0.24 mmol, 65%): ¹H-NMR (CDCl₃): δ = 8.30 (s, 1H, **a**), 7.00 (br t, 1H, **b**), 6.87 (s, 2H, **c**), 5.26 (t, 1H, **d**), 4.08 (d, 2H, *J* = 5.7 Hz, **e**), 4.0–3.8 (m, 6H, **f**), 3.84 (d, 2H, *J* = 5.7 Hz, **g**), 1.9–0.8 (m, 66H, **h** {57H}); s, 9H, **i**) ppm; ¹³C-NMR (CDCl₃): δ = 170.3 (**1**), 166.8 (**2**), 156.6 (**3**), 153.3 (**4**), 135.0 (**5**), 133.4 (**6**), 99.2 (**7**), 81.1 (**8**), 71.9 (*para*-**9**), 67.5 (*meta*-**9**), 44.9 (**10**), 44.1 (**11**), 39.5, 39.4, 37.7, 37.5, 37.5, 36.6 (**12**), 30.0 (**13**), 28.4, 28.1 (**14**), 24.9, 24.9 (**15**), 22.9, 22.8, 22.7, 19.7, 19.7 (**16**) ppm; FT-IR (ATR): ν = 3314, 2954, 2926, 2870, 1688 1663, 1608, 1505, 1428, 1383, 1367, 1290, 1226, 1169, 1117 cm⁻¹; MALDI-TOF: *m/z* [M]⁺ Calcd. 775.61; found: 775.50 [M]⁺, 798.50 [M+Na]⁺; elemental analysis: Calcd. for C₄₅H₈₁N₃O₇: 69.64% C, 10.52% H, 5.41% N; found: 69.91% C, 10.62% H, 5.41% N.

N^α-(tert-Butyloxycarbonyl)-N^ω-(3,4,5-trioctyloxyphenyl)-L-phenylalanyl-glycinamide (4b)

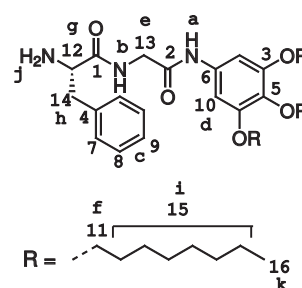
To a magnetically stirred solution of HBTU (3.18 g, 8.38 mmol) in dry dimethylformamide (17 mL), DiPEA (3 mL, 17 mmol) and Boc-L-PheGlyOH (2.41 g, 7.48 mmol) were added consecutively. This mixture was stirred for 5 min after which 3,4,5-trioctyloxyaniline (1.98 g, 4.15 mmol) was added. Stirring was continued overnight at room temperature. The reaction mixture was slowly added to a mixture of diethyl ether (200 mL), acidic water (pH < 3, 200 mL) and ice. The organic layer was washed with sat. KCl (150 mL), 1 N NaOH (3 × 150

mL) and 10 mM NaHCO₃ (3 × 150 mL) and dried over MgSO₄. After evaporation, the crude product was purified by column chromatography (silica, 2% methanol in dichloromethane) and subsequently washed with methanol to yield the pure compound as an off-white solid material (2.00 g, 2.56 mmol, 62%): ¹H-NMR (CDCl₃): δ = 8.27 (s, 1H, **a**), 7.4–7.1 (m, 5H, **b**), 6.87 (s, 2H, **c**), 6.58 (br t, 1H, **d**), 4.93 (d, 1H, *J* = 5.1 Hz, **e**), 4.28 (q, 1H, **f**), 4.1–3.8 (m, 8H, **g** {2H} + **h** {6H}), 3.10 (m, 2H, **i**), 1.9–1.2 (m, 45H, **j** {36H} + **k** {9H}), 0.86 (t, 9H, **l**) ppm; ¹³C-NMR (CDCl₃): δ = 172.2 (**1**), 166.8 (**2**), 156.1 (**3**), 153.2 (**4**), 136.2 (**5**), 134.8 (**6**), 133.4 (**7**), 129.2 (**8**), 129.1 (**9**), 127.5 (**10**), 99.4 (**11**), 81.2 (**12**), 73.6 (*para*-**13**), 69.2 (*meta*-**13**), 56.8 (**14**), 44.2 (**15**), 37.7 (**16**), 32.0, 32.0, (**17**) 30.4, 29.7, 29.5, 29.4, 28.4, 26.3, 26.2, 22.8, 22.8 (**18**), 14.2 (**19**) ppm; FT-IR (ATR): ν = 3296, 2924, 2855, 1683, 1653, 1606, 1525, 1504, 1428, 1379, 1365, 1228, 1114, 1022, 697 cm⁻¹; MALDI-TOF: *m/z* [M]⁺ Calcd. 781.56; found: 781.46 [M]⁺; elemental analysis: Calcd. for C₄₆H₇₅N₃O₇: 70.64% C, 9.67% H, 5.37% N; found: 70.72% C, 9.56% H, 5.32% N.

N^ω-[3,4,5-Tri((S)-3,7-dimethyloctyloxyphenyl)]glycylglycinamide (5a)

Compound **4a** (1.63 g, 2.10 mmol) was dissolved in TFA (10 mL). The solution was purged with argon for 15 min, after which the mixture was stirred for another 45 min. The reaction mixture was concentrated *in vacuo*. A mixture of diethyl ether, 1 N NaOH and ice was added and the layers were separated. The organic layer was washed several times with 1 N NaOH and dried over MgSO₄. After evaporation, the pure title compound was isolated (1.30 g, 1.92 mmol, 92%): ¹H-NMR (CDCl₃): δ = 8.58 (s, 1H, **a**), 8.12 (br t, 1H, **b**), 6.82 (s, 2H, **c**), 4.10 (d, 2H, *J* = 5.6 Hz, **d**), 4.0–3.9 (m, 6H, **e**), 3.45 (s, 2H, **f**), 1.90–0.8 (m, 59H, **g**

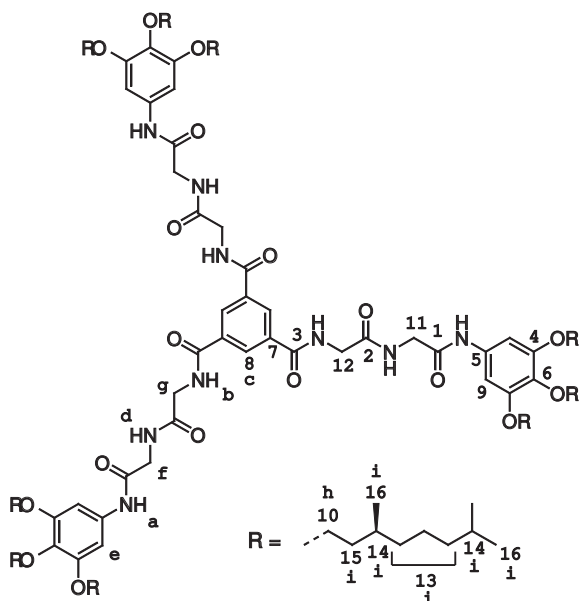
{57H} + **h** {2H}) ppm; ¹³C-NMR (CDCl₃): δ = 174.4 (**1**), 167.1 (**2**), 153.3 (**3**), 135.0 (**4**), 133.5 (**5**), 98.9 (**6**), 71.9 (*para*-**7**), 67.5 (*meta*-**7**), 44.7 (**8**), 39.5, 39.4, 37.7, 37.5, 37.5, 36.5 (**9**), 29.9, 29.8, 28.1 (**10**), 24.9, 24.9 (**11**), 22.9, 22.8, 22.7, 19.7 (**12**) ppm; FT-IR (ATR): ν = 3286, 2954, 2926, 2870, 1698, 1655, 1620, 1604, 1527, 1555, 1504, 1466, 1426, 1383, 1366, 1233, 1115, 834 cm⁻¹; MALDI-TOF: *m/z* [M]⁺ Calcd. 675.55; found: 675.55 [M]⁺, 698.55 [M+Na]⁺; elemental analysis: Calcd. for C₄₀H₇₃N₃O₅: 71.07% C, 10.88% H, 6.22% N; found: 70.95% C, 10.80% H, 6.09% N.

N^ω-[3,4,5-Trioctyloxyphenyl]-L-phenylalanyl-glycinamide (5b)

Compound **4b** (0.80 g, 1.02 mmol) was dissolved in TFA (10 mL). The solution was purged with argon for 15 min, after which the mixture was stirred for another 45 min. The reaction mixture was concentrated *in vacuo*. A mixture of ethyl acetate, 1 N NaOH and some ice was added and the layers were separated. The organic layer was washed with 1 N NaOH several times and dried over MgSO₄. After evaporation, the pure title compound was isolated (0.63 g, 0.92 mmol, 90%): ¹H-NMR (CDCl₃): δ = 8.75 (s, 1H, **a**), 8.20 (br t, 1H, **b**), 7.4–7.1 (m, 5H, **c**), 6.83 (s, 2H, **d**), 4.10 (d, 2H, *J* = 4.8 Hz, **e**), 4.0–3.8 (m, 6H, **f**), 3.70

(m, 1H, **g**), 3.72 + 2.77 (m, 2H, **h**), 1.9–1.2 (m, 38H, **i**{36H} + **j**{2H}), 0.86 (m, 9H, **k**) ppm; $^{13}\text{C-NMR}$ (CDCl_3): δ = 175.8 (**1**), 170.0 (**2**), 153.2 (**3**), 137.2 (**4**), 134.9 (**5**), 133.4 (**6**), 129.2 (**7**), 128.9 (**8**), 127.1 (**9**), 99.0 (**10**), 73.5 (*para*-**11**), 69.1 (*meta*-**11**), 56.2 (**12**), 44.7 (**13**), 40.8 (**14**), 31.9, 31.8, 30.3, 29.6, 29.4, 29.3, 26.1, 26.1, 22.7, 22.7 (**15**), 14.1 (**16**) ppm; **FT-IR (ATR)**: ν = 3289, 2923, 2855, 1694, 1648, 1603, 1555, 1502, 1426, 1384, 1227, 1115, 700 cm^{-1} ; **MALDI-TOF**: m/z $[\text{M}+\text{H}]^+$ Calcd. 682.51; found: 682.36 $[\text{M}+\text{H}]^+$, 704.35 $[\text{M}+\text{Na}]^+$; **elemental analysis**: Calcd. for $\text{C}_{41}\text{H}_{67}\text{N}_3\text{O}_5$: 72.21% C, 9.90% H, 6.16% N; found: 71.55% C, 9.60% H, 6.08% N.

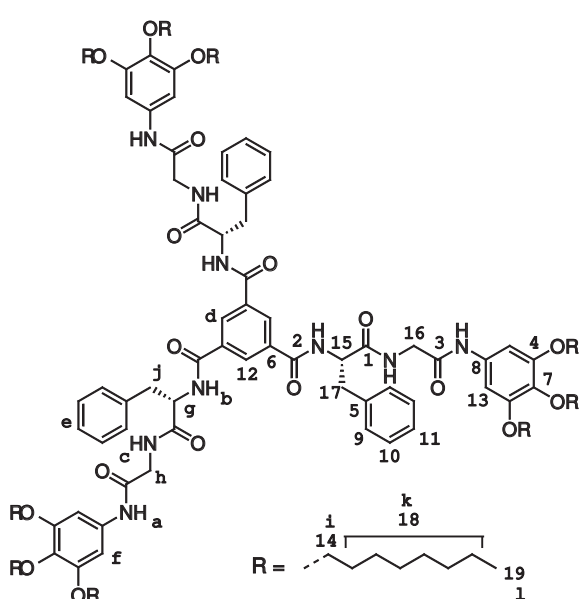
$\text{N}^\alpha, \text{N}^\omega, \text{N}^{\omega\omega}$ -(1,3,5-Benzenetricarbonyl)tris[N^ω -(3,4,5-tri((S)-3,7-dimethyloctyloxy)phenyl)glycyl-glycinamide (**1a**)



A solution of 1,3,5-benzenetricarbonyl trichloride (0.13 g, 0.51 mmol) in dry dichloromethane (5 mL) was added dropwise to a solution of **5a** (1.20 g, 1.77 mmol) and triethylamine (0.5 mL, 3.6 mmol) in dry dichloromethane (15 mL). After stirring overnight and evaporation of the dichloromethane the product was purified using column chromatography (silica, 2.5% methanol in ethyl acetate) to yield the title compound as a pink solid material (0.70 g, 0.32 mmol, 63%). The product was characterized using **GPC** (THF, 260 nm, purity based on UV > 98%): $^1\text{H-NMR}$ (THF- d_8): δ = 9.03 (br s, 6H, **a** {3H} + **b** {3H}), 8.42 (s, 3H, **c**), 8.23 (br t, 3H, **d**), 6.84 (s, 6H, **e**), 4.0–3.8 (m, 30H, **f** {6H} + **g** {6H} + **h** {18H}), 1.7–0.7 (m, 171H, **i**) ppm; $^{13}\text{C-NMR}$ (THF- d_8): δ = 170.8 (**1**), 169.4 (**2**), 167.5 (**3**), 154.3 (**4**), 136.0 (**5**), 135.6 (**6**, **7**), 130.4 (**8**), 100.1 (**9**),

72.2 (**10**), 45.3 (**11**), 44.5 (**12**), 40.8, 40.6, 39.0, 38.8, 37.8 (**13**), 31.1, 31.1, 29.3 (**14**), 23.5, 23.4 (**15**), 20.5, 20.3 (**16**) ppm; **FT-IR (ATR)**: ν = 3314, 2954, 2926, 2870, 1656, 1603, 1533, 1504, 1427, 1383, 1226, 1114 cm^{-1} ; **MALDI-TOF**: m/z $[\text{M}]^+$ Calcd. 2183.65; found: 2183.70 $[\text{M}]^+$, 2206.65 $[\text{M}+\text{Na}]^+$; **elemental analysis**: Calcd. for $\text{C}_{129}\text{H}_{219}\text{N}_9\text{O}_{18}$: 70.94% C, 10.11% H, 5.77% N; found: 70.33% C, 10.04% H, 5.63% N.

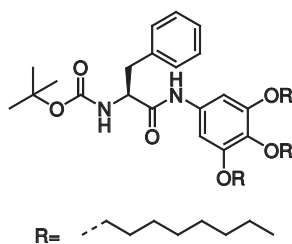
$\text{N}^\alpha, \text{N}^\omega, \text{N}^{\omega\omega}$ -(1,3,5-Benzenetricarbonyl)tris[N^ω -(3,4,5-trioctyloxyphenyl)]-L-phenylalanyl-glycinamide (**1b**)



A solution of 1,3,5-benzenetricarbonyl trichloride (66.7 mg, 0.25 mmol) in dry dichloromethane (2.5 mL) was added dropwise to a solution of **5b** (0.60 g, 0.88 mmol) and triethylamine (0.3 mL, 2.2 mmol) in dry dichloromethane (7.5 mL). After stirring overnight and evaporation of the dichloromethane the product was purified using column chromatography (silica, ethyl acetate/pentane 4/1) to yield the title compound as an off-white solid material (0.37 g, 0.17 mmol, 67%). The product was characterized using **GPC** (THF, 260 nm, purity based on UV > 99%): $^1\text{H-NMR}$ ($\text{DMSO}-d_6$, $T = 323\text{ K}$): δ = 9.73 (s, 3H, **a**), 8.87 (d, 3H, **b**, $J = 7.2\text{ Hz}$), 8.49 (br t, 3H, **c**), 8.31 (s, 3H, **d**), 7.4–7.1 (m, 15H, **e**), 6.93 (s, 6H, **f**), 4.79 (m, 3H, **g**), 4.0–3.6 (m, 24H, **h**{6H} + **i**{18H}), 3.2–3.0 (m,

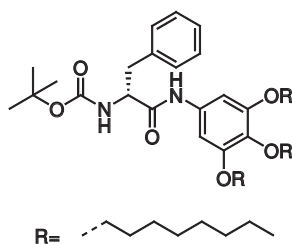
6H, j), 1.8–1.0 (m, 108H, k), 0.84 (t, 27H, l) ppm; $^{13}\text{C-NMR}$ (DMSO- d_6 , T = 323 K): δ = 171.5 (1), 167.2 (2), 165.7 (3), 152.3 (4), 138.1 (5), 134.6 (6), 134.4 (7), 133.1 (8), 129.1 (9), 128.1 (10), 126.2 (11, 12), 97.8 (13), 72.4 (*para*-14), 68.1 (*meta*-14), 55.8 (15), 42.8 (16), 37.3 (17), 31.3, 31.2, 29.8, 29.4, 28.9, 28.8, 28.7, 25.6, 25.6, 22.1 (18), 15.1 (19) ppm; **FT-IR (ATR)**: ν = 3300, 2924, 2855, 1645, 1603, 1536, 1503, 1427, 1380, 1226, 1112, 699 cm^{-1} ; **MALDI-TOF**: m/z [M] $^{+}$ Calcd. 2201.51; found: 2201.49 [M] $^{+}$, 2224.44 [M+Na] $^{+}$; **elemental analysis**: Calcd. for $\text{C}_{132}\text{H}_{201}\text{N}_9\text{O}_{18}$: 72.00% C, 9.20% H, 5.72% N; found: 71.63% C, 9.30% H, 5.44% N.

N^{α} -(*tert*-Butyloxycarbonyl)- N^{ω} -(3,4,5-trioctyloxyphenyl)-L-phenylalaninamide (7a)



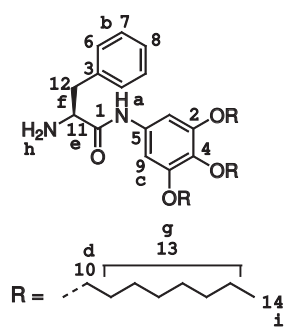
To a magnetically stirred solution of HBTU (3.24 g, 8.54 mmol) in dry dimethylformamide (17 mL), DiPEA (3 mL, 17 mmol) and Boc-L-PheOH (2.04 g, 7.69 mmol) were added consecutively. This mixture was stirred for 5 min after which 3,4,5-trioctyloxyaniline (2.00 g, 4.19 mmol) was added. Stirring was continued overnight at room temperature. The reaction mixture was slowly added to a mixture of diethyl ether (200 mL), acidic water (pH < 3, 200 mL) and ice. The organic layer was washed with sat. KCl (80 mL), 1 N NaOH (3 \times 80 mL) and 10 mM NaHCO_3 (3 \times 80 mL) and dried over MgSO_4 . The crude product obtained after evaporation was used as such for the preparation of **8a**.

N^{α} -(*tert*-Butyloxycarbonyl)- N^{ω} -(3,4,5-trioctyloxyphenyl)-D-phenylalaninamide (7b)

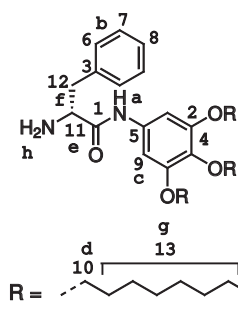


To a magnetically stirred solution of HBTU (3.20 g, 8.44 mmol) in dry dimethylformamide (17 mL), DiPEA (3 mL, 17 mmol) and Boc-D-PheOH (2.01 g, 7.57 mmol) were added consecutively. This mixture was stirred for 5 min after which 3,4,5-trioctyloxyaniline (2.04 g, 4.28 mmol) was added. Stirring was continued overnight at room temperature. The reaction mixture was slowly added to a mixture of diethyl ether (200 mL), acidic water (pH < 3, 200 mL) and ice. The organic layer was washed with sat. KCl (80 mL), 1 N NaOH (3 \times 80 mL) and 10 mM NaHCO_3 (3 \times 80 mL) and dried over MgSO_4 . The crude product obtained after evaporation was used as such for the preparation of **8b**.

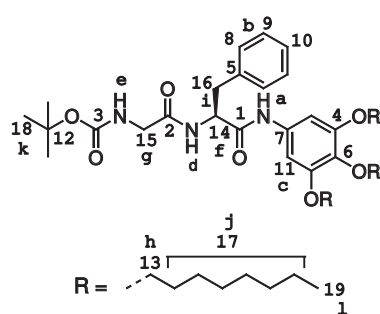
N^{ω} -(3,4,5-Trioctyloxyphenyl)-L-phenylalaninamide (8a)



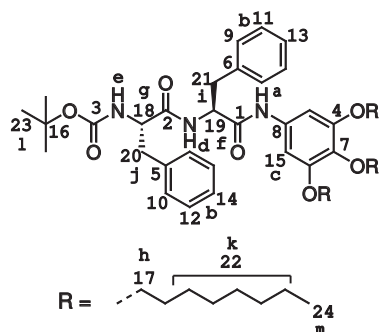
Crude **7a** (4.2 g) was dissolved in TFA (25 mL). The solution was purged with argon for 15 min, after which the mixture was stirred for another 45 min. The reaction mixture was concentrated *in vacuo*. A mixture of diethyl ether, 1 N NaOH and ice was added and the layers were separated. The organic layer was washed with 1 N NaOH several times and dried over MgSO_4 . After evaporation, the pure title compound was isolated (2.23 g, 3.56 mmol, 85% after two reactions): $^1\text{H-NMR}$ (CDCl_3): δ = 9.28 (s, 1H, a), 7.4–7.2 (m, 5H, b), 6.87 (s, 2H, c), 4.1–3.9 (m, 6H, d), 3.70 (m, 1H, e), 3.35 + 2.75 (m, 2H, f), 1.9–1.2 (m, 38H, g {36H} + h {2H}), 0.89 (t, 9H, i) ppm; $^{13}\text{C-NMR}$ (CDCl_3): δ = 172.1 (1), 153.2 (2), 137.8 (3), 134.7 (4), 133.3 (5), 129.3 (6), 128.8 (7), 127.0 (8), 98.4 (9), 73.5 (*para*-10), 69.0 (*meta*-10), 56.9 (11), 40.7 (12), 31.9, 31.8, 30.2, 29.6, 29.4, 29.3, 26.1, 26.1, 22.7, 22.7 (13), 14.1 (14) ppm; **FT-IR (ATR)**: ν = 3273, 2950, 2919, 2850, 1653, 1642, 1600, 1534, 1506, 1465, 1429, 1389, 1231, 1115, 743, 702 cm^{-1} ; **MALDI-TOF**: m/z [M+H] $^{+}$ Calcd. 625.49; found: 625.44 [M+H] $^{+}$, 647.43 [M+Na] $^{+}$; **elemental analysis**: Calcd. for $\text{C}_{39}\text{H}_{64}\text{N}_2\text{O}_4$: 74.95% C, 10.32% H, 4.48% N; found: 74.92% C, 10.52% H, 4.28% N.

N^ω-(3,4,5-Trioctyloxyphenyl)-D-phenylalaninamide (8b)

Crude **7b** (4.3 g) was dissolved in TFA (25 mL). The solution was purged with argon for 15 min, after which the mixture was stirred for another 45 min. The reaction mixture was concentrated *in vacuo*. A mixture of diethyl ether, 1 N NaOH and ice was added and the layers were separated. The organic layer was washed with 1 N NaOH several times and dried over MgSO₄. After evaporation, the pure title compound was isolated (2.24 g, 3.58 mmol, 85% after two reactions): ¹H-NMR (CDCl₃): δ = 9.28 (s, 1H, **a**), 7.4–7.2 (m, 5H, **b**), 6.87 (s, 2H, **c**), 4.1–3.9 (m, 6H, **d**), 3.70 (m, 1H, **e**), 3.35 + 2.75 (m, 2H, **f**), 1.9–1.2 (m, 38H, **g** {36H} + **h** {2H}), 0.89 (t, 9H, **i**) ppm; ¹³C-NMR (CDCl₃): δ = 172.1 (**1**), 153.2 (**2**), 137.8 (**3**), 134.7 (**4**), 133.3 (**5**), 129.3 (**6**), 128.8 (**7**), 127.0 (**8**), 98.4 (**9**), 73.5 (*para*-**10**), 69.1 (*meta*-**10**), 56.9 (**11**), 40.7 (**12**), 31.9, 31.8, 30.3, 29.6, 29.4, 29.3, 26.2, 26.1, 22.7, 22.7 (**13**), 14.1 (**14**) ppm; FT-IR (ATR): ν = 3270, 2950, 2919, 2850, 1652, 1642, 1600, 1536, 1506, 1465, 1430, 1389, 1231, 1115, 743, 702 cm⁻¹; MALDI-TOF: *m/z* [M+H]⁺ Calcd. 624.49; found: 624.38 [M+H]⁺; **elemental analysis**: Calcd. for C₃₉H₆₄N₂O₄: 74.95% C, 10.32% H, 4.48% N; found: 75.22% C, 10.57% H, 4.37% N.

N^α-(tert-Butyloxycarbonyl)-N^ω-(3,4,5-trioctyloxyphenyl)-glycyl-L-phenylalaninamide (6a)

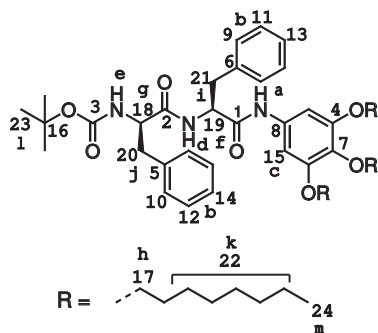
To a magnetically stirred solution of HBTU (0.69 g, 1.82 mmol) in dry dimethylformamide (3.6 mL), DiPEA (0.6 mL, 3.5 mmol) and Boc-GlyOH (0.29 g, 1.66 mmol) were added consecutively. This mixture was stirred for 5 min after which **8a** (0.57 g, 0.91 mmol) was added. Stirring was continued overnight at room temperature. The reaction mixture was slowly added to a mixture of diethyl ether (100 mL), acidic water (pH < 3, 100 mL) and ice. The organic layer was washed with sat. KCl (80 mL), 1 N NaOH (3 × 80 mL) and 10 mM NaHCO₃ (3 × 80 mL) and dried over MgSO₄. After evaporation, the crude product was purified by column chromatography (silica, 3% methanol in dichloromethane) to yield the pure compound as a sticky yellow solid material (0.56 g, 0.72 mmol, 79%). The product was characterized using **chiral HPLC** (isocratic, 10% isopropanol in hexane, purity based on UV > 99%): ¹H-NMR (CDCl₃): δ = 7.85 (s, 1H, **a**), 7.4–7.2 (m, 5H, **b**), 6.74 (s, 2H, **c**), 6.66 (d, 1H, *J* = 7.6 Hz, **d**), 5.07 (br t, 1H, **e**), 4.78 (q, 1H, **f**), 4.0–3.6 (m, 8H, **g** {2H} + **h** {6H}), 3.29 + 3.07 (m, 2H, **i**), 1.8–1.1 (m, 45H, **j** {36H} + **k** {9H}), 0.88 (t, 9H, **l**) ppm; ¹³C-NMR (CDCl₃): δ = 169.7 (**1**), 168.9 (**2**), 156.4 (**3**), 153.1 (**4**), 136.4 (**5**), 135.0 (**6**), 133.2 (**7**), 129.4 (**8**), 128.9 (**9**), 127.2 (**10**), 99.1 (**11**), 80.7 (**12**), 73.6 (*para*-**13**), 69.1 (*meta*-**13**), 54.9 (**14**), 44.7 (**15**), 38.2 (**16**), 32.0, 32.0, 30.4, 29.7, 29.5, 29.4 (**17**), 28.3 (**18**), 28.1, 26.2, 26.2, 22.8, 22.8 (**17**), 14.2 (**19**) ppm; FT-IR (ATR): ν = 3285, 2955, 2924, 2855, 1649, 1607, 1549, 1504, 1428, 1389, 1367, 1228, 1169, 1114, 698 cm⁻¹; MALDI-TOF: *m/z* [M]⁺ Calcd. 781.56; found: 781.57 [M]⁺; **elemental analysis**: Calcd. for C₄₆H₇₅N₃O₇: 70.64% C, 9.67% H, 5.37% N; found: 70.64% C, 9.85% H, 5.32% N.

N^α-(tert-Butyloxycarbonyl)-N^ω-(3,4,5-trioctyloxyphenyl)-L-phenylalanyl-L-phenylalaninamide (6b)

To a magnetically stirred solution of HBTU (0.80 g, 2.11 mmol) in dry dimethylformamide (4 mL), DiPEA (0.7 mL, 4.0 mmol) and Boc-L-PheOH (0.50 g, 1.88 mmol) were added consecutively. This mixture was stirred for 5 min after which **8a** (0.66 g, 1.05 mmol) was added. Stirring was continued overnight at room temperature. The reaction mixture was slowly added to a mixture of diethyl ether (100 mL), acidic water (pH < 3, 100 mL) and ice. The organic layer was washed with sat. KCl (60 mL), 1 N NaOH (3 × 60 mL) and 10 mM NaHCO₃ (3 × 60 mL) and dried over

MgSO₄. After evaporation, the crude product was purified by column chromatography (silica, 3% methanol in dichloromethane) and subsequently washed with methanol to yield the pure compound as a white solid material (0.68 g, 0.78 mmol, 74%). The product was characterized using **chiral HPLC** (isocratic, 10% isopropanol in hexane, purity based on UV > 99%): ¹H-NMR (CDCl₃): δ = 7.98 (s, 1H, **a**), 7.4–6.9 (m, 10H, **b**), 6.87 (s, 2H, **c**), 6.27 (d, 1H, *J* = 7.2 Hz, **d**), 4.9–4.7 (m, 2H, **e** {1H} + **f** {1H}), 4.26 (q, 1H, **g**), 4.0–3.8 (m, 6H, **h**), 3.37 + 2.89 (m, 2H, **i**) + 3.04 (m, 2H, **j**), 1.8–1.2 (m, 45H, **k** {36H} + **l** {9H}), 0.88 (t, 9H, **m**) ppm; ¹³C-NMR (CDCl₃): δ = 171.0 (**1**), 168.5 (**2**), 156.0 (**3**), 153.1 (**4**), 136.2 (**5**), 135.8 (**6**), 134.9 (**7**), 133.5 (**8**), 129.4 (**9**), 129.3 (**10**), 129.2 (**11**), 129.0 (**12**), 127.7 (**13**), 127.3 (**14**), 99.1 (**15**), 81.2 (**16**), 73.6 (**17**), 69.1 (**17**), 56.5 (**18**), 53.9 (**19**), 37.4 (**20**), 37.0 (**21**), 32.0, 32.0, 30.4, 29.7, 29.5, 29.4 (**22**), 28.4 (**23**), 28.2, 26.3, 26.2, 22.8, 22.8 (**22**), 14.3 (**24**) ppm; **FT-IR (ATR)**: ν = 3284, 2922, 2854, 1690, 1647, 1603, 1527, 1506, 1429, 1367, 1229, 1170, 1116, 697 cm⁻¹; **MALDI-TOF**: *m/z* [M]⁺; Calcd. 871.61; found: 871.61 [M]⁺; **elemental analysis**: Calcd. for C₅₃H₈₁N₃O₇: 72.98% C, 9.36% H, 4.82% N; found: 73.03% C, 9.56% H, 4.76% N.

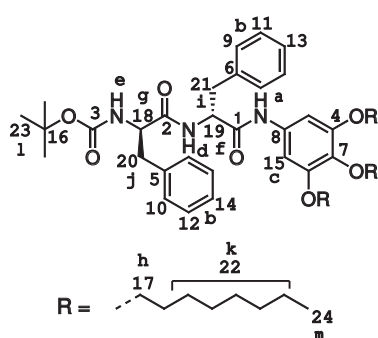
N^α-(*tert*-Butyloxycarbonyl)-N^ω-(3,4,5-trioctyloxyphenyl)-D-phenylalanyl-L-phenylalaninamide (**6c**)



To a magnetically stirred solution of HBTU (0.91 g, 2.40 mmol) in dry dimethylformamide (5 mL), DiPEA (0.8 mL, 4.6 mmol) and Boc-D-PheOH (0.57 g, 2.15 mmol) were added consecutively. This mixture was stirred for 5 min after which **8a** (0.75 g, 1.20 mmol) was added. Stirring was continued overnight at room temperature. The reaction mixture was slowly added to a mixture of diethyl ether (80 mL), acidic water (pH < 3, 80 mL) and ice. The organic layer was washed with sat. KCl (40 mL), 1 N NaOH (3 × 40 mL) and 10 mM NaHCO₃ (3 × 40 mL) and dried over MgSO₄. After evaporation, the crude product was purified by column

chromatography (silica, 2% methanol in dichloromethane) and subsequently washed with methanol to yield the pure compound as a white solid material (0.78 g, 0.90 mmol, 75%). The product was characterized using **chiral HPLC** (isocratic, 10% isopropanol in hexane, purity based on UV > 99%): ¹H-NMR (CDCl₃): δ = 7.99 (s, 1H, **a**), 7.4–6.9 (m, 10H, **b**), 6.72 (s, 2H, **c**), 6.15 (d, 1H, *J* = 6.4 Hz, **d**), 4.96 (br d, 1H, **e**), 4.76 (q, 1H, **f**), 4.08 (q, 1H, **g**), 4.0–3.8 (m, 6H, **h**), 3.26 + 2.80 (m, 2H, **i**), 3.00 (m, 2H, **j**), 1.8–1.2 (m, 45H, **k** {36H} + **l** {9H}), 0.88 (t, 9H, **m**) ppm; ¹³C-NMR (CDCl₃): δ = 171.5 (**1**), 168.5 (**2**), 155.8 (**3**), 153.1 (**4**), 136.4 (**5**), 136.3 (**6**), 135.3 (**7**), 133.1 (**8**), 129.6 (**9**), 129.4 (**10**), 129.0 (**11**), 129.0 (**12**), 127.4 (**13**), 127.3 (**14**), 99.9 (**15**), 81.0 (**16**), 73.6 (*para*-17), 69.3 (*meta*-17), 57.3 (**18**), 54.5 (**19**), 37.7 (**20**), 37.0 (**21**), 32.0, 32.0, 30.4, 29.7, 29.5, 29.4 (**22**), 28.3 (**23**), 26.3, 26.2, 22.8, 22.8 (**22**), 14.2 (**24**) ppm; **FT-IR (ATR)**: ν = 3295, 2921, 2852, 1688, 1648, 1603, 1526, 1508, 1428, 1388, 1367, 1231, 1170, 1130, 1117, 700 cm⁻¹; **MALDI-TOF**: *m/z* [M]⁺; Calcd. 871.61; found: 871.64 [M]⁺; **elemental analysis**: Calcd. for C₅₃H₈₁N₃O₇: 72.98% C, 9.36% H, 4.82% N; found: 73.31% C, 9.45% H, 4.77% N.

N^α-(*tert*-Butyloxycarbonyl)-N^ω-(3,4,5-trioctyloxy-phenyl)-D-phenylalanyl-D-phenylalaninamide (**6d**)

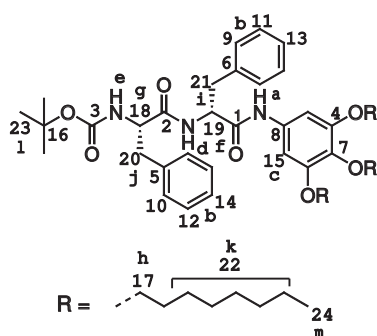


To a magnetically stirred solution of HBTU (1.19 g, 3.14 mmol) in dry dimethylformamide (7 mL), DiPEA (1.1 mL, 6.3 mmol) and Boc-D-PheOH (0.75 g, 2.83 mmol) were added consecutively. This mixture was stirred for 5 minutes after which **8b** (0.98 g, 1.57 mmol) was added. Stirring was continued overnight at room temperature. The reaction mixture was slowly added to a mixture of diethyl ether (80 mL), acidic water (pH < 3, 80 mL) and ice. The organic layer was washed with sat. KCl (40 mL), 1 N NaOH (3 × 40 mL) and 10 mM NaHCO₃ (3 × 40 mL) and dried over MgSO₄. After evaporation, the crude product was purified by

column chromatography (silica, 2% methanol in dichloromethane) and subsequently washed with methanol to

yield the pure compound as a white solid material (1.04 g, 1.19 mmol, 76%). The product was characterized using **chiral HPLC** (isocratic, 10% isopropanol in hexane, purity based on UV > 99%): **¹H-NMR** (CDCl₃): δ = 7.97 (s, 1H, **a**), 7.4–6.9 (m, 10H, **b**), 6.87 (s, 2H, **c**), 6.26 (d, 1H, *J* = 6.5 Hz, **d**), 4.9–4.7 (m, 2H, **e** {1H} + **f** {1H}), 4.26 (q, 1H, **g**), 4.0–3.8 (m, 6H, **h**), 3.37 + 2.89 (m, 2H, **i**) + 3.04 (m, 2H, **j**), 1.8–1.2 (m, 45H, **k** {36H} + **l** {9H}), 0.88 (t, 9H, **m**) ppm; **¹³C-NMR** (CDCl₃): δ = 170.9 (**1**), 168.5 (**2**), 156.1 (**3**), 153.1 (**4**), 136.2 (**5**), 135.8 (**6**), 134.9 (**7**), 133.5 (**8**), 129.4 (**9**), 129.3 (**10**), 129.2 (**11**), 129.1 (**12**), 127.7 (**13**), 127.3 (**14**), 99.1 (**15**), 81.2 (**16**), 73.6 (*para*-**17**), 69.1 (*meta*-**17**), 56.5 (**18**), 53.8 (**19**), 37.4 (**20**), 37.0 (**21**), 32.0, 32.0, 30.4, 29.7, 29.5, 29.4 (**22**), 28.2 (**23**), 26.3, 26.2, 22.8, 22.8 (**24**) ppm; **FT-IR (ATR)**: ν = 3289, 2922, 2852, 1691, 1648, 1602, 1527, 1506, 1428, 1388, 1367, 1297, 1229, 1168, 1129, 1116, 697 cm⁻¹; **MALDI-TOF**: *m/z* [M]⁺⁺ Calcd. 871.61; found: 871.45 [M]⁺⁺; **elemental analysis**: Calcd. for C₅₃H₈₁N₃O₇: 72.98% C, 9.36% H, 4.82% N; found: 73.22% C, 9.39% H, 4.75% N.

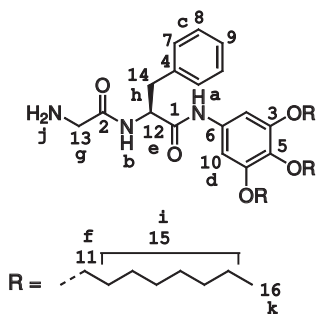
N^α-(*tert*-Butyloxycarbonyl)-N^ω-(3,4,5-trioctyloxyphenyl)-L-phenylalanyl-D-phenylalaninamide (**6e**)



To a magnetically stirred solution of HBTU (1.20 g, 3.16 mmol) in dry dimethylformamide (7 mL), DiPEA (1.1 mL, 6.3 mmol) and Boc-L-PheOH (0.76 g, 2.86 mmol) were added consecutively. This mixture was stirred for 5 min after which **8b** (0.99 g, 1.58 mmol) was added. Stirring was continued overnight at room temperature. The reaction mixture was slowly added to a mixture of diethyl ether (80 mL), acidic water (pH < 3, 80 mL) and ice. The organic layer was washed with sat. KCl (40 mL), 1 N NaOH (3 × 40 mL) and 10 mM NaHCO₃ (3 × 40 mL) and dried over MgSO₄. After evaporation, the crude product was purified by column

chromatography (silica, 2% methanol in dichloromethane) and subsequently washed with methanol to yield the pure compound as a white solid material (0.70 g, 0.80 mmol, 51%). The product was characterized using **chiral HPLC** (isocratic, 10% isopropanol in hexane, purity based on UV > 99%): **¹H-NMR** (CDCl₃): δ = 7.98 (s, 1H, **a**), 7.4–6.9 (m, 10H, **b**), 6.72 (s, 2H, **c**), 6.15 (d, 1H, *J* = 6.5 Hz, **d**), 4.96 (br d, 1H, **e**), 4.76 (q, 1H, **f**), 4.08 (q, 1H, **g**), 4.0–3.8 (m, 6H, **h**), 3.26 + 2.80 (m, 2H, **i**), 3.00 (m, 2H, **j**), 1.8–1.2 (m, 45H, **k** {36H} + **l** {9H}), 0.88 (t, 9H, **m**) ppm; **¹³C-NMR** (CDCl₃): δ = 171.4 (**1**), 168.5 (**2**), 155.8 (**3**), 153.1 (**4**), 136.4 (**5**), 136.3 (**6**), 135.3 (**7**), 133.1 (**8**), 129.6 (**9**), 129.4 (**10**), 129.0 (**11**), 129.0 (**12**), 127.4 (**13**), 127.3 (**14**), 99.9 (**15**), 81.0 (**16**), 73.6 (*para*-**17**), 69.3 (*meta*-**17**), 57.2 (**18**), 54.5 (**19**), 37.7 (**20**), 37.0 (**21**), 32.0, 32.0, 30.4, 29.7, 29.5, 29.4 (**22**), 28.3 (**23**), 26.3, 26.2, 22.8, 22.8 (**24**) ppm; **FT-IR (ATR)**: ν = 3289, 2922, 2852, 1691, 1648, 1602, 1527, 1506, 1428, 1388, 1367, 1297, 1229, 1168, 1129, 1116, 697 cm⁻¹; **MALDI-TOF**: *m/z* [M]⁺⁺ Calcd. 871.61; found: 871.55 [M]⁺⁺; **elemental analysis**: Calcd. for C₅₃H₈₁N₃O₇: 72.98% C, 9.36% H, 4.82% N; found: 73.00% C, 9.36% H, 4.80% N.

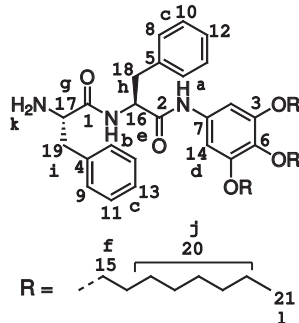
N^ω-(3,4,5-Trioctyloxyphenyl)-glycyl-L-phenylalaninamide (**9a**)



Compound **6a** (0.48 g, 0.61 mmol) was dissolved in TFA (6 mL). The solution was purged with argon for 15 min, after which the mixture was stirred for another 45 min. The reaction mixture was concentrated *in vacuo*. A mixture of diethyl ether, 1 N NaOH and ice was added and the layers were separated. The organic layer was washed with 1 N NaOH several times and dried over MgSO₄. After evaporation, the pure title compound was isolated (0.38 g, 0.56 mmol, 91%): **¹H-NMR** (CDCl₃): δ = 8.10 (s, 1H, **a**), 7.91 (d, 1H, *J* = 7.5 Hz, **b**), 7.4–7.1 (m, 5H, **c**), 6.66 (s, 2H, **d**), 4.71 (q, 1H, **e**), 4.0–3.8 (m, 6H, **f**), 3.35 (m, 2H, **g**), 3.18 (m, 2H, **h**), 1.9–1.2 (m, 38H, **i** {36H} + **j** {2H}), 0.89 (t, 9H, **k**) ppm; **¹³C-NMR** (CDCl₃): δ = 173.8 (**1**), 169.0 (**2**), 153.2 (**3**), 137.0 (**4**), 135.0 (**5**), 133.3 (**6**), 129.5, 129.4 (**7**), 128.8 (**8**), 127.1 (**9**), 99.1 (**10**), 73.6 (*para*-**11**), 69.2 (*meta*-**11**), 55.3 (**12**), 44.6 (**13**), 37.7 (**14**), 32.0, 32.0, 30.4, 29.7, 29.5, 29.4, 26.3, 26.2, 22.8, 22.8 (**15**), 14.2 (**16**) ppm; **FT-IR (ATR)**: ν = 3272, 2922, 2854, 1647, 1602, 1533, 1506, 1466, 1427,

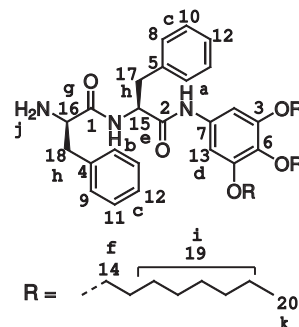
1388, 1230, 1116, 700 cm^{-1} ; **MALDI-TOF**: m/z $[M]^{++}$ Calcd. 681.51; found: 681.46 $[M]^{++}$, 721.49 $[M+K]^+$; **elemental analysis**: Calcd. for $\text{C}_{41}\text{H}_{67}\text{N}_3\text{O}_5$: 72.21% C, 9.90% H, 6.16% N; found: 71.48% C, 9.80% H, 6.16% N.

N^0 -(3,4,5-Trioctyloxyphenyl)-L-phenylalanyl-L-phenylalaninamide (9b)



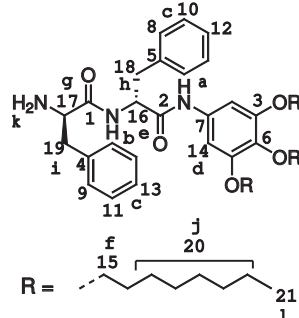
Compound **6b** (0.27 g, 0.31 mmol) was dissolved in TFA (3 mL). The solution was purged with argon for 15 min, after which the mixture was stirred for another 45 min. The reaction mixture was concentrated *in vacuo*. A mixture of ethyl acetate, 1 N NaOH and some ice was added and the layers were separated. The organic layer was washed with 1 N NaOH several times and dried over MgSO_4 . After evaporation, the pure title compound was isolated (0.22 g, 0.29 mmol, 93%): **$^1\text{H-NMR}$** (CDCl_3): δ = 8.32 (s, 1H, **a**), 7.97 (d, 1H, J = 4.4, **b**), 7.4–7.1 (m, 10H, **c**), 6.69 (s, 2H, **d**), 4.77 (q, 1H, **e**), 4.0–3.8 (m, 6H, **f**), 3.61 (d, 1H, J = 5.6 Hz, **g**), 3.23 (m, 2H, **h**), 3.11 + 2.45 (m, 2H, **i**), 1.9–1.2 (m, 36H, **j** {36H} + **k** {2H}), 0.88 (m, 9H, **l**) ppm; **$^{13}\text{C-NMR}$** (CDCl_3): δ = 175.4 (**1**), 168.9 (**2**), 153.2 (**3**), 137.2 (**4**), 136.8 (**5**), 135.0 (**6**), 133.3 (**7**), 129.5 (**8**), 129.3 (**9**), 128.9 (**10**), 128.8 (**11**), 127.1 (**12**), 127.0 (**13**), 99.1 (**14**), 73.6 (**15**), 69.2 (**15**), 56.3 (**16**), 55.2 (**17**), 40.7 (**18**), 37.7 (**19**), 32.0, 32.0, 30.4, 29.7, 29.5, 29.4, 26.3, 26.2, 22.8, 22.8 (**20**), 14.2 (**21**) ppm; **FT-IR (ATR)**: ν = 3283, 2954, 2923, 2855, 1644, 1605, 1539, 1506, 1467, 1455, 1428, 1387, 1231, 1116, 698 cm^{-1} ; **MALDI-TOF**: m/z $[M]^{++}$ Calcd. 771.55; found 771.53 $[M]^{++}$; **Elemental analysis**: Calcd. for $\text{C}_{48}\text{H}_{73}\text{N}_3\text{O}_5$: 74.67% C, 9.53% H, 5.44% N, found: 73.78% C, 9.45% H, 5.54% N.

N^0 -(3,4,5-Trioctyloxyphenyl)-D-phenylalanyl-L-phenylalaninamide (9c)



Compound **6c** (0.30 g, 0.34 mmol) was dissolved in TFA (3.5 mL). The solution was purged with argon for 15 min, after which the mixture was stirred for another 45 min. The reaction mixture was concentrated *in vacuo*. A mixture of ethyl acetate, 1 N NaOH and some ice was added and the layers were separated. The organic layer was washed with 1 N NaOH several times and dried over MgSO_4 . After evaporation, the pure title compound was isolated (0.24 g, 0.31 mmol, 91%): **$^1\text{H-NMR}$** (CDCl_3): δ = 8.26 (s, 1H, **a**), 7.90 (d, 1H, J = 7.6, **b**), 7.4–7.1 (m, 10H, **c**), 6.69 (s, 2H, **d**), 4.70 (q, 1H, **e**), 4.0–3.8 (m, 6H, **f**), 3.57 (m, 1H, **g**), 3.23 + 2.74 (m, 4H, **h**), 1.9–1.2 (m, 36H, **i** {36H} + **j** {2H}), 0.88 (m, 9H, **k**) ppm; **$^{13}\text{C-NMR}$** (CDCl_3): δ = 175.5 (**1**), 168.9 (**2**), 153.2 (**3**), 137.4 (**4**), 137.0 (**5**), 135.0 (**6**), 133.3 (**7**), 129.4 (**8**), 129.3 (**9**), 128.9 (**10**), 128.9 (**11**), 127.1 (**12**), 99.1 (**13**), 73.6 (*para*-**14**), 69.2 (*meta*-**14**), 56.3 (**15**), 55.4 (**16**), 40.9 (**17**), 37.3 (**18**), 32.0, 32.0, 30.4, 29.7, 29.5, 29.4, 26.3, 26.2, 22.8 (**19**), 14.2 (**20**) ppm; **FT-IR (ATR)**: ν = 3271, 2922, 2853, 1643, 1603, 1535, 1506, 1467, 1454, 1431, 1387, 1230, 1118, 698 cm^{-1} ; **MALDI-TOF**: m/z $[M]^{++}$ Calcd. 771.55; found: 771.64 $[M]^{++}$; **elemental analysis**: Calcd. for $\text{C}_{48}\text{H}_{73}\text{N}_3\text{O}_5$: 74.67% C, 9.53% H, 5.44% N, found: 74.82% C, 9.51% H, 5.29% N.

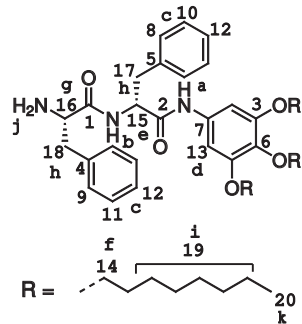
N^0 -(3,4,5-Trioctyloxyphenyl)-D-phenylalanyl-D-phenylalaninamide (9d)



Compound **6d** (0.30 g, 0.34 mmol) was dissolved in TFA (3.5 mL). The solution was purged with argon for 15 min, after which the mixture was stirred for another 45 min. The reaction mixture was concentrated *in vacuo*. A mixture of ethyl acetate, 1 N NaOH and some ice was added and the layers were separated. The organic layer was washed with 1 N NaOH several times and dried over MgSO_4 . After evaporation, the pure title compound was isolated (0.24 g, 0.31 mmol, 91%): **$^1\text{H-NMR}$** (CDCl_3): δ = 8.08 (s, 1H, **a**), 7.93 (d, 1H, J = 7.6, **b**), 7.4–7.1 (m, 10H, **c**), 6.68 (s, 2H, **d**), 4.70 (q, 1H, **e**), 4.0–3.8 (m, 6H, **f**), 3.60 (m,

1H, g), 3.23 (m, 2H, h), 3.11 + 2.45 (m, 2H, i), 1.9–1.2 (m, 38H, j {36H} + k {2H}), 0.88 (m, 9H, l) ppm; $^{13}\text{C-NMR}$ (CDCl_3): δ = 175.4 (1), 168.9 (2), 153.2 (3), 137.4 (4), 137.0 (5), 135.0 (6), 133.3 (7), 129.5 (8), 129.3 (9), 128.9 (10), 128.8 (11), 127.1 (12), 127.1 (13), 99.1 (14), 73.6 (*para*-15), 69.2 (*meta*-15), 56.3 (16), 55.2 (17), 40.7 (18), 37.5 (19), 32.0, 32.0, 30.4, 29.7, 29.5, 29.4, 26.3, 26.2, 22.8, 22.8 (20), 14.2 (21) ppm; **FT-IR (ATR)**: ν = 3283, 2955, 2922, 2855, 1646, 1606, 1540, 1506, 1467, 1455, 1430, 1231, 1119, 698 cm^{-1} ; **MALDI-TOF**: m/z [M] $^{+}$ Calcd. 771.55; found: 771.60 [M] $^{+}$; **elemental analysis**: Calcd. for $\text{C}_{48}\text{H}_{73}\text{N}_3\text{O}_5$: 74.67% C, 9.53% H, 5.44% N, found: 74.35% C, 9.53% H, 5.36% N.

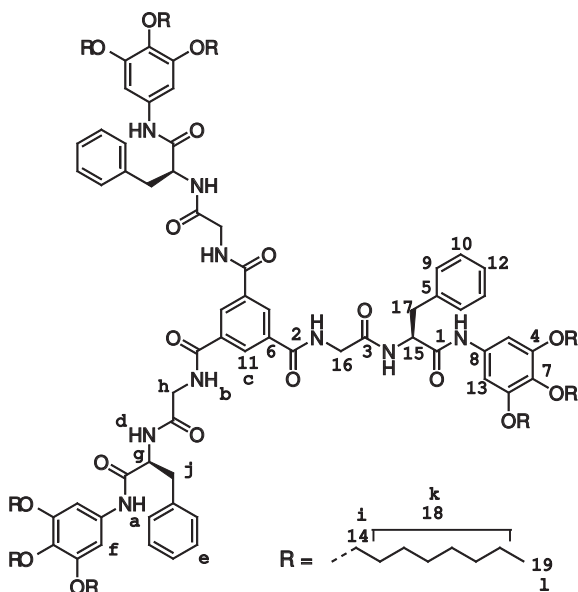
N^{α} -(3,4,5-Trioctyloxyphenyl)-L-phenylalanyl-D-phenylalaninamide (9e)



Compound **6e** (0.78 g, 0.90 mmol) was dissolved in TFA (9 mL). The solution was purged with argon for 15 min, after which the mixture was stirred for another 45 min. The reaction mixture was concentrated *in vacuo*. A mixture of ethyl acetate, 1 N NaOH and some ice was added and the layers were separated. The organic layer was washed with 1 N NaOH several times and dried over MgSO_4 . After evaporation, the pure title compound was isolated (0.49 g, 0.63 mmol, 71%): $^1\text{H-NMR}$ (CDCl_3): δ = 8.13 (s, 1H, a), 7.90 (d, 1H, J = 7.6, b), 7.4–7.1 (m, 10H, c), 6.68 (s, 2H, d), 4.70 (q, 1H, e), 4.0–3.8 (m, 6H, f), 3.57 (m, 1H, g), 3.23 + 2.74 (m, 4H, h), 1.9–1.2 (m, 38H, i {36H} + j {2H}), 0.87 (m, 9H, k)

ppm; $^{13}\text{C-NMR}$ (CDCl_3): δ = 175.6 (1), 168.9 (2), 153.3 (3), 137.3 (4), 137.0 (5), 135.1 (6), 133.3 (7), 129.4 (8), 129.4 (9), 128.9 (10), 128.9 (11), 127.1 (12), 99.1 (13), 73.6 (*para*-14), 69.3 (*meta*-14), 56.3 (15), 55.5 (16), 40.8 (17), 37.0 (18), 32.0, 32.0, 30.4, 29.7, 29.5, 29.4, 26.3, 26.2, 22.8, 22.8 (19), 14.2 (20) ppm; **FT-IR (ATR)**: ν = 3265, 2924, 2855, 1644, 1614, 1603, 1555, 1504, 1467, 1454, 1427, 1379, 1229, 1115, 698 cm^{-1} ; **MALDI-TOF**: m/z [M] $^{+}$ Calcd. 771.55; found: 771.58 [M] $^{+}$; **elemental analysis**: Calcd. for $\text{C}_{48}\text{H}_{73}\text{N}_3\text{O}_5$: 74.67% C, 9.53% H, 5.44% N, found: 74.81% C, 9.62% H, 5.32% N.

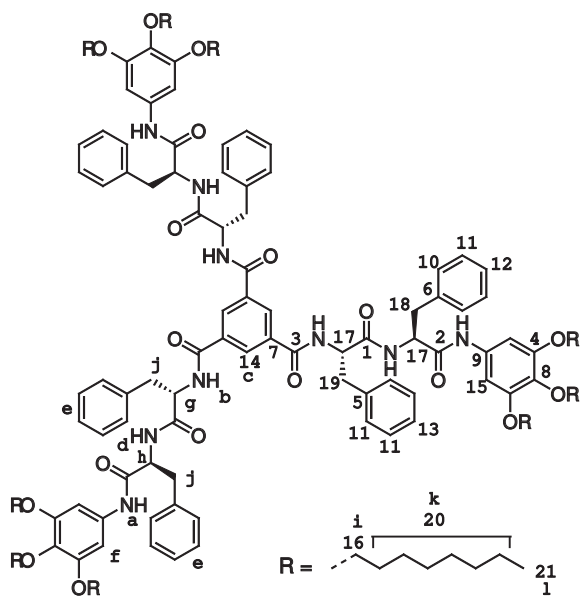
$\text{N}^{\alpha}, \text{N}^{\omega}, \text{N}^{\omega\omega}$ -(1,3,5-Benzenetricarbonyl)tris[N^{α} -(3,4,5-trioctyloxyphenyl)]-glycyl-L-phenylalaninamide (2a)



A solution of 1,3,5-benzenetricarbonyl trichloride (45.4 mg, 0.17 mmol) in dry tetrahydrofuran (1.7 mL) was added dropwise to a solution of **9a** (0.39 g, 0.57 mmol) and triethylamine (0.2 mL, 1.43 mmol) in dry tetrahydrofuran (5 mL). After stirring overnight and evaporation of the tetrahydrofuran the crude product was purified by column chromatography (silica, tetrahydrofuran/hexane 2/1). Subsequently, the product was recrystallized from a mixture of tetrahydrofuran/methanol (2/3) to yield the title compound as a white solid material (0.12 g, 0.05 mmol, 32%). The product was characterized by **GPC** (THF, 260 nm, purity based on UV ~ 100%): $^1\text{H-NMR}$ ($\text{DMSO-}d_6$, T = 323 K): δ = 9.71 (s, 3H, a), 8.78 (t, 3H, b), 8.48 (s, 3H, c), 8.18 (d, 3H, J = 7.5 Hz, d), 7.3–7.1 (m, 15H, e), 6.91 (s, 6H, f), 4.66 (q, 3H, g), 4.0–3.7 (m, 24H, h {6H} + i {18H}), 3.1 + 2.9 (m, 6H, j), 1.8–1.0 (m, 108H, k), 0.85 (t, 27H, l) ppm; $^{13}\text{C-NMR}$ ($\text{DMSO-}d_6$, T = 323 K): δ = 169.2 (1), 168.4 (2), 165.5 (3), 152.1 (4), 137.3 (5), 134.3 (6), 134.1 (7), 133.6 (8), 128.9 (9), 127.8 (10), 126.1 (11), 12, 98.6 (13), 72.3 (*para*-14), 68.2 (*meta*-14), 54.6 (15), 42.6 (16), 37.5 (17), 31.0, 31.0, 29.6, 28.7, 28.6, 28.5, 28.4, 25.4, 25.3, 21.8, 21.8 (18), 13.6 (19) ppm; **FT-IR (ATR)**: ν = 3280, 2923, 2854, 1651, 1604, 1536, 1506, 1467,

1428, 1386, 1228, 1116, 699 cm^{-1} ; **MALDI-TOF**: m/z $[M]^{+}$ Calcd. 2201.51; found: 2201.36 $[M]^{+}$, 2224.38 $[M+Na]^{+}$; **elemental analysis**: Calcd. for $\text{C}_{132}\text{H}_{201}\text{N}_9\text{O}_{18}$: 72.00% C, 9.20% H, 5.72% N; found: 71.41% C, 9.22% H, 5.77% N.

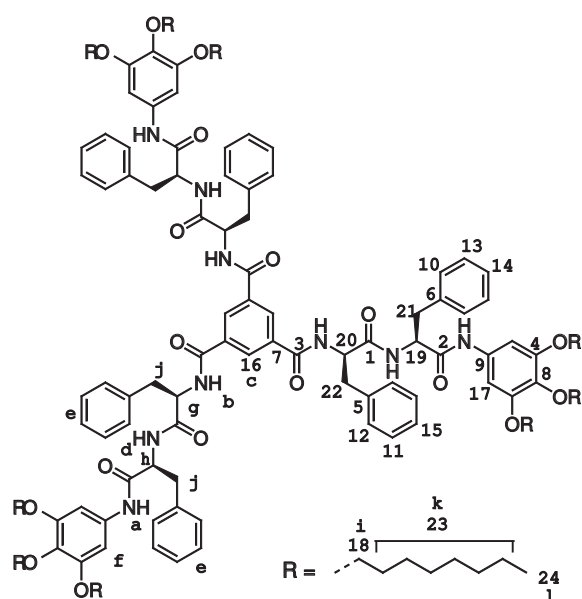
$\text{N}^{\alpha},\text{N}^{\omega},\text{N}^{\omega\omega}$ -(1,3,5-Benzenetricarbonyl)tris[N^{ω} -(3,4,5-trioctyloxyphenyl)]-L-phenylalanyl-L-phenylalaninamide (2b)



A solution of 1,3,5-benzenetricarbonyl trichloride (33.4 mg, 0.13 mmol) in dry tetrahydrofuran (1.3 mL) was added dropwise to a solution of **9b** (0.30 g, 0.39 mmol) and triethylamine (0.1 mL, 0.7 mmol) in dry dichloromethane (4 mL). After stirring overnight the reaction mixture was filtered to yield the title compound as an off-white solid material (0.19 g, 0.07 mmol, 59%): $^1\text{H-NMR}$ ($\text{DMSO-}d_6$, $T = 323$ K): $\delta = 9.74$ (s, 3H, **a**), 8.60 (d, 3H, $J = 8.0$ Hz, **b**), 8.24 (s, 3H, **c**), 8.16 (d, 3H, $J = 7.5$ Hz, **d**), 7.3–7.0 (m, 30H, **e**), 6.87 (s, 6H, **f**), 4.79 (q, 3H, **g**), 4.69 (q, 3H, **h**), 4.0–3.7 (m, 18H, **i**), 3.1–2.9 (m, 12H, **j**), 1.8–1.0 (m, 108H, **k**), 0.84 (t, 27H, **l**) ppm; $^{13}\text{C-NMR}$ ($\text{DMSO-}d_6$, $T = 323$ K): $\delta = 170.6$ (**1**), 169.1 (**2**), 165.2 (**3**), 152.1 (**4**), 137.7 (**5**), 137.1 (**6**), 134.2 (**7**), 134.1 (**8**), 133.6 (**9**), 128.9 (**10**), 127.8 (**11**), 126.1 (**12**), 125.9 (**13**, **14**), 98.6 (**15**), 72.3 (*para*-**16**), 68.2 (*meta*-**16**), 54.6 (**17**), 37.5 (**18**), 37.0 (**19**), 31.0, 31.0, 29.6, 28.6, 28.5, 28.4, 25.3, 21.8 (**20**), 13.5 (**21**) ppm;

FT-IR (ATR): $\nu = 3273, 2923, 2854, 1639, 1603, 1532, 1506, 1467, 1455, 1428, 1387, 1230, 1117, 697$ cm^{-1} ; **MALDI-TOF**: m/z $[M]^{+}$ Calcd. 2471.65; found: 2471.78 $[M]^{+}$, 2494.75 $[M+Na]^{+}$, 2511.73 $[M+K]^{+}$; **elemental analysis**: Calcd. for $\text{C}_{153}\text{H}_{219}\text{N}_9\text{O}_{18}$: 74.33% C, 8.93% H, 5.10% N; found: 74.06% C, 8.94% H, 5.04% N.

$\text{N}^{\alpha},\text{N}^{\omega},\text{N}^{\omega\omega}$ -(1,3,5-Benzenetricarbonyl)tris[N^{ω} -(3,4,5-trioctyloxyphenyl)]-D-phenylalanyl-L-phenylalaninamide (2c)

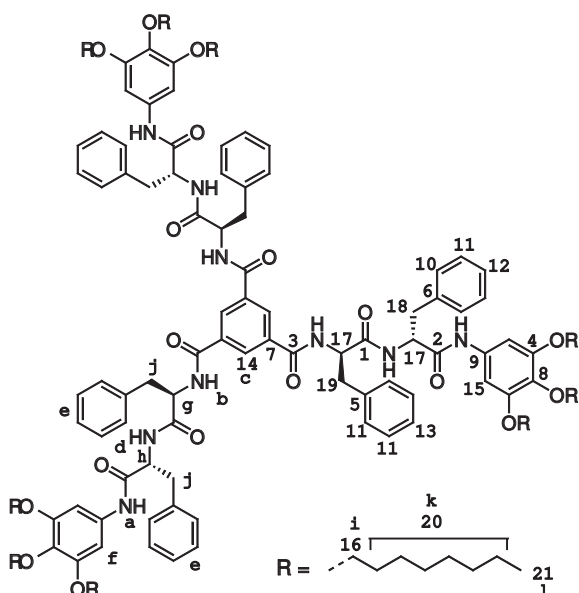


A solution of 1,3,5-benzenetricarbonyl trichloride (30.0 mg, 0.11 mmol) in dichloromethane (1.2 mL) was added dropwise to a solution of **9c** (0.29 g, 0.37 mmol) and triethylamine (0.1 mL, 0.7 mmol) in dry dichloromethane (3.5 mL). After stirring overnight and evaporation of the dichloromethane, the compound was separated from the crude mixture using column filtration (silica, 2% methanol in dichloromethane). Subsequently, refluxing in methanol for 30 min and filtration afforded the product as a white solid in pure form (0.20 g, 0.08 mmol, 71%). The product was characterized using **GPC** (THF, 260 nm, purity based on UV > 99%): $^1\text{H-NMR}$ ($\text{DMSO-}d_6$, $T = 373$ K): $\delta = 9.43$ (s, 3H, **a**), 8.27 (d, 3H, $J = 8.5$ Hz, **b**), 8.18 (s, 3H, **c**), 8.03 (d, 3H, $J = 7.5$ Hz, **d**), 7.3–7.0 (m, 30H, **e**), 6.88 (s, 6H, **f**), 4.77 (q, 3H, **g**), 4.69 (q, 3H, **h**), 4.0–3.7 (m, 18H, **i**), 3.1–2.9

(m, 12H, **j**), 1.8–1.0 (m, 108H, **k**), 0.84 (t, 27H, **l**) ppm; $^{13}\text{C-NMR}$ ($\text{DMSO-}d_6$, $T = 373$ K): $\delta = 170.2$ (**1**), 168.7 (**2**), 165.0 (**3**), 151.9 (**4**), 137.2 (**5**), 136.9 (**6**), 134.3 (**7**), 134.1 (**8**), 133.6 (**9**), 128.5 (**10**), 128.4 (**11**), 128.1 (**12**), 127.3

(13), 125.6 (14), 125.5 (15, 16), 99.5 (17), 72.1 (18), 68.5 (18), 54.6 (19), 54.2 (20), 37.4 (21), 37.0 (22), 30.6, 30.5, 29.2, 28.4, 28.2, 28.0, 28.0, 28.0, 25.0, 25.0, 21.3, 21.3 (23), 13.0 (24) ppm; FT-IR (ATR): $\nu = 3267, 2954, 2922, 2854, 1640, 1603, 1536, 1505, 1467, 1455, 1430, 1388, 1231, 1117, 697 \text{ cm}^{-1}$; MALDI-TOF: $m/z [M]^+$ Calcd. 2471.65; found: 2471.88 $[M]^+$, 2494.94 $[M+Na]^+$, 2510.92 $[M+K]^+$; elemental analysis: Calcd. for $C_{153}H_{219}N_9O_{18}$: 74.33% C, 8.93% H, 5.10% N; found: 74.35% C, 8.87% H, 4.90% N.

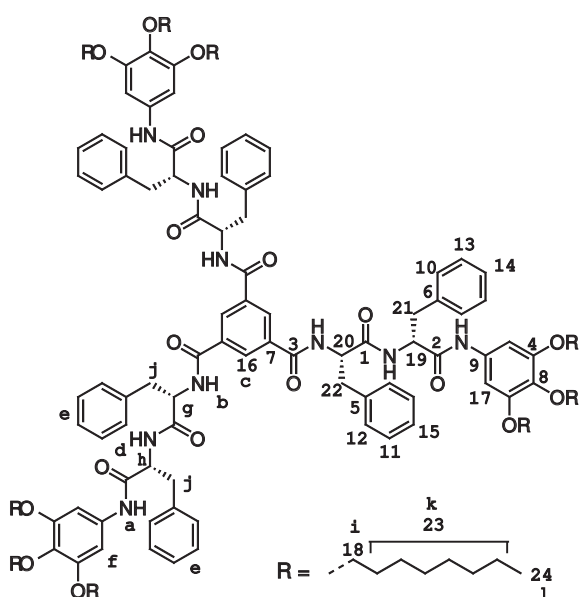
$N^\alpha, N^\omega, N^{\omega'}$ -(1,3,5-Benzenetricarbonyl)tris[N^ω -(3,4,5-trioctyloxyphenyl)]-D-phenylalanyl-D-phenylalaninamide (2d)



A solution of 1,3,5-benzenetricarbonyl trichloride (5.8 mg, 21.8 μmol) in dry dichloromethane (0.2 mL) was added dropwise to a solution of **9d** (52.6 mg, 68.1 μmol) and triethylamine (20 μL , 143 μmol) in dry dichloromethane (0.7 mL). After stirring overnight the reaction mixture was filtered to yield the title compound as an off-white solid material (20 mg, 8.1 μmol , 37%): $^1\text{H-NMR}$ (DMSO- d_6 , T = 323 K): $\delta = 9.74$ (s, 3H, **a**), 8.60 (d, 3H, $J = 8.0$ Hz, **b**), 8.24 (s, 3H, **c**), 8.16 (d, 3H, $J = 7.5$ Hz, **d**), 7.3–7.0 (m, 30H, **e**), 6.87 (s, 6H, **f**), 4.79 (q, 3H, **g**), 4.69 (q, 3H, **h**), 4.0–3.7 (m, 18H, **i**), 3.1–2.9 (m, 12H, **j**), 1.8–1.0 (m, 108H, **k**), 0.84 (t, 27H, **l**) ppm; $^{13}\text{C-NMR}$ (DMSO- d_6 , T = 323 K): $\delta = 170.6$ (1), 169.1 (2), 165.2 (3), 152.1 (4), 137.7 (5), 137.1 (6), 134.2 (7), 134.1 (8), 133.6 (9), 128.9 (10), 127.8 (11), 126.1 (12), 125.9 (13, 14), 98.6 (15), 72.3

(*para*-16), 68.2 (*meta*-16), 54.6 (17), 37.5 (18), 37.0 (19), 31.0, 31.0, 29.6, 28.6, 28.5, 28.4, 25.3, 21.8 (20), 13.5 (21) ppm; FT-IR (ATR): $\nu = 3273, 2923, 2854, 1639, 1603, 1532, 1506, 1467, 1455, 1428, 1387, 1230, 1117, 697 \text{ cm}^{-1}$; MALDI-TOF: $m/z [M]^+$ Calcd. 2471.65; found: 2471.78 $[M]^+$, 2494.75 $[M+Na]^+$, 2511.73 $[M+K]^+$; elemental analysis: Calcd. for $C_{153}H_{219}N_9O_{18}$: 74.33% C, 8.93% H, 5.10% N; found: 74.06% C, 8.94% H, 5.04% N.

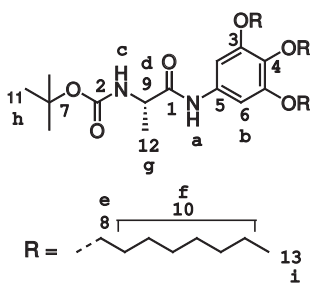
$N^\alpha, N^\omega, N^{\omega'}$ -(1,3,5-Benzenetricarbonyl)tris[N^ω -(3,4,5-trioctyloxyphenyl)]-L-phenylalanyl-D-phenylalaninamide (2e)



A solution of 1,3,5-benzenetricarbonyl trichloride (44.2 mg, 0.17 mmol) in dichloromethane (1.7 mL) was added dropwise to a solution of **9e** (0.43 g, 0.56 mmol) and triethylamine (0.16 mL, 1.15 mmol) in dry dichloromethane (5 mL). After stirring overnight and evaporation of the dichloromethane, the crude product was purified using column chromatography (silica, 2% methanol in dichloromethane) and subsequently washed with acetonitrile to yield the title compound as an off-white solid material (0.23 g, 0.09 mmol, 55%). The product was characterized by GPC (THF, 260 nm, purity based on UV ~ 100%): $^1\text{H-NMR}$ (DMSO- d_6 , T = 373 K): $\delta = 9.43$ (s, 3H, **a**), 8.27 (d, 3H, $J = 8.0$ Hz, **b**), 8.18 (s, 3H, **c**), 8.03 (d, 3H, $J = 6.5$ Hz, **d**), 7.3–7.0 (m, 30H, **e**), 6.88 (s, 6H, **f**), 4.77 (q, 3H, **g**),

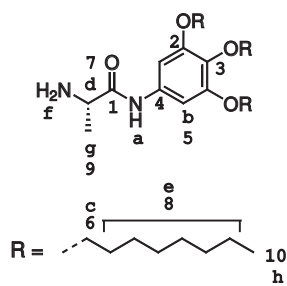
4.69 (q, 3H, **h**), 4.0–3.7 (m, 18H, **i**), 3.1–2.9 (m, 12H, **j**), 1.8–1.0 (m, 108H, **k**), 0.84 (t, 27H, **l**) ppm; $^{13}\text{C-NMR}$ (DMSO- d_6 , T = 373 K): δ = 170.2 (**1**), 168.7 (**2**), 165.0 (**3**), 152.0 (**4**), 137.2 (**5**), 136.9 (**6**), 134.3 (**7**), 134.2 (**8**), 133.6 (**9**), 128.6 (**10**), 128.5 (**11**), 128.1 (**12**), 127.4 (**13**), 125.7 (**14**), 125.6 (**15**, **16**), 99.6 (**17**), 72.1 (*para*-**18**), 68.5 (*meta*-**18**), 54.6 (**19**), 54.2 (**20**), 37.4 (**21**), 37.1 (**22**), 30.6, 30.5, 29.2, 28.4, 28.2, 28.1, 28.0, 28.0, 25.0, 25.0, 21.3, 21.3 (**23**), 13.0 (**24**) ppm; **FT-IR (ATR)**: ν = 3276, 2923, 2854, 1640, 1603, 1537, 1505, 1467, 1455, 1429, 1387, 1230, 1116, 697 cm^{-1} ; **MALDI-TOF**: m/z [M] $^{++}$ Calcd. 2471.65; found: 2471.05 [M] $^{++}$, 2494.07 [$\text{M}+\text{Na}$] $^{+}$; **elemental analysis**: Calcd. for $\text{C}_{153}\text{H}_{219}\text{N}_9\text{O}_{18}$: 74.33% C, 8.93% H, 5.10% N; found: 73.72% C, 8.85% H, 4.87% N.

N^{α} -(tert-Butyloxycarbonyl)- N^{ω} -(3,4,5-trioctyloxyphenyl)-L-alaninamide (**10b**)

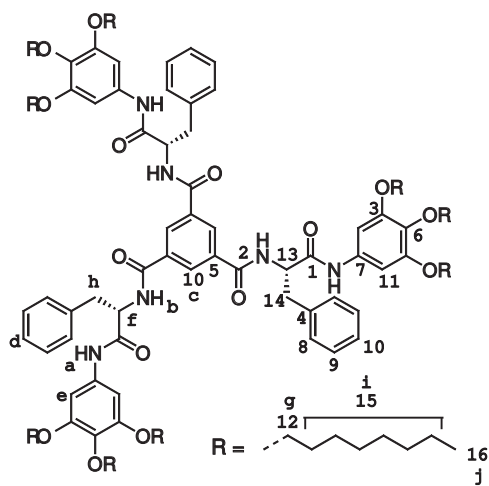


To a magnetically stirred solution of HBTU (0.48 g, 1.26 mmol) in dry dimethylformamide (2.5 mL), DiPEA (0.5 mL, 2.9 mmol) and Boc-L-AlaOH (0.21 g, 1.11 mmol) were added consecutively. This mixture was stirred for 5 min after which 3,4,5-trioctyloxyaniline (0.31 g, 0.65 mmol) was added. Stirring was continued overnight at room temperature. The reaction mixture was slowly added to a mixture of diethyl ether (25 mL), acidic water (pH < 3, 25 mL) and ice. The organic layer was washed with sat. KCl (15 mL), 1 N NaOH (3 \times 15 mL) and 10 mM NaHCO_3 (3 \times 15 mL) and dried over MgSO_4 . After evaporation, the crude product was purified by column chromatography (silica, 2% methanol in dichloromethane) to yield the pure compound as a purple, sticky oil (0.31 g, 0.48 mmol, 74%): $^1\text{H-NMR}$ (CDCl_3): δ = 8.22 (s, 1H, **a**), 6.78 (s, 2H, **b**), 4.93 (br s, 1H, **c**), 4.27 (bt, 1H, **d**), 4.0–3.8 (m, 6H, **e**), 1.9–0.8 (m, 48H, **f** {36H} + **g** {3H} + **h** {9H}), 0.88 (t, 9H, **i**) ppm; $^{13}\text{C-NMR}$ (CDCl_3): δ = 170.8 (**1**), 156.3 (**2**), 153.2 (**3**), 134.9 (**4**), 133.6 (**5**), 98.8 (**6**), 80.8 (**7**), 73.6 (**8**), 69.1 (**8**), 51.0 (**9**), 32.0, 32.0, 30.4, 29.7, 29.5, 29.4 (**10**), 28.4(**11**), 26.3, 26.2, 22.8, 22.8 (**10**), 17.6 (**12**), 14.2 (**13**) ppm; **FT-IR (ATR)**: ν = 3312, 2955, 2925, 2855, 1669, 1607, 1504, 1426, 1379, 1367, 1227, 1168, 1114 cm^{-1} ; **MALDI-TOF**: m/z [M] $^{++}$ Calcd. 648.51; found: 648.46 [M] $^{++}$; **elemental analysis**: Calcd. for $\text{C}_{38}\text{H}_{68}\text{N}_2\text{O}_6$: 70.33% C, 10.56% H, 4.32% N; found: 70.30% C, 10.51% H, 4.45% N.

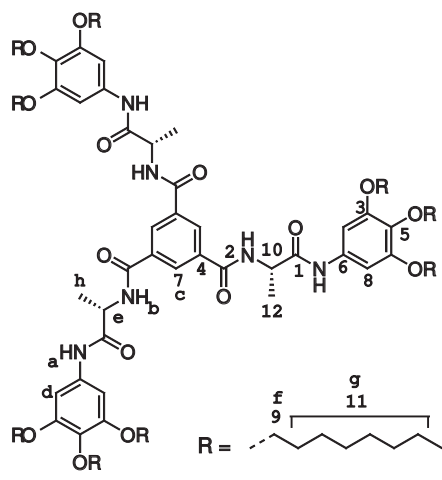
N^{ω} -(3,4,5-Trioctyloxyphenyl)-L-alaninamide (**11b**)



Compound **10b** (0.26 g, 0.40 mmol) was dissolved in TFA (4 mL). The solution was purged with argon for 15 min, after which the mixture was stirred for another 45 min. The reaction mixture was concentrated *in vacuo*. A mixture of ethyl acetate, 1 N NaOH and some ice was added and the layers were separated. The organic layer was washed with 1 N NaOH several times and dried over MgSO_4 . After evaporation, the pure title compound was isolated (0.20 g, 0.36 mmol, 90%): $^1\text{H-NMR}$ (CDCl_3): 9.35 (s, 1H, **a**), 6.88 (s, 2H, **b**), 4.0–3.8 (m, 6H, **c**), 3.60 (m, 1H, **d**), 1.9–1.2 (m, 41H, **e** {36H} + **f** {2H} + **g** {3H}), 0.86 (t, 9H, **h**) ppm; $^{13}\text{C-NMR}$ (CDCl_3): δ = 173.5 (**1**), 153.3 (**2**), 134.7 (**3**), 133.6 (**4**), 98.3 (**5**), 73.6 (**6**), 69.2 (**6**), 51.3 (**7**), 32.1, 32.0, 30.4, 29.7, 29.5, 29.4, 26.3, 26.2, 22.8 (**8**), 21.8 (**9**), 14.3 (**10**) ppm; **FT-IR (ATR)**: ν = 3299, 2925, 2855, 1724, 1675, 1601, 1527, 1505, 1424, 1378, 1227, 1114 cm^{-1} ; **MALDI-TOF**: m/z [$\text{M}+\text{H}$] $^{+}$ Calcd. 548.45; found: 548.40 [$\text{M}+\text{H}$] $^{+}$; **elemental analysis**: Calcd. for $\text{C}_{33}\text{H}_{60}\text{N}_2\text{O}_4$: 72.22% C, 11.02% H, 5.10% N; found: 72.00% C, 10.82% H, 5.12% N.

$N^\alpha, N^\omega, N^{\omega\omega}$ -(1,3,5-Benzenetricarbonyl)tris[N^ω -(3,4,5-trioctyloxyphenyl)]-L-phenylalaninamide (**3a**)

A solution of 1,3,5-benzenetricarbonyl trichloride (66.9 mg, 0.25 mmol) in dry dichloromethane (2.5 mL) was added dropwise to a solution of **8a** (0.49 g, 0.78 mmol) and triethylamine (0.3 mL, 2.2 mmol) in dry dichloromethane (7.5 mL). After stirring overnight and evaporation of the dichloromethane the crude product was purified by column chromatography (silica, ethyl acetate/pentane 4/1; silica, methanol in dichloromethane (gradient 0–2%). Subsequently, recrystallization from a mixture of tetrahydrofuran/methanol (4/7) afforded the pure title compound as an off-white solid material (0.19 g, 0.19 mmol, 76%). The product was characterized by GPC (THF, 260 nm, purity based on UV > 99%): $^1\text{H-NMR}$ (DMSO- d_6 , T = 373 K): δ = 9.74 (s, 3H, **a**), 8.58 (d, 3H, *J* = 7.5 Hz, **b**), 8.34 (s, 3H, **c**), 7.4–7.1 (m, 15H, **d**), 6.96 (s, 6H, **e**), 4.95 (q, 3H, **f**), 4.0–3.6 (m, 18H, **g**), 3.3–3.0 (m, 6H, **h**), 2.0–1.0 (m, 108H, **i**), 0.87 (t, 27H, **j**) ppm; $^{13}\text{C-NMR}$ (DMSO- d_6 , T = 323 K): δ = 169.5 (**1**), 165.5 (**2**), 152.2 (**3**), 137.7 (**4**), 134.3 (**5**), 134.2 (**6**), 133.5 (**7**), 129.0 (**8**), 128.0 (**9**), 126.1 (**10**), 98.5 (**11**), 72.3 (*para*-**12**), 68.2 (*meta*-**12**), 55.6 (**13**), 37.3 (**14**), 31.1, 31.0, 29.6, 28.7, 28.7, 28.5, 28.5, 25.4, 25.4, 21.9, 21.8 (**15**), 13.6 (**16**) ppm; FT-IR (ATR): ν = 3263, 2956, 2923, 2854, 1646, 1604, 1536, 1505, 1428, 1386, 1229, 1115, 699 cm^{-1} ; MALDI-TOF: m/z [M] $^{+}$ Calcd. 2030.45; found: 2030.68 [M] $^{+}$; elemental analysis: Calcd. for $\text{C}_{126}\text{H}_{192}\text{N}_6\text{O}_{15}$: 74.52% C, 9.53% H, 4.14% N; found: 74.21% C, 9.45% H, 4.15% N.

 $N^\alpha, N^\omega, N^{\omega\omega}$ -(1,3,5-Benzenetricarbonyl)tris[N^ω -(3,4,5-trioctyloxyphenyl)]-L-alaninamide (**3b**)

A solution of 1,3,5-benzenetricarbonyl trichloride (24.7 mg, 0.09 mmol) in dichloromethane (0.9 mL) was added dropwise to a solution of **11b** (0.16 g, 0.29 mmol) and triethylamine (0.1 mL, 0.7 mmol) in dry dichloromethane (2.9 mL). After stirring overnight and evaporation of the dichloromethane, the compound was separated from the crude mixture by column filtration (silica, methanol in dichloromethane (gradient 0–2%) and ethyl acetate/pentane 1/1). Subsequently, repetitive recrystallization from a mixture of tetrahydrofuran/methanol (1/3) afforded the pure title compound as a light pink solid material (0.11 g, 0.06 mmol, 67%). The product was characterized using GPC (THF, 260 nm, purity based on UV ~ 100%): $^1\text{H-NMR}$ (DMSO- d_6 , T = 373K): δ = 9.61 (s, 3H, **a**), 8.42 (d, 3H, *J* = 7.2 Hz, **b**), 8.50 (s, 3H, **c**), 6.96 (s, 6H, **d**), 4.69 (quintet, 3H, **e**), 4.0–3.7 (m, 18H, **f**), 1.8–1.0 (m, 117H, **g** {108H} + **h** {9H}), 0.84 (t, 27H, **i**) ppm; $^{13}\text{C-NMR}$ (DMSO- d_6 , T = 373K): δ = 170.3 (**1**), 165.1 (**2**), 152.0 (**3**), 134.2 (**4**), 134.1 (**5**), 133.9 (**6**), 128.7 (**7**), 99.1 (**8**), 72.1 (*para*-**9**), 68.4 (*meta*-**9**), 49.6 (**10**), 30.7, 30.7, 29.3, 28.5, 28.4, 28.2, 28.1, 28.1, 25.1, 25.1, 21.5 (**11**), 17.4 (**12**), 13.2 (**13**) ppm; FT-IR (ATR): ν = 3293, 2955, 2924, 2855, 1651, 1604, 1531, 1504, 1467, 1426, 1380, 1223, 1111 cm^{-1} ; MALDI-TOF: m/z [M] $^{+}$ Calcd. 1802.35; found: 1802.40 [M] $^{+}$; elemental analysis: Calcd. for $\text{C}_{108}\text{H}_{180}\text{N}_6\text{O}_{15}$: 71.96% C, 10.06% H, 4.66% N; found: 71.36% C, 9.81% H, 4.53% N.

2.7 References and notes

- [1] C. Moberg, *Angew. Chem.* **1998**, *110*, 260–281; *Angew. Chem., Int. Ed.* **1998**, *37*, 248–268.
- [2] S.E. Gibson, M.P. Castaldi, *Chem. Commun.* **2006**, 3045–3062.
- [3] S.E. Gibson, M.P. Castaldi, *Angew. Chem.* **2006**, *118*, 4834–4837; *Angew. Chem., Int. Ed.* **2006**, *45*, 4718–4720.
- [4] E. Fan, J. Yang, S.J. Geib, T.C. Stoner, M.D. Hopkins, A.D. Hamilton, *J. Chem. Soc., Chem. Commun.* **1995**, 1251–1252.
- [5] M.P. Lightfoot, F.S. Mair, R.G. Pritchard, J.E. Warren, *Chem. Commun.* **1999**, 1945–1946.
- [6] Y. Matsunaga, N. Miyajima, Y. Nakayasu, S. Sakai, M. Yonenaga, *Bull. Chem. Soc. Jpn.* **1988**, *61*, 207–210.
- [7] Y. Yasuda, E. Ishi, H. Inada, Y. Shirota, *Chem. Lett.* **1996**, 575–576.
- [8] K. Hanabusa, C. Kato, M. Kimura, H. Shirai, A. Takechi, *Chem. Lett.* **1997**, 429–430.
- [9] S.Y. Ryu, S. Kim, J. Seo, Y.-W. Kim, O.-H. Kwon, D.-J. Jang, S.Y. Park, *Chem. Commun.* **2004**, 70–71.
- [10] S.J. Lee, C.R. Park, J.Y. Chang, *Langmuir* **2004**, *20*, 9513–9519.
- [11] K.J.C. van Bommel, C. van der Pol, I. Muizebelt, A. Friggeri, A. Heeres, A. Meetsma, B.L. Jeringa, J. van Esch, *Angew. Chem.* **2004**, *116*, 1695–1699; *Angew. Chem., Int. Ed.* **2004**, *43*, 1663–1667.
- [12] T.-Q. Nguyen, R. Martel, P. Avouris, M.L. Bushey, L. Brus, C. Nuckolls, *J. Am. Chem. Soc.* **2004**, *126*, 5234–5242.
- [13] P.P. Bose, M.G.B. Drew, A.K. Das, A. Banerjee, *Chem. Commun.* **2006**, 3196–3198.
- [14] M. de Loos, *Thesis: Hydrogen-bonded low molecular weight gelators*; University of Groningen: Groningen (The Netherlands), **2005**.
- [15] A.R.A. Palmans, J.A.J.M. Vekemans, E.E. Havinga, E.W. Meijer, *Angew. Chem.* **1997**, *109*, 2763–2765; *Angew. Chem., Int. Ed.* **1997**, *36*, 2648–2651.
- [16] A.R.A. Palmans, J.A.J.M. Vekemans, R.A. Hikmet, H. Fischer, E.W. Meijer, *Adv. Mater.* **1998**, *10*, 873–876.
- [17] E.W. Meijer, J.A.J.M. Vekemans, A.R.A. Palmans, P. Breure, J. de Kraker, L. Brunsveld, *Polym. Prepr.* **2000**, *41*, 902–903.
- [18] J. van Herrikhuyzen, P. Jonkheijm, A.P.H.J. Schenning, E.W. Meijer, *Org. Biomol. Chem.* **2006**, *4*, 1539–1545.
- [19] J.J. van Gorp, J.A.J.M. Vekemans, E.W. Meijer, *J. Am. Chem. Soc.* **2002**, *124*, 14759–14769.
- [20] 3,4,5-Trioctyloxylaniline was synthesized as described for 3,4,5-tridodecyloxylaniline by K. Pieterse, *Thesis: Electron deficient materials based on azaheterocycles*, Eindhoven University of Technology, Eindhoven (The Netherlands), **2001**. The obtained data correspond to those described for the compound by A. Zinsou, M. Veber, H. Strzelecka, C. Jallabert, P. Fourré, *New J. Chem.* **1993**, *17*, 309.
- [21] K. Pieterse, *Thesis: Electron deficient materials based on azaheterocycles*, Eindhoven University of Technology, Eindhoven (The Netherlands), **2001**.
- [22] X. Lou, K.P. van den Hout, M.H.C.J. van Houtem, J.L.J. van Dongen, J.A.J.M. Vekemans, E.W. Meijer, *J. Mass Spectrom.* **2006**, *41*, 659–669.
- [23] Y. Okada, *Curr. Org. Chem.* **2001**, *5*, 1–43.
- [24] A. Berkessel, F. Cleemann, S. Mukherjee, T.N. Müller, J. Lex, *Angew. Chem.* **2005**, *117*, 817–821; *Angew. Chem., Int. Ed.* **2005**, *44*, 807–811.
- [25] K. Gottwald, D. Seebach, *Tetrahedron* **1999**, *55*, 723–738.

3

Self-assembly of peptide discotics with aliphatic solubilizing tails

Characterization in the neat state and in solution

ABSTRACT: *The self-assembly of C_3 -symmetrical molecules that consist of a 1,3,5-benzenetricarboxamide core extended with three peptide fragments decorated with peripheral mesogenic groups containing aliphatic solubilizing tails is described. Small structural modifications in the peptide fragments have been applied to demonstrate their influence on the stability of the self-assembled structures. Seven dipeptide discotics have been investigated, all with different combinations of glycine and L- and/or D-phenylalanine. Characterization of these discotics in the neat state using DSC and polarized optical microscopy (POM) and in solution with CD, UV/Vis, $^1\text{H-NMR}$ and IR reveals that there is a clear upward trend in the stack stability, going from the glycine-phenylalanine combinations to the phenylalanine-phenylalanine motifs. A larger hydrophobic core and additional π - π interaction contribute to enhanced stability of the stacks. In addition, stacking properties of two mono-peptide discotics containing an L-phenylalanine or an L-alanine fragment have been investigated and compared, both in the neat state and in solution. It is unambiguously shown that the L-phenylalanine based discs form more stable stacks compared to the L-alanine based discs.*

* Part of this work has been published: K.P. van den Hout, R. Martín-Rapún, J. A. J. M. Vekemans, E. W. Meijer, *Chem. Eur. J.* **2007**, *13*, 8111–8123.

3.1 Introduction

Self-assembled architectures are envisioned to serve as important building blocks in the fields of biology as well as material science.^[1-11] The interplay of secondary interactions fulfils a key role in the formation of stable conformers that still can express their reversible nature. It is known that minor changes in the molecule may dramatically influence the subtle balance of non-covalent interactions between molecules, in the most extreme cases resulting in the loss of reversibility or in preventing the formation of stable self-assembled structures.^[12-16] The challenge is to develop new molecules that self-assemble and allow functionalization and fine-tuning of the structure in an easily accessible manner.

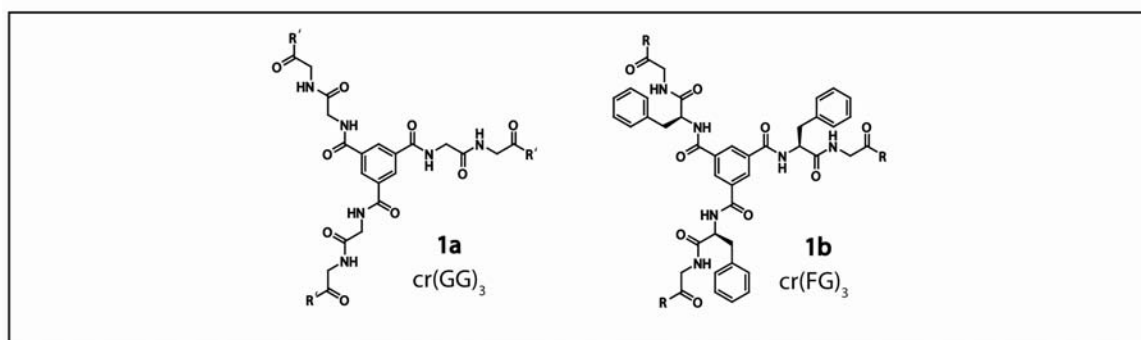
Peptide fragments are widely used as structuring elements in self-assembled architectures for their biocompatibility, hydrogen-bonding properties and versatile nature.^[17-25] Amphiphilic dendritic dipeptides that self-assemble into helical pores have been described by Percec and coworkers.^[26] Stupp and collaborators have reported peptide amphiphiles that self-assemble into nanofibers and they demonstrate the ability of such systems to tolerate chemical modifications by changing the peptide sequence.^[27] In the group of Van Esch excellent low molecular weight hydrogelators have been developed that possess a cyclohexane core extended with peptides.^[28] They show that the properties of the gels can easily be tuned by changing the hydrophobic substituents or the number of hydrogen bonding moieties. Recently, Kimizuka and coworkers have also reported C_3 -symmetrical conjugates that bear three β -sheet forming peptides (FKFEFKFE) that form anti-parallel β -sheets in water.^[29] These C_3 -symmetrical peptide conjugates spontaneously self-assemble into virus-sized peptide nanospheres.

In our laboratory, the self-assembly of various 1,3,5-benzenetricarboxamide derivatives, which have a strong tendency to form columnar aggregates in solution, has been extensively studied.^[30-33] In our present design the 1,3,5-benzenetricarboxamide centre is extended with peptide fragments providing additional driving forces for self-assembly (like hydrogen bonding and π - π interaction).

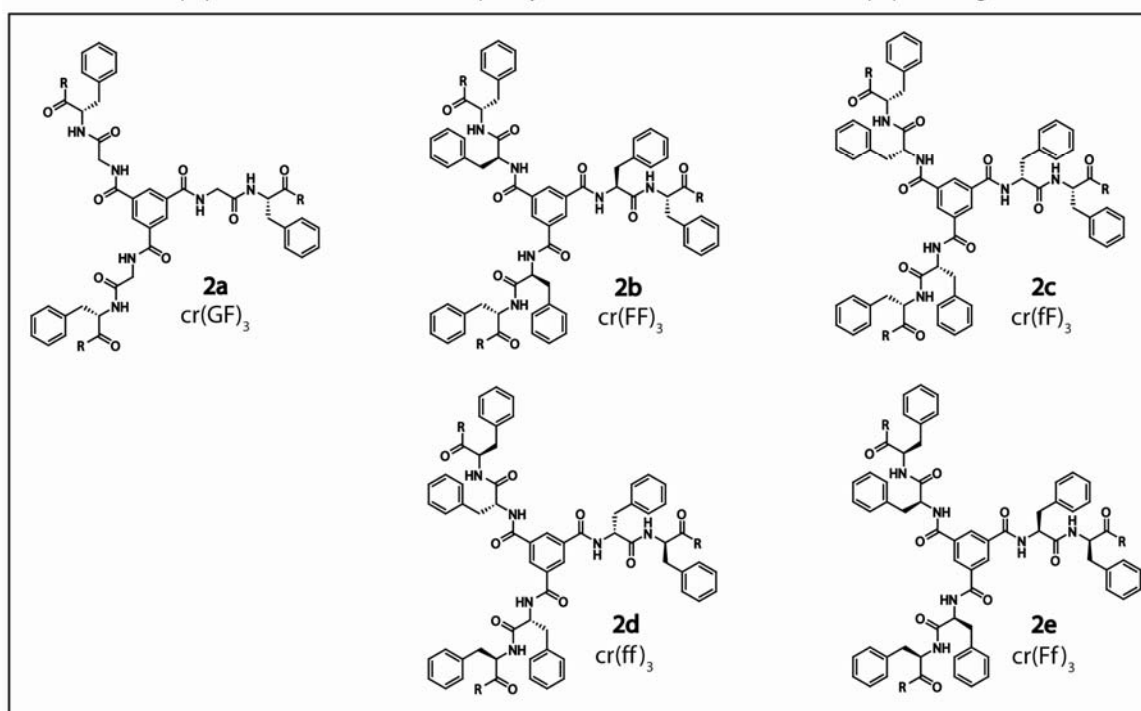
In this Chapter, the self-assembly behaviour of all nine peptide discotics introduced in the previous Chapter (Figure 1) will be evaluated. The self-assembly processes of all these molecules are studied in the neat state using DSC, POM and XRD as well as in solution with CD, UV/Vis, low concentration $^1\text{H-NMR}$ and IR spectroscopy.

Library of discs

Dipeptide discotics with an achiral glycine at the C-terminus of the dipeptide fragment



Dipeptide discotics with a chiral phenylalanine at the C-terminus of the peptide fragment



Monopeptide discotics

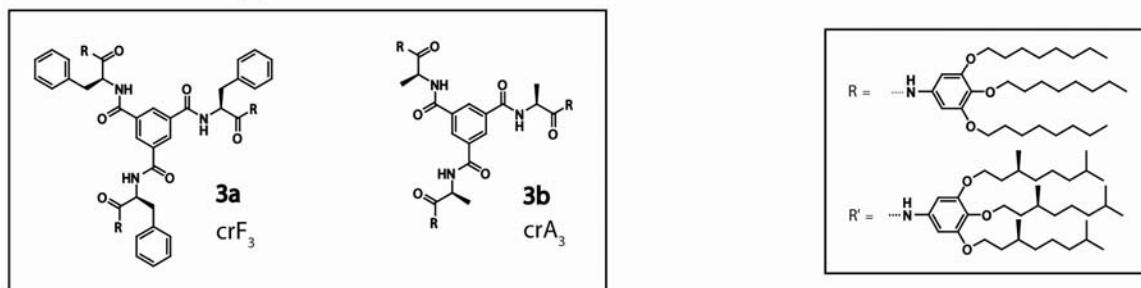


Figure 3.1 Library of peptide discotics; G = glycine, F = L-phenylalanine, f = D-phenylalanine, A = alanine, cr = 1,3,5-benzenetricarbonyl core.

3.2 Self-assembly behaviour of dipeptide discotics in the neat state

The self-assembly behaviour of all dipeptide discotics was examined in the neat state with DSC and POM.^[34] Some of the discotics were also investigated with XRD. The DSC data of the second heating run (rate 10 °C·min⁻¹) for dipeptide discotics **1a,b** and **2a–e** are depicted in Table 3.1.

Table 3.1 The onsets of the transitions (T_{onset} [°C]) and the corresponding enthalpies (ΔH [kJ·mol⁻¹]) for compounds **1a,b** and **2a–e** (second heating run; 10 °C·min⁻¹).^[a]

Compound		T_{onset} [°C]	ΔH [kJ·mol ⁻¹]	
1a = cr(GG) ₃	G ^[b]	113	-	M ^[c]
1b = cr(FG) ₃	K*	133	14	I
2a = cr(GF) ₃	K*	186	18	I
2b = cr(FF) ₃	K*	115 ^[d]	6.8	M ^[c]
2c = cr(ff) ₃	K*	175/186 ^[e]	16 ^[e]	I
2d = cr(ff) ₃	- ^[f]	-	-	- ^[c]
2e = cr(Ff) ₃	K* ^[g]	175/184 ^[e]	13 ^[e]	I

[a] - = phase is not observed; K* = crystalline-like phase with a low degree of order; M = unidentified mesophase; I = isotropic phase; [b] A T_g is observed at 113 °C; [c] The clearing is accompanied by decomposition of the sample; [d] Temperature of transition maximum instead of transition onset; [e] The onset temperatures of overlapping peaks with corresponding total enthalpy; [f] Cooling the sample to -100 °C did not show any transition; [g] An enantiotropic transition with an onset at 110(0.7) was present, probably originating from an undetectably small amount of impurity.

Polarized optical microscopy (POM) showed that compound **1a** melted at 240 °C, but the clearing was accompanied by decomposition of the sample; therefore we measured DSC up to 220 °C. Upon heating the sample from -100 to 220 °C a glass transition temperature was found at 113 °C. Compound **1b** was heated in the second run at a rate of 10 °C·min⁻¹ from -100 to 160 °C and exhibited a transition to the isotropic state with an onset at 133 °C. Upon cooling, a transition at 132 °C was observed. Remarkably, no hysteresis of the transition was observed upon cooling, which normally indicates a transition into a mesophase instead of a transition into a crystalline phase. However, slowly cooling from the isotropic state did not afford an LC-texture for **1b** and it was also not possible to induce formation of the mesophase by pressing on the sample. XRD data, discussed later on, showed that this crystalline-like phase showed a low degree of order—Hence, this phase is referred to as K* (Table 3.1)—Discotic **2a** was heated at a rate of 10 °C·min⁻¹ from -100 to 230 °C and showed a broad K*–I transition at 186 °C. The cooling run, in contrast, showed a sharp transition with an onset at

176 °C. Polarized optical microscopy pointed out that a monotropic mesophase was present at around 202 °C. The texture of the mesophase could be grown as is shown in Figure 3.2. Probably, the enthalpy associated to this I–M transition was too small to be detected with DSC.

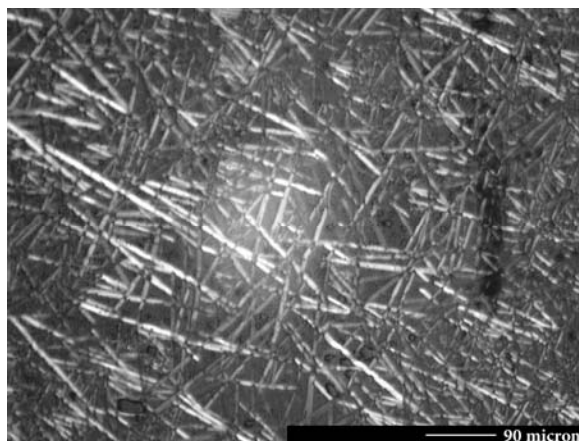


Figure 3.2 Polarized optical microscopy texture of compound **2a** at 187 °C.

Homochiral enantiomers $cr(FF)_3$ (**2b**) and $cr(ff)_3$ (**2d**) started to show some decomposition around 240 °C, before reaching the clearing point (around 305 °C); therefore these discotics were heated from –100 to 220 °C in DSC. Discotic **2b** showed a reversible transition with a maximum at 115 °C in the heating run and a maximum at 107 °C in the cooling run. Surprisingly, enantiomer **2d** did not exhibit any transition upon cooling to –100 °C. Heterochiral enantiomers $cr(fF)$ (**2c**) and $cr(Ff)_3$ (**2e**) melted around 200 °C. Upon heating discotic **2e** from –100 to 220 °C three transitions could be discerned, a small transition with a maximum at 110 °C and a transition that was overlapping the transition to the isotropic state with an onset at 175 °C. Upon cooling, just one I–K* transition was observed with a maximum at 153 °C. The DSC curve of discotic **2c** was similar to the one of **2e**, except for the small transition at 110 °C in the heating run, which was missing. Most likely, this small peak originated from a small amount of impurity, which could not be detected by MALDI-TOF MS and GPC.

Dipeptide discotics **1a,b** and **2a,b,e** have also been investigated with XRD. The data are gathered in table 3.2. The XRD patterns of compounds **1a,b** consist of an intense peak and a diffuse halo in the small and the wide angle region, respectively. The position of the former is temperature-independent up to the clearing point and corresponds to a distance of 32 Å for **1a** and 27 Å for **1b**, which are in the range of the diameters of the molecules. The diffuse halo is attributed to the aliphatic chains in the periphery although the associated spacings, 4.8 Å for **1a** and 4.6 Å for **1b** at room temperature, are somehow larger than the expected 4.4–4.6 Å. Increasing the temperature leads to an increase in the distance corresponding to the halo.

Table 3.2 XRD data of the compounds **1a,b** and **2a,b,e**.

Compound	T (°C)	d (Å) ^[a]
1a = cr(GG) ₃	25	32.7 (s), 4.8 (h)
	130	32.4 (s), 4.9(h)
1b = cr(FG) ₃	25	26.5 (s), 4.6 (h)
	152	27.2 (s), 4.8 (h)
2a = cr(GF) ₃	Pristine	36.8 (s), 17.8 (b), 4.5 (h)
	200	29.2 (s), 17.5 (b), 4.9 (h)
	25	28.1 (s), 16.2 (b), 4.5 (h)
2b = cr(FF) ₃	64	30.0 (b), 15.8 (b), 4.9 (h)
	120	30.8 (b), 16.0 (b), 4.9 (h)
2e = cr(Ff) ₃	25	34.9 (s), 4.9 (h)
	211	21.8 (b), 5.0 (h)

^[a] s = sharp; b = broad; h = halo.

The pattern of compound **2a** in the virgin state exhibits an intense peak corresponding to 37 Å and a hump centred at 17.8 Å in the small angle region and a non-symmetric halo in the wide angle region, with its centre corresponding to 4.5 Å and a sharper edge towards smaller angles. When heated above the isotropization temperature of 186 °C, the new phase exhibits the same pattern, but with the intense peak corresponding to 28–29 Å; and the hump becoming weaker and broader. The diffuse halo becomes symmetric and the distance associated with it increases to 4.9 Å. Upon cooling back to room temperature the spacing of the peak remains at 28–29 Å, the hump is recovered as a broad peak with a spacing of 16 Å and the diffuse halo moved back to 4.5 Å. The XRD pattern of **2b** stays invariant from room temperature to 190 °C. No change is observed when the compound undergoes the DSC transition at 115 °C. The XRD pattern comprises two broad peaks with spacings in an approximate ratio 2:1, at 30 and 16 Å. In the wide angle region the halo is not symmetric and exhibits a sharper edge towards the smaller angles. The XRD pattern of compound **2e** shows an intense peak of which the corresponding spacing increases from 35 Å at room temperature to 41 Å at 185 °C. However, at a temperature as high as 211 °C there is a second phase, as is proven by an intense peak appearing with a smaller spacing (~22 Å) than the original peak, still present at this temperature but vanishing with time or upon further heating. Upon cooling to room temperature the pattern of the pristine sample is recovered.

It has to be noted that the spacing corresponding to the diffuse halo is in all cases larger than expected for the molten alkyl chains in a liquid crystalline phase. The lack of reflections prevents the assignment of any phase, but also excludes a well-ordered crystalline state for all of the compounds. In some cases the intense reflection in the small angle region corresponds to a spacing comparable to the expected diameter of these molecules, pointing to a columnar phase, which would be disordered in any case due to the absence of a peak corresponding to a spacing of 3.3–4.0 Å. Another remarkable observation, which holds for all

presented materials, is that the XRD patterns do not disappear at temperatures well above the clearing point as measured by POM. This behaviour has been previously reported^[35-37] and has been attributed to the persistence of local stacking of discs above the clearing point.

3.3 Self-assembly behaviour of dipeptide discotics in solution

The self-assembly behaviour of all dipeptide discotics was examined in dilute solutions in chloroform and in heptane with CD, UV/Vis, ¹H-NMR and IR. From ordinary solubility experiments it became clear that a trend in aggregate stability was noticeable. Compounds cr(FF)₃ (**2b**) and cr(ff)₃ (**2d**), both containing two phenylalanines with equal chirality, were neither soluble in chloroform nor in heptane, even at concentrations in the micromolar range. Therefore, it was not possible to characterize these discotics in solution. Discotics cr(fF)₃ (**2c**) and cr(Ff)₃ (**2e**), both having two phenylalanines with opposite chirality, were only soluble in chloroform and not in heptane. Disc cr(GF)₃ (**2a**) was soluble in both solvents, but to dissolve **2a** in heptane external heating was needed. Finally, dipeptide discotics cr(GG)₃ (**1a**) and cr(FG)₃ (**1b**), which contain a glycine at the C-terminus of the dipeptide fragments were easily soluble in both solvents.

The CD and UV/Vis spectra of discotics **1a,b** and **2a,c,e** in chloroform and of **1a,b** and **2a** in heptane are shown in Figure 3.3. Compound **1a** does not show a Cotton effect in heptane or in chloroform. Presumably, the glycyglycine tails are too flexible, which makes it impossible to transfer the chiral information embedded in the alkyl chains to a higher level of organization. In heptane, **1b** induces a coupled CD curve centred at 242 nm with a negative extreme at 255 nm and a positive extreme at 234 nm, while in chloroform a much smaller CD effect is observed with a negative extreme at 262 nm. Compound **2a** also shows a coupled CD curve in heptane, of which the effect is even stronger compared to **1b**. This curve is centred at 235 nm and shows a broad negative CD band around 263 nm. The CD spectrum of **2a** in chloroform is less active than the CD spectrum in heptane, as is also observed for discotic **1b**. Compound **2c** shows a Cotton effect in chloroform that decreases going to lower wavelengths, while compound **2e** in chloroform shows a Cotton effect that increases going to lower wavelengths. From Figure 3.3 it can be deduced that the CD spectra of **2c** and **2e** are mirror images, as is expected for enantiomers. Obviously, they form chiral assemblies with reversed helicity.

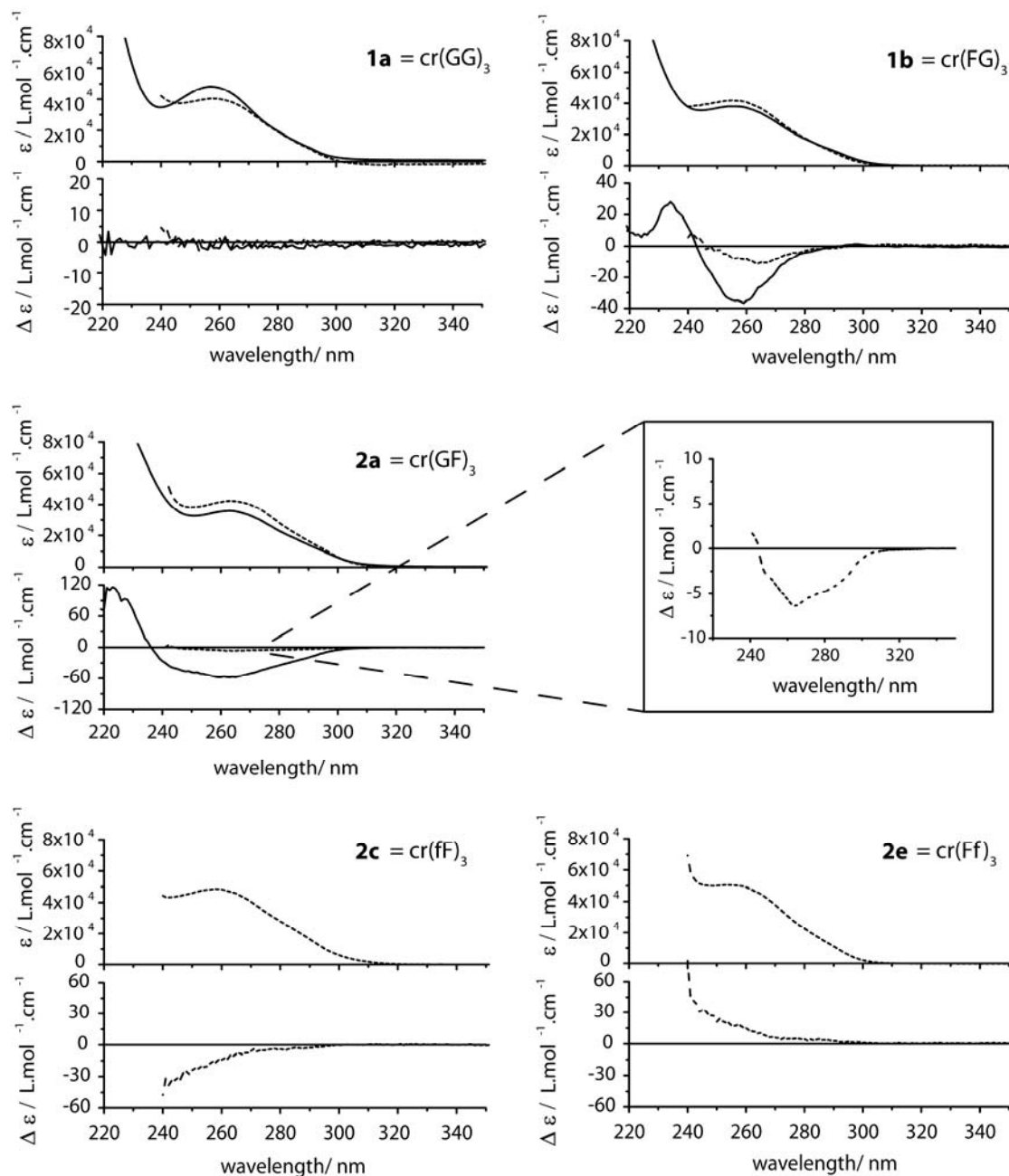
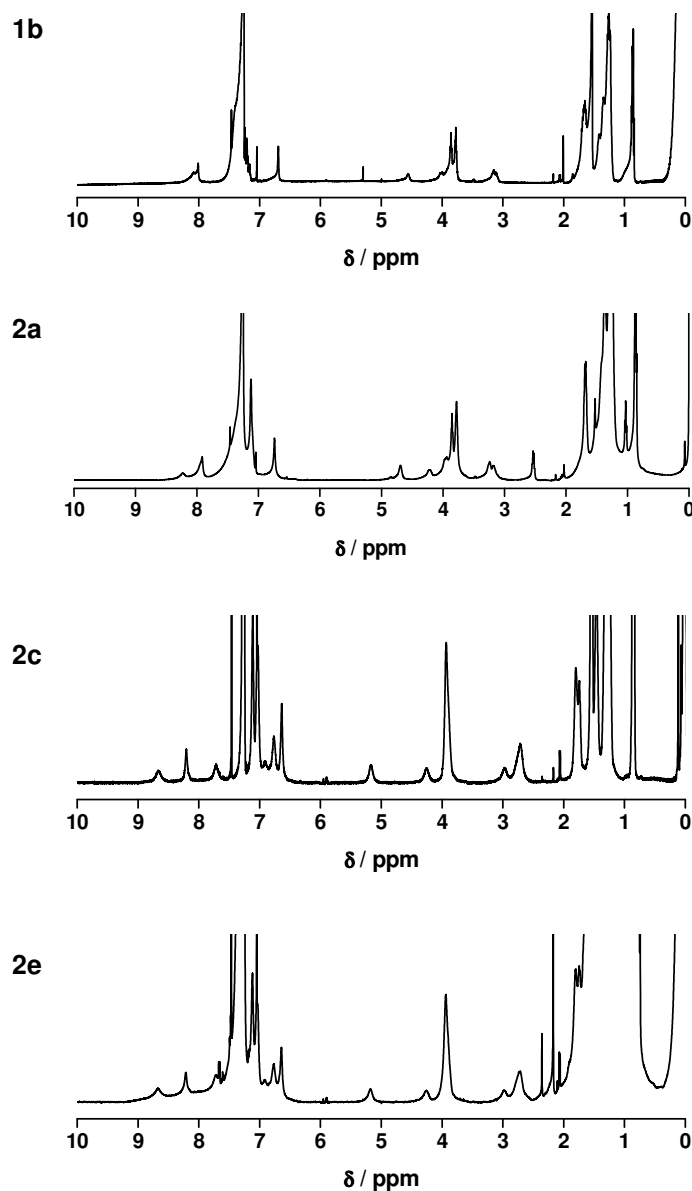


Figure 3.3 UV/Vis and CD spectra for dipeptide discotics **1b** and **2a,c,e** in heptane, 4×10^{-5} M (solid line) and chloroform, 4×10^{-5} M (dashed line). The insertion in the graph of **2a** is an enlargement of the CD spectrum of **2a** in chloroform.

Temperature-dependent CD and UV/Vis measurements reveal that discotics **1b** and **2a,c,e** do not show a temperature-dependent behaviour in chloroform. To investigate whether the weak, temperature insensitive Cotton effects in chloroform originate from molecularly dissolved discotics or less ordered self-assembled structures, IR spectra in chloroform (Table 3.3) and $^1\text{H-NMR}$ spectra in deuterated chloroform (Figure 3.4) have been recorded.

Table 3.3 Wavenumbers ν [cm^{-1}] of the N–H stretch vibrations of **1b** and **2a,c,e** in the solid state and in 2×10^{-5} M solutions in chloroform at 20 °C.

Compound	1b = cr(FG) ₃	2a = cr(GF) ₃	2c = cr(fF) ₃	2e = cr(Ff) ₃
ν solid state	3315	3300	3267	3276
ν chloroform	3322	3327	3322	3322

**Figure 3.4** ¹H-NMR spectra at 25 °C of compounds **1b** and **2a,c,e**; 2×10^{-5} M in CDCl₃.

The measurements have been performed on solutions with concentrations similar to those used for the CD measurements. The ¹H-NMR measurements suggest that assemblies are still present, because all peaks in the spectra are broadened as can clearly be deduced from the

signals above 7.5 ppm, corresponding to the chemical shifts of the aromatic protons of the core and the protons of the amide groups. IR experiments support this hypothesis, since the N–H stretch vibrations in chloroform are very broad for all samples measured. The optimum of the broad peak can in general be found around 3322 cm^{-1} , which is indicative for hydrogen bonding.

CD and UV/Vis measurements reveal that solutions of discs $\text{cr}(\text{FG})_3$ (**1b**) and $\text{cr}(\text{GF})_3$ (**2a**) in heptane do show a temperature-dependent Cotton effect, while the optical density is not temperature-dependent. The graphs depicted in Figure 3.5 are heating curves of compounds **1b** and **2a**, starting from $10\text{ }^\circ\text{C}$ to $80\text{ }^\circ\text{C}$ in steps of $10\text{ }^\circ\text{C}$. The heating curve of discotic **1b** shows two plateaus, one at low temperatures with $\Delta\varepsilon = -36\text{ L}\cdot\text{mol}^{-1}\text{cm}^{-1}$ and one at higher temperatures with $\Delta\varepsilon = -13\text{ L}\cdot\text{mol}^{-1}\text{cm}^{-1}$, and a melting temperature around $62\text{ }^\circ\text{C}$. The cooling curve of discotic **1b** lies exactly on top of the heating curve and these temperature scans are reproducible, meaning that the system is in thermodynamic equilibrium. The heating curve of discotic **2a** only shows a plateau at low temperatures with $\Delta\varepsilon = -53\text{ L}\cdot\text{mol}^{-1}\text{cm}^{-1}$. At $80\text{ }^\circ\text{C}$, the second plateau is still not reached. Furthermore, the cooling curve of disc **2a** is completely different from the heating curve and is not reproducible at all, suggesting that this molecule possesses a complex energy landscape with multiple kinetic minima.

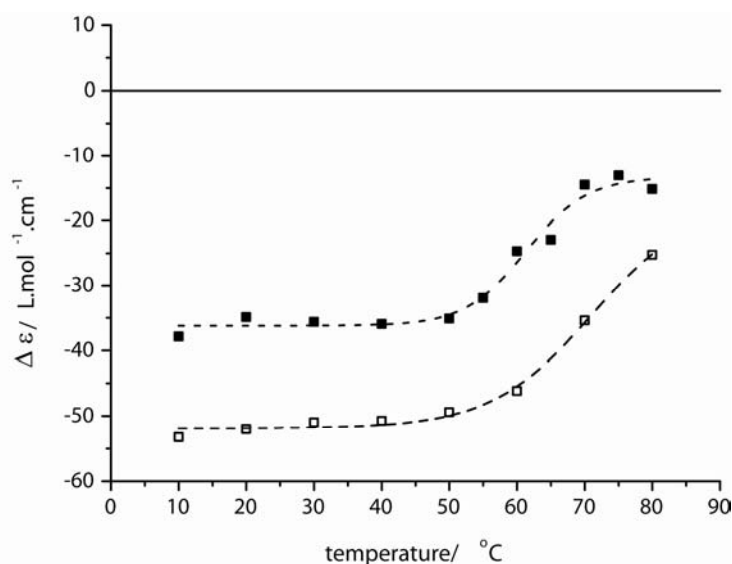


Figure 3.5 Temperature-dependent CD measurements for compounds **1b** (solid squares) and **2a** (open squares) at $\lambda = 255\text{ nm}$ and $\lambda = 263\text{ nm}$ respectively, in heptane, $2 \times 10^{-5}\text{ M}$ from $10\text{ }^\circ\text{C}$ to $80\text{ }^\circ\text{C}$ in steps of $10\text{ }^\circ\text{C}$.

IR and $^1\text{H-NMR}$ spectroscopy have been used to judge whether helically ordered assemblies or molecularly dissolved discotics of compounds **1b** and **2a** are present at $70\text{ }^\circ\text{C}$.

The IR spectra have been taken in heptane, while the $^1\text{H-NMR}$ spectra have been measured in deuterated cyclohexane, both at concentrations similar to those used in the CD measurements. According to the N–H stretch vibrations of **1b** and **2a**, which appear as sharp peaks at 3286 cm^{-1} and 3272 cm^{-1} , respectively, hydrogen bonding is still present at $70\text{ }^\circ\text{C}$ suggesting that assemblies are still present (Table 3.4).

Table 3.4 Wavenumbers ν [cm^{-1}] of the N–H stretch vibrations of **1b** and **2a** in the solid state and in $2 \times 10^{-5}\text{ M}$ solutions in heptane at $70\text{ }^\circ\text{C}$.

Compound	1b = cr(FG) ₃	2a = cr(GF) ₃
ν solid state	3315	3300
ν heptane	3286	3272

The completely broadened $^1\text{H-NMR}$ spectra in deuterated cyclohexane at $70\text{ }^\circ\text{C}$ (Figure 3.6) also confirm this observation. Presumably, the deaggregation of the stacks in heptane is a multiple-step process of which just the first step, going from ordered to less ordered assemblies, can be monitored with CD due to the restricted temperature window. This also explains why the optical density is not temperature-dependent in this temperature frame.

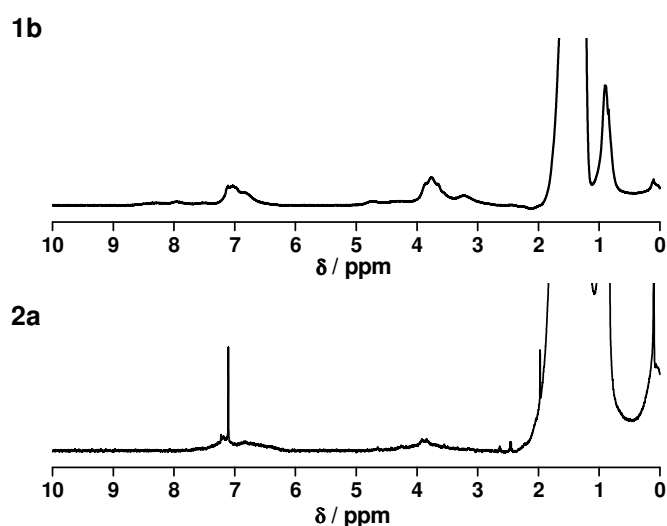


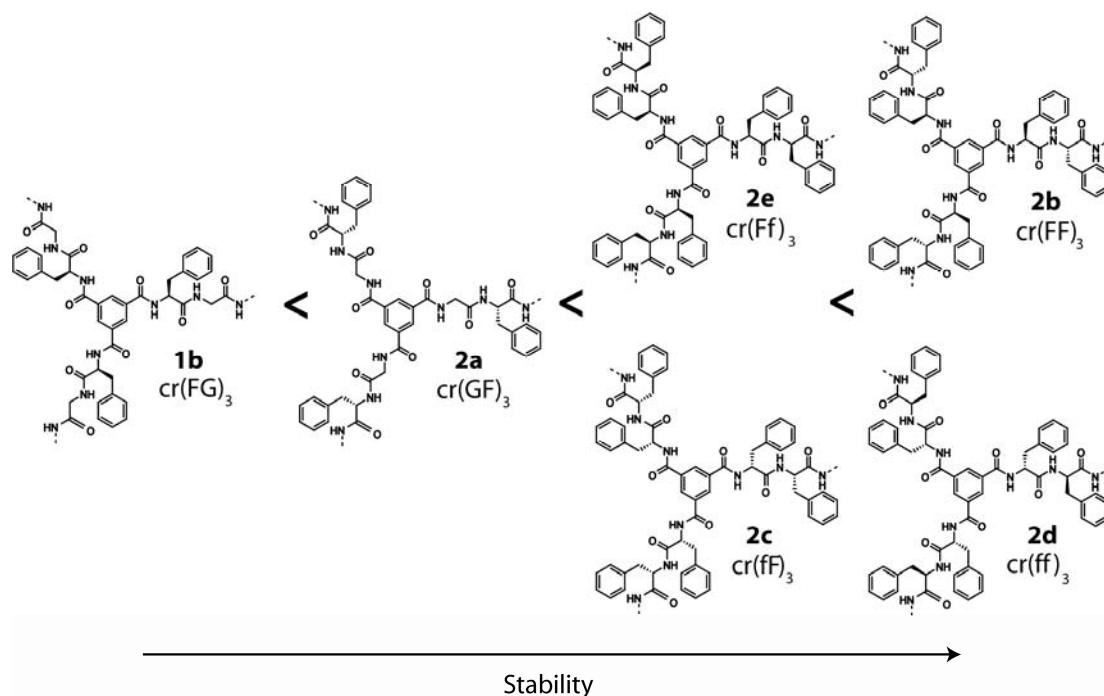
Figure 3.6 $^1\text{H-NMR}$ spectra at $70\text{ }^\circ\text{C}$ for compounds **1b**, $2 \times 10^{-5}\text{ M C}_6\text{D}_{12}$ and **2a**, $2 \times 10^{-5}\text{ M C}_6\text{D}_{12}$.

In general, the UV/Vis and CD measurements in combination with IR and $^1\text{H-NMR}$ demonstrate that discotics **1b** and **2a,c,e** do aggregate and that it is impossible to reach the molecularly dissolved state, even in chloroform at $50\text{ }^\circ\text{C}$. The transition observed in the

temperature-dependent CD measurements of **1b** in heptane appears to be a transition from an ordered self-assembled state to a less ordered one. It is proven that **1b** is in thermodynamic equilibrium during this transition, while **2a** is not. An explanation for the different behaviour of **1b** and **2a** may be embedded in the structure of the molecules. They both contain a 1,3,5-benzenetriscarboxamide centre that favours to self-assemble in a ship-screw fashion, in order to make sure that both π - π interaction and hydrogen bonding can take place. They also contain a dipeptide fragment of which it is known that it prefers to form hydrogen bonds perpendicular to its backbone, like in a β -sheet. This may result in an ongoing competition between the centre of the discotic and the dipeptide fragment depending on the strength of the interactions of the different moieties. For compound **1b**, there is apparently one dominant conformation. This probably means that the supramolecular interactions of either the 1,3,5-benzenetriscarboxamide centre or the dipeptide fragment are far more dominant, so competition is not an issue. In the case of **2a** there is obviously competition, meaning that the strengths of the interactions are in the same order of magnitude.

3.4 Stability of assemblies of dipeptide discotics

It has been demonstrated that the stability of all dipeptide assemblies is very high, nevertheless, a clear trend in stability of the stacks can be observed. Characterization in the neat state points out that the clearing temperatures increase going from discotic **1b** to **2a** to **2c,2e** to **2b,2d** (Scheme 3.1). Discotic **1a** behaves totally different compared to the other discotics. It shows a glass transition temperature, while all the other discotics show a crystalline-like phase at a certain point. The clearing temperature, on the other hand, is very high and the clearance is accompanied by decomposition of the sample. In this way, the behaviour of **1a** resembles the behaviour of homochiral discotics **2b** and **2d**, which also decompose before the isotropic state is reached, meaning that strong interactions are present preventing the molecules to flow. The solubility experiments in chloroform and in heptane show the same trends as observed in the neat state; the solubility decreases from **1b** to **2a** to heterochiral **2c,2e** to homochiral **2b,2d** (Scheme 3.1). Again, discotic **1a** behaves completely different compared to the other discotics. It does not show a Cotton effect, neither in chloroform nor in heptane. Probably, the glycylglycine tails of **1a** are too flexible, which makes it impossible to transfer the chiral information embedded in the alkyl tails to a higher level of organization. This does not necessarily mean that aggregation, in which the transfer of chirality to a higher level of organization is not possible, cannot be present in solution. In contrast, according to the high stability in the neat state, it is most likely that assemblies are present also in solution.



Scheme 3.1 Cores of compounds **1b** and **2a–e** shown in order of increasing stability.

Scheme 3.1 demonstrates that the stack stability increases when two phenylalanines are present in the core (**2b–e**). An explanation for the increased stability may be that two phenylalanines provide a larger hydrophobic core and additional π - π interaction. The measurements also reveal that the stack stability is higher when two phenylalanines with equal chirality (**2b,2d**) are present compared to two phenylalanines with opposite chirality (**2c,2e**). This may be due to more efficient packing when two phenylalanines with equal chirality are introduced. Unexpectedly, the data also point out that when a combination of L-phenylalanine and glycine is used, the stack stability increases when the L-phenylalanine is situated remote from the core. To explain this observation, a more detailed understanding of the self-assembly mechanism is required. When the centre starts to self-assemble first, followed by the mesogenic groups at the periphery, it would be more beneficial to have the phenylalanine close to the centre to enlarge the core and provide a more confined packing. Nevertheless, the opposite is observed, which suggests that stacking is not initiated from the centre of the discotics, but from the periphery. Preliminary investigation of the stacking mechanism of **1b** in solution with CD also supports this hypothesis.

3.5 Self-assembly behaviour of mono-peptide discotics in the neat state

The self-assembly behaviour of the mono-peptide discotics was examined in the neat state with DSC and POM. The DSC data of the second heating run (rate $10\text{ }^{\circ}\text{C}\cdot\text{min}^{-1}$) for **3a,b** are shown in Table 3.5.

Table 3.5 The onsets of the transitions (T_{onset} [$^{\circ}\text{C}$]) and the corresponding enthalpies (ΔH [$\text{kJ}\cdot\text{mol}^{-1}$]) for compounds **3a,b** (second heating run; $10\text{ }^{\circ}\text{C}\cdot\text{min}^{-1}$).^[a]

Compound	T_{onset}		ΔH		T_{onset}		ΔH			
	[$^{\circ}\text{C}$]	[$\text{kJ}\cdot\text{mol}^{-1}$]	[$^{\circ}\text{C}$]	[$\text{kJ}\cdot\text{mol}^{-1}$]	[$^{\circ}\text{C}$]	[$\text{kJ}\cdot\text{mol}^{-1}$]	[$^{\circ}\text{C}$]	[$\text{kJ}\cdot\text{mol}^{-1}$]		
3a = crF ₃	K*	162	14	I	-	-	-	-	-	
3b = crA ₃	K*	113	0.2	M	125	0.3	M	156	2.1	I

[a] - = phase is not observed; K* = crystalline-like phase; M = unidentified mesophase; I = isotropic phase.

Compound **3a** was heated in the second run at a rate of $10\text{ }^{\circ}\text{C}\cdot\text{min}^{-1}$ from -100 to $185\text{ }^{\circ}\text{C}$ and showed a broad K*–I transition with an onset at $162\text{ }^{\circ}\text{C}$. The cooling run, in contrast, showed a sharp transition with an onset at $156\text{ }^{\circ}\text{C}$. There were no indications for the presence of a mesophase. Discotic **3b** was heated from -100 to $185\text{ }^{\circ}\text{C}$. Three transitions could be discerned; two small transition with onsets at $113\text{ }^{\circ}\text{C}$ and $125\text{ }^{\circ}\text{C}$, respectively, and a transition to the isotropic phase at $156\text{ }^{\circ}\text{C}$. Upon cooling, only two transitions could be discerned, an I–M transition at $148\text{ }^{\circ}\text{C}$ and an M–K* transition at $95\text{ }^{\circ}\text{C}$. A mesophase could be grown by slowly cooling from the isotropic state, but the contrast of the pattern was low (Figure 3.7).

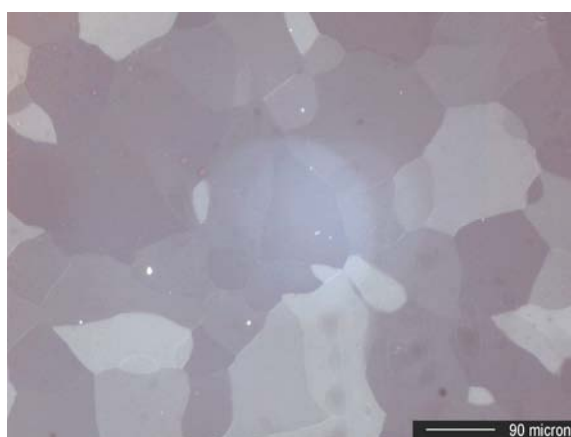


Figure 3.7 Polarized optical microscopy texture of compound **3b** at $115\text{ }^{\circ}\text{C}$.

3.6 Self-assembly behaviour of mono-peptide discotics in solution

The self-assembly behaviour of both mono-peptide discotics has been examined in dilute solutions in chloroform and in heptane with CD, UV/Vis and IR spectroscopy. The CD and UV/Vis spectra of discotics **3a,b** in chloroform and in heptane are shown in Figure 3.8.

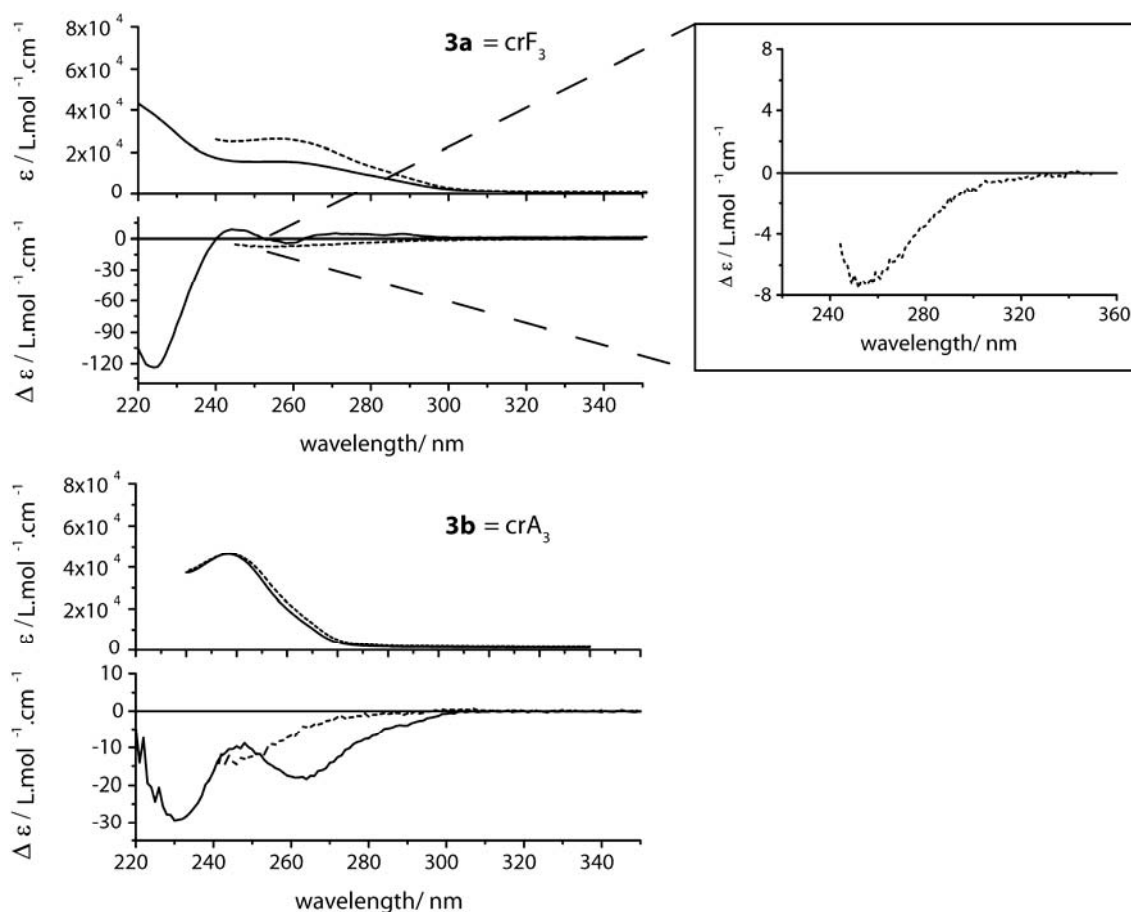


Figure 3.8 UV/Vis and CD spectra for mono-peptide discotics **3a,b** in heptane, 2×10^{-5} M (solid line) and chloroform, 2×10^{-5} M (dashed line).

In heptane, compound **3a** induces a complex CD curve with weak maxima at 244 nm and 288 nm, a very strong minimum at 224 nm and a weak minimum at 258 nm. The CD curve of **3a** in chloroform is completely different; it gives rise to a negative CD effect over the whole spectrum with a minimum at 255 nm. The CD curve of compound **3b** in heptane has two minima at 230 nm and 264 nm and one maximum at 248 nm, which still gives rise to a negative CD effect. Compound **3b** shows a Cotton effect in chloroform that decreases going to smaller wavelengths. The CD spectrum of **3b** in chloroform is less active than the one in heptane, as was also observed for discotic **3a**.

CD and UV/Vis measurements reveal that discotics **3a** and **3b** do not show a temperature-dependent behaviour in chloroform. To investigate whether the weak,

temperature insensitive Cotton effects in chloroform originate from molecularly dissolved discotics or from less ordered self-assembled structures, IR spectra in chloroform (Table 3.6) have been recorded.

Table 3.6 Wavenumbers ν [cm^{-1}] of the N–H stretch vibrations of **3a** and **3b** in the solid state and in 1×10^{-4} M solutions in chloroform at 20 °C.

Compound	3a = crF ₃	3b = crA ₃
ν solid state	3263	3293
ν chloroform	3300	3324
	3421	3423

The N–H stretch vibrations in chloroform are very broad for all samples measured. The maximum of the broad peak can in general be found around 3322 cm^{-1} , which is indicative for hydrogen bonding. There is also a much smaller and sharper peak at 3422 cm^{-1} , suggesting that a small fraction of the molecules is molecularly dissolved.

CD measurements reveal that solutions of compounds **3a,b** in heptane do show a temperature-dependent Cotton effect. The graphs depicted in Figure 3.9 are cooling curves of **3a** and **3b**, recorded at a rate of $1 \text{ }^\circ\text{C}\cdot\text{min}^{-1}$.

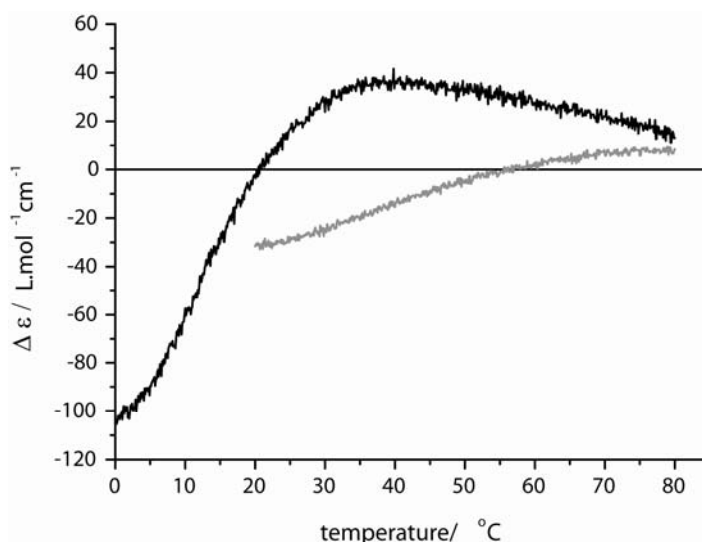


Figure 3.9 Temperature-dependent CD measurements in heptane for compounds **3a** (black line); 1×10^{-4} M at $\lambda = 225 \text{ nm}$ from 80 °C to 0 °C and **3b** (grey line); 2×10^{-5} M at $\lambda = 230 \text{ nm}$ from 85 °C to 20 °C, both with a cooling rate of $1 \text{ }^\circ\text{C}\cdot\text{min}^{-1}$.

The cooling curve of **3a** does not show any real plateaus. Going from 80 °C to 40 °C the Cotton effect at 225 nm slowly increases to a $\Delta\epsilon = 37 \text{ L}\cdot\text{mol}^{-1}\text{cm}^{-1}$. Further cooling leads to

a more rapid decrease of the CD signal. At around 25 °C, the Cotton effect changes sign and, finally, at 0 °C it seems that a plateau will be reached with $\Delta\epsilon = -106 \text{ L}\cdot\text{mol}^{-1}\text{cm}^{-1}$. Unfortunately, the cooling curves are not reproducible. This behaviour has already been observed before for certain dipeptide discotics and illustrates that these molecules display a very complex energy landscape. The cooling curve of **3b** shows two plateaus, one at low temperatures at around $\Delta\epsilon = -30 \text{ L}\cdot\text{mol}^{-1}\text{cm}^{-1}$ and one at higher temperatures with $\Delta\epsilon = 8 \text{ L}\cdot\text{mol}^{-1}\text{cm}^{-1}$, and a melting temperature around 45 °C. The cooling curve of **3b** is reproducible, but does not lie exactly on top of the heating curve, meaning that the system is not in thermodynamic equilibrium. IR spectroscopy has been performed to judge whether helically ordered assemblies or molecularly dissolved discotics of **3a** and **3b** are present in heptane at 70 °C. The IR spectra are taken in heptane at concentrations similar to those used in the CD measurements. According to the N–H stretch vibrations of **3a** and **3b**, which appear as sharp peaks at 3289 cm^{-1} and 3351 cm^{-1} respectively, hydrogen bonding is still present (Table 3.7). The hydrogen bonds present in assemblies of **3a** are stronger than the ones for **3b**, suggesting that, when a phenylalanine is used as structuring element, more stable assemblies are formed.

Table 3.7 Wavenumbers ν [cm^{-1}] of the N–H stretch vibrations of **3a** and **3b** in the solid state and in $1 \times 10^{-4} \text{ M}$ solutions in heptane at 80 °C.

Compound	3a = crF ₃	3b = crA ₃
ν solid state	3263	3293
ν heptane	3289	3351

3.7 Stability of assemblies of mono-peptide discotics

It has been demonstrated that the stabilities of the mono-peptide assemblies are still very high despite the lack of one amide functionality compared to the dipeptide discotics. Characterization in the neat state points out that the clearing temperature of the phenylalanine-based disc **3a** (162 °C) is somewhat higher than the one of the alanine-based disc **3b** (156 °C), indicating that the interactions between the molecules are somewhat stronger in the case of **3a**. In solution, the same trend has been observed with IR experiments performed in heptane, which show that hydrogen bonding is stronger for **3a** than for **3b** as can be deduced from a smaller wavenumber for the N–H stretch vibration of the former. Explanation for the increased stability of **3a** may be that the extra phenyl group provides more confinement of space and/or additional π – π interaction. The additional phenyl moiety also plays a role in determining the degree of order present in the assemblies, since significantly larger Cotton effects are obtained for **3a** compared to **3b**, especially in heptane. The mono-peptide discotics can, in terms of stability and order within the stacks, be situated in

between dipeptide discotics **1b** [cr(FG)₃] and **2a** [cr(GF)₃]. For this reason, phenylalanine-based discotic **3a** looks the most attractive candidate for future functionalization; the assemblies of **3a** possess appropriate stack stability in relation with the dipeptide discotics, while from a synthetic point a view they are much easier to prepare than the dipeptide discotics.

3.8 Conclusions

The self-assembly behaviour of seven dipeptide discotics and two mono-peptide discotics is described both in the neat state and in solution. Although all discotics form very stable assemblies, a clear trend in the stability of the different stacks is observed depending on the peptide fragment incorporated.

The assemblies are not very well-ordered in the neat state. Furthermore, some of the self-assembled structures show very complex energy landscapes in solution. This indicates that small changes in the balance between the secondary interactions originating from the benzenetricarboxamide core and the peptide fragments have a strong influence on the order within the stack. The balance between these supramolecular interactions is very subtle and a small modification can already make the difference between thermodynamically stable or completely frustrated stacks.

The results presented over here show that it is possible to alter the stacking properties of these peptide discotics by modifying the peptide fragments, but the results also stress the importance of understanding the self-assembly mechanisms in order to clarify the self-assembly behaviour of the different C₃-symmetrical molecules. Finally, it is shown that phenylalanine-based discotic **3a** is the most attractive candidate for future functionalization, since assemblies of **3a** possess appropriate stabilities and are easily accessible.

3.9 Experimental section

General

UV/VIS spectra were obtained on a Perkin Elmer Lambda 40 spectrometer. CD measurements were performed on a Jasco J-600 spectropolarimeter connected to a Jasco PTC-348WI temperature controller. Infrared spectra of the liquid samples were recorded using a Biorad FTS 6000 spectrometer. The heatable cell used to perform the measurements was controlled by a home made temperature controller and fitted with KBr windows and a Teflon spacer that makes the path length 1 mm. Each spectrum was recorded with a resolution of 4 cm⁻¹, co-adding 200 scans. Low concentration ¹H-NMR spectra were recorded on a Varian Unity Inova 500 spectrometer. The optical properties of the neat state were determined using a Jenaval polarization microscope equipped with a Linkam THMS 600 heating device and a Polaroid digital camera model PDMC-2. DSC data were collected on a Perkin Elmer Pyris 1 under nitrogen atmosphere. The X-ray measurements were carried out on a home-built system consisting of a sealed X-ray tube (Cu K α radiation), a primary graphite monochromator, a pinhole collimator, a sample stage, and a Siemens Hi-Star area detector. All components were mounted on an

optical bench to provide maximal flexibility and easy alignment. Samples were prepared in a 0.9 mm diameter Lindemann capillary tube and mounted in a home-built furnace, based on a TMS94 Linkam hot stage. Wide angle X-ray (WAXS) patterns were recorded with a sample-to-detector distance of 8.1 cm.

Synthesis

The syntheses of compounds **1a,b**, **2a–e** and **3a,b** are described in Chapter 2.

3.10 References and notes

- [1] L.J. Prins, D.N. Reinhoudt, P. Timmerman, *Angew. Chem.* **2001**, *113*, 2446–2492; *Angew. Chem., Int. Ed.* **2001**, *40*, 2382–2426.
- [2] D.J. Hill, M.J. Mio, R.J. Prince, T.S. Hughes, J.S. Moore, *Chem. Rev.* **2001**, *101*, 3893–4011.
- [3] L. Brunsveld, B.J.B. Folmer, E.W. Meijer, R.P. Sijbesma, *Chem. Rev.* **2001**, *101*, 4071–4097.
- [4] D.C. Sherrington, K.A. Taskinen, *Chem. Soc. Rev.* **2001**, *30*, 83–93.
- [5] L.M. Greig, D. Philip, *Chem. Soc. Rev.* **2001**, *30*, 287–302.
- [6] D.T. Bong, T.D. Clark, J.R. Granja, M.R. Ghadiri, *Angew. Chem.* **2001**, *113*, 1016–1041; *Angew. Chem., Int. Ed.* **2001**, *40*, 989–1011.
- [7] T. Kato, *Science*, **2002**, *295*, 2414–2418.
- [8] A. Ciferri, *Macromol. Rapid Commun.* **2002**, *23*, 511–529.
- [9] H.M. Keizer, R.P. Sijbesma, *Chem. Soc. Rev.* **2005**, *34*, 226–234.
- [10] A.L. Sisson, M.R. Shah, S. Bhosale, S. Matile, *Chem. Soc. Rev.* **2006**, *35*, 1269–1286.
- [11] K. Sada, M. Takeuchi, N. Fujita, M. Numata, S. Shinkai, *Chem. Soc. Rev.* **2007**, *36*, 415–435.
- [12] E.W. Meijer, J.A.J.M. Vekemans, A.R.A. Palmans, P. Breure, J. de Kraker, L. Brunsveld, *Polym. Prep.* **2000**, *41*, 902–903.
- [13] J.J. van Gorp, *Thesis: Helices by hydrogen bonding, folding and stacking of chiral supramolecular scaffolds*; Eindhoven University of Technology: Eindhoven (The Netherlands), **2004**.
- [14] M. de Loos, *Thesis: Hydrogen-bonded low molecular weight gelators*; University of Groningen: Groningen (The Netherlands), **2005**.
- [15] V. Percec, A.E. Dulcey, M. Peterca, M. Iies, M.J. Sienkowska, P.A. Heiney, *J. Am. Chem. Soc.* **2005**, *127*, 17902–17909.
- [16] R.E. Gillard, F.M. Raymo, J.F. Stoddart, *Chem. Eur. J.* **1997**, *3*, 1933–1940.
- [17] S. Zhang, X. Zhao, *J. Mater. Chem.* **2004**, *14*, 2082–2086.
- [18] K. Rajagopal, J.P. Schneider, *Curr. Opin. Struct. Biol.* **2004**, *14*, 480–486.
- [19] N. Ashkenasy, W.S. Horne, M.R. Ghadiri, *Biomaterials* **2006**, *2*, 99–102.
- [20] J.R. Dunetz, C. Sandstrom, E.R. Young, P. Baker, S.A. van Name, T. Cathopolous, R. Fairman, J.C. de Paula, K.S. Åkerfeldt, *Org. Lett.* **2005**, *7*, 2559–2561.
- [21] J. Couet, J.D. Jeyaprakash, S. Samuel, A. Kopyshev, S. Santer, M. Biesalski, *Angew. Chem.* **2005**, *117*, 3361–3365; *Angew. Chem., Int. Ed.* **2005**, *44*, 3297–3301.
- [22] A. Rösler, H-A. Klok, I.W. Hamley, V. Castelletto, O.O. Mykhaylyk, *Biomacromolecules* **2003**, *4*, 859–863.
- [23] H-A. Klok, G.W.M. Vandermeulen, H. Nuhn, A. Rösler, I.W. Hamley, V. Castelletto, H. Xu, S.S. Sheiko, *Faraday Discuss.* **2004**, *128*, 29–41.
- [24] D. Aili, K. Enander, J. Rydberg, I. Lundström, L. Baltzer, B. Liedberg, *J. Am. Chem. Soc.* **2006**, *128*, 2194–2195.
- [25] P.P. Bose, M.G.B. Drew, A.K. Das, A. Banerjee, *Chem. Commun.* **2006**, 3196–3198.

- [26] V. Percec, A.E. Dulcey, V.S.K. Balagurusamy, Y. Miura, J. Smidrkal, M. Peterca, S. Nummelin, U. Edlund, S.D. Hudson, P.A. Heiney, D.A. Hu, S.N. Magonov, S.A. Vinogradov, *Nature*, **2004**, *430*, 764–768.
- [27] J.D. Hartgerink, E. Beniash, S.I. Stupp, *Proc. Natl. Acad. Sci. U. S. A.* **2002**, *99*, 5133–5138.
- [28] K.J.C. van Bommel, C. van der Pol, I. Muizebelt, A. Friggeri, A. Heeres, A. Meetsma, B.L. Feringa, J. van Esch, *Angew. Chem.* **2004**, *116*, 1695–1699; *Angew. Chem., Int. Ed.* **2004**, *43*, 1663–1667.
- [29] K. Matsuura, K. Murasato, N. Kimizuka, *J. Am. Chem. Soc.* **2005**, *127*, 10148–10149.
- [30] A.R.A. Palmans, J.A.J.M. Vekemans, H. Fischer, R.A. Hikmet, E.W. Meijer, *Chem. Eur. J.* **1997**, *3*, 300–307.
- [31] L. Brunsveld, H. Zhang, M. Glasbeek, J.A.J.M. Vekemans, E.W. Meijer, *J. Am. Chem. Soc.* **2000**, *122*, 6175–6182.
- [32] L. Brunsveld, B.G.G. Lohmeijer, J.A.J.M. Vekemans, E.W. Meijer, *J. Incl. Phenom. Macrocycl. Chem.* **2001**, *41*, 61–64.
- [33] J.J. van Gorp, J.A.J.M. Vekemans, E.W. Meijer, *J. Am. Chem. Soc.* **2002**, *124*, 14759–14769.
- [34] A preliminary AFM study did not give information about the dimensions of the assemblies.
- [35] R. Festag, R. Kleppinger, M. Soliman, J.H. Wendorff, G. Lattermann, G. Staufer, *Liq. Cryst.* **1992**, *11*, 699–710.
- [36] R. Kleppinger, C.P. Lillya, C. Yang, *J. Am. Chem. Soc.* **1997**, *119*, 4097–4102.
- [37] A. Hayer, V. de Halleux, A. Köhler, A. El-Garouhy, E.W. Meijer, J. Barberá, J. Tant, J. Levin, M. Lehmann, J.C. Gierschner, Y.H. Geerts, *J. Phys. Chem. B* **2006**, *110*, 7653–7659.

4

From apolar media to water: Self-assembly of a peptide-based discotic amphiphile

Characterization in solution

ABSTRACT: *A C_3 -symmetrical molecule with a 1,3,5-benzenetricarboxamide core decorated with L-phenylalanine residues bearing peripheral mesogenic groups containing oligo(ethylene oxide) tails is described. A convergent synthetic strategy, similar to the one reported for the mono-peptide discotics described in Chapter 2 has been applied to obtain the target product. To investigate the stacking properties of phenylalanine-based discotic **1** a combination of techniques including UV/Vis spectroscopy, circular dichroism, NMR spectroscopy and cryoTEM has been applied. The measurements demonstrate that this molecule forms ordered aggregates in solutions in chloroform and in water. The stacks are well-defined, nanometer-sized objects (containing 11 monomers within an aggregate), of which the size is independent of concentration within the investigated concentration regime (10^{-5} to 10^{-3} M). Their water-solubility in combination with their well-defined nanometer-size and their ability to display multiple functional groups make these assemblies potential supramolecular scaffolds for biomedical applications.*

4.1 Introduction

Nanotechnology aims at constructing materials or operative systems at nanoscale dimensions. In the biomedical world alone, several potential applications can be envisioned, like scaffolds for targeted drug delivery, imaging or tissue engineering.^[1-3] Suitable scaffolds should fulfil several biological demands. They should be water-soluble, non-toxic and non-immunogenic. Monodisperse scaffolds with a well-defined structure are important in order to achieve systems displaying homogeneous and reproducible properties. The presence of multiple functional groups at the surface of the scaffold to which targeting groups or imaging modalities can be coupled, fulfils a key role in obtaining highly selective and efficient systems. And, the scaffold molecules have to stay in circulation for the time needed to have a clinical effect, but on the other hand may not accumulate in the body over a larger period of time. Numerous covalent systems, mostly based on polymeric architectures^[4-7], quantum dots^[8,9], inorganic nanoparticles^[10] or dendrimers^[11-13], have been reported. Recently, self-assembling micellar systems^[14-17] are receiving much attention, because accumulation of covalently linked macromolecular systems in the body is a serious problem. Another advantage of self-assembling systems is that they display easily controlled properties and good pharmacological characteristics. Examples of self-assembling systems utilized as contrast agents for MRI are described in Chapter 1.

In this Chapter, the synthesis will be reported of a discotic amphiphile (Figure 4.1) that may act as self-assembling scaffold for biomedical applications. A single phenylalanine unit is introduced as the peptide fragment in line with the experiments described in Chapter 3, which show that the apolar variant of phenylalanine-based disc **1** (compound **3a** in Chapter 3) displays good self-assembly properties and is rather easily accessible. To obtain water-solubility oligo(ethylene oxide) tails are introduced within the peripheral mesogenic groups.

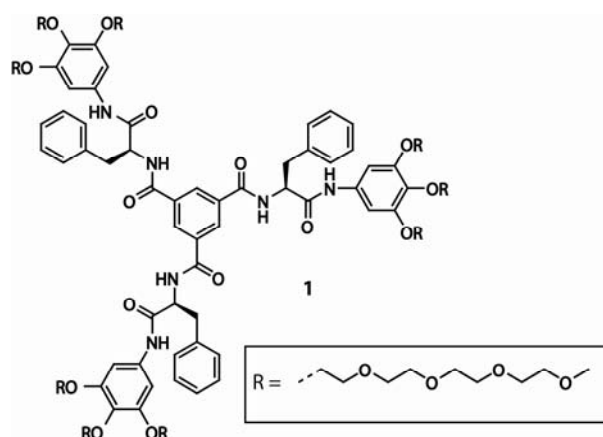
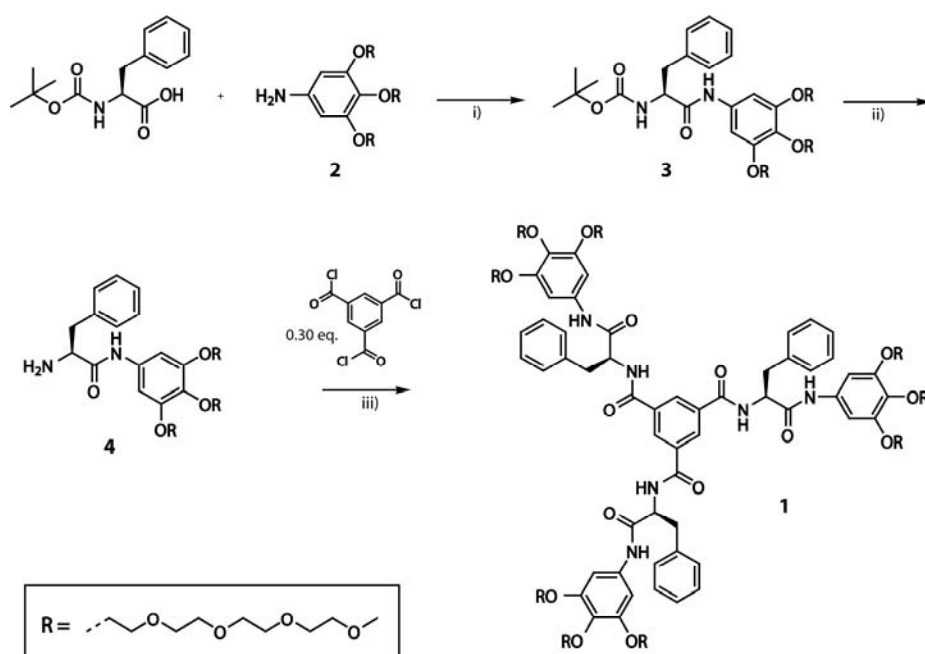


Figure 4.1 Molecular structure for water-soluble, phenylalanine-based disc **1**.

Next to the synthesis, the self-assembly properties of discotic **1** in solutions in chloroform and in water and the dimensions of the stacks of **1** in water will be discussed. Owing to these properties, the potential of discotic **1** to act as a scaffold for biomedical applications will be determined.

4.2 Synthesis

The phenylalanine-based disc was synthesized as depicted in Scheme 4.1. As a starting material for compound **2**, 3,4,5-tris(2-{2-[2-(2-methoxyethoxy)ethoxy]ethoxy}ethoxy)ethoxy) phenylisocyanate was used, which was synthesized according to a described procedure.^[18]



Scheme 4.1 Synthetic route towards L-phenylalanine-based water soluble disc **1**: i) HBTU, DiPEA, DMF, RT, overnight, ~76%; ii) 1) TFA, RT, 1 h, 2) ion exchange column, ~95%; iii) Et₃N, DCM, RT, overnight, ~51%.

Direct coupling of Boc-protected L-phenylalanine with **2** was accomplished using HBTU as a coupling reagent and DiPEA as a base. (HBTU is preferred as the coupling reagent because it precludes racemization of the activated amino acid.^[19,20]) Deprotection of **3** with trifluoroacetic acid, followed by ion-exchange, gave **4** in a 95% yield. Discotic **1** was obtained after coupling of compound **4** with 0.30 equivalents of trimesic chloride in the presence of triethylamine as a base. Extraction followed by dialysis and column chromatography yielded pure disc **1** in a yield of 51%. All compounds were characterized with a combination of analytical techniques including MALDI-TOF MS, ¹H- and ¹³C-NMR spectroscopy and IR. The

purity of target discotic **1** was also demonstrated with GPC and elemental analysis. Figure 4.2 shows the GPC trace together with the MALDI-TOF MS spectrum of **1**.

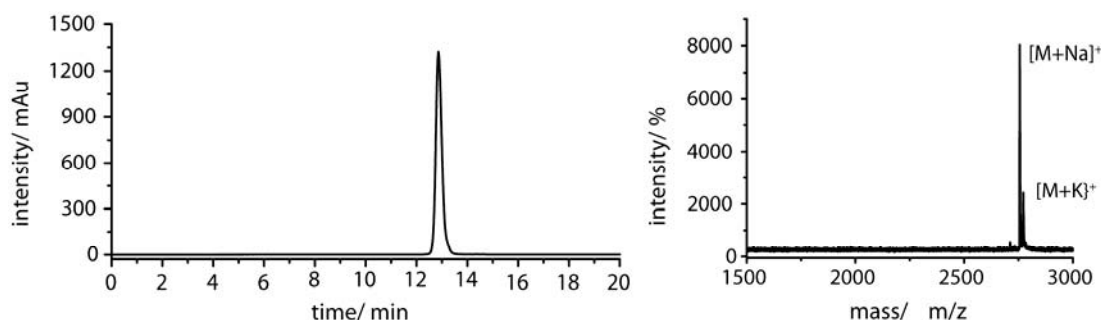


Figure 4.2 GPC trace and MALDI-TOF MS spectrum of compound **1**.

4.3 Self-assembly in solution

The self-assembly behaviour of **1** has been investigated in dilute solutions in chloroform and in water using CD, UV/Vis, IR spectroscopy and/or various NMR techniques. The CD and UV/Vis spectra of **1** in chloroform or in water are shown in Figure 4.3.

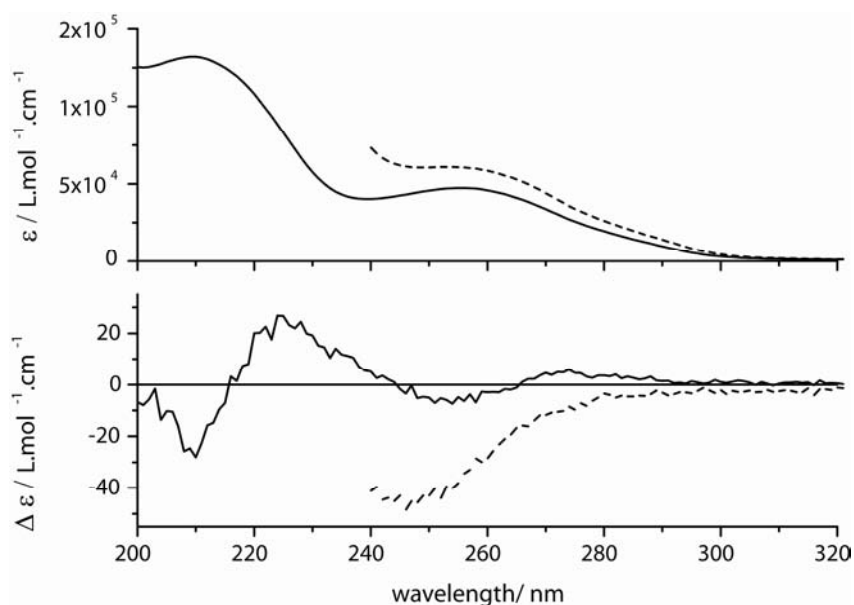


Figure 4.3 UV/Vis and CD spectra for phenylalanine-based discotic **1** in water, 1×10^{-4} M (solid line) and chloroform, 1×10^{-4} M (dashed line).

In chloroform, compound **1** induces a large negative Cotton effect with a minimum at 246 nm with $\Delta\epsilon = -48 \text{ L}\cdot\text{mol}^{-1}\cdot\text{cm}^{-1}$. The CD curve of discotic **1** in water shows two coupled CD effects, one centred at 216 nm with a negative extreme at 210 nm and a positive extreme at 225 nm and the other centred at 266 nm with a minimum at 254 nm and a maximum at

274 nm. Figure 4.3 demonstrates that the assemblies in water are less ordered than those in chloroform. This is expected, since water is a stronger hydrogen bond acceptor than chloroform.

CD as well as UV/Vis measurements reveal that discotic **1** does not show a temperature-dependent behaviour in chloroform. This indicates that the interactions between the molecules within the aggregate are quite strong. IR experiments performed in dilute solution in chloroform support this hypothesis, because the N–H stretch vibration appears at 3274 cm^{-1} . Remarkably, this value is even lower than the value of the N–H stretch vibration of **1** in the neat state, which indicates that the hydrogen bond interactions between the molecules in solutions of chloroform are even stronger than in the neat state.

Table 4.1 Wavenumbers ν [cm^{-1}] of the N–H stretch vibration of **1** in the solid state and in a $1 \times 10^{-4}\text{ M}$ solution in chloroform at $20\text{ }^\circ\text{C}$.

Compound	1
ν solid state	3318
ν chloroform	3274

In water, discotic **1** does show a temperature-dependent behaviour both in CD as well as in UV/Vis. The CD and UV/Vis spectra are presented in Figure 4.4.

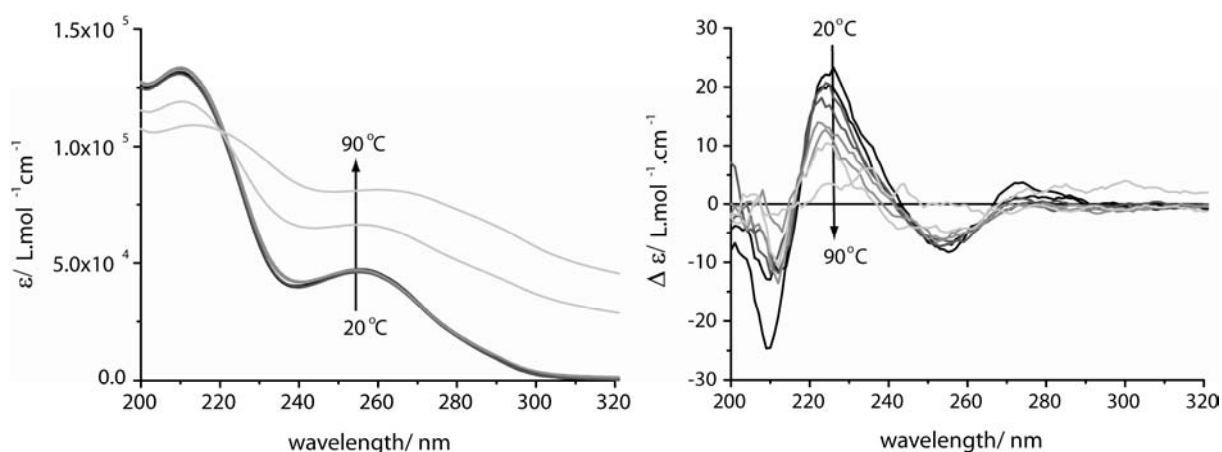


Figure 4.4 Temperature-dependent UV/Vis and CD spectra for phenylalanine-based discotic **1** in water, $1 \times 10^{-4}\text{ M}$; $T = 20\text{--}90\text{ }^\circ\text{C}$.

The UV/Vis spectra do not show any temperature-dependence up to $70\text{ }^\circ\text{C}$. Above $70\text{ }^\circ\text{C}$, a temperature-dependence is observed, but as illustrated by Figure 4.4 the baseline also starts to deviate from zero. This phenomenon has already been observed for water-soluble C_3 -symmetrical bipyridine molecules^[21] and has been attributed to the low critical solution

temperature behaviour of oligo(ethylene oxide)s in water.^[22] Strong aggregation of oligo(ethylene oxide) tails may lead to large objects that cause scattering of the sample and hence a deviating baseline. The CD spectra at the different temperatures show that the CD curves become less active at higher temperatures, which can be explained by a loss of order within the assemblies. Again, the spectra at 80 °C and 90 °C have an unstable baseline, as is also observed in UV/Vis.

The UV/Vis and CD measurements both show that it is impossible to reach the molecularly dissolved state by increasing the temperature due to aggregation of the oligo(ethylene oxide) tails. It has been tried to reach the molecularly dissolved state by decreasing the concentration, but even at 5×10^{-6} M an identical $\Delta\epsilon$ -value is found as at 1×10^{-4} M. This suggests that the assemblies that are formed are very stable.

4.4 Size of the self-assembled structures in water

A combination of NMR techniques has been explored to provide additional proof for the presence of aggregates and to determine the dimensions of the stacks of compound **1** in water. Figure 4.5 shows an ^1H -NMR spectrum of **1** in D_2O .

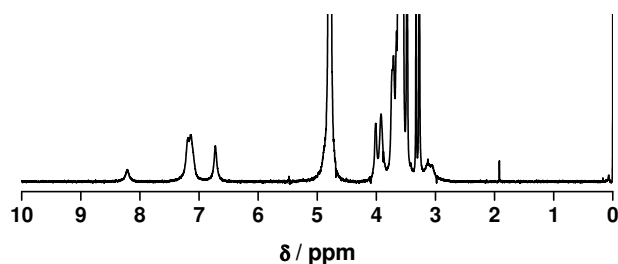


Figure 4.5 ^1H -NMR spectrum for phenylalanine-based discotic **1** in D_2O , 1×10^{-3} M; $T = 25$ °C.

The spectrum indicates the presence of assemblies, because all peaks in the spectrum are broadened as can clearly be deduced from the signal around 8.2 ppm, corresponding to the chemical shift of the aromatic core protons.

The longitudinal (T_1) and transverse (T_2) relaxation times have been determined to give some extra insight into the local freedom of movement of the different hydrogen atoms. The T_1 has been measured with the inversion-recovery sequence while the T_2 has been measured with the Carr–Purcell–Meiboom–Gill (CPMG) sequence.^[23,24] Figure 4.6 shows the T_1 and T_2 relaxation times as a function of temperature for three selected resonances, namely: the aromatic core protons at 8.2 ppm, the aromatic protons of the aminobenzoyl unit at 6.7 ppm and the ethylene oxide protons closest to the centre of the core at 4.0 ppm.

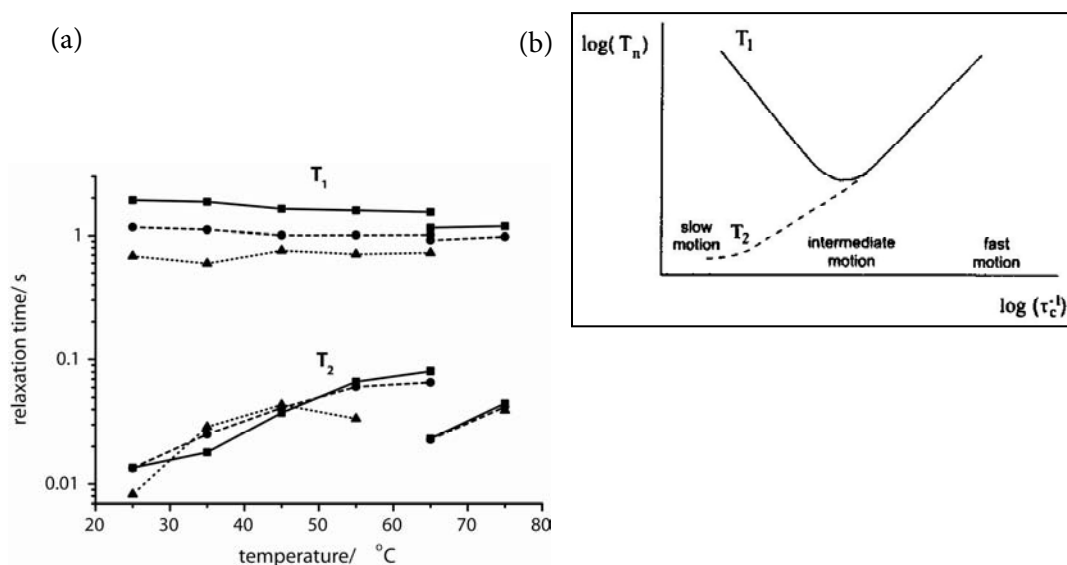


Figure 4.6 a) Longitudinal (T_1) and transverse (T_2) relaxation times versus temperature for discotic **1** in D_2O , 1×10^{-3} M; $T = 25$ – 80 °C. The investigated resonances were at 8.2 (squares), 6.7 (circles) and 4.0 (triangles) ppm. b) A schematic representation of the dependence of the T_1 and T_2 on the molecular tumbling rate.^[25]

The T_1 is more or less constant in this temperature regime for all resonances investigated. The T_2 on the other hand, appears to be temperature-dependent. The transverse relaxation time increases going from 25 °C to 55 °C; At 70 °C this increasing trend is disrupted, which can be attributed to clustering of the oligo(ethylene oxide) tails. Moreover Figure 4.6a shows that the T_2 values are lower than the T_1 values for each temperature measured and that the values are converging going to higher temperatures, which indicates that all investigated resonances are in the intermediate motion regime (Figure 4.6b).

Temperature-dependent 1H -DOSY NMR experiments have been performed to determine the diffusion coefficients of the aggregates, from which the sizes of the assemblies can be deduced. The measurements have been performed using the DOSY bipolar pulse paired stimulated echo with convection compensation (Dbppste_cc) pulse sequence^[26]. The steady state pulse sequence has been used to compensate for the long relaxation times of HDO, and the self-diffusion of HDO is used to calibrate the measurements. A sample of discotic **1** in D_2O (1×10^{-3} M) has been measured at different temperatures ranging from 25 °C to 80 °C. Table 4.2 lists, besides the theoretical diffusion coefficients of HDO, the measured diffusion coefficients of HDO and of the stacks in the sample. At temperatures between 25 °C and 55 °C, the measured self-diffusion of HDO does not deviate from its theoretical value. This implies that the dynamic viscosity of the sample is equal to the dynamic viscosity of pure D_2O .^[27] At 70 °C and 80 °C, the measured self-diffusion coefficients of HDO are much lower than the theoretical values. This is expected since the oligo(ethylene oxide)

tails of discotic **1** start to aggregate above 70 °C, which will lead to higher viscosities than theoretically calculated.

Table 4.2 Diffusion coefficients and hydrodynamic radii of assemblies of **1** in D₂O; $T = 25\text{--}75$ °C, 1×10^{-3} M. The resonance peak at ~ 8.2 ppm was used to determine the diffusion coefficients.

Temperature [°C]	D_t (HDO) / 10^{-10} m ² s ⁻¹		D_t (stack) / 10^{-10} m ² s ⁻¹	$R_{H, \text{stack}}$ [10^{-10} m]
	theoretical	measured		
25	19	19	1.0	20
35	25	25	1.5	19
45	31	30	1.7	19
55	37	36	2.1	19
70	50	41	-	-
80	59	48	-	-

The diffusion coefficient of the stacks increases going from 25 °C to 55 °C. When compensated for temperature and viscosity of pure D₂O by the Stokes–Einstein equation^[28], it can be concluded that this increase is only caused by increased mobility. The Stokes–Einstein^[28] relationship for the diffusion of a spherical particle is used to calculate the dimensions of the aggregates, since the model of Tirado and Garcia de la Torre^[29] for the diffusion of a cylindrical particle is not valid, due to the aspect ratio of the assemblies ($L/d < 2$). The calculated hydrodynamic radii are listed in Table 4.2. The radii are constant at 19–20 Å between 25 °C and 55 °C, which corresponds to aggregates consisting of 11 monomers (assuming an interdisc distance of 3.5 Å).

Cryo-electron microscopy measurements have been performed to support the data obtained by ¹H-DOSY NMR and to visualize the assemblies present in water. Three solutions, namely 10^{-5} , 10^{-4} and 10^{-3} M discotic **1** in water, respectively, are investigated. The cryoTEM images for the different concentrations are all very similar. Figure 4.7 shows a characteristic image of discotic **1** in water. Since no large assemblies can be deduced from this image, it indirectly indicates that the aggregates indeed are very small (a few nanometers; 4 nm corresponds to 11 monomers), which is in agreement with the ¹H-DOSY NMR experiments. Apparently, the sizes of the aggregates are not very sensitive to changes in

temperature or concentration, which indicates that the stacks have a relatively well-defined size within the investigated concentration regime (10^{-5} to 10^{-3} M).

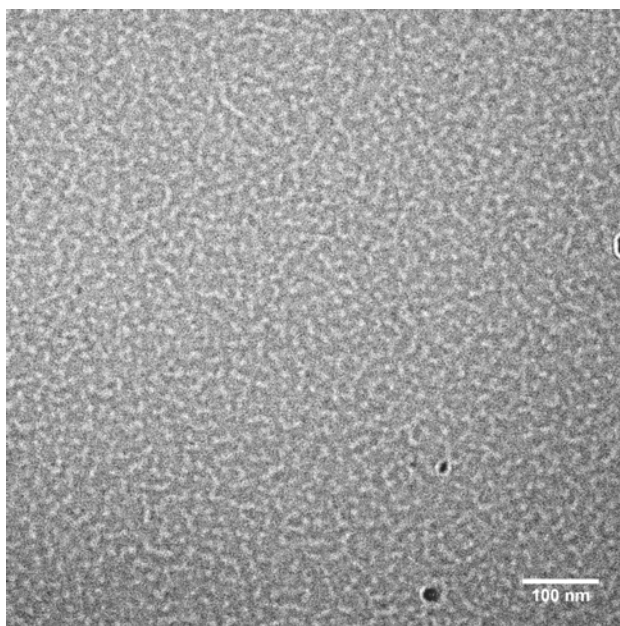


Figure 4.7 CryoTEM image for discotic **1** in water; 1×10^{-4} M. Images were obtained with an underfocus value of $-1.5 \mu\text{m}$.

The fact that only 11 monomers are able to stack on top of each other is presumably caused by steric crowding, but so far no experimental proof for this hypothesis has been found. However, there are other discotic amphiphiles reported that resemble disc **1** and show similar characteristics in apolar media. These discotics have been investigated by De Loos *et al.*^[30] and possess a 1,3,5-benzenetricarboxamide core decorated with phenylalanine moieties each containing one alkyl tail. They demonstrate that these discotics are rather poor organogelators compared to their *cis-cis*-1,3,5-cyclohexanetricarboxamide analogues. This suggests that aggregates of benzene-based discotics are much smaller in size (restricted growth) compared to the aggregates of cyclohexane-based discs. When combining these results with our findings, a possible relationship between the restricted growth and the combination of the 1,3,5-benzenetricarboxamide core with the phenylalanines is deduced. Our hypothesis is supported by the work of Hanabusa *et al.*^[31] They show that small 1,3,5-benzenetricarboxamide discotics lacking the phenylalanine moiety do form long fibres and, therefore, do show good gelating properties. Regarding disc **1**, the additional aminobenzene units may also play a critical role in the self-assembly process, since it is possible to stack the phenyl groups of phenylalanines on top of the aminobenzene units by means of π - π interaction.

4.5 Conclusions

In this chapter the synthesis of phenylalanine-based disc **1**, using a convergent synthetic approach, is described. Disc **1** self-assembles in solutions in chloroform and in water as has been demonstrated by means of CD. The molecularly dissolved state can not be reached, neither via raising the temperature due to clustering of the oligo(ethylene oxide) tails nor via lowering the concentration; even at a concentration as low as 5×10^{-6} M aggregates are still present, which suggests that the aggregates are quite stable. NMR techniques in combination with *cryo*TEM have been performed and show that the stacks are well-defined nanometer-sized objects (at an estimate 11 monomers within an aggregate). The sizes of the aggregates are almost independent of concentration (investigated concentration 10^{-5} M to 10^{-3} M) and temperature (10^{-3} M, 25–55 °C). The combination of properties like, water solubility and a well-defined nanometer-size makes these discotic molecules attractive supramolecular scaffolds for drug delivery or imaging.

4.6 Experimental section

General

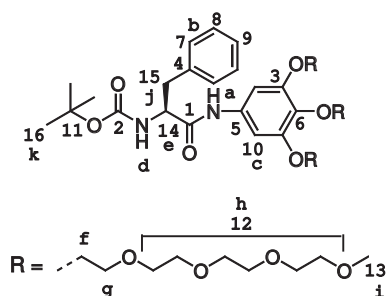
Compounds **1–4** were all kindly provided by B. F. M. de Waal. Unless stated otherwise, all reagents and chemicals were obtained from commercial sources and used without further purification. Water was demineralised prior to use. Dichloromethane and tetrahydrofuran were obtained by distillation over Merck molecular sieves (4 Å). ^1H -NMR, ^1H - ^1H COSY and ^{19}F -NMR spectra were recorded on a Varian Gemini 300 spectrometer, a Varian Mercury Vx 400 spectrometer or a Varian Unity Inova 500 spectrometer at 298 K. Chemical shifts are given in ppm (δ) values relative to tetramethylsilane (TMS). Splitting patterns are designated as s, singlet; d, doublet; dd, double doublet; t, triplet; q, quartet; m, multiplet and br stands for broad. Neat state IR spectra were measured at 298 K on a Perkin-Elmer 1605 FT-IR spectrophotometer. Matrix assisted laser desorption/ionization mass spectra were obtained on a PerSeptive Biosystems Voyager DE-PRO spectrometer using α -cyano-4-hydroxycinnamic acid (CHCA) and 2-[(2E)-3-(4-tert-butylphenyl)-2-methylprop-2-enylidene]malononitrile (DCTB) as matrices. Elemental analyses were carried out using a Perkin Elmer 2400. UV/VIS spectra were obtained on a Perkin Elmer Lambda 40 spectrometer. CD measurements were performed on a Jasco J-600 spectropolarimeter connected to a Jasco PTC-348WI temperature controller. Infrared spectra of the liquid samples were recorded using a Biorad FTS 6000 spectrometer. The heatable cell used to perform the measurements was fitted with KBr windows and a Teflon spacer that makes the path length 1 mm. Each spectrum was recorded with a resolution of 4 cm^{-1} , co-adding 200 scans. The longitudinal and transverse relaxation time and ^1H -DOSY NMR experiments were recorded on a Varian Unity Inova 500 spectrometer operating at 500.618 MHz and equipped with a 5 mm ID-PFG probe from Varian. Additional, experimental ^1H -DOSY NMR data can be found at the end of this experimental section. Cryogenic transmission microscopy measurements were performed on a FEI Titan Krios TEM equipped with a field emission gun (FEG) operating at 300 kV. Images were recorded using a 2k x 2k Gatan CCD camera equipped with a post column Gatan energy filter (GIF). TEM grids, (R2/2 Quantifoil Jena grids) were purchased from Aurion. The Quantifoil grids underwent a surface plasma treatment using a Cressington 208 carbon coater operating at 5 mA for 40 s prior to the vitrification procedure. The *cryo*TEM images of the discotics were obtained by applying small aliquots (3 μL) of the aqueous discotic solutions to Quantifoil grids (R2/2 Quantifoil Jena) within the environmental chamber

(relative humidity 100%) of the VitroBot™ at room temperature. The vitrified specimens were stored under liquid nitrogen and observed at $-170\text{ }^{\circ}\text{C}$ (Gatan cryo holder) in the Titan microscope. Micrographs were taken at 300 kV using low dose conditions.

3,4,5-Tris(2-{2-[2-(2-methoxyethoxy)ethoxy]ethoxy}ethoxy)aniline (2)

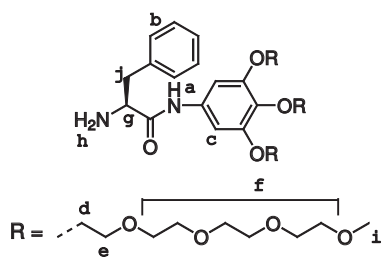
As a starting material 3,4,5-tris(2-{2-[2-(2-methoxyethoxy)ethoxy]ethoxy}ethoxy)phenylisocyanate was used, which was synthesized according to a described procedure.^[18] 3,4,5-tris(2-{2-[2-(2-methoxyethoxy)ethoxy]ethoxy}ethoxy)aniline was synthesized as described for 3,4,5-tris[2-(2-{2-[2-(2-methoxyethoxy)ethoxy]ethoxy}ethoxy)ethoxy]aniline by L. Brunsveld.^[21] The purification procedure was somewhat adjusted. The reaction mixture was evaporated *in vacuo*. The crude product was purified by stirring with hexane ($2 \times 10\text{ mL}$) followed by decantation. Subsequently, it was dissolved in dichloromethane (15 mL) and washed with water ($4 \times 15\text{ mL}$) and brine (15 mL). The organic layer was then dried with Na_2SO_4 and evaporated. LC-ESI-MS: m/z calcd. for 711.44 [M]^+ ; found: 711.40 [M]^+ .

N^{α} -*tert*-Butoxycarbonyl- N^{ω} -(3,4,5-tris(2-{2-[2-(2-methoxyethoxy)ethoxy]ethoxy}ethoxy)phenyl)-L-phenylalaninamide (3)



To a magnetically stirred solution of HBTU (2.77 g, 7.30 mmol) in dry dimethylformamide (15 mL), DiPEA (5 mL) and Boc-L-PheOH (1.93 g, 7.27 mmol) were added consecutively. This mixture was stirred for 5 min after which it was added to a solution of **2** (4.49 g, 6.31 mmol) in dichloromethane. After stirring overnight at room temperature, the solvents were removed *in vacuo*. The residue was dissolved in dichloromethane (200 mL) and washed with NaHCO_3 ($3 \times 100\text{ mL}$) and brine (200 mL). The organic layer was dried over Na_2SO_4 . After evaporation, the crude product was purified by column chromatography (silica, gradient of 0–10% ethanol in dichloromethane) and subsequently washed with hexane ($3 \times 50\text{ mL}$) and precipitated from dichloromethane (30 mL) in 300 mL of hexane to yield the pure compound as a yellow oil (4.60 g, 4.80 mmol, 76%): $^1\text{H-NMR}$ (CDCl_3): $\delta = 7.93$ (s, 1H, **a**), 7.35–7.20 (m, 5H, **b**), 6.81 (s, 2H, **c**), 5.17 (bs, 1H, **d**), 4.42 (q, 1H, **e**), 4.15–4.05 (m, 6H, **f**), 3.85–3.50 (m, 42H, **g** {6H} + **h** {36H}), 3.34 (s, 9H, **i**), 3.20–3.00 (m, 2H, **j**), 1.40 (s, 9H, **k**) ppm; $^{13}\text{C-NMR}$ (CDCl_3): $\delta = 169.9$ (**1**), 155.6 (**2**), 152.1 (**3**), 136.7 (**4**), 134.1 (**5**), 133.8 (**6**), 129.3 (**7**), 128.5 (**8**), 126.8 (**9**), 99.7 (**10**), 80.1 (**11**), 72.2, 71.7, 70.4, 70.4, 70.3, 70.3, 70.2, 70.1, 69.3, 68.3 (**12**), 58.9 (**13**), 56.7 (**14**), 38.5 (**15**), 28.2 (**16**) ppm; FT-IR (ATR): $\nu = 3333, 2954, 2924, 2854, 1727, 1698, 1604, 1536, 1507, 1468, 1424, 1390, 1367, 1297, 1229, 1163, 1114\text{ cm}^{-1}$; MALDI-TOF MS: m/z calcd. for 958.52 [M]^+ ; found: 958.54 [M]^+ , 981.55 [M+Na]^+ , 997.54 [M+K]^+ .

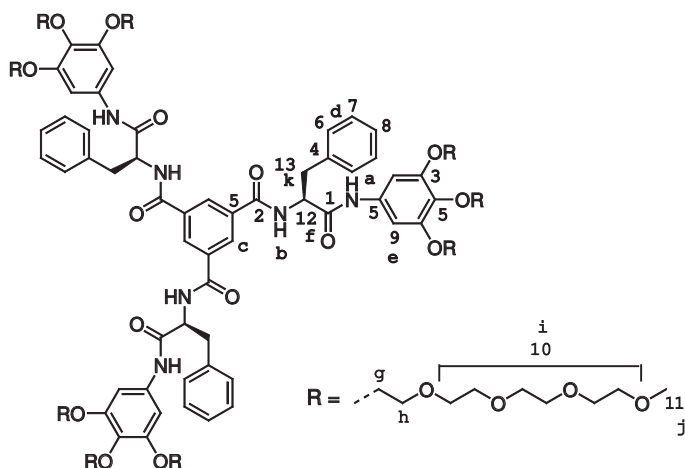
N^{ω} -(3,4,5-Tris(2-{2-[2-(2-methoxyethoxy)ethoxy]ethoxy}ethoxy)phenyl)-L-phenylalaninamide (4)



Compound **3** (1.4 g, 1.45 mmol) was dissolved in H_2O (60 mL) to which 20 mL of TFA was added. The solution was stirred for 3.5 h at room temperature in a nitrogen atmosphere. After evaporation of the solvents at room temperature, the product was stripped with toluene (3 \times) and acetonitrile. A Dowex 550A OH^- column was prepared and washed with water and methanol. The product was dissolved in methanol and applied to the column. Elution with methanol yielded 800 mg of product (0.93 mmol, 65%). With F-NMR no TFA could be detected: $^1\text{H-NMR}$ (CDCl_3): $\delta = 9.35$ (s, 1H, **a**), 7.40–7.20 (m, 5H, **b**), 6.93 (s, 2H, **c**), 4.16 (t, 4H, *meta*-**d**), 4.10 (t, 2H, *p*-**d**), 3.84 (t, 4H, *m*-**e**), 3.77 (t, 2H, *p*-**e**), 3.73–3.52 (m, 37H, **f** {36H} + **g** {1H} + **h** {2H}), 3.37 (s, 3H, *p*-**i**), 3.36 (s, 6H, *m*-**i**), 3.36 + 2.75 + 2.40

(m, 2H, j) ppm; **FT-IR (ATR)**: $\nu = 3503, 2873, 1682, 1603, 1505, 1455, 1426, 1349, 1297, 1242, 1220, 1096 \text{ cm}^{-1}$; **MALDI-TOF MS**: m/z calcd. for 859.47 $[M]^+$; found: 859.40 $[M]^+$, 881.40 $[M+Na]^+$; 897.43 $[M+K]^+$. Unidentified $[X]^+$ Obsd. 901.47.

$N^\alpha, N^\omega, N^{\omega'}$ -(1,3,5-Benzenetricarbonyl)tris[N^ω -(3,4,5-tris(2-{2-[2-(2-methoxyethoxy)ethoxy]ethoxy}ethoxy)-phenyl)-L-phenylalaninamide (1)



A solution of 1,3,5-benzenetricarbonyl trichloride (41.0 mg, 0.15 mmol) in dry dichloromethane (1.0 mL) was added dropwise to a solution of **4** (0.48 g, 0.56 mmol) and triethylamine (0.4 mL) in dry dichloromethane (2.0 mL). After stirring overnight, 50 mL dichloromethane was added and the organic layer was consecutively washed with 1 M KHSO_4 ($2 \times 50 \text{ mL}$), 1 M NaOH ($2 \times 50 \text{ mL}$) and brine (50 mL). The turbid organic layer was dried over MgSO_4 . After evaporation, the crude product was then dialysed, first with 1.1 L water/10 mL triethylamine/ 5 g NaCl and

second with water. After co-evaporation with acetonitrile column chromatography (silica, gradient 0–10% methanol in chloroform) gave the title compound as yellow oil (0.21 g, 0.08 mmol, 51%). The product was characterized using **GPC** (THF, 260 nm, purity based on UV > 99%): **$^1\text{H-NMR}$** (DMSO-d_6): $\delta = 10.14$ (s, 3H, **a**), 8.91 (d, 3H, $J = 8.8 \text{ Hz}$, **b**), 8.32 (s, 3H, **c**), 7.4–7.1 (m, 15H, **d**), 6.98 (s, 6H, **e**), 4.85 (q, 3H, **f**), 4.02 (t, 4H, *meta-g*), 3.94 (t, 2H, *para-g*), 3.72 (t, 4H, *meta-h*), 3.63 (t, 2H, *para-h*), 3.60–3.35 (m, 36H, **i**), 3.20 (s, 3H, *para-j*), 3.19 (s, 6H, *meta-j*), 3.18–3.00 (m, 6H, **k**) ppm; **$^{13}\text{C-NMR}$** (D_2O): $\delta = 170.9$ (**1**), 166.6 (**2**), 151.8 (**3**), 136.2 (**4**), 133.6 (**5**), 129.1 (**6**), 128.5 (**7**), 127.2 (**8**), 99.6 (**9**), 72.2, 70.9, 69.1, 69.6, 69.5, 69.4, 68.9, 68.0, 58.0 (**10**, **11**), 57.1 (**12**), 37.6 (**13**) ppm; **FT-IR (ATR)**: $\nu = 3318, 2872, 1661, 1603, 1530, 1504, 1455, 1426, 1349, 1287, 1226, 1096 \text{ cm}^{-1}$; **MALDI-TOF MS**: m/z calcd. for 2755.17 $[M+Na]^+$; found: 2755.63 $[M+Na]^+$, 2771.55 $[M+K]^+$; **elemental analysis**: calcd. for $\text{C}_{135}\text{H}_{210}\text{N}_6\text{O}_{51}$: 59.33% C, 7.74% H, 3.07% N; found: 58.98% C, 7.71% H, 2.98% N.

¹H-DOSY NMR data

The measurements were executed using the DOSY bipolar pulse paired stimulated echo convection compensation (Dbppste_cc) pulse sequence^[26], to avoid effects of convection within the sample. The steady state pulse sequence was used to compensate for the long relaxation times of HDO. The *gt1* and *del* values for each sample are listed in the Table E1.

Table E1: *gt1* and *del* values for each sample.

T / °C		del / s	gt1 / s
25	Sample	0.060	0.0080
	Standard	0.060	0.0020
35	Sample	0.060	0.0040
	Standard	0.030	0.0020
45	Sample	0.040	0.0040
	Standard	0.015	0.0017
55	Sample	0.040	0.0040
	Standard	0.015	0.0015
65	Sample	0.15	0.0080
	Standard	0.020	0.0015
75	Sample	0.15	0.0080
	Standard	0.020	0.0010

The self-diffusion of HDO was used to calibrate the measurements. It is known from literature that the self-diffusion of HDO in D₂O at 298 K is $19.0 \times 10^{-9} \text{ m}^2\text{s}^{-1}$.^[32] This value was used to modify the original Speedy–Angell power law^[33] reported for the self-diffusion of HDO in water. The theoretical self-diffusion coefficients of HDO in D₂O at the other temperatures were calculated using this modified Speedy–Angell power law^[27,32]:

$$D_{HDO} = 1.635 \times 10^{-8} * \left(\frac{(T - 7.295)}{215.05} - 1 \right)^{2.063}$$

The self-diffusion of HDO in D₂O was measured in a VARIAN 2 Hz D₂O standard sample and calibrated to its theoretical value. Figure E1 shows the measured self-diffusion coefficients of HDO in the sample at different temperatures. Furthermore, the self-diffusion coefficients of HDO in D₂O at three temperatures, 278, 298 and 318 K, as reported by Longworth *et al.*^[32] are included. The modified Speedy–Angell power law^[27,32] is used to fit a line through the measured datapoints. It is clear that the modified Speedy–Angell power law nicely describes the temperature-dependence of the self-diffusion of HDO in D₂O and in the measured samples.

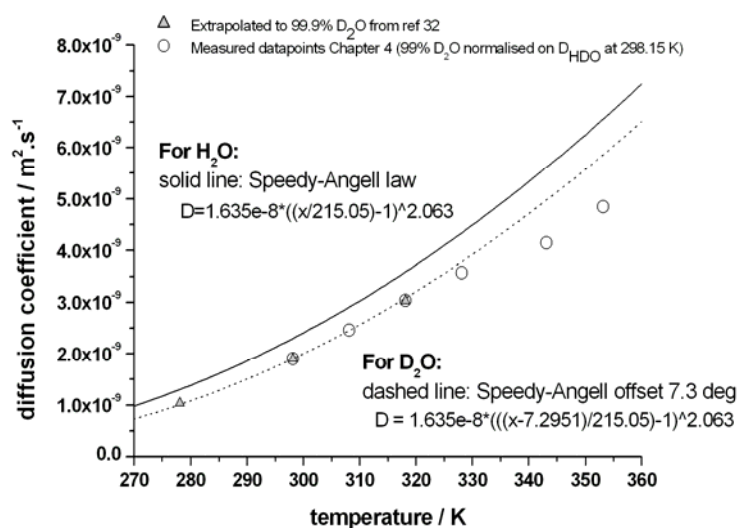


Figure E1: Temperature-dependent diffusion of HDO in D₂O and in the samples fitted with the modified Speedy-Angell power law.^[32]

The model used to calculate the hydrodynamic radii of the aggregates is the Stokes–Einstein relationship^[28] for the diffusion of a spherical particle:

$$D_t = \frac{kT}{6\pi\eta R_H}$$

k = Boltzmann constant

T = absolute temperature

η = dynamic viscosity of the D₂O^(*)

R_H = hydrodynamic radius of the aggregate

(*) The measurements in Chapter 4 show that the self-diffusion of HDO in the sample does not deviate from its theoretical value between 25 °C and 55 °C. In order to estimate the size of the aggregates present at 25 °C to 55 °C the dynamic viscosity of pure D₂O^[27] is used. At 70 °C (343.15 K) and higher, the measured self-diffusion of HDO does deviate from its theoretical value.

4.7 References and notes

- [1] M. Goldberg, R. Langer, X. Jia, *J. Biomater. Sci. Polymer Edn.* **2007**, *18*, 241–268.
- [2] Y. Liu, H. Miyoshi, M. Nakamura, *Int. J. Cancer* **2007**, *120*, 2527–2537.
- [3] T. Barrett, H. Kobayashi, M. Brechbiel, P.L. Choyke, *Eur. J. Radiol.* **2006**, *60*, 353–366.
- [4] L.Y. Qiu, Y.H. Bae, *Pharm. Res.* **2006**, *23*, 1–30.
- [5] F. Kiessling, M. Heilmann, T. Lammers, K. Ulbrich, V. Subr, P. Peschke, B. Waengler, W. Mier, H-H. Schrenk, M. Bock, L. Schad, W. Semmler, *Bioconjugate Chem.* **2006**, *17*, 42–51.
- [6] V.S. Vexler, O. Clement, H. Schmitt-Willich, R.C. Brasch, *J. Magn. Res. Imaging* **1994**, *4*, 381–388.
- [7] T.S. Desser, L.D. Rubin, H.H. Muller, F. Qing, S. Khodor, G. Zanazzi, S.W. Young, D.L. Ladd, J.A. Wellons, K.E. Kellar, *J. Magn. Res. Imaging* **1994**, *4*, 467–472.
- [8] I.L. Medintz, H.T. Uyeda, E.R. Goldman, H. Mattoussi, *Nat. Mater.* **2005**, *4*, 435–446.

- [9] W.J.M. Mulder, A.W. Griffioen, G.J. Strijkers, D.P. Cormode, K. Nicolay, Z.A. Fayad, *Nanomedicine* **2007**, *2*, 307–324.
- [10] Z.P. Xu, Q.H. Zeng, G.Q. Lu, A.B. Yu, *Chem. Eng. Sci.* **2006**, *61*, 1027–1040.
- [11] U. Boas, P.M.H. Heegard, *Chem. Soc. Rev.* **2004**, *33*, 43–63.
- [12] E.R. Gillies, J.M.J. Fréchet, *Drug Discovery Today* **2005**, *10*, 35–43.
- [13] S. Langereis, A. Dirksen, T.M. Hackeng, M.H.P. van Genderen, E.W. Meijer, *New J. Chem.* **2007**, *31*, 1152–1160.
- [14] A. Barge, G. Cravotto, B. Robaldo, E. Gianolio, S. Aime, *J. Incl. Phenom. Macrocycl. Chem.* **2007**, *57*, 489–495.
- [15] S.R. Bull, M.O. Guler, R.E. Bras, P.N. Venkatasubramanian, S.I. Stupp, T.J. Meade, *Bioconjugate Chem.* **2005**, *16*, 1343–1348.
- [16] G.M. Nicolle, E. Tóth, K-P. Eisenwiener, H.R. Mäcke, A.E. Merbach, *J. Biol. Inorg. Chem.* **2002**, *7*, 757–769.
- [17] E.R. Gillies, T.B. Jonsson, J.M.J. Fréchet, *J. Am. Chem. Soc.* **2004**, *126*, 11936–11943.
- [18] M.A.C. Broeren, B.F.M. de Waal, M.H.P. van Genderen, H.M.H.F. Sanders, G. Fytas, E.W. Meijer, *J. Am. Chem. Soc.* **2005**, *127*, 10334–10343.
- [19] R. Knorr, A. Trzeciak, W. Bannwarth, D. Gillessen, *Tetrahedron Lett.* **1989**, *30*, 1927–1930.
- [20] The enantiomeric excess of intermediate 3 was not determined with chiral HPLC.
- [21] L. Brunsveld, Thesis: *Supramolecular chirality from molecules to helical assemblies in polar media*, Eindhoven University of Technology, Eindhoven (The Netherlands), **2001**.
- [22] F. Jr. Bailey, J. Koleske, *Poly (Ethylene Oxide)* Academic Press Inc., New York, **1976**.
- [23] H.Y. Carr, E.M. Purcell, *Phys. Rev.* **1954**, *94*, 630–638.
- [24] S. Meiboom, D. Gill, *Rev. Scient. Instr.* **1958**, *29*, 688–691.
- [25] Claridge T.D.W.; *Tetrahedron Organic Chemistry Series Volume 19: High Resolution NMR Techniques in Organic Chemistry*, Elsevier, **1999**, 13–44.
- [26] A. Jerschow, N. Müller, *J. Magn. Reson.* **1997**, *125*, 372–375.
- [27] C. H. Cho, J. Urquidi, S. Singh, G. Wilse Robinson, *J. Phys. Chem. B* **1999**, *103*, 1991–1994.
- [28] Stokes, G.G.; *Trans. Cambridge Philos. Soc.*, **1845**, *8*, 287.
- [29] Tirado, M.M.; Garcia de la Torre, J.; *J. Chem Phys.*, **1979**, *71*, 2581–2587.
- [30] M. de Loos, Thesis: *Hydrogen-bonded low molecular weight gelators*; University of Groningen: Groningen (The Netherlands), **2005**.
- [31] A. Sakamoto, D. Ogata, T. Shikata, O. Urakawa, K. Hanabusa, *Polymer* **2006**, *47*, 956–960.
- [32] L.G. Longsworth, *J. Phys. Chem.* **1960**, *64*, 1914–1917.
- [33] R.J. Speedy, C.A. Angell, *J. Chem Phys.* **1976**, *65*, 851–858.

5

Self-assembly of paramagnetic discotic amphiphiles

ABSTRACT: *The syntheses are described of four paramagnetic discotic molecules, which all possess 1,3,5-benzenetricarboxamide cores, but differ in their linker units and/or peripheral chelating ligands. Three of the discs contain peripheral Gd^{III}-DTPAs and are referred to as small (1a), medium (2a) and large (3a) Gd^{III}-DTPA discotics, respectively. Going from disc 1a to disc 3a, the capability to undergo secondary interactions and the hydrophobic character both increase. Discotic 4 is very similar to disc 3a; the only difference is that the peripheral Gd^{III}-DTPA moieties are replaced by Gd^{III}-DOTA units. The self-assembly behaviour of these molecules has been studied in aqueous solution using longitudinal relaxation time (T₁) measurements. Concentration-dependent T₁ measurements demonstrate that the self-assembly process of paramagnetic discotics can indeed be probed. Furthermore, by modifying the number of secondary interactions and the size of the hydrophobic core, the self-assembly processes of these molecules can be tuned, which might be important to meet the requirements for use in vivo. From the four paramagnetic discotics synthesized, Gd^{III}-complex 3a is the most promising candidate for a columnar self-assembling contrast agent, in view of its low aggregation concentration and its high ionic relaxivity in the aggregated form (~30 mM⁻¹s⁻¹ at 20 °C and 1.5 T). Furthermore, the well-defined nanometer-size of assemblies of 3a may be advantageous in relation to its pharmacokinetic properties.*

5.1 Introduction

Since the approval of the first magnetic resonance (MR) contrast agent in 1988, there has been a remarkable growth in the utilization of these agents in the clinics. To date, it is estimated that almost 50% of all the MR examinations are contrast-enhanced. Most of the clinically approved contrast agents^[1,2] are complexes incorporating gadolinium (Gd^{III}) as this ion is highly paramagnetic and has a long electronic relaxation time. Drawbacks of the approved contrast agents are their non-specificity and their low efficiency, which only stems from their preference to be in the blood stream, in view of their hydrophilicity. Therefore, there is a strong need for new contrast agents with improved performance. In recent years, various strategies have been explored in order to improve the proton relaxivity of MRI contrast agents.^[3-5] Low molecular weight contrast agents have been coupled to various macromolecules, either covalently^[6-13] or non-covalently^[14-17], to reduce the molecular tumbling rate of the Gd^{III}-complex and, as a result, to increase the proton relaxivity. However, a high molecular weight alone does not guarantee a low tumbling rate and hence a high proton relaxivity. In fact, many flexible linear polymeric systems do not show an appreciable increase in proton relaxivity as molecular weights increase beyond 10 kDa, indicating that segmental flexibility dominates the tumbling rate of the Gd^{III}-complex.^[18,19] Another problem of covalently linked macromolecular systems is non-specific accumulation in the body due to their high molecular weight. As a result, self-assembling contrast agents have recently gained attention owing to their easily controlled properties, good pharmacological characteristics and/or their reversible nature, which allows combining the benefits of both low and high molecular weight contrast agents. Modified micelles^[20,21], liposomes^[22-26], peptide nanofibers^[27] and a system based on cyclodextrins^[28] with ionic relaxivities ranging from 4.1 to 43 mM⁻¹s⁻¹ (at 0.5 T, 25 °C) were reported as potential self-assembling contrast agents for MRI. In addition, it has been shown that T₁ measurements can be used to probe the self-assembly process of these systems, as was reported for biotin-avidin complexes^[29,30] and micelles^[31,32] (see Chapter 1).

So far, research has focused on the use of classical linear amphiphiles mainly forming spherical self-assembled structures, leaving the use of discotic amphiphiles unexplored. Discotic molecules are a special class of amphiphiles that form columnar objects in solution. Compared to spherical assemblies, columnar structures have the advantage of being able to become very long, hence ensuring higher local concentrations of gadolinium. Another benefit of the use of discotic amphiphiles compared to linear amphiphiles is their multivalent character, which leads to higher molecular relaxivities and opens possibilities for the use of asymmetric target-specific discotics. Furthermore, the self-assembly of discotics, especially C₃-symmetrical (C₃)-discotics, has been well-studied. In our laboratory, the self-assembly behaviour of various 1,3,5-benzenetricarboxamide-based discotics has been extensively investigated.^[33-37] In Chapter 4, it has been shown that L-phenylalanine-based discotic

amphiphiles self-assemble into oligomeric structures (11 discs on top of each other) in aqueous solution. These assemblies resemble fourth generation poly(propylene imine) (PPI)-dendrimers in shape, molecular weight as well as the number of endgroups. PPI dendrimers have been applied as multivalent scaffolds for Gd^{III} -DTPA chelates and show high proton relaxivities.^[6] It may therefore be rewarding to synthesize paramagnetic phenylalanine-based discotics in order to study their self-assembly and their potential to act as self-assembling MR contrast agents.

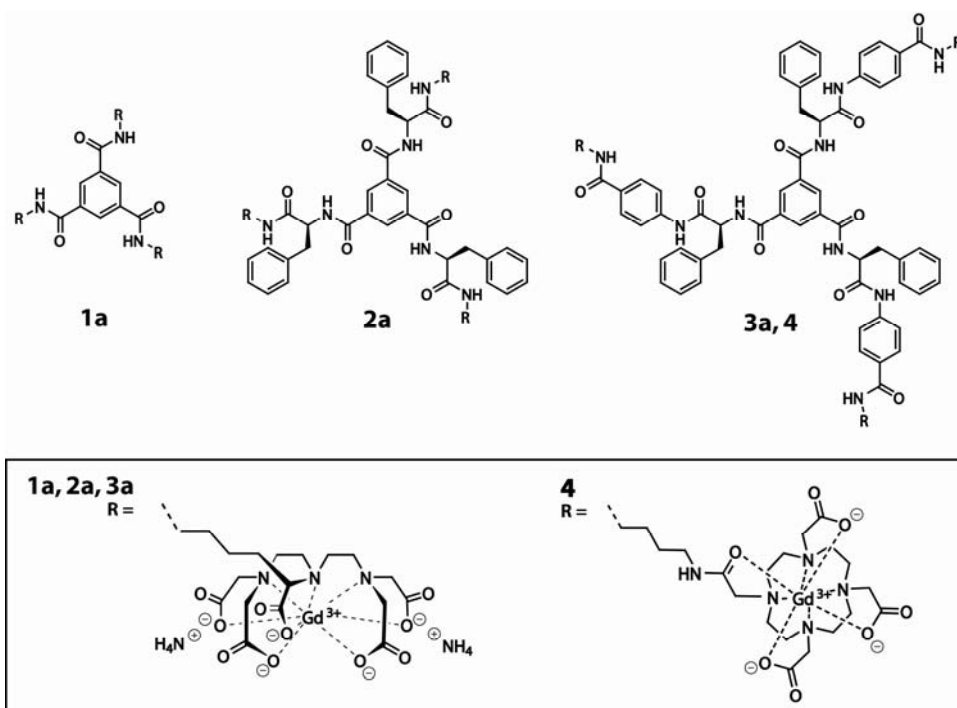


Figure 5.1 Molecular structures of Gd^{III} -DTPA discs **1a** (small), **2a** (medium), **3a** (large) and Gd^{III} -DOTA disc **4** (large).

In this Chapter, the syntheses of three paramagnetic discotics that differ in hydrophobicity of the core and in their ability to undergo secondary interactions are described. The first disc (**1a**) contains lysine-functionalized Gd^{III} -DTPAs, which are directly coupled to the 1,3,5-benzenetricarboxamide core. The second disc (**2a**) contains additional L-phenylalanines in between the core and the lysine-functionalized Gd^{III} -DTPA moieties and the third disc (**3a**) contains, besides additional L-phenylalanines, extra aminobenzoyl units in between the L-phenylalanines and the lysine-functionalized Gd^{III} -DTPA moieties. To enable 1H -NMR based structural elucidation also the corresponding yttrium complexes **1b**, **2b** and **3b** have been synthesized. Paramagnetic discotics (**1a–3a**) have been developed with the aim to determine their proton relaxivities, both in the molecularly dissolved as well as in the self-assembled state. Secondly, this series has been prepared to investigate the possibility to alter

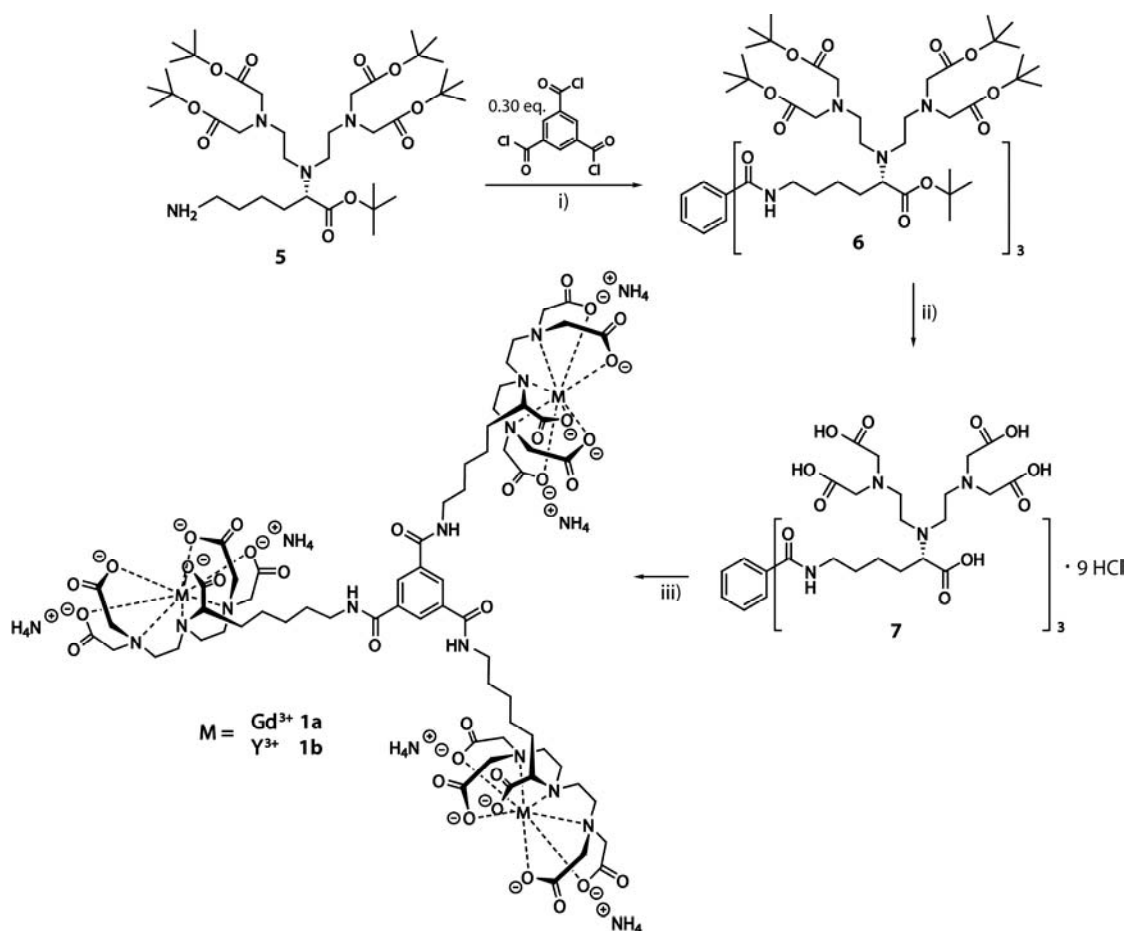
the self-assembly properties by modifying the molecular structure. It is expected that a larger hydrophobic core and increased opportunities for secondary interactions promote self-assembly, so **3a** should self-assemble at much lower concentrations compared to **2a**, which in turn, should aggregate at lower concentrations than **1a**. To demonstrate the universality of our approach a fourth disc, very similar to disc **3a**, has been synthesized. Discs **3a** and **4** only differ in the ligands chelating the gadolinium ions; for **3a** DTPAs and for **4** DOTAs are used (Figure 5.1). The self-assembly processes of **3a** and **4** are, therefore, expected to be very similar. And the final aim is to investigate whether T_1 measurements can be used as a valuable tool to study the more complex self-assembly behaviour of discotic molecules.

5.2 Small Gd^{III}-DTPA discotics (**1a,b**)

5.2.1 Syntheses

The synthetic routes towards small Gd^{III}- and Y^{III}-DTPA complexes (**1a,b**) are depicted in Scheme 5.1. Lysine-functionalized DTPA **5**^[38,39] was directly coupled with 0.30 molar equivalents of trimesic chloride in the presence of triethylamine as a base to afford molecule **6** in 78% yield. Removal of the Boc-groups of compound **6** was accomplished in two steps. During the first hour, compound **6** was treated with 2 M HCl in dioxane/chloroform. The suspension was concentrated *in vacuo* and the reaction was completed by the addition of 2 M aqueous HCl. Finally, metal complexes **1a,b** were prepared by adding Gd(OAc)₃ or Y(OAc)₃, respectively, to compound **7** in water. The pH of the solution was monitored and maintained at 7 by adding small aliquots of 0.1 M NH₄OH. The exact amount of Gd^{III} or Y^{III} needed was predetermined by performing a UV titration with xylenol orange as the indicator.^[40,41] After lyophilizing the reaction mixture and precipitating the lyophilized product from water in ethanol, compounds **1a,b** were obtained as off-white solid materials.

Structural characterization of all intermediates was performed with a combination of analytical techniques including ¹H- and ¹³C-NMR spectroscopy, IR spectroscopy, MALDI-TOF MS and elemental analysis. Characterization of metal complexes **1a,b** was performed with IR and ESI-MS, while the Gd^{III}- or Y^{III}-content was determined with inductively coupled plasma mass spectrometry (ICP-MS). The Gd^{III}-content of **1a** was 92% of the theoretical value, while the Y^{III}-content of **1b** was 80% of the theoretical value.



Scheme 5.1 Synthetic routes towards discs **1a,b**. i) Et_3N , DCM , 78%; ii) 1) HCl , dioxane/ CHCl_3 (1:1 v/v), 2) HCl , H_2O , 92%; iii) **1a**) $\text{Gd}(\text{OAc})_3 \cdot x\text{H}_2\text{O}$, H_2O , 0.1 M NH_4OH (pH 7), 64%, **1b**) $\text{Y}(\text{OAc})_3 \cdot x\text{H}_2\text{O}$, H_2O , NaOAc buffer (pH 5.3), 91%.

5.2.2 Self-assembly in solution

T_1 measurements for Gd^{III} -complex **1a** were performed at concentrations ranging between 0.0 and 1.5 mM Gd^{III} in 200 mM Tris buffer (pH 7.4). The T_1 of an 18 mM Gd^{III} solution of **1a** was also measured. All longitudinal relaxation time measurements were performed at 1.5 T and 20 °C. Figure 5.2 shows that the datapoints in the low concentration regime (0.0–1.5 mM Gd^{III}) can be fitted by a single line, which possesses a correlation coefficient of 0.99987 and crosses the y-axis exactly at the measured R_1^{d} (0.39 s^{-1}) of the Tris buffer. If the fitted line is extrapolated to higher concentrations, it crosses the datapoint of the solution with a Gd^{III} -concentration of 18 mM (Figure 5.3). This suggests that Gd^{III} -complex **1a** is molecularly dissolved over the whole concentration regime (0–18 mM). The ionic longitudinal relaxivity for **1a** is 8.2 $\text{mM}^{-1}\text{s}^{-1}$.

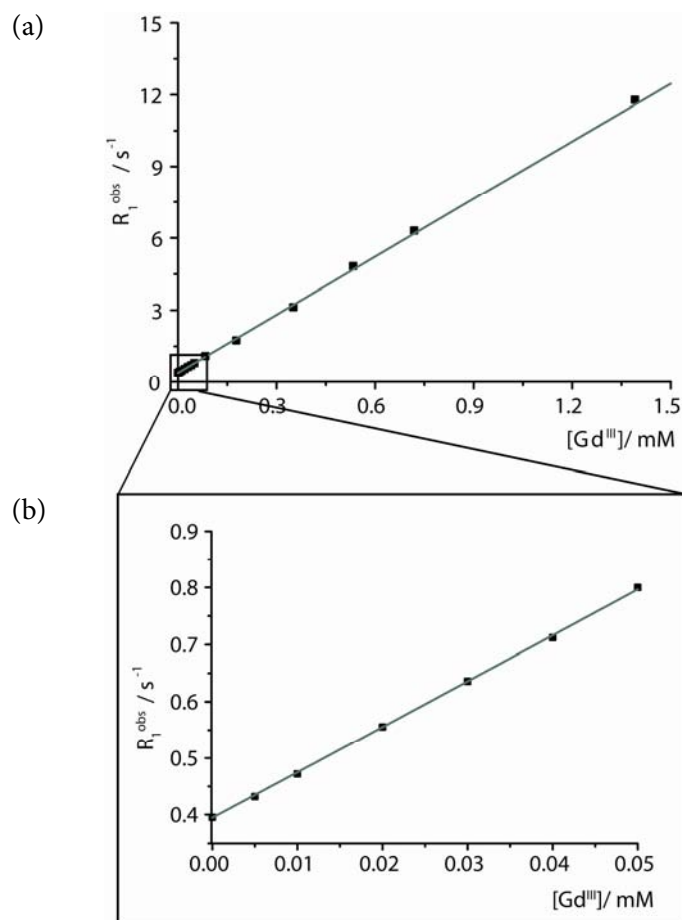


Figure 5.2 The longitudinal relaxation rate ($R_1^{obs} = 1/T_1^{obs}$) is plotted against the gadolinium concentration for Gd^{III} -complex **1a**; (a) concentration window 0.0–1.5 mM; (b) concentration window 0.00–0.05 mM. The correlation coefficient R of the fit through all datapoints is 0.99987.

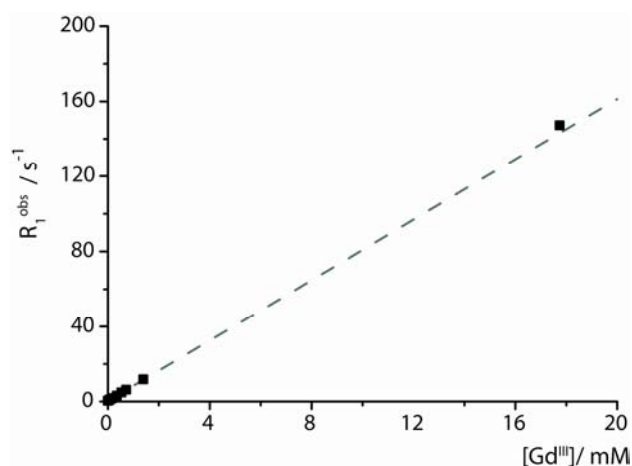


Figure 5.3 The fitted line is extrapolated to higher concentrations of gadolinium for Gd^{III} -complex **1a**.

Gd^{III} -complex **1a** was further investigated with *cryo*TEM, CD and UV/Vis spectroscopy, while 1H -NMR spectroscopy was performed on yttrium version **1b**. Solutions

with different concentrations of **1a** (2, 10 and 20 mM Gd^{III}) in D₂O were visualized with *cryo*TEM, but no assemblies could be observed (images not included). Figure 5.4 shows the CD and UV/Vis spectra for compound **1a** in water at 20 °C. The CD curve of **1a** does not show a Cotton effect, which is in full agreement with the relaxation time data because it also indicates the absence of aggregates.

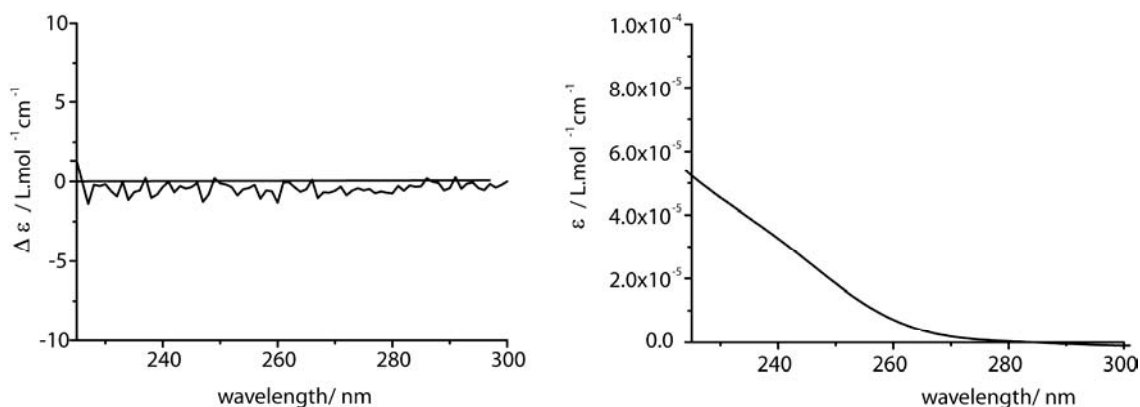


Figure 5.4 CD and UV/Vis spectra of Gd^{III}-complex **1a** in 200 mM Tris (pH 7.4) at 20 °C; [Gd^{III}] = 5.1 mM.

Figure 5.5 shows the ¹H-NMR spectrum of compound **1b** in D₂O at 25 °C. All peaks in the spectrum are sharp, even those corresponding to the central core protons, which appear around 8 ppm.

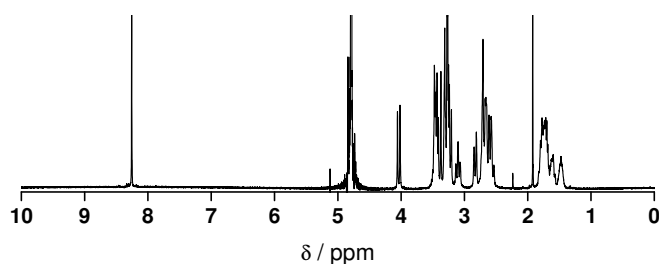


Figure 5.5 ¹H-NMR spectrum of Y^{III}-complex **1b** in D₂O at 25 °C; [Y^{III}] = 20 mM.

5.2.3 Conclusions

The self-assembly behaviour of discotics **1a** and **1b** has been studied using T₁ measurements and CD/UV spectroscopy and *cryo*TEM and ¹H-NMR spectroscopy, respectively. The T₁ measurements suggest that Gd^{III}-complex **1a** does not form aggregates within the investigated concentration regime, which is supported by a sharp ¹H-NMR spectrum of Y^{III}-complex **1b** and the absence of aggregates in the *cryo*TEM image. Most likely,

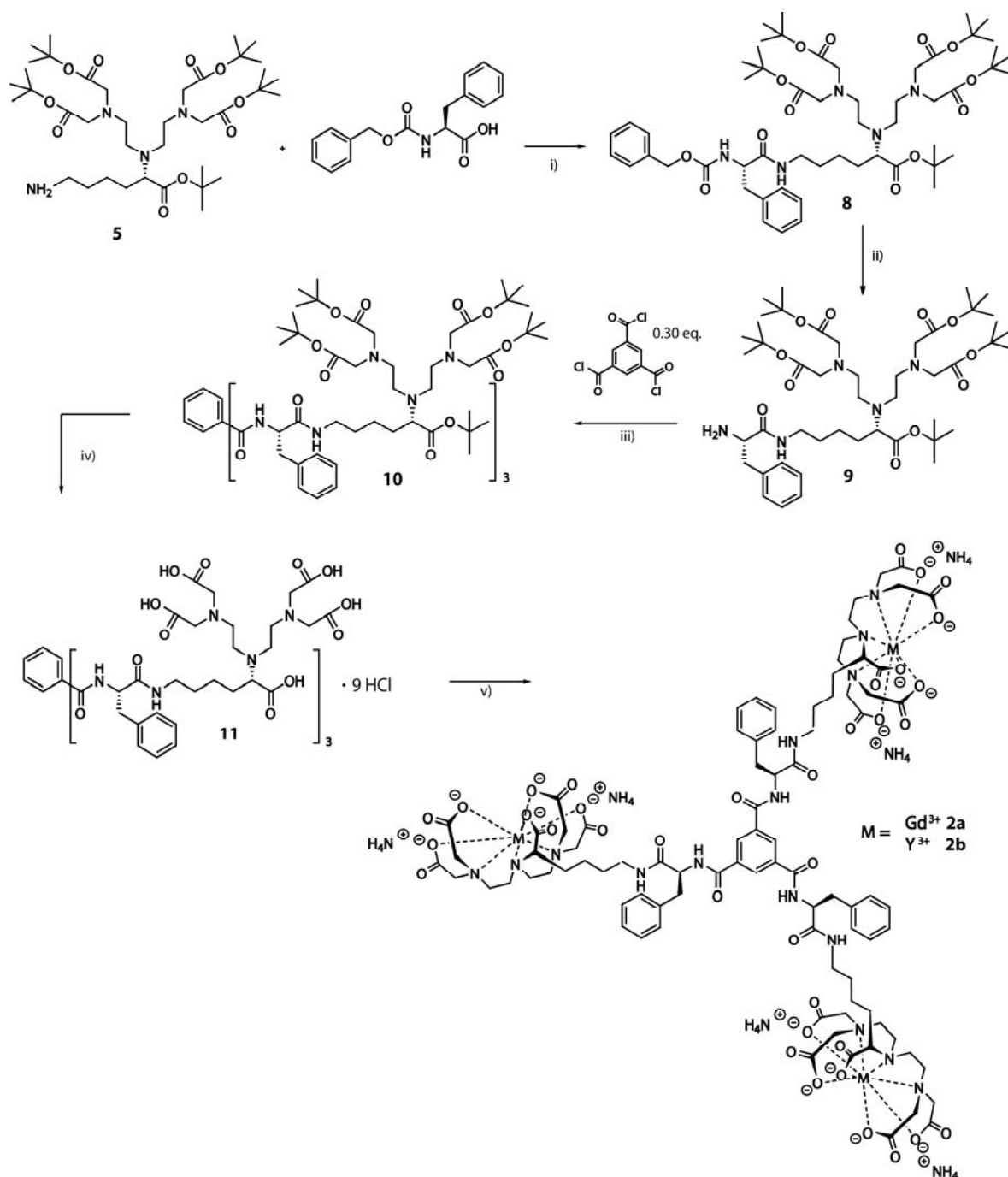
the hydrophobic core is too small, in relation to the bulky Gd^{III}-DTPA units that are highly hydrophilic, to generate a tendency for the discs to stack on top of each other. The ionic relaxivity of molecularly dissolved Gd^{III}-complex **1a** is 8.2 mM⁻¹s⁻¹. This value is in full agreement with the reported ionic relaxivities for Gd^{III}-DTPA units coupled to small molecules.^[42] Discs **2a**, **3a** and **4** are expected to show stronger tendencies for self-assembly, since these discs possess a larger hydrophobic core and increased opportunities for secondary interaction, therefore, the focus has been directed to these discotics.

5.3 Medium Gd^{III}-DTPA discotics (**2a,b**)

Compounds **2a,b** contain additional L-phenylalanines in between the core and the lysine-functionalized DTPAs. These phenylalanines provide extra secondary amide functionalities, which allow for intermolecular hydrogen bonding; the embedded phenyl groups may promote additional π - π interaction and the hydrophobic phenyl groups could also promote self-assembly in water. Therefore, it is expected that the additional phenylalanines will improve the self-assembly properties of these molecules. Another advantage of these molecules (**2a,b**) compared to the previous ones (**1a,b**), is the presence of additional stereocentres closer to the core of the disc, which may function as a chiral tool to study the self-assembly behaviour of these molecules with CD spectroscopy.

5.3.1 Syntheses

The syntheses of intermediate Gd^{III}- and Y^{III}-DTPA complexes **2a,b** are depicted in Scheme 5.2. Lysine-functionalized DTPA **5** was coupled with *N*-benzyloxycarbonyl-L-phenylalanine using HBTU as a coupling reagent and DiPEA as a base. HBTU was used as the coupling reagent because it is known to preclude racemization of the activated amino acid.^[43,44] The benzyloxycarbonyl group of compound **8** was removed with catalytic hydrogenation affording compound **9**. Amino-terminated intermediate **9** was reacted with 0.30 molar equivalents of trimesic chloride in the presence of triethylamine as a base. Removal of the Boc-groups and complexation of the DTPA-ligand with Gd^{III} gave compounds **11** and **2a,b** as described for compounds **7** and **1a,b**, respectively. The Gd^{III}-content of **2a** was 80% of the theoretical value, while the Y^{III}-content of **2b** was 93% of the theoretical value.



Scheme 5.2 Synthetic routes towards discs **2a,b**. i) HBTU, DiPEA, DMF, 72%; ii) H_2 (g), 10% Pd/C, MeOH/ CH_3COOH (10/1 v/v), 62%; iii) Et_3N , DCM, 34%; iv) 1] HCl, dioxane/ CHCl_3 (1:1 v/v), 2] HCl, H_2O , quantitative yield; v) **2a**) $\text{GdCl}_3 \cdot 6\text{H}_2\text{O}$, H_2O , 0.1 M NH_4OH (pH 7), quantitative yield, **2b**) $\text{YCl}_3 \cdot 6\text{H}_2\text{O}$, H_2O , 0.1 M NH_4OH , (pH 7), quantitative yield.

5.3.2 Self-assembly in solution

T_1 measurements for Gd^{III} -complex **2a** were performed in a concentration regime ranging from 0 to 9 mM Gd^{III} , in 200 mM Tris buffer (pH 7.4). The measurements were performed at 1.5 T and 20 °C.

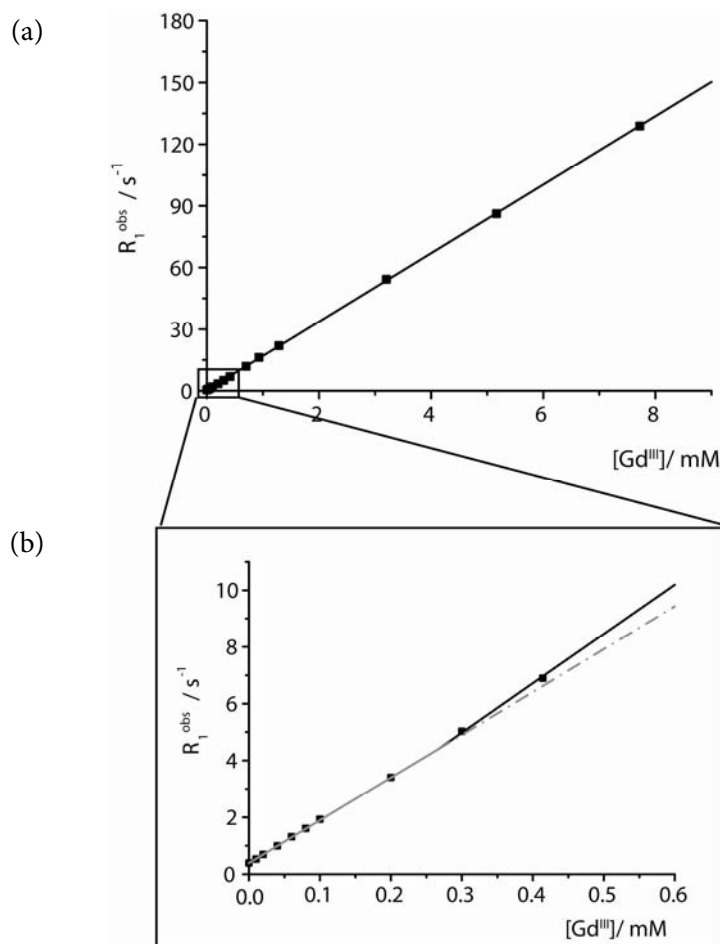


Figure 5.6 The longitudinal relaxation rate (R_1^{obs}) is plotted against the gadolinium concentration for Gd^{III} -complex **2a**; (a) concentration window 0–9 mM; (b) concentration window 0.0–0.6 mM; The solid and dotted lines are just to guide the eye.

Figure 5.6 shows the measured datapoints for discotic **2a**. If a line to guide the eye is drawn through these points, it becomes clear that it is difficult to describe all datapoints with one single line. Therefore, two lines are included in Figure 5.6. At the lower concentrations, the line crosses the y-axis at the measured R_1^d of the Tris buffer and has a correlation coefficient of 0.99993. This suggests that the molecules are in the molecularly dissolved state. The ionic relaxivity of molecularly dissolved **2a** is $\sim 15 \text{ mM}^{-1}\text{s}^{-1}$. At around 0.27 mM Gd^{III} , a subtle deviation from linearity takes place suggesting that the discs are aggregating. Aggregation of the paramagnetic discotics most likely limits the local freedom of movement of the Gd^{III} -DTPAs and thereby increases the ionic relaxivity; an estimated ionic relaxivity of $\sim 17 \text{ mM}^{-1}\text{s}^{-1}$ is obtained in the second regime.

Gd^{III} -complex **2a** was further investigated with *cryo*TEM and CD/UV spectroscopy, while ^1H -NMR spectroscopy was performed on the yttrium version **2b** in order to gather additional proof for the presence of aggregated molecules at higher concentrations. Figure 5.7 shows two *cryo*TEM images at different concentrations, 1.3 mM Gd^{III} and 13 mM Gd^{III} .

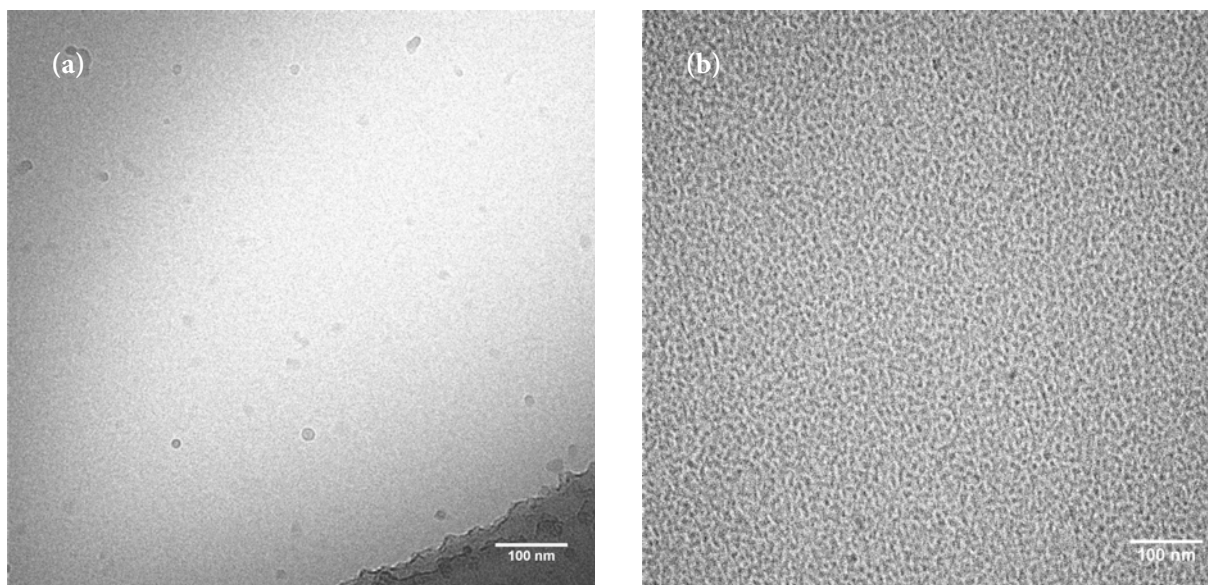


Figure 5.7 CryoTEM images of Gd^{III} -complex **2a** in 200 mM Tris buffer (pH 7.4) have been obtained with an underfocus value of $-1 \mu\text{m}$; (a) $[Gd^{III}] = 1.3 \text{ mM}$; (b) $[Gd^{III}] = 13 \text{ mM}$.

In Figure 5.7a, which is at the lowest concentration, no aggregates can be observed. This does not necessarily mean that the molecules do not aggregate. It is possible that small aggregates (smaller than 2 nm) are present, which are too small to be visualized with cryoTEM. Figure 5.7b, which is the highest concentration, does show the presence of aggregates. Since no large assemblies can be deduced from this image, it indirectly indicates that the assemblies are very small (a few nanometers).

The CD and UV/Vis spectra of **2a** at two concentrations, 0.055 mM Gd^{III} and 0.55 mM Gd^{III} , and two temperatures, 20 °C and 90 °C, are depicted in Figure 5.8.

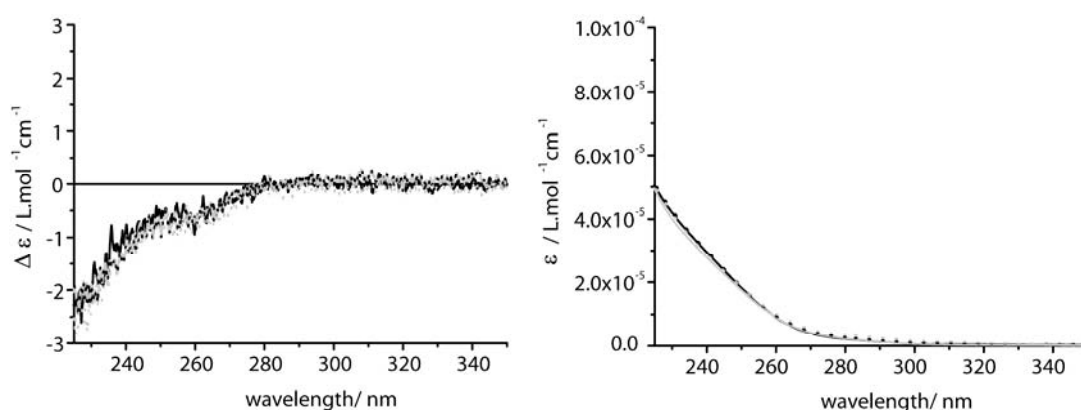


Figure 5.8 CD and UV/Vis spectra of Gd^{III} -complex **2a** in 200 mM Tris (pH 7.4) at 20 °C (black) and 90 °C (grey); (—) $[Gd^{III}] = 0.55 \text{ mM}$ and (---) $[Gd^{III}] = 0.055 \text{ mM}$.

Both solutions are CD active, but no concentration- or temperature-dependence is observed. A possible explanation, which is in agreement with the previous results, is that at the lowest concentration molecularly dissolved species are present, which display a Cotton effect that is inherent to the molecule. Conversely, at the higher concentration assemblies are present, but they are not able to transfer the chirality present in the L-phenylalanine moieties to a higher level of organization, either because the aggregates are still too small or because the order within the aggregates is too low.

Figure 5.9 shows an $^1\text{H-NMR}$ spectrum of Y^{III} -complex **2b** in D_2O ($[\text{Y}^{\text{III}}] = 17 \text{ mM}$). In this spectrum no significant broadening of the proton resonances could be observed.

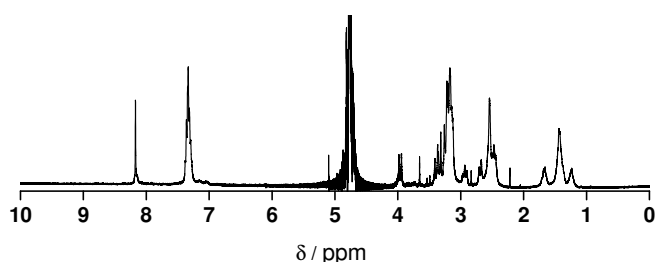


Figure 5.9 $^1\text{H-NMR}$ spectrum of Y^{III} -complex **2b** in D_2O at $25 \text{ }^\circ\text{C}$; $[\text{Y}^{\text{III}}] = 17 \text{ mM}$.

5.3.3 Conclusions

The self-assembly behaviour of discotics **2a** and **2b** has been studied using T_1 measurements, CD and UV/Vis spectroscopy and *cryo*TEM and $^1\text{H-NMR}$ spectroscopy, respectively. The T_1 measurements suggest that Gd^{III} -complex **2a** self-assembles in aqueous solution. This observation is supported by *cryo*TEM measurements, which also show that assemblies are present at higher concentrations. The $^1\text{H-NMR}$ measurements, on the other hand, could not give additional proof for the presence of aggregates at higher concentrations.

According to the T_1 measurements, the ionic relaxivity of molecularly dissolved Gd^{III} -complex **2a** is $\sim 15 \text{ mM}^{-1}\text{s}^{-1}$, which is comparable to the ionic relaxivity of a third generation poly(propylene imine) dendrimer.^[6] This value is significantly higher than the value obtained for molecularly dissolved **1a** ($8.2 \text{ mM}^{-1}\text{s}^{-1}$). In general, higher molecular weights result in reduced global mobilities and hence higher ionic relaxivities, so this may explain the higher ionic relaxivity observed for discotic **2a**. On the other hand, the extra L-phenylalanines in **2a** may rigidify the Gd^{III} -DTPA moieties thereby decreasing their local freedom of movement. This may also contribute to a higher ionic relaxivity for discotic **2a**. The ionic relaxivity of discs of **2a** present within an aggregate can only be estimated ($\sim 17 \text{ mM}^{-1}\text{s}^{-1}$) since the mechanism of self-assembly and the association constant(s) describing the self-assembly process are not known.

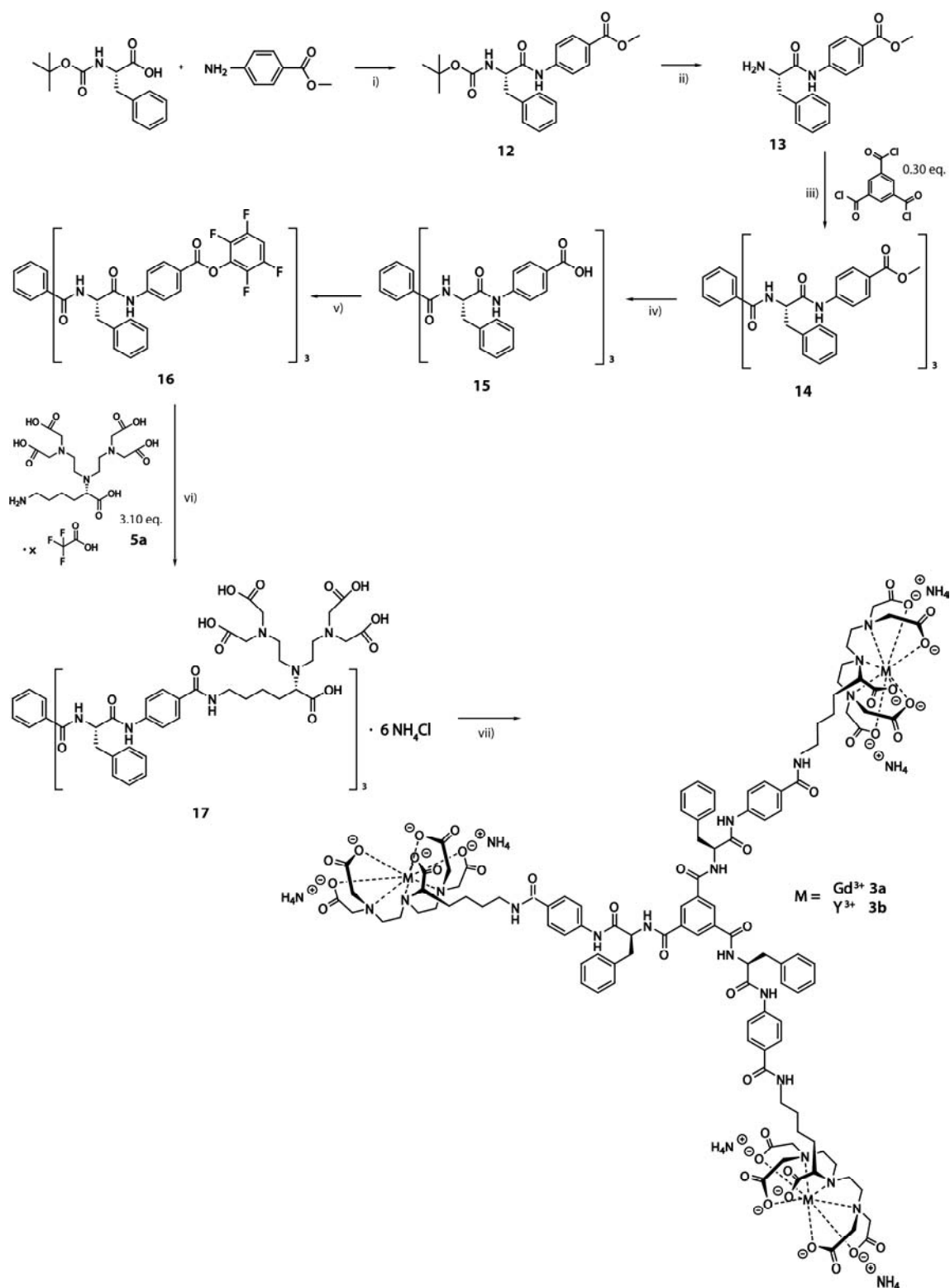
Since medium-size discotic **2a** does self-assemble and small disc **1a** does not, it is demonstrated that the aggregation properties of these discotic amphiphiles can indeed be improved by increasing the number of the secondary interactions and enlarging the hydrophobic core. According to the T_1 measurements, aggregation of disc **2a** starts around a gadolinium concentration of 0.27 mM (which corresponds to 0.09 mM discs). Since *in vivo* concentrations would be expected at or below 1 mM^[32], an aggregation concentration of 0.27 mM Gd^{III} is already rather high. Hence, the self-assembly of disc **2a** has not been investigated in more detail, and the focus has been fixed on large Gd^{III}-DTPA discotic **3a**.

5.4 Large Gd^{III}-DTPA discotics (**3a,b**)

Compounds **3a,b** contain, besides additional L-phenylalanines, extra amino-benzoyl units in between the phenylalanines and the lysine-functionalized DTPA moieties. These units may offer additional hydrogen bonding interactions and the possibility of π - π interaction in order to strengthen the secondary interactions to improve the self-assembly properties at even lower concentrations.

5.4.1 Syntheses

The syntheses of the intermediate Gd^{III}- and Y^{III}-DTPA complexes **3a,b** are depicted in Scheme 5.3. Commercially available Boc-L-PheOH was reacted with methyl-4-aminobenzoate using HATU as the coupling reagent and DiPEA as a base. The enantiomeric purity of compound **12** was determined with chiral HPLC and exceeded 99%. Deprotection of the Boc-groups of **12** was accomplished with a one hour treatment with TFA. Subsequently, free amine **13** was isolated via a basic work up. Compound **13** was reacted with 0.30 molar equivalents of trimesic chloride in the presence of DiPEA as a base. Saponification of **14** was carried out in a mixture of THF/ 3.5 M aqueous NaOH. The solution had to be stirred for four days to get the reaction to completion. Subsequently, intermediate **15** was reacted with tetrafluorophenol in the presence of a catalytic amount of DMAP, using EDC as a coupling reagent. Active ester **16** was coupled to 3.10 molar equivalents of deprotected lysine-DTPA analogue **4a** in the presence of DiPEA as a base. Finally, metal complexes **3a** and **3b** were prepared by adding Gd(OAc)₃ and Y(OAc)₃, respectively, to compound **17**. After lyophilizing the reaction mixtures, compounds **3a,b** were obtained as fluffy white powders. Structural characterization of all intermediates was performed with a combination of analytical techniques including ¹H- and ¹³C-NMR spectroscopy, IR spectroscopy, MALDI and elemental analysis. Characterization of metal complexes **3a,b** was performed with IR and ESI-MS, while the Gd^{III}- or Y^{III}-content was determined with ICP-MS. The Gd^{III}-content of **3a** was 63% of the theoretical value, while the Y^{III}-content of **3b** was 84% of the theoretical value.



Scheme 5.3 Synthetic routes towards discs **3a,b**. i) HATU, DiPEA, DMF, 24%; ii) [1] TFA, [2] basic work up, 87%; iii) DiPEA, DCM, 71%; iv) 1] THF / 3.5 M NaOH(aq), 2] acidify to pH 3 and centrifugation, 104%; v) 2,3,5,6-tetrafluorophenol, DMAP, EDC, DCM, 57%; vi) 1] DiPEA, DMSO, 2] acidify to pH 3 and centrifugation, 3] treatment with NH₄OH, 69%; vii) **3a**) Gd(OAc)₃·x H₂O, ultra pure water, 0.1 M NH₄OH (pH 7), 133%; **3b**) Y(OAc)₃·xH₂O, ultra pure water, 0.1 M NH₄OH (pH 7), quantitative yield.

5.4.2 Self-assembly in solution

T_1 measurements on Gd^{III} -complex **3a** were performed in a concentration regime ranging from 0 to 4 mM Gd^{III} , in 200 mM Tris buffer (pH 7.4). The measurements were performed at 1.5 T and 20 °C. Figure 5.10 shows the measured datapoints for discotic **3a**.

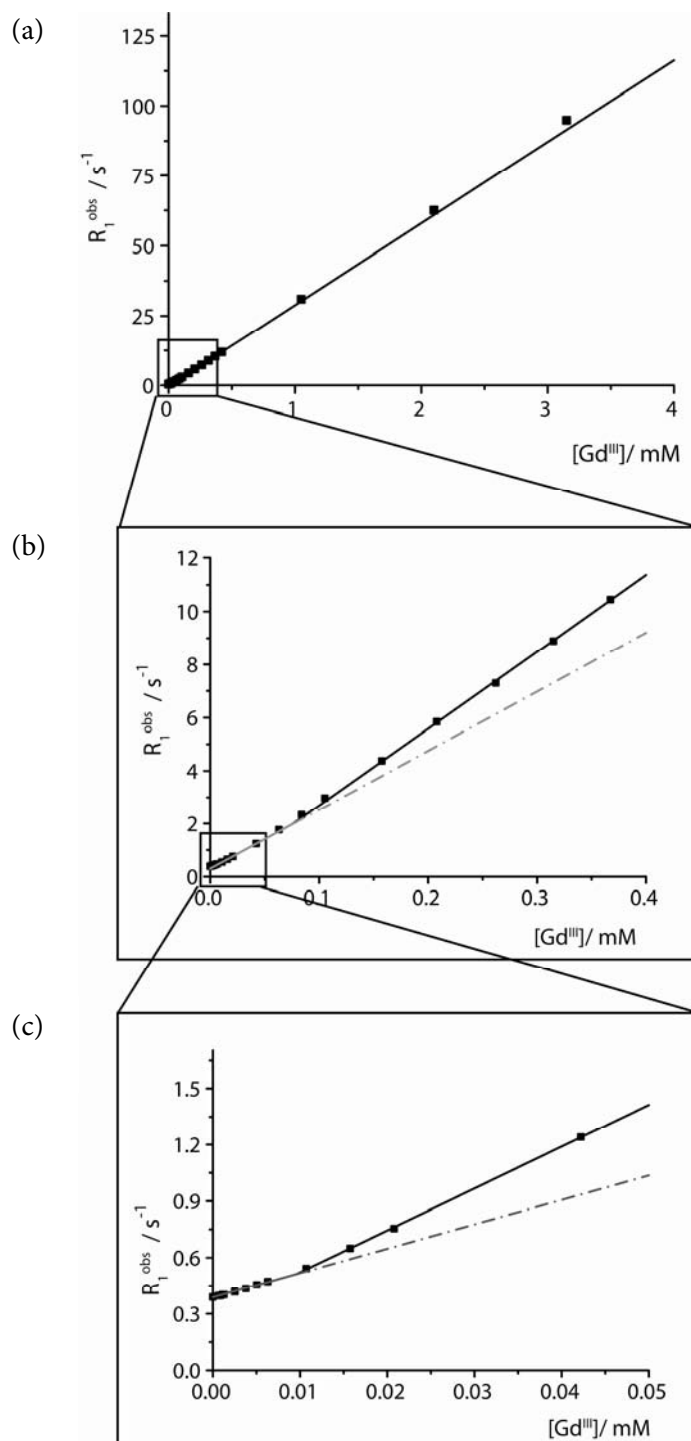


Figure 5.10 The longitudinal relaxation rate (R_1^{obs}) is plotted against the gadolinium concentration for Gd^{III} -complex **3a**; (a) concentration window 0–4 mM; (b) concentration window 0.0–0.4 mM; (c) concentration window 0.00–0.05 mM. The lines are just to guide the eye.

If a line to guide the eye is drawn through these points, it becomes clear that it is impossible to describe all datapoints with one single line. Three lines are needed to follow the datapoints, which suggests that aggregation takes place. It also suggests that three regimes can be discerned during the self-assembly process, presumably corresponding to molecularly dissolved discs, small aggregates and higher order aggregates. The three lines are included in Figure 5.10. It has to be stressed that these lines are just to guide the eye. The line at the lower concentrations crosses the y-axis at the measured R_1^d of the Tris buffer, but the correlation coefficient of the line is not good ($R = 0.99792$). This proves that a model is needed to fit the data in order to determine the ionic relaxivity of molecularly dissolved discs of **3a**, the concentration at which aggregation starts. However, as a rough estimate for the ionic relaxivity of molecularly dissolved discotic **3a** the slope of the line at the lowest concentrations can be taken, which is $13 \text{ mM}^{-1}\text{s}^{-1}$. Furthermore, it can be deduced that the concentration at which aggregation starts lies below $0.01 \text{ mM Gd}^{\text{III}}$, which is, as expected, much lower than the corresponding aggregation concentration found for discotic **2a** ($0.27 \text{ mM Gd}^{\text{III}}$).

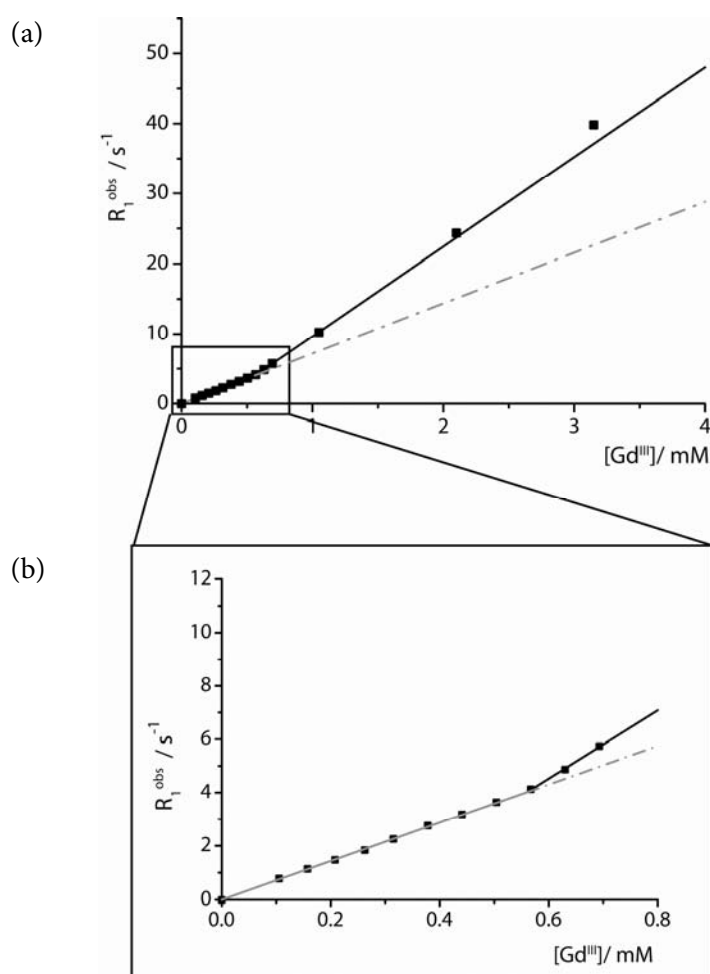


Figure 5.11 The longitudinal relaxation rate (R_1^{obs}) at $80 \text{ }^\circ\text{C}$ is plotted against the gadolinium concentration for Gd^{III} -complex **3a**; (a) concentration window 0–4 mM; (b) concentration window 0.0–0.8 mM. The lines are just to guide the eye.

To show the influence of a higher temperature on the proton relaxivity, the measurements were also performed at 80 °C and 1.5 T (Figure 5.11). It was not possible to measure the datapoints at a concentration lower than 0.1 mM Gd^{III}, because the relaxation times became too long. The only datapoint below 0.1 mM Gd^{III} that could be obtained was the R_1^d , because it could be estimated via extrapolation of the R_1^d measured at 20, 30, 35 and 40 °C (Appendix A). From 0.00 mM to 0.56 mM Gd^{III}, the datapoints lie on a straight line that crosses the y-axis exactly at the estimated R_1^d of the Tris buffer (the correlation coefficient is $R = 0.99976$), which suggests that the compound is in the molecularly dissolved state. Furthermore, the concentration at which aggregation starts is considerably shifted to higher concentrations (0.56 mM Gd^{III} at 80 °C compared to < 0.01 mM Gd^{III} at 20 °C).

In order to arrive at a model that is able to fit the relaxation time data measured at 20 °C more details concerning the self-assembly process of this discotic are needed. For this reason, Gd^{III}-complex **3a** has been further investigated with CD and UV/Vis spectroscopy, while *cryo*TEM images have been taken and NMR measurements have been performed on yttrium version **3b**.

The CD and UV/Vis spectra of **3a** at three concentrations selected in the three regimes determined by the T_1 measurements, namely 0.2 mM Gd^{III}, 0.02 mM Gd^{III} and 0.004 mM Gd^{III}, and two temperatures, 20 °C and 90 °C, are depicted in Figures 5.12 and 5.13.

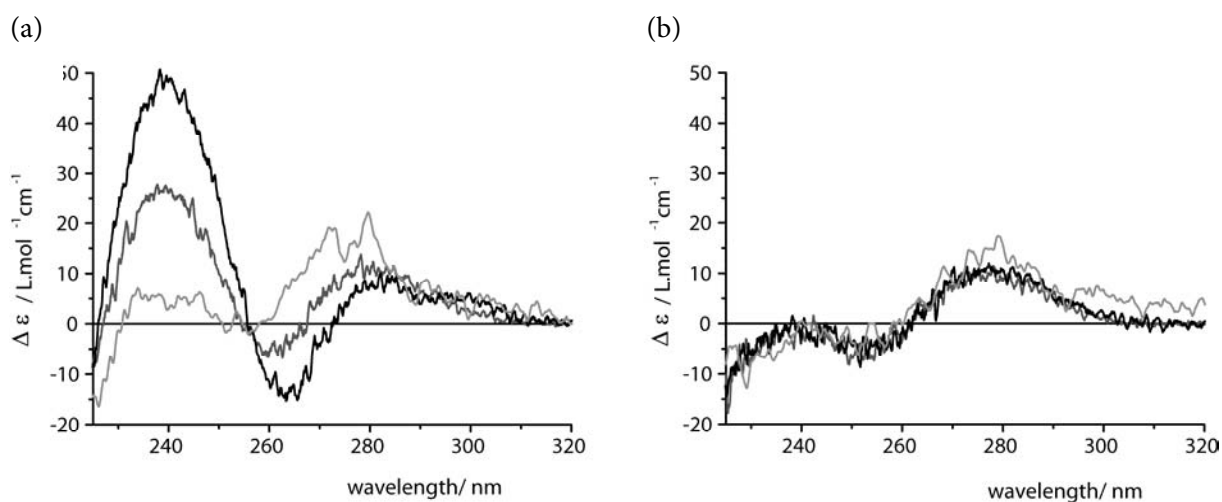


Figure 5.12 CD spectra of Gd^{III}-complex **3a** in 200 mM Tris (pH 7.4) (a) at 20 °C and (b) at 90 °C; $[\text{Gd}^{\text{III}}] = 0.2 \text{ mM}$ (black), $[\text{Gd}^{\text{III}}] = 0.02 \text{ mM}$ (dark grey) and $[\text{Gd}^{\text{III}}] = 0.004 \text{ mM}$ (grey).

All solutions are CD active both at 20 °C and at 90 °C. The graphs at 20 °C are all different, which suggests that different regimes in the aggregation process are visualized. The spectra at 90 °C are all identical, what suggests that at this temperature all samples are in the molecularly dissolved state. According to the CD curves at 20 °C, discotic **3a** is at none of the

measured concentrations completely molecularly dissolved even at 0.004 mM Gd^{III}. Although the CD curve at this concentration is almost similar to the one at 90 °C. The increase in Cotton effect going from 0.004 to 0.2 mM Gd^{III} can be rationalized by the fact that the ratio aggregated species/molecularly dissolved species increases with concentration.

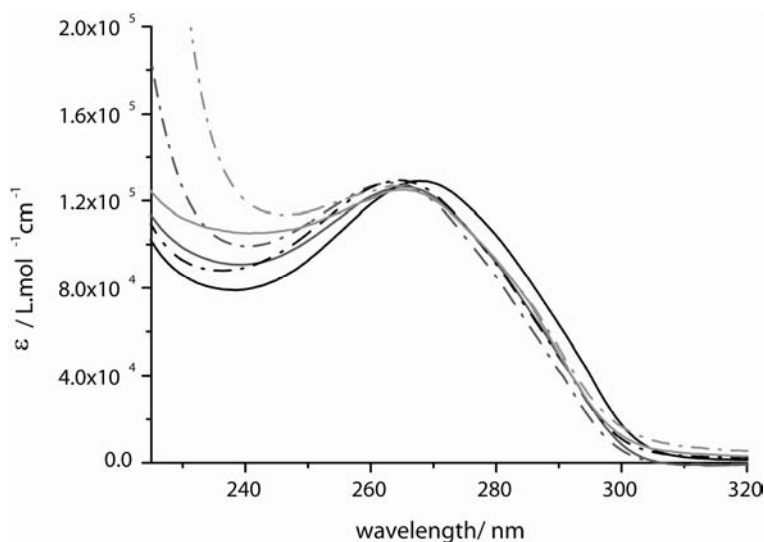


Figure 5.13 UV/Vis spectra of Gd^{III}-complex **3a** in 200 mM Tris (pH 7.4) at 20 °C (—) and at 90 °C (---); [Gd^{III}] = 0.2 mM (black), [Gd^{III}] = 0.02 mM (dark grey) and [Gd^{III}] = 0.004 mM (grey).

The UV/Vis spectra are more or the less the same. The spectrum of 0.2 mM Gd^{III} at 20 °C is 3 nm red-shifted compared to the others, but this difference is too small to draw any conclusions.

Temperature-dependent CD measurements at a concentration of 0.2 mM Gd^{III} were performed to determine via which mechanism these molecules self-assemble, a nucleation–elongation^[45–47] or an isodesmic^[47,48] mechanism. Figure 5.14a shows the cooling curve of **3a**; the sample is cooled from 90 °C to 20 °C at a rate of 1 °C·min⁻¹. The heating curve is not shown, but the curves lie on top of each other, meaning that the system is in thermodynamic equilibrium. This curve can be fitted with a sigmoidal (Boltzmann) model meaning that the self-assembly follows an isodesmic mechanism. The sigmoidal (Boltzmann) fit is used to normalize the data as is shown in Figure 5.14b, in which the degree of polymerization is plotted against the temperature. To normalize the data the assumption that all aggregated discs contribute in equal amounts to the CD effect is made.

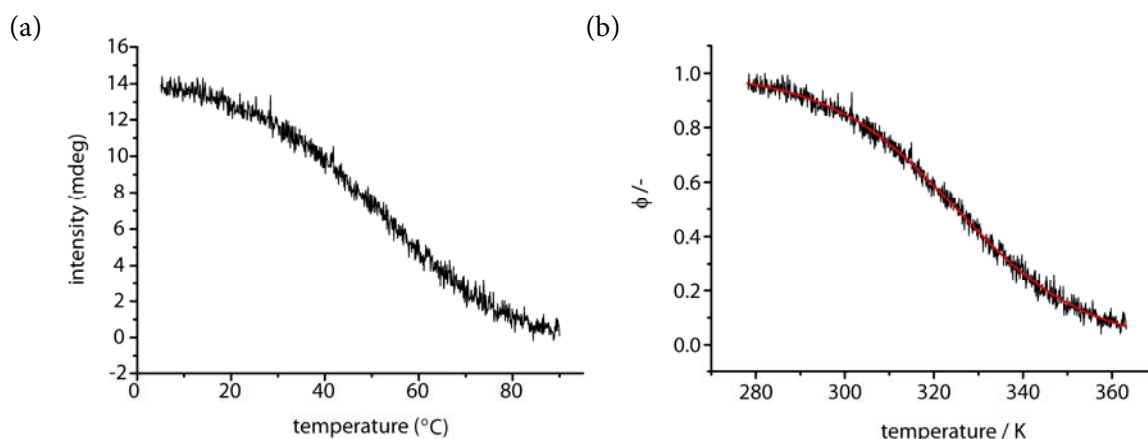


Figure 5.14 (a) Temperature-dependent CD measurement of Gd^{III} -complex **3a** in 200 mM Tris (pH 7.4) from 10 °C to 90 °C with 1 °C·min⁻¹; $[Gd^{III}] = 0.2$ mM and $\lambda = 243$ nm; (b) Normalized CD curve: the degree of aggregation ϕ is plotted against the temperature in K.

Assuming an isodesmic model, the association constant that describes the self-assembly process can be calculated (see appendix B equations (16) and (17) and appendix C for the association constant as function of the temperature); the association constant at 25 °C is 5×10^4 L·mol⁻¹. When this association constant is used to determine the weight-averaged degree of polymerization (DP_w) as function of the Gd^{III} -concentration, it can be calculated that at a concentration of 0.2 mM Gd^{III} there are on average 3–4 monomers within a single stack (Figure 5.15; see appendix B, equation (13)).

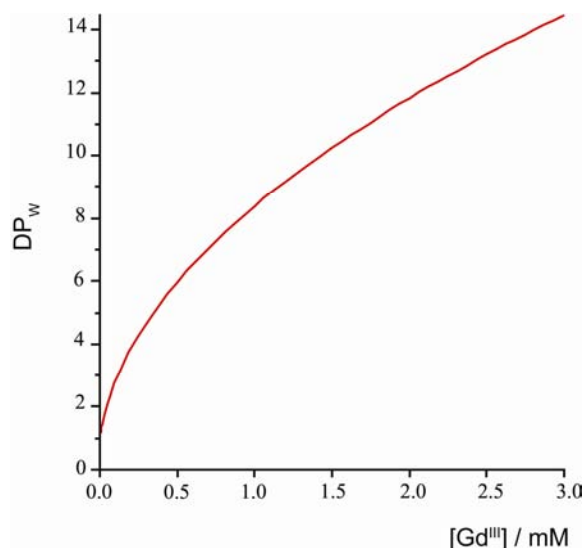


Figure 5.15 The theoretically calculated DP_w is plotted as function of the Gd^{III} -concentration for discotic **3a** at 25 °C.

The weight-averaged molecular weights were also calculated from ¹H-DOSY NMR experiments.^[49–51] The measurements were executed using the DOSY bipolar pulse paired

stimulated echo with convection compensation (Dbppste_cc) pulse sequence.^[52] The steady state pulse sequence was used to compensate for the long relaxation times of HDO, and the self-diffusion of HDO was used to calibrate the measurements. Three samples containing 1.7, 8.3 and 25 mM Y^{III} , respectively, were measured at different temperatures. Table 5.1 lists, besides the theoretical diffusion coefficients of HDO, the measured diffusion coefficients of HDO and of the stacks in the sample.

Table 5.1 Diffusion coefficients, hydrodynamic radii assuming spherical aggregates and the calculated number of monomers within an aggregate for **3b**; $[Y^{III}] = 1.7, 8.3$ or 25 mM in D_2O .

$[Y^{III}] / \text{mM}$	$T / ^\circ\text{C}$	$D_t(\text{HDO}) / 10^{-10} \text{m}^2\text{s}^{-1}$		$D_t(\text{compound}) / 10^{-10} \text{m}^2\text{s}^{-1}$	$R_H(\text{sample}) / \text{\AA}$	n
		theoretical	measured			
1.7	25	19	19	1.3	15	9
	41	28	28	2.0	15	9
	54	37	37	2.8	14	8
	67	47	46	3.5	14	8
	81	60	64	-	-	-
8.3	25	19	19	1.1	18	10
25	25	19	19	0.6	31	18

At temperatures between 25 °C and 67 °C, the measured self-diffusion of HDO in the sample deviates little from its theoretical value. This implies that the dynamic viscosity of the sample is approximately equal to the dynamic viscosity of pure D_2O .^[53] Only at 81 °C, the measured self-diffusion of HDO in the sample is different from its theoretical value. The diffusion coefficient for **3b**, at 1.7 mM Y^{III} , increases when going to higher temperatures. When compensated for temperature and viscosity of pure D_2O by the Stokes–Einstein equation^[54], it is concluded that this increase is only caused by increased mobility. The Stokes–Einstein^[54] relationship for the diffusion of a spherical particle is used to calculate the dimensions of the aggregates, since the model of Tirado and Garcia de la Torre^[55] for the diffusion of a cylindrical particle is not valid, due to the aspect ratio of the assemblies ($L/d < 2$). The calculated hydrodynamic radii, together with the corresponding number of monomers within the aggregate—assuming an average distance of 3.5 Å between the monomers—are

listed in Table 5.1. The aggregates are almost constant in length (9 monomers) at 1.7 mM Y^{III} . This length corresponds to the calculated weight average degree of polymerization at 1.7 mM Gd^{III} —Figure 5.15 gives a DP_w of 10–11 at 25 °C. Higher concentrations of disc **3b** in D_2O do not lead to an enormous increase in stack length; even at 25 mM Y^{III} the average stack length only doubled. A possible explanation for the doubled stack length might be that the nona- to decamers start to aggregate at this concentration. According to these measurements rather well-defined nanometer-sized objects are present within a broad concentration window as was also shown for water-soluble discotic **1** described in Chapter 4.

CryoTEM measurements were performed to visualize the self-assembled structures. The concentrations used in these experiments are $[Y^{III}] = 1.7, 8.3$ and 25 mM, respectively. Figure 5.16 shows the *cryoTEM* images for the investigated samples with the two highest concentrations. The *cryoTEM* image of 1.7 mM Y^{III} is not included, since the density of the aggregates was very low. In general, the images prove that the aggregates are indeed spherical, which validates the use of the Stokes–Einstein relationship for the calculations mentioned above. For the sample with an Y^{III} -concentration of 8.3 mM, the *cryoTEM* image shows small spherical objects with diameters in the order of ~ 4 nm (corresponds to 11 monomers). The image for the sample with an Y^{III} -concentration of 25 mM shows mainly spherical objects (very similar to the ones at a concentration of 8.3 mM Y^{III}). As expected, the density of the spherical aggregates present at 25 mM Y^{III} was higher compared to that at 8.3 mM Y^{III} .

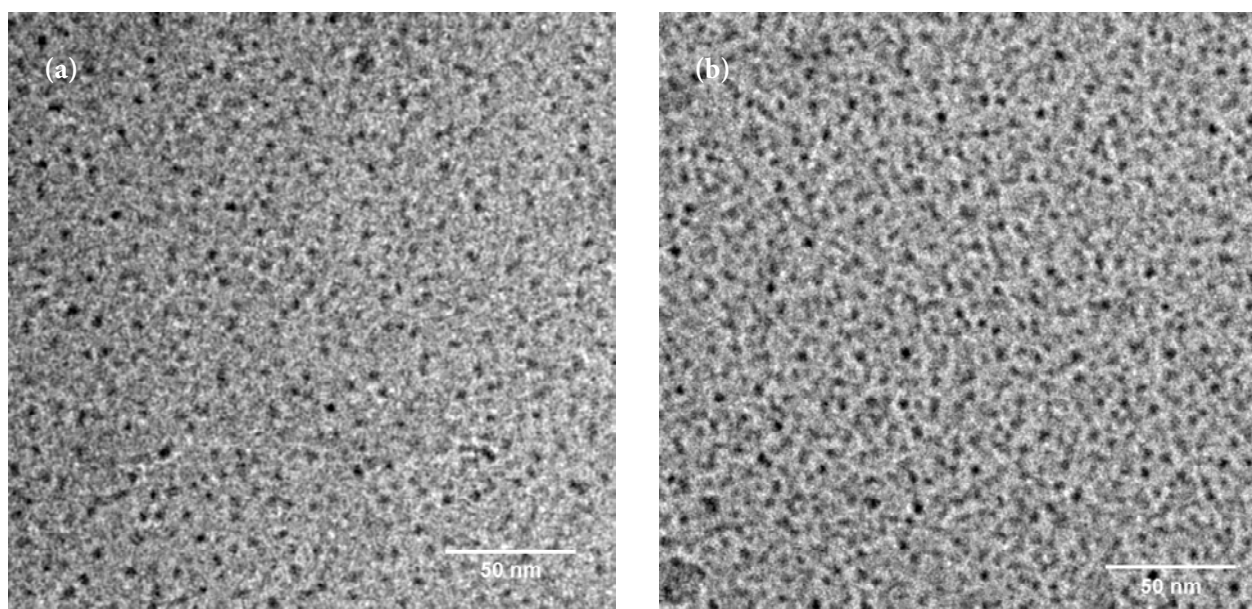


Figure 5.16 *CryoTEM* images of Y^{III} -complex **3b** in 200 mM Tris buffer (pH 7.4) were obtained with an underfocus value of $-4 \mu m$; (a) $[Y^{III}] = 8.3$ mM; (b) $[Y^{III}] = 25$ mM.

5.4.3 Fitting of the T_1 measurements

The *cryo*TEM and ^1H DOSY-NMR experiments show that aggregates with rather well-defined sizes (9–10 monomers) are formed. And, it is shown that clustering of the stacks can be ruled out within the concentration regime studied with the T_1 measurements. Since the size of the aggregates is restricted, one would expect different values for the different association constants. Especially, the association constant describing the process going from a nonamer to a decamer should be much lower compared to the others. However, since the CD measurements show that the self-assembly of **3a** resembles an isodesmic mechanism, it is assumed that all association constants are equal ($K = 8 \times 10^4 \text{ L}\cdot\text{mol}^{-1}$ at 20°C ; see appendix C).

The first model used to fit the longitudinal relaxation time data assumes, furthermore, that there are two kinds of discs, molecularly dissolved discs and discs within an aggregate that display different ionic relaxivities. It is expected that discs within the aggregate possess higher ionic relaxivities since the global and possibly also the local tumbling rates are lower upon aggregation. The water ^1H relaxation rate can now be expressed as in equation E1, in which R_1^d is the diamagnetic contribution (the relaxation rate of pure Tris buffer), r_1^m represents the ionic relaxivity of molecularly dissolved discs (in $\text{mM}^{-1}\text{s}^{-1}$), r_1^a gives the ionic relaxivity of discs within an aggregate (in $\text{mM}^{-1}\text{s}^{-1}$), $[A]$ is the free disc concentration (in mM) and C is the Gd^{III} -concentration (in mM) (see Appendix D, equation (20)).

$$R_1^{obs} - R_1^d = r_1^m \cdot 3[A] + r_1^a \cdot (C - 3[A]) \quad \text{E1}$$

The obtained ionic relaxivities are $r_1^m \approx 0 \text{ mM}^{-1}\text{s}^{-1}$ and $r_1^a = 30.2 \text{ mM}^{-1}\text{s}^{-1}$ and $\chi^2 = 0.2415$. At first glance it seems that this fit is not good; especially at the lower concentrations the fit deviates from the measured datapoints, which could be expected since the value for $r_1^m \approx 0 \text{ mM}^{-1}\text{s}^{-1}$. Therefore, a second model is derived. This model assumes that there are three types of discs present in solution each displaying different ionic relaxivities, namely molecularly dissolved discs, discs within an aggregate that only have one neighbour (the ends) and discs within an aggregate that have two neighbours (the inside). Equation E2 describes the water ^1H relaxation rate, in which $[A_{out}]$ represents the concentration of discs at the ends of an aggregate, r_1^{out} gives the ionic relaxivity of discs at the ends of an aggregate, $[A_{in}]$ is the concentration of discs inside an aggregate and r_1^{in} gives the ionic relaxivity of discs inside an aggregate (see Appendix D, equations (21–25)).

$$R_1^{obs} - R_1^d = r_1^m \cdot 3[A] + r_1^{out} \cdot 3[A_{out}] + r_1^{in} \cdot 3[A_{in}] \quad \text{E2}$$

Figure 5.17 shows the water ^1H relaxation rate data obtained for disc **3a** together with the fit based on model 2. By using this model three ionic relaxivities and the sum-of-squares are determined, $r_1^m = 9.2 \text{ mM}^{-1}\text{s}^{-1}$, $r_1^{\text{out}} = 25.5 \text{ mM}^{-1}\text{s}^{-1}$, $r_1^{\text{in}} = 31.3 \text{ mM}^{-1}\text{s}^{-1}$ and $\chi^2 = 0.02554$. This model seems to describe the measured datapoints very well, even at the lower Gd^{III} -concentrations. A comparison of the two models using the corrected Akaike's information criteria, which takes the number of parameters and the sum-of-squares (χ^2) into account, supports our findings since it is shown that the probability that model 1 is correct is 0%, while the probability that model 2 is correct is 100%.

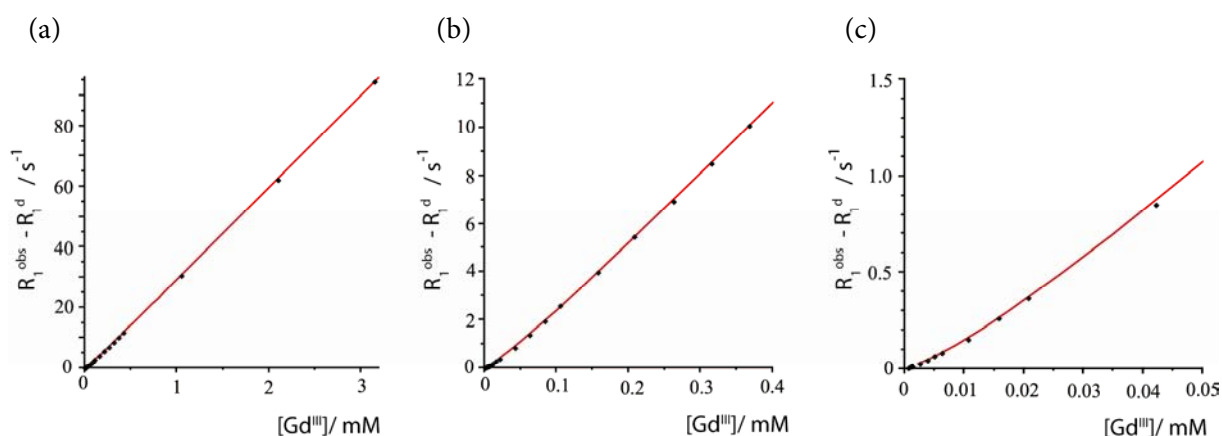


Figure 5.17 Model 2 is used to fit the measured relaxation rate data for discotic **3a** obtained in 200 mM Tris (pH 7.4) at 20 °C and 1.5 T. (a) concentration regime from 0.0–3.2 mM Gd^{III} ; (b) concentration regime from 0.0–0.4 mM Gd^{III} ; (c) concentration regime from 0.00–0.05 mM Gd^{III} .

The gain in relaxivity going from a molecularly dissolved disc to a disc within an aggregate (either at the end or inside) is high, while the gain in relaxivity going from a disc at the end of an aggregate to a disc inside an aggregate is much smaller. This indicates that the ionic relaxivity of a dimer is not very different from the ionic relaxivity of a decamer.

5.4.4 Evaluation of the aggregation concentration

Assuming an isodesmic model and an association constant of $8 \times 10^4 \text{ L}\cdot\text{mol}^{-1}$ at 20 °C, the concentration at which aggregation of disc **3a** starts can be estimated and lies around $3 \times 10^{-4} \text{ mM Gd}^{\text{III}}$. This value cannot directly be compared to the critical micelle concentration of micellar contrast agents, since the mechanisms of self-assembly are completely different. At the point at which the discotic molecules start to aggregate almost all discs are in the molecularly dissolved state (isodesmic self-assembly), while at the critical micelle concentration almost all linear amphiphiles are incorporated into aggregated structures (extreme case of nucleation–elongation).

A requirement for our discotic system is that almost all discotic molecules are in the aggregated state at concentrations relevant for *in vivo* use. Therefore, we would like to define a 95% aggregate concentration (95% *ac*: concentration at which 95% of all discotics are in the aggregated state and 5% of all discotics are in the molecularly dissolved state.) The 95% *ac* of discotic **3a** at 37 °C is 3 mM Gd^{III} = 1 mM disc, which is in the range of useful concentrations *in vivo* (around 1 mM). Moreover, the effect of going below the 95% *ac* is less dramatic than in the case of critical micelle concentrations, because the observed relaxivity only slowly decreases because the fraction of monomer in the aggregated state only slowly decreases. As an example, at 0.12 mM Gd^{III} = 0.04 mM disc the degree of aggregation is 0.5, which means that the observed ionic relaxivity is still above 17 mM⁻¹s⁻¹. This value of the observed ionic relaxivity is much higher than the one for molecularly dissolved discotics ($r_1^m = 9.2 \text{ mM}^{-1}\text{s}^{-1}$), so the benefit of aggregation is still present.

5.4.5 Conclusions

The self-assembly behaviour of discotics **3a** and **3b** has been studied using T₁ measurements, CD and UV/Vis spectroscopy and *cryo*TEM and NMR spectroscopy, respectively. The T₁ measurements suggest that Gd^{III}-complex **3a** self-assembles in aqueous solution. This observation is supported by CD, *cryo*TEM and ¹H-DOSY NMR measurements, which also show that assemblies are present. In addition, the ¹H-DOSY NMR measurements show that the size of the assemblies is limited to nonamers. This limited growth has already been observed before for a similar discotic described in Chapter 4 (deca/undecamers).

The CD measurements, furthermore, show that discotic **3a** self-assembles via an isodesmic mechanism. The association constant describing this self-assembly process at 20 °C is $8 \times 10^4 \text{ L}\cdot\text{mol}^{-1}$. With this association constant the fraction of molecularly dissolved discs at each Gd^{III}-concentration can be calculated. It is shown that aggregation of disc **3a** starts around a gadolinium concentration of $3 \times 10^{-4} \text{ mM}$. As expected, this concentration is significantly lower than the 0.27 mM Gd^{III} obtained for disc **2a**.

According to the T₁ measurements, there are three regimes within the self-assembly process. The relaxivity data can be fitted with a model assuming the presence of three types of discotics during the self-assembly process; molecularly dissolved discs, discs within an aggregate that only have one neighbour (the ends) and discs within an aggregate that have two neighbours (the inside). The ionic relaxivity of molecularly dissolved Gd^{III}-complex **3a** is 9.2 mM⁻¹s⁻¹. This value is higher than that obtained for molecularly dissolved **1a** (8.2 mM⁻¹s⁻¹), which was expected since the molecular weight of the discs increase significantly going from **1a** to **3a**. On the other hand, this value is lower than the value obtained for discotic **2a** (~15 mM⁻¹s⁻¹). Apparently, the decrease in ionic relaxivity as a consequence of more local freedom of movement due to the larger core of **3a** is bigger than the increase in ionic relaxivity as a

consequence of slower global tumbling due to a higher overall molecular weight. The ionic relaxivities of outer and inner discs are $25.5 \text{ mM}^{-1}\text{s}^{-1}$ and $31.3 \text{ mM}^{-1}\text{s}^{-1}$, respectively. These values are promising since they are comparable to the values obtained for micelle- and liposome-based systems displaying relaxivities ranging from 12 to $29 \text{ mM}^{-1}\text{s}^{-1}$ and 5 to $43 \text{ mM}^{-1}\text{s}^{-1}$, respectively.

The molecular relaxivity of an undecamer can be calculated and compared to a fourth generation Gd^{III} -DTPA containing PPI dendrimer, which has a somewhat lower molecular weight but a comparable size and number of endgroups (Figure 5.18). The molecular relaxivity of the dendrimer is $576 \text{ mM}^{-1}\text{s}^{-1}$ (1.5 T, $20 \text{ }^\circ\text{C}$)^[56], while the molecular relaxivity of an aggregate containing 11 discotics is $998 \text{ mM}^{-1}\text{s}^{-1}$ (1.5 T, $20 \text{ }^\circ\text{C}$). This illustrates that the Gd^{III} -DTPA units are more tightly packed in a stack compared to a dendrimer, which can also be deduced from the molecular pictures shown in Figure 5.18.

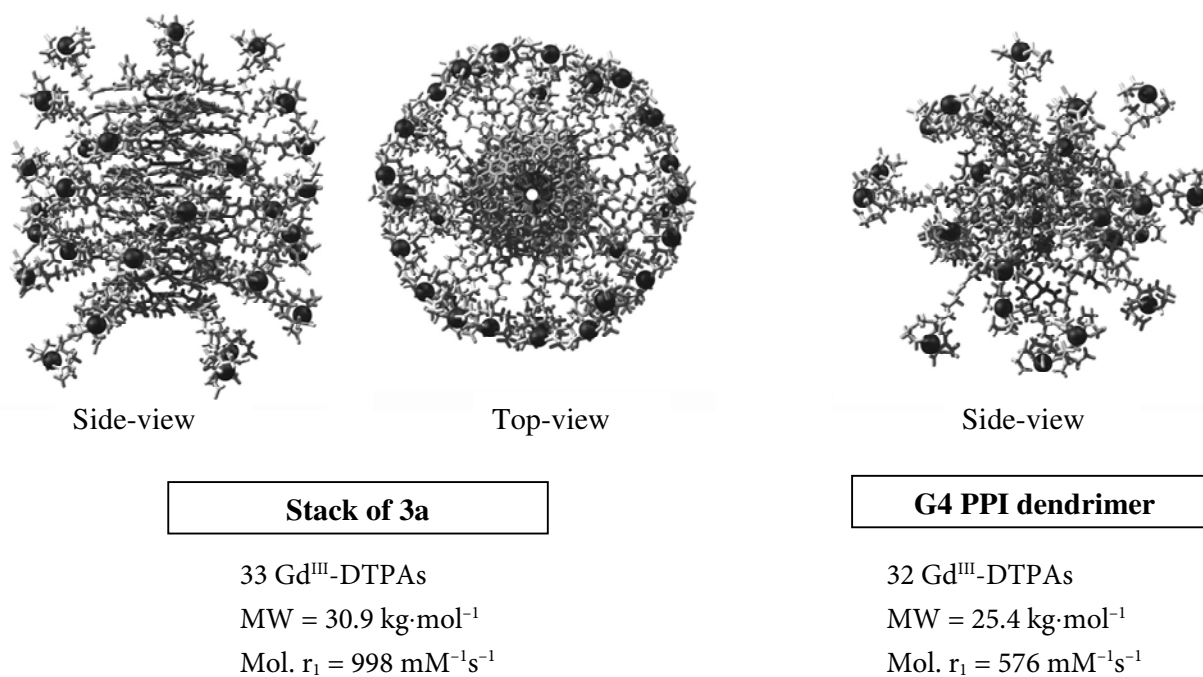


Figure 5.18 3D-models of a stack of **3a** (11 monomers) and of a fourth generation Gd^{III} -DTPA containing PPI dendrimer.

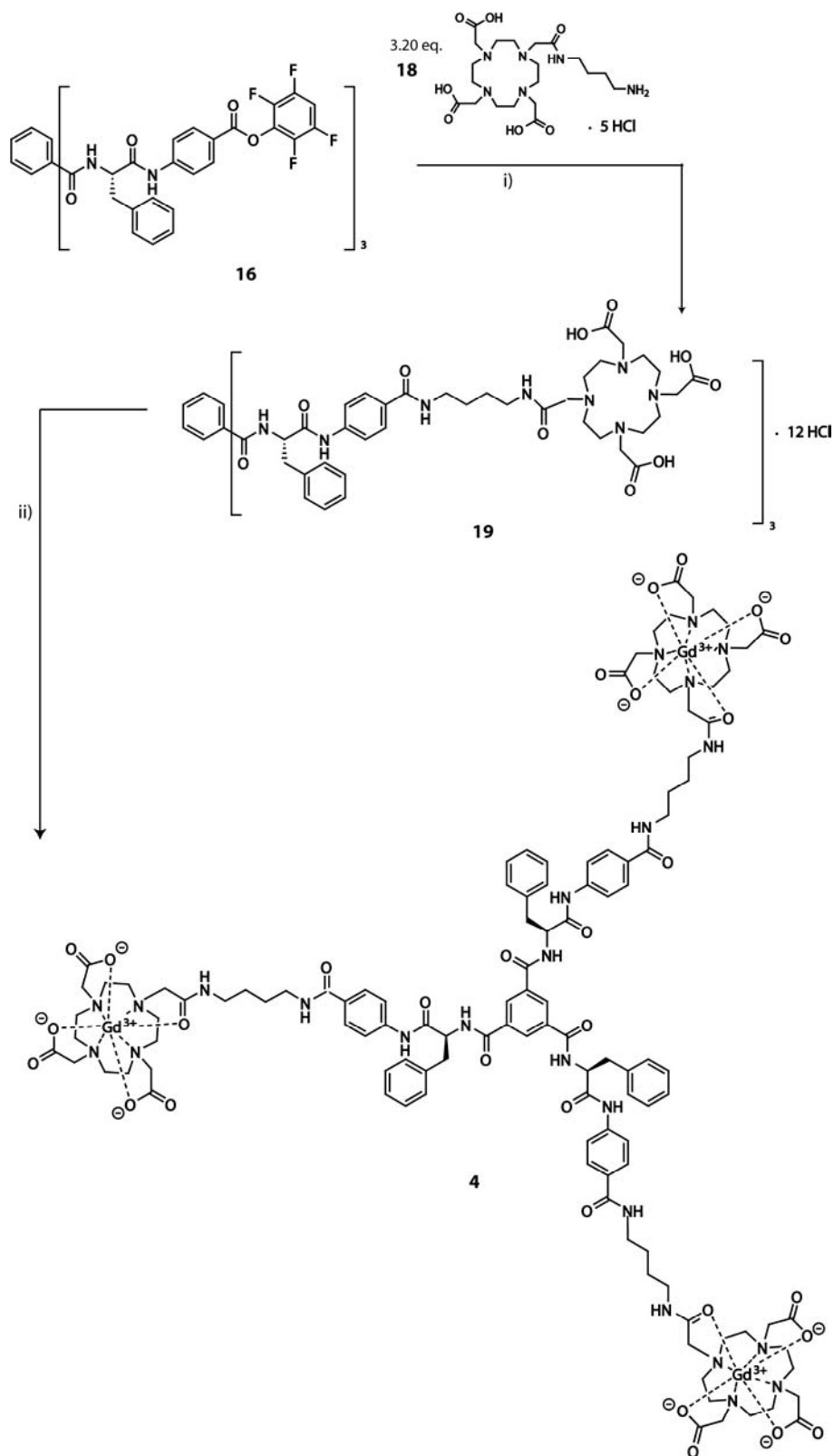
5.5 Large Gd^{III}-DOTA discotic (4)

Because large DTPA discotics **3a,b** displayed high relaxivities and low aggregation concentrations, the ligand in **3** was replaced. Large DOTA discotic **4** was synthesized to show the universality of our approach. Switching the ligand from DTPA to DOTA may result in a higher association constant, since electrostatic repulsion does not play a role in the case of Gd^{III}-DOTA. This complex is neutral, which makes it easier for the Gd^{III}-DOTA discs to self-assemble. Gd^{III}-DTPA complexes, on the other hand, have a charge of 2-, so the overall charge of one discotic is 6-. Electrostatic repulsion may, therefore, hinder aggregation. The ionic relaxivities for the molecularly dissolved discs are expected to be comparable since DOTA and DTPA ligands display similar ionic relaxivities.^[3]

5.5.1 Synthesis

Gd^{III}-DOTA discotic **4** was prepared as depicted in Scheme 5.4. DOTA derivative **18** was kindly provided by SyMO-Chem BV. Activated disc **16** was reacted with 3.20 equivalents of compound **18** in deuterated DMSO in the presence of an excess of base. Dilution of the reaction mixture with ultra pure water and consecutive acidification to pH 3 with concentrated HCl did not result in precipitation of target compound **19**, hence the aqueous solution was lyophilized to yield crude **19** as a off-white solid material. Purification by eluting a solution of crude **19** in water over a size-exclusion PD10 column followed by preparative RP HPLC gave pure disc **19**. Finally, metal complex **4** was prepared by adding an excess of Gd(OAc)₃ to compound **19** in water. The pH of the solution was monitored and maintained at 7 by adding pyridine. After stirring overnight, a CHELEX 100 sodium form resin was added to capture the excess of gadolinium ions. After three days, the removal of the Gd^{III}-ions was completed as was indicated by an UV test experiment with xylenol orange.^[40,41] The solution was carefully isolated from the resin beads and was subsequently lyophilized to yield the product as a white fluffy powder.

Structural characterization of discotic **4** was performed with LC-MS. The Gd^{III}-content of disc **4** was determined with ICP-MS. The values for the observed Gd^{III}- and Y^{III}-contents for all complexes (**1-3**) were very close to their theoretical values, typically between 80–100%, except for discotics **4** for which a Gd^{III}-content of 28% was found. This may be attributed to the presence of residual salts originating from the pyridine, which was not used during the complexation of the other discotics. Despite this low number, the self-assembly of discotic **4** has been evaluated in a preliminary study.



Scheme 5.4 Synthetic route to Gd^{III} -DOTA discotic **4**; i) 1] DiPEA, $\text{DMSO-}d_6$, 2] acidify to pH 3 and centrifugation, 24%; ii) $\text{Gd}(\text{OAc})_3 \cdot x\text{H}_2\text{O}$, H_2O , pyridine (pH 7), 113%.

5.5.2 Longitudinal relaxation time measurements

T_1 measurements for Gd^{III}-complex **4** were performed at concentrations between 0 and 2.0 mM Gd^{III} in 200 mM Tris buffer (pH 7.4). All longitudinal relaxation time measurements were performed at 1.5 T and 20 °C. Figure 5.19 shows the inverse of the measured longitudinal relaxation times at different concentrations for discotic **4**. As a reference, the obtained datapoints for compound **3a** are included. The graphs for discotics **3a** and **4** follow the same trend, especially at concentrations above 0.05 mM Gd^{III}, which suggests that the self-assembly mechanism of discotic **4** is also isodesmic. Furthermore, it indicates that the ionic relaxivities of the outer and inner discs of compound **4** display values that are comparable to those obtained for compound **3a**. Below 0.05 mM Gd^{III} some differences are observed. The ionic relaxivity of molecularly dissolved discs of **4** appears to be lower than the value obtained for disc **3a**. Furthermore, the data suggest that the association constant describing the self-assembly process of disc **4** is comparable to the one for disc **3a**, since it seems that the discs start to aggregate at similar concentrations as is estimated by drawing lines to guide the eye through the datapoints. So, the data suggest that electrostatic repulsion between Gd^{III}-DTPA complexes does not play a crucial role in the self-assembly process. However, to draw hard conclusions additional measurements, as were also performed for discotic **3a**, are needed in order to fit these relaxivity data and to determine the ionic relaxivities of molecularly dissolved, outer and inner discs of compound **4**.

5.5.3 Conclusions

The self-assembly behaviour of discotic **4** has been studied in a preliminary investigation using T_1 measurements. The T_1 measurements show that Gd^{III}-complex **4** self-assembles in aqueous solution. The measurements also suggest that the mechanism of self-assembly, the association constant and the values of the ionic relaxivities for discotic **4** are comparable to those obtained for discotic **3a**. These relaxation time measurements, of course, must be supported by additional techniques and duplo measurements using another batch of disc **4**, but they do show the universality of our approach since the results are reproducible with a different type of ligand.

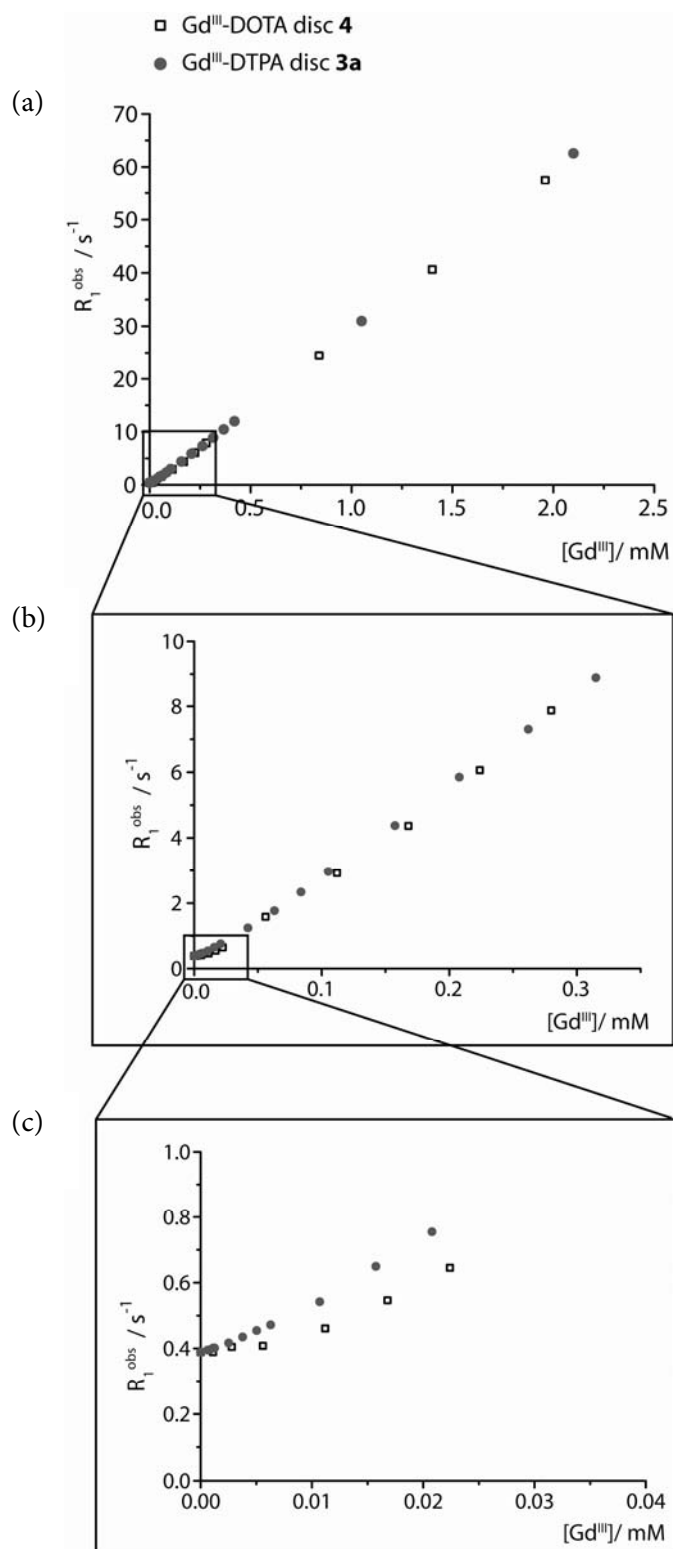


Figure 5.19 The longitudinal relaxation rate (R_1^{obs}) is plotted against the gadolinium concentration for Gd^{III} -complex 4; As a reference, the relaxation rates of Gd^{III} -complex 3a are included; (a) concentration window 0.0–2.5 mM; (b) concentration window 0.00–0.35 mM; (c) concentration window 0.00–0.04 mM.

5.6 Overall conclusions

Four paramagnetic discotics that differ in their complexity and capability to undergo secondary interactions have been successfully synthesized. As expected, it has been shown that increased opportunities for secondary interactions and larger hydrophobic cores lead to lower concentrations at which aggregation starts; the aggregation concentration decreased going from Gd^{III}-DTPA discotic **1a** (does not aggregate) to **2a** (aggregation starts at 0.27 mM Gd^{III}) to **3a** (aggregation starts at 3×10^{-4} mM Gd^{III}). Furthermore, it has been shown that changing the ligand from DTPA to DOTA only slightly affects the self-assembly process, which illustrates the universality of our approach. To be able to alter self-assembly processes and thus aggregation concentrations is very important because it allows designing systems that may benefit from their aggregation *in vivo*. The self-assembly studies also point out that, next to CD spectroscopy, T₁ measurements can be used to probe the self-assembly process of the paramagnetic discotics described in this chapter. However, it has to be noted that self-assembly mechanisms can be most easily studied using CD spectroscopy, since it takes less time and the data are easier to interpret.

From the three Gd^{III}-DTPA discotics synthesized, Gd^{III}-complex **3a** is the most promising building block for a supramolecular contrast agent for MRI, in view of its low aggregation concentration, its high ionic relaxivity in the aggregated form ($\sim 30 \text{ mM}^{-1}\text{s}^{-1}$ at 20 °C and 1.5 T) and its rather well-defined assemblies with dimensions in the nanometer range. *In vitro* these paramagnetic assemblies show higher ionic relaxivities than fourth generation Gd^{III}-DTPA containing PPI dendrimers, which are comparable in size, molecular weight and the number of endgroups, and they also show higher relaxivities compared to many of the micellar and liposomal contrast agents reported thus far. Future research should point out whether these new self-assembling contrast agents based on discotic amphiphiles also show high proton relaxivities *in vivo*.

5.7 Epilogue

The results described in this chapter show that paramagnetic discotic molecules can be designed in such a way that they display good self-assembling properties and high molecular relaxivities in 200 mM Tris (pH 7.4) *in vitro*. Future research is, however, necessary in order to determine whether this new type of self-assembling contrast agents offers opportunities for use *in vivo*.

First of all, the influence of the presence of serum proteins, like BSA, on the performance of discotic **3a** should be investigated. These proteins may affect the behaviour of discs of **3a** in the molecularly dissolved and/or the self-assembled state, because they are known to bind to hydrophobic molecules. Especially the core of discotic **3a** is quite hydrophobic, so aspecific binding may play an important role *in vivo*. For molecularly

dissolved species this may be beneficial because it is known that non-covalent binding of a small molecule to a protein leads to an increased ionic relaxivity and an increased residence time in the body, while the paramagnetic complex can still be excreted from the body due to the reversible nature of the binding. For self-assembled structures, the effect of aspecific binding on their performance is not so straightforward. It is proposed that there are three possibilities; firstly, there is no aspecific binding because the hydrophilic Gd^{III}-complexes shield the core of the stack from the protein, secondly, the entire stack of **3a** binds to the serum protein, and thirdly, aspecific binding of the discs to the protein is stronger than the binding between the discs, hence the paramagnetic assemblies break up. In the first two scenarios, the molecular relaxivity of the assemblies stays the same or increases somewhat, in the third scenario, the molecular relaxivity decreases since the benefit from aggregation has disappeared. Preliminary *in vitro* relaxation time measurements of discotic **3a** in serum and in blood suggest that the assemblies do break up, since the observed proton relaxivities are much lower than expected. It seems that stronger interactions between the discs are needed to keep the assemblies intact. The results described in Chapters 2 and 3 illustrate that by using phenylalanyl-phenylalanines as structuring elements in the core of the discotic, the stack stability can be increased. The introduction of an additional phenylalanine in the structure of **3a** may, therefore, avoid deaggregation. Another strategy for creating stronger interactions between discs may be based on the incorporation of fluorophobic interactions. This type of interaction is unknown to proteins, so proteins are not able to disturb fluorophobic interactions between discs. One way to obtain fluorinated discs is by replacing the phenylalanines by fluorinated phenylalanines. Future research should focus on these aspects because self-assembly of paramagnetic discotic molecules is a key requirement for obtaining systems displaying high relaxivities.

Secondly, it is important to investigate the dynamics of the system for reasons concerning excretion from the body, stability of the assemblies and possibilities for introducing active targeting. Excretion of paramagnetic complexes is important, due to the toxicity of gadolinium ions that may be released from the complexes. Assemblies of discotic **3a** are relatively small (diameters in the order of 4 nm) hence accumulation in the body should not be an issue. Therefore, in this particular case reversible binding between discs within an aggregate is not a necessity for excretion. However, when replacing the 1,3,5-benzenetricarboxamide centre of disc **3a** by a *cis-cis*-1,3,5-cyclohexanetricarboxamide centre self-assembling contrast agents forming long columnar structures in solution presumably become accessible. These agents may act as potential intravascular agents because of their high molecular weight. For these types of systems, reversible binding between the discs within an aggregate is required to ensure complete excretion of the paramagnetic complexes from the body. On the other hand, the assembly must be stable enough, so the interactions between the discs within the aggregate should not be too weak (this is a general requirement and thus

holds also for assemblies of discotic **3a**); otherwise the benefit of a high relaxivity due to aggregation vanishes. As a consequence, the dynamics must be balanced in an appropriate way for an optimal performance *in vivo*. Dynamic systems may also open possibilities for the introduction of active targeting in an easily accessible manner demanding less synthetic effort, since symmetrical discs with similar core-fragments but displaying peptide sequences at their periphery may simply be mixed with paramagnetic discs. In this way, even more efficient contrast agents can be prepared.

And finally, the potential of the use of asymmetric discotic molecules containing peripheral Gd^{III}-complexes and an active peptide sequence should be investigated because this may be an alternative strategy for introducing active targeting to the system. The main advantage of this method compared to the method using at least two types of symmetrical discs is that the molecularly dissolved paramagnetic discs themselves display peptide sequences and thus are target-specific. Drawback, on the other hand, is that it takes much more synthetic effort to synthesize asymmetric discs incorporating various peptide sequences.

All these aspects together may give new insights in the performance of paramagnetic discotic amphiphiles *in vivo*. This is of general importance in order to demonstrate whether paramagnetic discotic molecules are efficient self-assembling contrast agents for MR imaging.

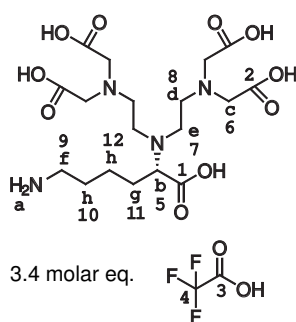
5.8 Experimental section

General

Unless stated otherwise, all reagents and chemicals were obtained from commercial sources and used without further purification. Lysine-DTPA **5** and its benzyloxycarbonyl protected analogue **5b** were synthesized according to literature.^[38,39] Water was demineralised prior to use. Dichloromethane and tetrahydrofuran were obtained by distillation over Merck molecular sieves (4Å). Semi-preparative HPLC was performed on a Varian Prostar HPLC system with a Vydac C18 column (2.5 × 20 cm, flow 10 mL·min⁻¹), eluted with a linear gradient of 30–50% CH₃CN in 0.1% aqueous TFA in 90 min. ¹H-NMR, ¹H-¹H COSY, ¹³C-NMR and ¹⁹F-NMR spectra were recorded on a Varian Gemini 300 spectrometer, a Varian Mercury Vx 400 spectrometer or a Varian Unity Inova 500 spectrometer at 298 K. Chemical shifts are given in ppm (δ) values relative to tetramethylsilane (TMS). Splitting patterns are designated as s, singlet; br s, broad singlet, d, doublet; dd, double doublet; t, triplet; q, quartet; m, multiplet. Neat state IR spectra were measured at 298 K on a Perkin-Elmer 1605 FT-IR spectrophotometer. Matrix assisted laser desorption/ionization mass spectra were obtained on a PerSeptive Biosystems Voyager DE-PRO spectrometer using α -cyano-4-hydroxycinnamic acid (CHCA) and 2-[(2E)-3-(4-*tert*-butylphenyl)-2-methylprop-2-enylidene]malononitrile (DCTB) as matrices. (LC)-ESI-MS measurements were performed on a Finnigan LCQ Deca XP Max ion trap mass spectrometer (Thermo Electron Corporation, San Jose, USA). Elemental analyses were carried out using a Perkin Elmer 2400. Gd^{III}- and Y^{III}-contents were determined by means of inductively coupled plasma mass spectrometry (ICP-MS) conducted by Philips Research-Materials Analysis in Eindhoven. Chiral HPLC was performed on a Shimadzu system consisting of a Shimadzu LC-10 ADvp pump, a Spark Midas autosampler and a Shimadzu SPD-10ADvp UV-Vis detector. A DNBPG column (covalent, 5 μ m; 0.46 x 25 cm) was used, with a 9/1 (v/v) hexane/isopropanol mixture as the eluent. The T₁ measurements were performed at 1.5 T on a Bruker Minispec mq60 NMR analyzer. The sample volume was 300 μ L and the samples were measured in tubes with a diameter of 7.5 mm. Longitudinal relaxation times were determined with an inversion recovery pulse sequence. Gd^{III}-concentrations of the aqueous solutions used for the T₁-relaxivity measurements were determined by means of inductively coupled plasma mass spectrometry (ICP-MS) conducted by Philips Research-Materials Analysis in Eindhoven. UV/VIS spectra were obtained on a Perkin Elmer Lambda 40 spectrometer. CD measurements were performed on a Jasco J815 CD spectrometer connected to a Jasco PTC-348WI temperature controller. Cryogenic transmission microscopy measurements were performed on a FEI Titan Krios TEM equipped with a field emission gun (FEG) operating at 300 kV. Images were recorded using a 2k x 2k Gatan CCD camera equipped with a post column Gatan energy filter (GIF). TEM grids, (R2/2 Quantifoil Jena grids) were purchased from Aurion. The Quantifoil grids underwent a surface plasma treatment using a Cressington 208 carbon coater operating at 5 mA for 40 s prior to the vitrification procedure. The *cryo*TEM images of the discotics were obtained by applying small aliquots (3 μ L) of the aqueous discotic solutions to Quantifoil grids (R2/2 Quantifoil Jena) within the environmental chamber (relative humidity 100%) of the Vitrobot™ at room temperature. The vitrified specimens were stored under liquid nitrogen and observed at -170°C (Gatan cryo holder) in the Titan microscope. Micrographs were taken at 300 kV using low dose conditions. ¹H-DOSY NMR experiments were recorded on a Varian Unity Inova 500 spectrometer operating at 500.618 MHz and equipped with a 5 mm ID-PFG probe from Varian. Additional, experimental ¹H-DOSY NMR data can be found at the end of this experimental section.

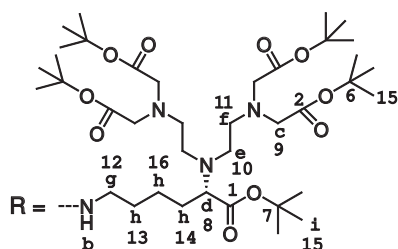
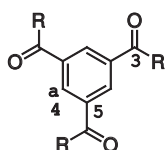
***tert*-Butyl 6-amino-2-[bis-{2-[bis-(*tert*-butoxycarbonylmethyl)amino]ethyl}amino]hexanoate (5)**

A detailed description of the synthesis of this lysine-DTPA building block was reported.^[38,39]

6-Amino-2-(bis-{2-[bis-(carboxymethyl)amino]ethyl}amino)hexanoic acid (TFA-salt) (5a)


The benzyloxycarbonyl protected lysine-DTPA analogue (1.25 g, 1.52 mmol), precursor of compound **5**^[38,39], was dissolved in TFA (5 mL). The solution was purged with argon for 15 min, after which the mixture was stirred for another 45 min. The reaction mixture was concentrated *in vacuo*. The remaining product was dissolved in water (20 mL) and lyophilized. A suspension of the obtained sticky material in water (10 mL) and 10% Pd supported on activated carbon (90 mg) was subjected to hydrogenation under a H₂ blanket at room temperature for 24 h. After filtration over Celite, the solution was lyophilized giving the title compound as an off-white sticky product (1.05 g, 1.23 mmol, 81% over two steps). The

amount of TFA was determined with ¹⁹F-NMR spectroscopy using 4-fluorobiphenyl as an internal standard: compound **5a** contained 3.4 molar eq. TFA: ¹H-NMR (DMSO-d₆): δ = 7.83 (br s, 3H, **a**), 4.51 (br t, 1H, **b**), 3.59 (br s, 8H, **c**), 3.32 (br s, 4H, **d**), 3.06 (br s, 4H, **e**), 2.79 (br s, 2H, **f**), 1.85 (br s, 2H, **g**), 1.56 (m, 4H, **h**) ppm; ¹³C-NMR (DMSO-d₆): δ = 172.0 (**1**), 170.8 (**2**), 158.6 (**3**, **q**), 116.3 (**4**, **q**), 63.8 (**5**), 54.2 (**6**), 50.3 (**7**), 50.0 (**8**), 38.6 (**9**), 27.0 (**10**), 26.5 (**11**), 23.2 (**12**) ppm; FT-IR (ATR): ν = 2967, 2541, 1723, 1659, 1424, 1177, 1131 cm⁻¹; ESI-MS (negative mode): *m/z* calcd. for [M+TFA]⁻ 576.5; found: 576.7 [M+TFA]⁻, 690.5 [M+2TFA]⁻, 1040.5 [2M+TFA]²⁻.

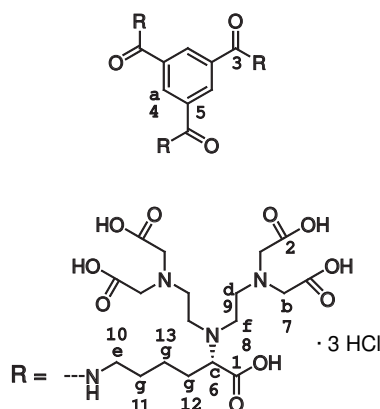
N,N',N''-Tris[{5-*tert*-butoxycarbonyl}{5-(bis-[2-{bis-(*tert*-butoxycarbonylmethyl)amino}ethyl]amino)}-pentyl]-1,3,5-benzenetricarboxamide (6**)**


A solution of 1,3,5-benzenetricarboxyl trichloride (122 mg, 0.46 mmol) in dry dichloromethane (5 mL) was added dropwise to a solution of lysine-DTPA analogue **6** (1.06 g, 1.42 mmol) and triethylamine (250 μL, 1.79 mmol) in dry dichloromethane (15 mL). After stirring overnight under an atmosphere of argon and at room temperature, the reaction mixture was concentrated *in vacuo* at 40 °C. The crude product was purified using column chromatography (silica, CH₂Cl₂ / THF 3:1, R_f = 0.77). Finally, the pure compound **6** was obtained as a yellow oil (854 mg, 0.35 mmol, 78%): ¹H-NMR (CDCl₃): δ = 8.38 (s, 3H, **a**), 7.07 (s, 3H, **b**), 3.43 (s, 24H, **c**), 3.33 (t, 3H, **d**), 2.9–2.6 (m, 30H, **e** {12H} + **f** {12H} + **g** {6H}), 1.7–1.3 (m, 153H, **h** {18H} + **i** {135H}) ppm; ¹³C-NMR (CDCl₃): δ = 172.3 (**1**), 170.3 (**2**), 165.5 (**3**), 135.1 (**4**), 128.0 (**5**), 80.4 (**6**), 80.3 (**7**), 63.5 (**8**), 55.7 (**9**), 53.2 (**10**),

49.8 (**11**), 39.8 (**12**), 29.1 (**13**), 28.8 (**14**), 27.9, 27.8 (**15**), 23.4 (**16**) ppm; FT-IR (ATR): ν = 3382, 2978, 2934, 2868, 1723, 1664, 1533, 1457, 1393, 1366, 1281, 1255, 1219 and 1135 cm⁻¹; ESI-MS (positive mode): *m/z* calcd. for 1195.8 [M+2H]²⁺; found: 1196.1 [M+2H]²⁺; elemental analysis: calcd. for C₁₂₃H₂₁₆N₁₂O₃₃: 61.78% C, 9.11% H, 7.03% N; found: 61.33% C, 8.90% H, 6.74% N.

N,N',N''-Tris[{5-carboxy}{5(bis-[2-{bis-(carboxymethyl)amino}ethyl]amino)}pentyl]-1,3,5-benzenetricarboxamide · 9 HCl (7**)**

To a solution of **6** (699 mg, 0.292 mmol) in chloroform (30 mL), 4 M HCl-dioxane solution (30 mL) was added dropwise. After 1 h, the reaction mixture was concentrated *in vacuo* at 50 °C. The concentrate was dissolved in water (25 mL) and a 12 M aqueous HCl solution (20 mL) was added dropwise. After stirring overnight, the reaction mixture was concentrated *in vacuo* at 80 °C. The crude product was dissolved in methanol (5 mL) and precipitated from diethyl ether (20 mL). Finally, the precipitate was filtered under a flow of argon and lyophilized during 3 days resulting in pure **7** as a yellow/orange hygroscopic solid (503 mg, 0.27 mmol, 92%): ¹H-NMR



(D₂O): δ = 8.19 (s, 3H, **a**), 4.81 (s, 24H, **b**), 3.58 (t, 3H, **c**), 3.5–3.3 (m, 18H, **d** {12H} + **e** {6H}), 3.16 (m, 12H, **f**), 1.7–1.4 (m, 18H, **g**) ppm; ¹³C-NMR (D₂O): δ = 175.6 (**1**), 169.6 (**2**), 168.9 (**3**), 135.4 (**4**), 129.3 (**5**), 63.8 (**6**), 55.8 (**7**), 53.7 (**8**), 47.0 (**9**), 40.3 (**10**), 28.7 (**11**), 28.2 (**12**), 24.0 (**13**) ppm; FT-IR (ATR): ν = 3288, 2942, 2521, 1728, 1635, 1543, 1403 and 1203 cm⁻¹; ESI-MS (negative mode): m/z calcd. for [M-(H+9HCl)]⁻ 1548.6; found: 1548.6 [M-(H+9HCl)]⁻; **elemental analysis**: calcd. for C₆₃H₉₆N₁₂O₃₃ · 9HCl: 40.30% C, 5.64% H, 8.95% N; found: 41.11% C, 5.93% H, 8.87% N.

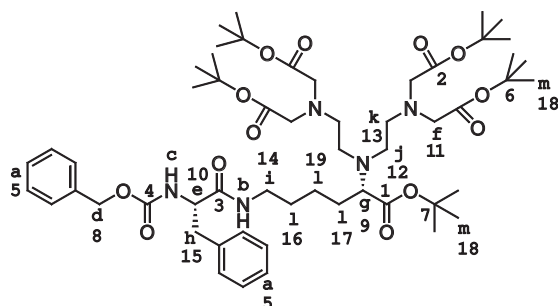
Gd^{III} complex (**1a**)

Compound **7** (50.7 mg, 27.0 μ mol) was dissolved in water (5 mL) and the pH was adjusted to 7 by adding aliquots of a 2 M ammonia solution. The gadolinium complex was prepared by adding Gd(OAc)₃·xH₂O (33.3 mg) as predetermined by UV-titration. The solution was vigorously stirred for 6 h at room temperature at pH 7. After lyophilizing the reaction mixture overnight, the crude product was dissolved in water (1 mL) and precipitated in ethanol (10 mL). Filtration of the precipitate under a flow of argon yielded title compound **1a** as an off-white hygroscopic solid (36.6 mg, 17.3 μ mol, 64%): FT-IR (ATR): ν = 3145, 3040, 2868, 1575, 1435, 1401, 1323 and 1087 cm⁻¹; ESI-MS (negative mode): m/z calc. for [M-(2H+6NH₃)]²⁻ 1005.3; found: 1005.1 [M-(2H+6NH₃)]²⁻; ICP-MS (Gd^{III}): calcd. 14.1 ng/g, found: 13.0 ng/g.

Y^{III} complex (**1b**)

Compound **7** (202 mg, 108 μ mol) was dissolved in a sodium acetate buffer (25 mL, pH = 5.3). The yttrium complex was prepared by adding Y(OAc)₃·xH₂O (117 mg) as predetermined by UV-titration. The solution was vigorously stirred for 4 h at room temperature at pH 5.3. After lyophilizing the reaction mixture during three days, the crude product was dissolved in water (2 mL) and precipitated in ethanol (20 mL). Filtration of the precipitate under a flow of argon yielded title **1b** compound as a white hygroscopic solid (187 mg, 97.9 μ mol, 91%). FT-IR (ATR): ν = 3283, 2935, 1590, 1440, 1406, 1325 and 1088 cm⁻¹; MALDI-TOF-MS (negative mode): m/z calc. for [M-(H+6NH₃)]⁻ 1806.2; found 1806.6 [M-(H+6NH₃)]⁻; ICP-MS (Y^{III}): calcd. 106 ng/g, found: 85.0 ng/g.

N ^{α} -[Benzyloxycarbonyl]-N ^{ω} -[5-*tert*-Butoxycarbonyl]{5-(bis-[2-{bis-(*tert*-butoxycarbonylmethyl)amino}-ethyl]amino)}pentyl]-L-phenylalaninamide (**8**)

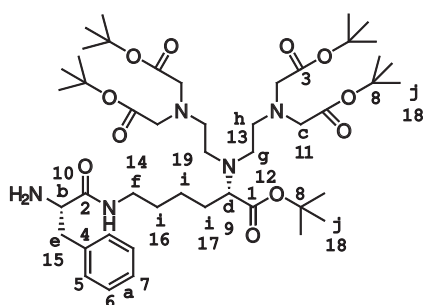


To a solution of HBTU (1.02 g, 2.68 mmol) in dry DMF (5.5 mL), DiPEA (0.93 mL, 5.35 mmol) and Z-Phe-OH (0.735 g, 2.46 mmol) were added. The mixture was stirred for 20 min under an atmosphere of argon. To the yellow solution, lysine-DTPA-analogue **5** (0.990 g, 1.33 mmol) was added. The solution was stirred overnight at room temperature under an atmosphere of argon. The reaction mixture was added dropwise to an ice-cold mixture of aqueous HCl (pH < 3, 50 mL) and diethyl ether (50 mL).

After washing the organic layer with 1 M NaOH (3 \times 25 mL) and 10 mM NaHCO₃ (3 \times 25 mL), the combined aqueous layers were extracted with diethyl ether (45 mL). The organic layers were combined, dried over Na₂SO₄,

filtered and concentrated *in vacuo* at 40 °C. After purification by column chromatography (silica, CH₂Cl₂/Et₃N 25:1, R_f = 0.26) pure **8** was obtained as a yellow oil (0.976 g, 0.95 mmol, 72%): ¹H-NMR (CDCl₃): δ = 7.4–7.2 (m, 10H, **a**), 5.88 (t, 1H, **b**), 5.50 (d, 1H, **c**), 5.05 (d + d, 2H, **d**), 4.34 (d + d, 1H, **e**), 3.43 (s, 8H, **f**), 3.2–3.0 (m, 5H, **g** {1H} + **h**{2H} + **i**{2H}), 2.8–2.6 (m, 8H, **j**{4H} + **k**{4H}), 1.7–1.0 (m, 51H, **l**{6H} + **m**{45H}) ppm; ¹³C-NMR (CDCl₃): δ = 172.9 (**1**), 170.8 (**2**), 170.6 (**3**), 155.7 (**4**), 136.8, 136.4, 129.5, 128.8, 128.7, 128.3, 128.2, 127.1 (**5**), 81.0 (**6**), 80.9 (**7**), 67.0 (**8**), 64.2 (**9**), 56.5 (**10**), 56.1 (**11**), 53.9 (**12**), 50.4 (**13**), 39.5 (**14**), 39.2 (**15**), 29.6 (**16**), 29.1 (**17**), 28.5, 28.3 (**18**), 23.7 (**19**) ppm; FT-IR (ATR): ν = 3324, 2977, 2933, 2867, 1722, 1662, 1533, 1455, 1392, 1367, 1284, 1250, 1218 and 1147 cm⁻¹; MALDI-TOF-MS: *m/z* calc. for [M+H]⁺ 1026.6; found: 1026.7 [M+H]⁺; **elemental analysis**: calcd. for C₅₅H₈₇N₅O₁₃: 64.37% C, 8.54% H, 6.82% N; found: 64.73% C, 8.51% H, 6.92% N.

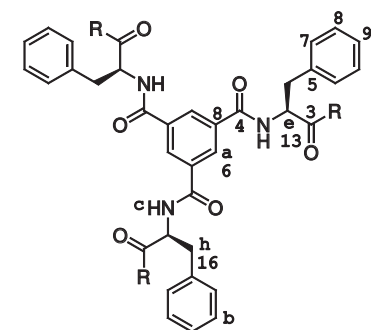
N^o-[5-*tert*-Butoxycarbonyl]{5-(bis-[2-{bis(*tert*-butoxycarbonylmethyl)amino}ethyl]amino)}pentyl]-L-phenylalaninamide (9**)**



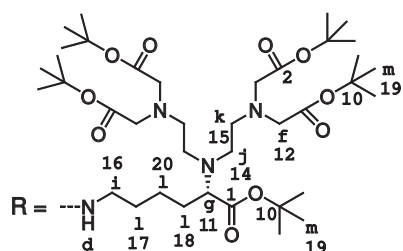
To a solution of Z-Phe-DTPA **8** (502 mg, 0.489 mmol) in MeOH (10 mL), acetic acid (1 mL) was added. The solution was purged with nitrogen gas for 15 min. Subsequently, 10% Pd supported on activated carbon (32.2 mg) was added and the heterogeneous mixture was shaken in a Parr-reactor for 22 h under an atmosphere of hydrogen (70 psi). The reaction mixture was filtered and the filtrate was concentrated *in vacuo* at 60 °C to give a yellow oil, which was dissolved in diethyl ether (20 mL). The diethyl ether phase was washed with 2 M NaOH (2 × 10 mL) and the combined aqueous layers were extracted with diethyl ether

(10 mL). Finally, the combined organic layers were washed with brine (2 × 10 mL) and concentrated *in vacuo* at 60 °C, resulting in pure **9** as a yellow oil (270 mg, 0.30 mmol, 62%): ¹H-NMR (CDCl₃): δ = 7.4–7.2 (m, 5H, **a**), 3.60 (q, 1H, **b**), 3.43 (s, 8H, **c**), 3.3–3.2 (m, 5H, **d** {1H} + **e** {2H} + **f** {2H}), 2.9–2.7 (m, 8H, **g** {4H} + **h** {4H}), 1.7–1.2 (m, 51H, **i** {6H} + **j** {45H}) ppm; ¹³C-NMR (CDCl₃): δ = 174.2 (**1**), 172.9 (**2**), 170.8 (**3**), 138.4 (**4**), 129.4 (**5**), 128.8 (**6**), 126.9 (**7**), 80.9, 80.8 (**8**), 64.5 (**9**), 56.7 (**10**), 56.2 (**11**), 54.0 (**12**), 50.6 (**13**), 41.3 (**14**), 39.1 (**15**), 29.9 (**16**), 29.5 (**17**), 28.5, 28.3 (**18**), 23.9 (**19**) ppm; FT-IR (ATR): ν = 3373, 2977, 2933, 2867, 1725, 1673, 1520, 1455, 1392, 1367, 1254, 1219 and 1149 cm⁻¹; MALDI-TOF-MS: *m/z* calc. for [M+H]⁺ 892.6; found: 892.4 [M+H]⁺; **elemental analysis**: calcd. for C₄₇H₈₁N₅O₁₁: 63.27% C, 9.15% H, 7.85% N; found: 63.55% C, 9.11% H, 7.73% N.

N,N',N''-Tris[[(S)-benzyl]{5-*tert*-butoxycarbonyl}(5-[bis-2-(bis-[*tert*-butoxycarbonylmethyl]amino)-ethyl)amino)}pentylaminocarbonyl]methyl]-1,3,5-benzenetricarboxamide (10**)**

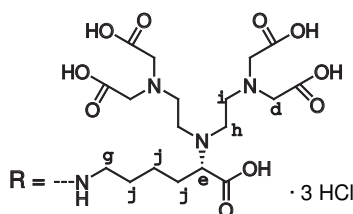
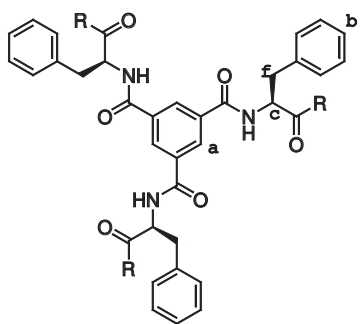


A solution of 1,3,5-benzenetricarbonyl trichloride (49.5 mg, 0.186 mmol) in dry dichloromethane (0.5 mL) was added dropwise to a solution of **9** (515 mg, 0.578 mmol) and triethylamine (103 μL, 0.74 mmol) in dry dichloromethane (5 mL). After stirring overnight at room temperature under an atmosphere of argon, the reaction mixture was concentrated *in vacuo* at 35 °C. The crude product was purified by column chromatography (silica, gradient 0–20% THF in dichloromethane). Product **10** was obtained as a thick, yellow oil (180 mg, 0.06 mmol, 34%): ¹H-NMR (CDCl₃): δ = 8.34 (s, 3H, **a**), 7.4–7.2 (m, 18H, **b** {15H} + **c** {3H}), 5.94 (t, 3H, **d**), 4.78 (q, 3H, **e**), 3.43 (s, 24H, **f**), 3.4–3.0 (m, 15H, **g** {3H} + **h** {6H} + **i** {6H}), 2.8–2.6 (m, 24H, **j** {12H} + **k** {12H}), 1.7–1.1 (m, 153H, **l** {18H} + **m** {135H}) ppm; ¹³C-NMR (CDCl₃): δ = 172.8 (**1**), 170.8 (**2**), 170.3 (**3**), 165.1 (**4**), 136.8 (**5**), 135.1 (**6**), 129.5 (**7**), 128.8 (**8**), 127.3 (**9**),



81.0, 80.9 (**10**), 64.1 (**11**), 56.0 (**12**), 55.6 (**13**), 53.8 (**14**), 50.4 (**15**), 39.5, 39.4 (**16**), 29.6 (**17**), 29.0 (**18**), 28.5, 28.4, 28.3 (**19**), 23.7 (**20**) ppm; **FT-IR (ATR)**: $\nu = 3303, 2977, 2933, 2867, 1726, 1658, 1538, 1456, 1392, 1368, 1250, 1219$ and 1150 cm^{-1} ; **MALDI-TOF-MS**: m/z calc. for $[M+H]^+$ 2831.8; found: 2832.1 $[M+H]^+$; **GPC** (Tetrahydrofuran): $t_{\text{ret.}} = 16.6$ min; **elemental analysis**: calcd. for $C_{150}H_{243}N_{15}O_{36}$: 63.60% C, 8.65% H, 7.42% N; found: 63.58% C, 8.54% H, 6.63% N.

N,N',N''-Tris[[(S)-benzyl][[5-carboxy][5-(bis-[2-(bis-[carboxymethyl]amino)ethyl)amino]]pentylamino-carbonyl]methyl]-1,3,5-benzenetricarboxamide · 9 HCl (11**)**



To a solution of **10** (181 mg, 63 μmol) in chloroform (6.5 mL), a 4 M HCl-dioxane solution (6.5 mL) was added dropwise. After 2 h at room temperature, the reaction mixture was concentrated *in vacuo* at 40 °C and the concentrate was redissolved in a 2 M aqueous HCl solution (26 mL). After 44 h, the reaction mixture was freeze dried during 3 days resulting in off-white hygroscopic solid **11** (152 mg, 66 μmol , 105%): **¹H-NMR** (D_2O , 363 K): $\delta = 8.09$ (s, 3H, a), 7.31 (m, 15H, b), 4.77 (3H, c), 3.94 (s, 24H, d), 3.62 (b, 3H, e), 3.4–3.2 (m, 36H, f {6H} + g {6H} + h {12H} + i {12H}), 1.8–1.3 (m, 18H, j) ppm; **FT-IR (ATR)**: $\nu = 3303, 2977, 2933, 2867, 1726, 1658, 1538, 1456, 1392, 1368, 1250, 1219$ and 1150 cm^{-1} ; **ESI-MS** (negative mode): m/z calcd. for $[M-(2H+9HCl)]^{2-}$ 994.5; found: 994.0 $[M-(2H+9HCl)]^{2-}$; **elemental analysis**: calcd. for $C_{90}H_{123}N_{15}O_{36} \cdot 9HCl$: 45.19% C, 5.65% H, 8.78% N; found 45.64% C, 5.85% H, 8.45% N.

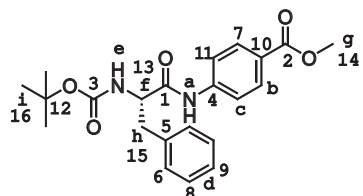
Gd^{III} complex (2a)

Compound **11** (60.0 mg, 25.8 μmol) was dissolved in ultra-pure water (95 mL) and the pH was adjusted to 7 by adding aliquots of 0.1 N NH_4OH . The gadolinium complex was prepared by adding $GdCl_3 \cdot 6H_2O$ (77.4 μmol) as predetermined by UV-titration. The solution was vigorously stirred for 6 h at room temperature at a pH of 7. After freeze drying, **2a** was obtained as a white hygroscopic solid (66.4 mg, 26.0 μmol , quantitative yield): **FT-IR (ATR)**: $\nu = 3129, 3042, 2811, 1575, 1440, 1400, 1322$ and 1086 cm^{-1} ; **ESI-MS** (negative mode): m/z calcd. for $[M-(2H+6NH_3)]^{2-}$ 1225.8; found: 1225.7 $[M-(2H+6NH_3)]^{2-}$; **ICP-MS** (Gd^{III}): calcd. 25.5 ng/g, found 20.0 ng/g.

Y^{III} complex (2b)

Compound **11** (35.2 mg, 15.2 μmol) was dissolved in ultra-pure water (50 mL) and the pH was adjusted to 7 by adding aliquots of 0.1 N NH_4OH . The yttrium complex was prepared by adding an amount of $YCl_3 \cdot 6H_2O$ (46.2 μmol) predetermined by UV-titration. The solution was vigorously stirred for 6 h at room temperature at a pH of 7. After freeze drying, **2b** was obtained as a white hygroscopic solid (35.5 mg, 15.1 μmol quantitative yield). **FT-IR (ATR)**: $\nu = 3131, 3042, 2829, 1583, 1442, 1400, 1324$ and 1088 cm^{-1} ; **ESI-MS** (negative mode): m/z calcd. for $[M-(2H+6NH_3)]^{2-}$ 1123.4; found: 1123.4 $[M-(2H+6NH_3)]^{2-}$; **ICP-MS** (Y^{III}): calcd. 16.1 ng/g, found 15.0 ng/g.

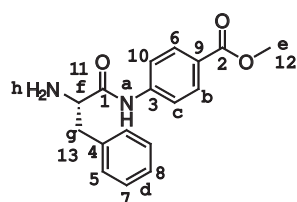
N^a-(tert-Butoxycarbonyl)-N^w-[4-(methoxycarbonyl)phenyl]-L-phenylalaninamide (12**)**



To a magnetically stirred solution of HATU (9.0 g, 23.7 mmol) in dry dimethylformamide (50 mL), DiPEA (9 mL) and Boc-L-PheOH (6.3 g, 23.7 mmol) were added consecutively. This mixture was stirred for 5 min after which methyl-4-aminobenzoate (2.00 g, 13.2 mmol) was added. Stirring was

continued overnight at room temperature. Then, the reaction mixture was slowly added to a mixture of diethyl ether (150 mL), acidic water (pH < 3, 150 mL) and ice. A precipitate was formed. The layers were separated and the diethyl ether layer together with the precipitate were washed with sat. KCl (2 × 72 mL) and 1 N NaOH (2 × 75 mL). The precipitate was filtered, washed with cold ether and isolated as a white powder (1.25 g, 3.14 mmol, 23.8%). Product **12** was characterized using chiral HPLC (isocratic, 10% isopropanol in hexane, purity based on UV = 100%): ¹H-NMR (CDCl₃): δ = 7.97 (br s, 1H, **a**); d, 2H, *J* = 8.8 Hz, **b**), 7.46 (d, 2H, *J* = 8.4 Hz, **c**), 7.3–7.2 (m, 5H, **d**), 5.06 (br s, 1H, **e**), 4.46 (q, 1H, **f**), 3.89 (s, 3H, **g**), 3.16 (d, 2H, *J* = 7.2 Hz, **h**), 1.43 (s, 9H, **i**) ppm; ¹³C-NMR (CDCl₃): δ = 170.2 (**1**), 166.7 (**2**), 156.2 (**3**), 141.7 (**4**), 136.5 (**5**), 130.8 (**6**), 129.4 (**7**), 129.0 (**8**), 127.3 (**9**), 125.9 (**10**), 119.1 (**11**), 81.0 (**12**), 57.0 (**13**), 52.1 (**14**), 38.3 (**15**), 28.4 (**16**) ppm; FT-IR (ATR): ν = 3346, 3316, 1716, 1681, 1665, 1607, 1593, 1519, 1445, 1434, 1407, 1367, 1317, 1283, 1245, 1212, 1177, 1160 and 1111 cm⁻¹; MALDI-TOF-MS: *m/z* calcd. for [M+Na]⁺ 421.17; found: 421.24 [M+Na]⁺, 437.24 [M+K]⁺; elemental analysis: calcd. for C₂₂H₂₆N₂O₅: 66.32% C, 6.58% H, 7.03% N; found: 66.37% C, 6.59% H, 7.24% N.

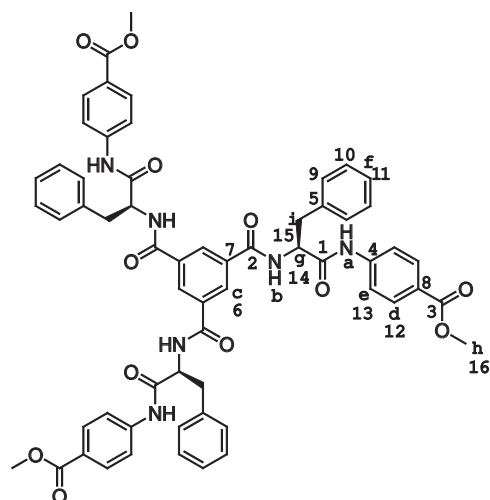
N^ω-[4-(Methoxycarbonyl)phenyl]-L-phenylalaninamide (**13**)



Compound **12** (4.28 g, 10.74 mmol) was dissolved in TFA (20 mL). The solution was purged with argon for 15 min, after which the mixture was stirred for another 45 min. Then, the reaction mixture was concentrated *in vacuo*. A Dowex 550A OH⁻ column was prepared and washed with water and methanol. The product was dissolved in methanol and applied to the column. Elution with methanol yielded 2.78 g of pure title compound **13** (9.62 mmol, 87%), not contaminated with TFA

according to ¹⁹F-NMR: ¹H-NMR (CDCl₃): = 9.68 (s, 1H, **a**), 8.02 (d, 1H, *J* = 8.8 Hz, **b**), 7.68 (d, 1H, *J* = 8.8 Hz, **c**), 7.4–7.2 (m, 5H, **d**), 3.90 (s, 3H, **e**), 3.76 (dd, 1H, **f**), 3.38 + 2.80 (m, 2H, **g**), 1.50 (s, 2H, **h**) ppm; ¹³C-NMR (CDCl₃): = 172.8 (**1**), 166.8 (**2**), 142.0 (**3**), 137.6 (**4**), 131.0 (**5**), 129.4 (**6**), 129.0 (**7**), 127.2 (**8**), 125.7 (**9**), 118.7 (**10**), 57.0 (**11**), 52.1 (**12**), 40.7 (**13**) ppm; FT-IR (ATR): ν = 3389, 3272, 1702, 1674, 1607, 1587, 1520, 1494, 1457, 1434, 1409, 1343, 1318, 1270, 1245, 1182, 1174, 1105 and 1074 cm⁻¹; MALDI-TOF-MS: *m/z* calc. for [M+H]⁺ 299.13; found: 299.05 [M+H]⁺; elemental analysis: calcd. for C₁₇H₁₈N₂O₃: 68.44% C, 6.08% H, 9.39% N; found: 68.19% C, 6.00% H, 9.50% N.

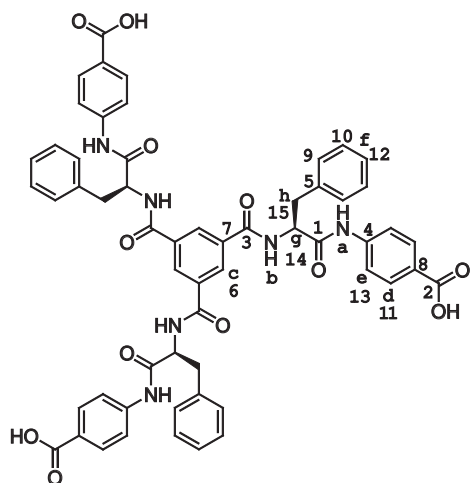
N,N',N''-Tris[*[(S)*-benzyl]{4-(methoxycarbonyl)phenylaminocarbonyl}methyl]-1,3,5-benzenetricarboxamide (**14**)



A solution of 1,3,5-benzenetricarbonyl trichloride (51.3 mg, 0.19 mmol) in dry tetrahydrofuran (1.8 mL) was added dropwise to a solution of **13** (0.19 g, 0.62 mmol) and DiPEA (0.25 mL) in dry tetrahydrofuran (7 mL). After stirring overnight the tetrahydrofuran was evaporated and the residual product was purified using column chromatography (silica, gradient 50–80% ethyl acetate in chloroform). The small excess of **13** used for the reaction could not be completely separated from the product by column chromatography, but this impurity could be easily removed in the next reaction step. Therefore, no effort was made to purify **14** any further (0.14 g, 0.14 mmol, 71%): ¹H-NMR (DMSO-*d*₆): δ = 10.61 (s, 3H, **a**), 9.09 (d, 3H, *J* = 7.6 Hz, **b**), 8.37 (s, 3H, **c**), 7.93 (6H, d, *J* = 8.8 Hz, **d**), 7.76 (6H, d, *J* = 8.8 Hz, **e**), 7.4–7.1 (m, 15H, **f**), 4.91 (q, 3H, **g**), 3.82 (s, 9H, **h**), 3.2–3.1 (m, 6H, **i**) ppm; ¹³C-NMR (DMSO-*d*₆): δ = 170.9 (**1**), 165.9 (**2**), 165.8 (**3**), 143.2 (**4**), 137.8 (**5**), 134.2 (**6**), 130.3 (**7**), 129.5 (**8**), 129.2 (**9**), 128.2 (**10**), 126.5 (**11**), 124.2 (**12**), 118.8 (**13**), 56.1 (**14**), 51.9 (**15**), 37.1 (**16**) ppm; FT-IR (ATR): ν = 3284, 3063, 3029, 2952, 1696, 1643, 1600,

1512, 1455, 1435, 1409, 1277, 1252, 1174, 1107, 1031, 1017 cm^{-1} ; **MALDI-TOF-MS**: m/z calcd. for $[\text{M}+\text{Na}]^+$ 1073.38; found: 1073.23 $[\text{M}+\text{Na}]^+$, 2124.36 $[2\text{M}+\text{Na}]^+$; **elemental analysis**: calcd. for $\text{C}_{60}\text{H}_{54}\text{N}_6\text{O}_{12}$: 68.56% C, 5.18% H, 8.00% N; found: 66.84% C, 5.05% H, 7.49% N.

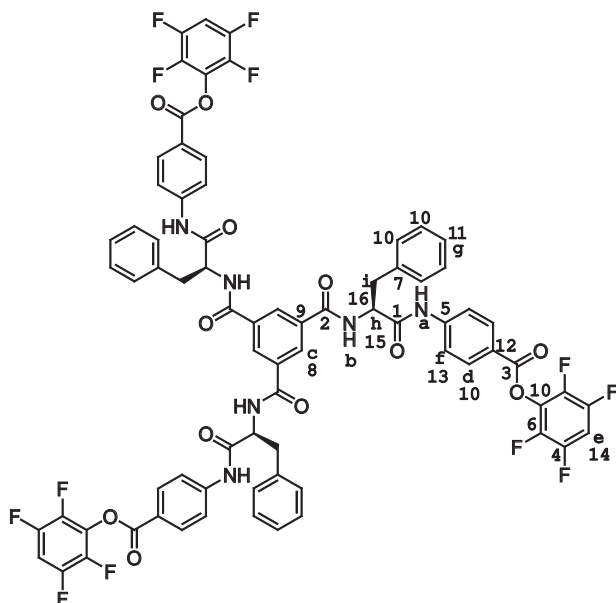
N,N',N''-Tris[[(S)-benzyl]{4-(carboxy)phenylaminocarbonyl}methyl]-1,3,5-benzenetricarboxamide (15)



A solution of **14** (888 mg, 0.85 mmol) in tetrahydrofuran / 1.8 M NaOH (aq) (1.25/1 v/v) (3.6 mL) was stirred for 4 days at room temperature. Then, the gel-like reaction mixture was diluted with H_2O (60 mL) to give a clear solution that was acidified with concentrated HCl to $\text{pH} < 3$. The gel that formed was centrifuged, the water was decanted and the remaining gel washed with acidic water (30 mL). These consecutive steps were repeated three times after which the gel was lyophilized. The title compound **15** was isolated as a fine white powder (0.89 g, 0.88 mmol, 104%): $^1\text{H-NMR}$ (DMSO-d_6): $\delta = 10.60$ (s, 3H, **a**), 9.10 (m, 3H, **b**), 8.42 + 8.40 (s + s, 1H + 2H, **c**), 7.92 (6H, d, $J = 8.4$ Hz, **d**), 7.75 (6H, d, $J = 8.4$ Hz, **e**), 7.5–7.1 (m, 15H, **f**), 4.94 (q, 3H, **g**), 3.2–3.0 (m, 6H, **h**) ppm; $^{13}\text{C-NMR}$ (DMSO-d_6): $\delta = 170.8$ (**1**), 167.0 (**2**), 165.8 (**3**, **t**),

142.8 (**4**), 137.8 (**5**), 134.2 (**6**, **d**), 130.4 (**7**), 129.5 (**8**), 129.2 (**9**), 128.2 (**10**), 126.5 (**121**), 125.6 (**12**), 118.6 (**13**), 56.1 (**14**), 37.1 (**15**) ppm; **FT-IR (ATR)**: $\nu = 3283, 3064, 1684, 1646, 1598, 1512, 1455, 1410, 1308, 1246, 1173, 1099$ cm^{-1} ; **MALDI-TOF-MS**: m/z calcd. for $[\text{M-H}]^-$ 1007.33; found: 1007.29 $[\text{M-H}]^-$; **elemental analysis**: calcd. for $\text{C}_{57}\text{H}_{48}\text{N}_6\text{O}_{12}$: 65.48% C, 4.72% H, 8.04% N; found: 65.40% C, 4.65% H, 7.62% N.

N,N',N''-Tris[[(S)-benzyl]{4-(2,3,5,6-tetrafluorophenoxy)phenylaminocarbonyl}methyl]-1,3,5-benzenetricarboxamide (16)

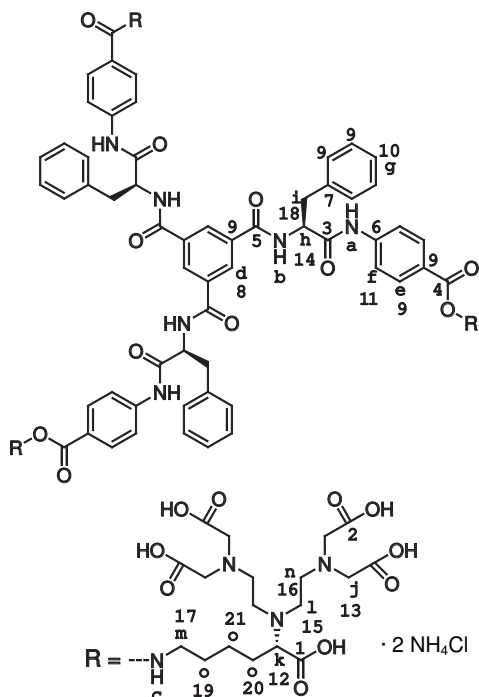


To a solution of **15** (498 mg, 0.49 mmol), tetrafluorophenol (280 mg, 1.69 mmol) and DMAP (18.4 mg, 0.15 mmol) in dry dichloromethane (3 mL) a solution of EDC (316 mg, 1.64 mmol) in dry dichloromethane (3 mL) was added. After the reaction mixture was stirred overnight in an atmosphere of argon, the solvent was evaporated *in vacuo*. Purification was achieved with column chromatography (silica, gradient 0–10% tetrahydrofuran in dichloromethane). The pure title compound **16** was isolated as a fine white solid material (410 mg, 0.28 mmol, 57%): $^1\text{H-NMR}$ (DMSO-d_6): $\delta = 10.80$ (s, 3H, **a**), 9.12 (m, 3H, **b**), 8.44 + 8.42 (s + s, 1H + 2H, **c**), 8.17 (6H, d, $J = 8.8$ Hz, **d**), 8.00 (m, 3H, **e**), 7.90 (6H, d, $J = 8.8$ Hz, **f**), 7.5–7.1 (m, 15H, **g**), 4.95 (q, 3H, **h**), 3.3–3.0 (m, 6H, **i**) ppm;

$^{13}\text{C-NMR}$ (DMSO-d_6): $\delta = 171.3$ (**1**), 165.9 (**2**, **t**), 161.8 (**3**), 146.9 (**4**, **t**), 145.1 (**5**), 144.4 (**6**, **t**), 141.5 (**4**, **d**), 139.0 (**6**, **d**), 137.8 (**7**), 134.2 (**8**, **d**), 131.9 (**9**), 129.6, 129.2, 129.0, 128.9, 128.2 (**10**), 126.5 (**11**), 120.2 (**12**), 119.2 (**13**), 104.8, 104.5, 104.3 (**14**), 56.3 (**15**), 37.1 (**16**) ppm; **FT-IR (ATR)**: $\nu = 3287, 3073, 1756, 1645, 1598, 1521, 1488, 1456, 1411, 1372, 1309, 1278, 1240, 1175, 1132, 1074$ cm^{-1} ; **MALDI-TOF-MS**: m/z calcd. for $[\text{M}+\text{Na}]^+$ 1475.31;

found: 1475.36 [M+Na]⁺, 1491.31 [M+K]⁺; **elemental analysis**: calcd. for C₇₅H₄₈F₁₂N₆O₁₂: 61.99% C, 3.33% H, 5.78% N; found: 61.21% C, 3.26% H, 5.01% N.

N,N',N''-Tris[[(S)-benzyl]{4-[(5-carboxy)(5-[bis-{2-[bis-(carboxymethyl)amino]ethyl)amino})pentylamino-carbonyl]}phenylaminocarbonyl]methyl]-1,3,5-benzenetricarboxamide · 6 NH₄Cl (17)



To a solution of **5a** (221 mg, 0.26 mmol) and DiPEA (475 μ L, 2.73 mmol) in DMSO-*d*₆ (2 mL), compound **15** (122 mg, 0.08 mmol) was added as solid material. After the reaction was stirred overnight in an atmosphere of argon, the reaction mixture was diluted with water (8 mL) and acidified to pH < 3 with 2 M aqueous HCl. The gel that was formed was centrifuged, the water was decanted and the remaining gel washed with 30 mL water. These consecutive steps were repeated three times after which the gel was dissolved in 0.1 M NH₄OH and lyophilized. The pure title compound **17** was isolated as a fluffy, white powder (148 mg, 55.4 μ mol, 69%): ¹H-NMR (DMSO-*d*₆): δ = 10.47 (s, 3H, **a**), 9.08 (m, 3H, **b**), 8.57 (s, 3H, **c**), 8.40 + 8.37 (s + s, 1H + 2H, **d**), 7.88 (6H, d, *J* = 8.0 Hz, **e**), 7.67 (6H, d, *J* = 8.0 Hz, **f**), 7.5–7.1 (m, 15H, **g**), 4.91 (q, 3H, **h**), 3.6–3.0 (m, 45H, **i** {6H} + **j** {24H} + **k** {3H} + **l** {12H}), 3.0–2.4 (m, 18H, **m** {6H} + **n** {12H}), 1.8–1.2 (m, 18H, **o**) ppm; ¹³C-NMR (DMSO-*d*₆): δ = 173.5 (**1**), 171.8 (**2**), 170.6 (**3**), 165.8 (**4**), 165.5 (**5**), 141.2 (**6**), 137.9 (**7**), 134.3 (**8**), 129.4, 129.2, 128.2 (**9**), 126.4 (**10**), 118.6 (**11**), 63.4 (**12**), 57.7 (**13**), 56.1 (**14**), 52.1

(**15**), 48.2 (**16**), covered by DMSO (**17**), 37.2 (**18**), 28.9 (**19**), 28.5 (**20**), 23.7 (**21**) ppm; **FT-IR (ATR)**: ν = 3198, 3031, 1603, 1536, 1503, 1457, 1436, 1391, 1313, 1253, 1094 cm⁻¹; **ESI-MS** (negative mode): *m/z* calcd. for 1173.21 [M-(2H+6NH₄Cl)]²⁻; found: 1173.1 [M-(2H+6NH₄Cl)]²⁻, 1184.5 [M-(2H+6NH₄Cl) + Na]²⁻, 1196.5 [M-(2H+6NH₄Cl) + 2Na]²⁻, 781.7 [M-(3H+6NH₄Cl)]³⁻; **elemental analysis**: calcd. for C₁₁₁H₁₃₈N₁₈O₃₉ · 6 NH₄Cl: 49.95% C, 6.12% H, 12.59% N; found: 50.48% C, 6.63% H, 12.26% N.

Gd^{III} complex (3a)

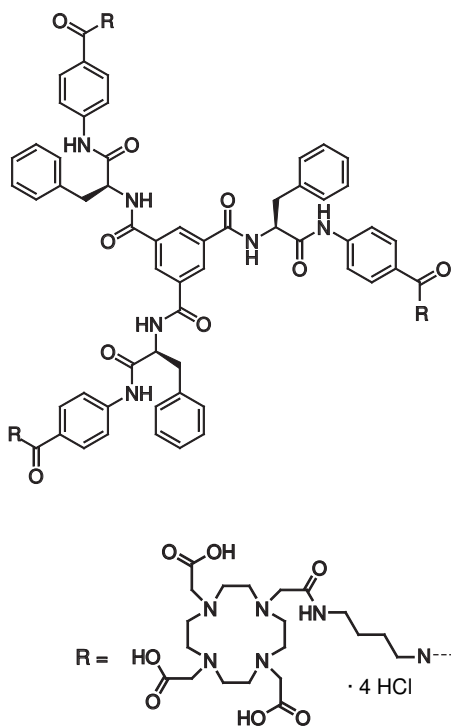
Compound **17** (49.2 mg, 18.9 μ mol) was dissolved in ultra-pure water (30 mL) and the pH was adjusted to 7 by adding aliquots of 0.1 N NH₄OH. The gadolinium complex was prepared by adding Gd(OAc)₃·xH₂O (43.6 μ mol) as predetermined by UV-titration. The solution was vigorously stirred overnight at room temperature at a pH of 7. After freeze drying, **3a** was obtained as a white fluffy powder could be obtained (66.9 mg, 25.1 μ mol, 133%): **FT-IR (ATR)**: ν = 3267, 1589, 1539, 1506, 1440, 1405, 1319, 1256, 1185, 1090 cm⁻¹; **ICP-MS** (Gd^{III}): calcd. 885 ng/g, found 560 ng/g.

Y^{III} complex (3b)

Compound **17** (50.0 mg, 19.2 μ mol) was dissolved in ultra-pure water (30 mL) and the pH was adjusted to 7 by adding aliquots of 0.1 N NH₄OH. The yttrium complex was prepared by adding an amount of Y(OAc)₃·xH₂O (37.7 μ mol) predetermined by UV-titration. The solution was vigorously stirred overnight at room temperature at a pH of 7. After freeze drying, **3b** was obtained as a white fluffy powder could be obtained (46.6 mg, 18.9 μ mol, quantitative yield). **FT-IR (ATR)**: ν = 3261, 1599, 1539, 1506, 1440, 1408, 1319, 1257, 1185, 1091 cm⁻¹; **ICP-MS** (Y^{III}): calcd. 500 ng/g, found 420 ng/g.

1,4,7,10-Tetraazacyclododecane-1,4,7-tris(acetic acid)-10-(aminobutylaminocarbonylmethyl) · 5 HCl (18)

This compound was kindly provided by Dr. H. Keizer (SyMO-chem BV).

N,N',N''-Tris[*S*-(benzyl){4-(1-[4,7,10-tris(carboxymethyl)]-1,4,7,10-tetraazacyclododecyl)methylcarbonylaminobutylaminocarbonyl}phenylaminocarbonyl]methyl]-1,3,5-benzenetricarboxamide · 12 HCl (19)

To a solution of **18** (75 mg, 0.12 mmol) and DiPEA (310 μ L, 1.81 mmol) in DMSO- d_6 (1 mL), compound **16** (53.7 mg, 37 μ mol) was added as solid material. After the reaction was stirred overnight in an atmosphere of argon, extra amounts of **18** (15.0 mg, 0.02 mmol) in DMSO- d_6 (0.2 mL) and DiPEA (60 μ L, 0.35 mmol) were added. The reaction mixture was stirred overnight, diluted with water (4 mL) and acidified to pH < 3 with concentrated HCl. No gel was formed so the solution was further diluted with water (100 mL) and lyophilized. Crude **19** was dissolved in water (2.5 mL) and eluted over a size exclusion PD10 column to remove the salts. Subsequently, semi-preparative HPLC and freeze-drying yielded **19** (25 mg, 8.9 μ mol, 24%) as a white powder. LC-ESI-MS: *m/z* calcd. for 1190.4 [M+2H-12HCl]²⁺; found: 1190.1 [M+2H-12HCl]²⁺, 793.7 [M+3H-12HCl]³⁺, 595.6 [M+4H-12HCl]⁴⁺, 476.6 [M+5H-12HCl]⁵⁺, [M+3H-12HCl]³⁺, 391.2 [M+6H-12HCl]⁶⁺.

Gd^{III} complex (4)

Compound **19** (17.3 mg, 6.1 μ mol) was dissolved in ultra-pure water (1.6 mL) and the pH was adjusted to 7 by adding aliquots of pyridine. The gadolinium complex was prepared by adding Gd(OAc)₃·xH₂O (9.81 mg) to the solution. The solution was stirred overnight at room temperature at a pH of 7. CHELEX 100 sodium form resin (115 mg) was added to capture the excess of gadolinium. After gently stirring over three nights, the solution was isolated from the beads using a pipette and lyophilized. The pure title compound **4** was obtained as a white fluffy powder (19.7 mg, 6.9 μ mol, 113%). LC-ESI-MS: *m/z* calcd. for 1421.5 [M+2H]²⁺; found: 1421.9 [M+2H]²⁺, 948.1 [M+3H]³⁺, 711.2 [M+4H]⁴⁺; ICP-MS (Gd^{III}): calcd. 500 ng/g, found 140 ng/g.

¹H-DOSY NMR data

The measurements were executed using the DOSY bipolar pulse paired stimulated echo convection compensation (Dbppste_cc) pulse sequence^[52], to avoid effects of convection within the sample. The steady state pulse sequence was used to compensate for the long relaxation times of HDO. The gt1 and del values for each sample are listed in Table E1. The self-diffusion of HDO was used to calibrate the measurements (see Chapter 4: Experimental section).

Table E1: gt1 and del values for each sample.

[Y ^{III}] / mM	T / °C		del / s	gt1 / s
1.7	25	Molecule	0.070	0.0025
		HDO	0.015	0.0020
	41	Molecule	0.075	0.0025
		HDO	0.015	0.0017
	54	Molecule	0.07	0.0025
		HDO	0.015	0.0015
67	Molecule	0.060	0.0020	
	HDO	0.015	0.0013	
81	Molecule	0.050	0.0017	
	HDO	0.015	0.0011	
8.3	25	Molecule	0.075	0.0025
		HDO	0.015	0.0020
	81	Molecule	0.020	0.0019
		HDO	0.020	0.0011
25	25	Molecule	23	0.75
		HDO	0.015	0.0020

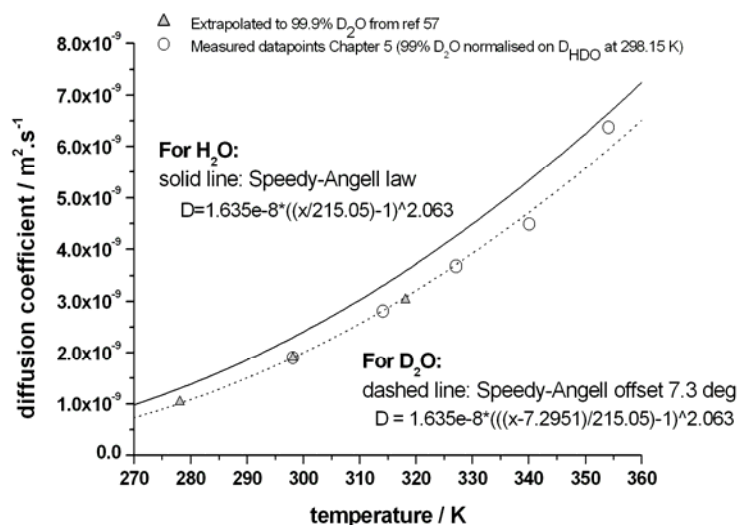


Figure E1: Temperature-dependent diffusion of HDO in D₂O^[57] and in the samples fitted with the modified Speedy–Angell power law.

Figure E1 shows the measured self-diffusion coefficients of HDO in the sample at different temperatures. Furthermore, the self-diffusion coefficients of HDO in D₂O at three temperatures, 278, 298 and 318 K, as reported by Longworth *et al.*^[57] are included.

The model used to calculate the hydrodynamic radii of the aggregates is the Stokes–Einstein relationship^[54] for the diffusion of a spherical particle:

$$D_t = \frac{kT}{6\pi\eta R_H}$$

k = Boltzmann constant

T = absolute temperature

η = dynamic viscosity of the D₂O^(*)

R_H = hydrodynamic radius of the aggregate

(*) The measurements in Chapter 5 show that the measured self-diffusion of HDO in the sample does not deviate from its theoretical value between 25 °C and 67 °C. At 81 °C (354.15 K) and higher, the measured self-diffusion of HDO does deviate from its theoretical value. In order to estimate the size of the aggregates present at 25 °C to 67 °C the dynamic viscosity of pure D₂O is used.

5.9 Appendices

Appendix A

Linear relationship between temperature and $1/T_{1,diamagn.}$ ^[58,59]

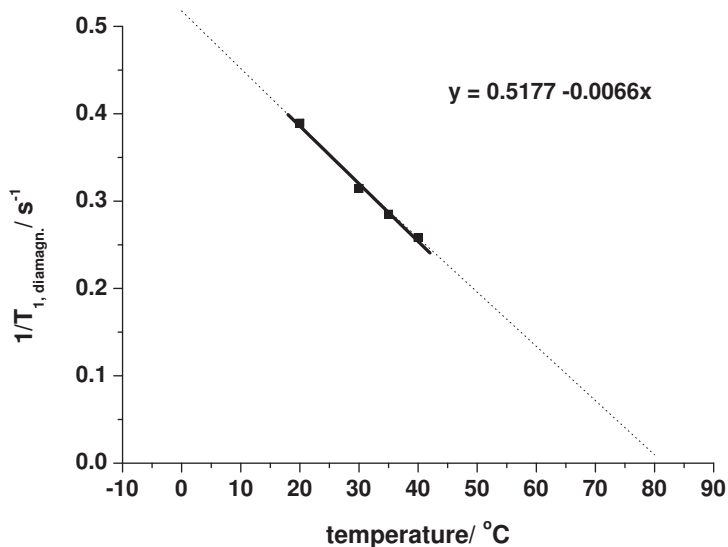
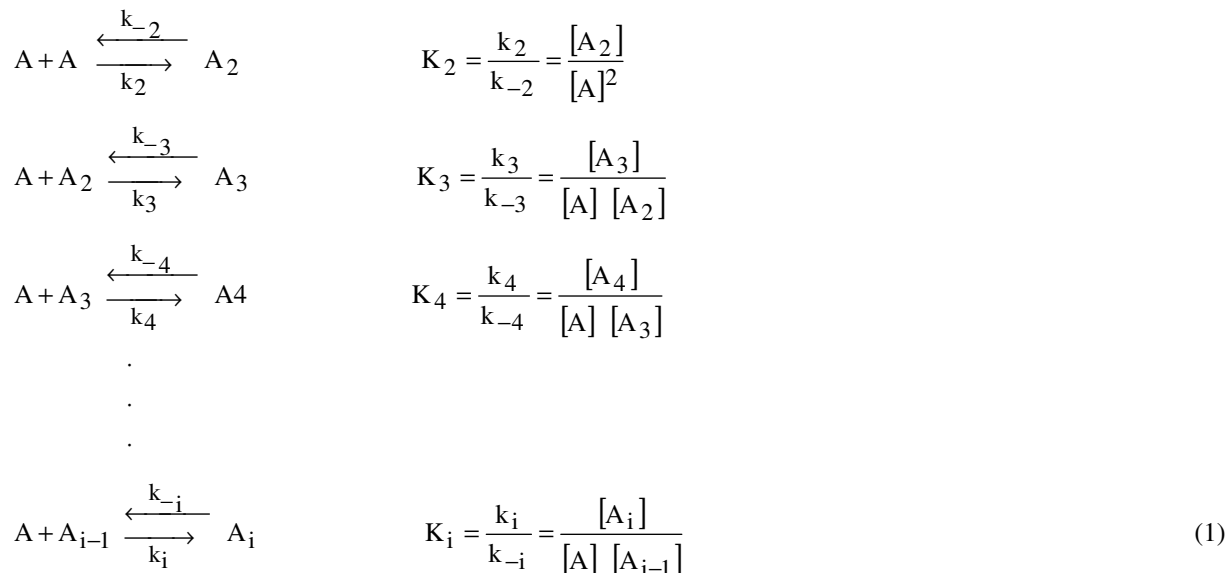


Figure A1. Extrapolation of the $1/T_{1,diamagn.}$

Appendix B*Theory isodesmic polymerization*

Consider the following polymerization of free discotics $[A]$ in solution



According to equation (1), the molar concentration of all aggregates with different degree of polymerization i at equilibrium can be written as:

$$\begin{array}{l}
 [A_2] = K_2[A]^2 \\
 [A_3] = K_3[A_2][A] = K_3K_2[A]^3 \\
 [A_4] = K_4[A_3][A] = K_4K_3K_2[A]^4 \\
 \vdots \\
 \vdots \\
 \vdots \\
 [A_i] = K_i[A_{i-1}][A] = K_i \dots K_3K_2[A]^i = [A]^i \prod_{j=2}^i K_j \quad (2) \\
 \vdots \\
 \vdots \\
 \vdots
 \end{array}$$

$$c_t = \sum_{i=1}^{\infty} i[A_i] \quad (3)$$

$$c_p = \sum_{i=1}^{\infty} [A_i] \quad (4)$$

Where c_t is the initial total concentration of free discotics, and c_p is the total concentration of all i -mers including the free discotics. In the isodesmic model, the equilibrium constants for all free discotic additions are identical ($K_2 = K_3 = \dots = K_i = \dots = K$). Therefore, equation (2) reduces to:

$$[A_i] = K^{-1}(K[A])^i = K^{i-1}[A]^i \quad (5)$$

And the mole fraction of an i -mer is defined as:

$$x_i = \frac{[A_i]}{c_t} \quad (6)$$

The degree of aggregation ϕ , which can be deduced from spectroscopic measurements and can be written as:

$$\phi = 1 - x_1 \quad (7)$$

Due to equation (5), the initial total free disc concentration can be written as:

$$c_t = \sum_{i=1}^{\infty} iK^{-1}(K[A])^i \quad (8)$$

If $K[A] < 1$ this sum can be conveniently written as :

$$c_t = \frac{[A]}{(1 - K[A])^2} \quad (9)$$

And c_p is written as:

$$c_p = \frac{[A]}{(1 - K[A])} \quad (10)$$

The free disc concentration $[A]$ can be isolated from equation (9):

$$[A] = \frac{1}{2} \frac{2c_t K + 1 - \sqrt{4c_t K + 1}}{c_t K^2} \quad (11)$$

For each given value of K and initial concentration c_0 , the corresponding concentration of free disc $[A]$ can be calculated and hence, the concentration of each i -mer too. The mole fraction of each i -mer is then defined via equation (6).

The weight average degree of polymerization PD_w is defined by equation (12):

$$DP_w = \frac{\sum_{i=1}^{\infty} i^2 N_i}{\sum_{i=1}^{\infty} i N_i} \quad (12)$$

The numerator of equation (12) is proportional to the summation of the molar concentrations of all i -mers multiplied by i^2 , whereas the denominator is proportional to the initial free disc concentration, c_t . In other words, equation (12) can be written as:

$$DP_w = \frac{\sum_{i=1}^{\infty} i^2 [A_i]}{c_t} = \frac{\sum_{i=1}^{\infty} i^2 K^{i-1} [A]^i}{c_t} = \frac{1 + K[A]}{1 - K[A]} \quad (13)$$

The number average degree of polymerization DP_N is defined by equation (14):

$$DP_N = \frac{\sum_{i=1}^{\infty} i N_i}{\sum_{i=1}^{\infty} N_i} \quad (14)$$

Where N_i is the number of aggregates of a given i -mer. Now, the numerator of equation (14) is proportional to the initial free disc concentration, c_t , whereas the denominator is proportional to the summation of the molar concentrations of all the i -mers. In other words, equation (14) can be written as:

$$DP_N = \frac{c_t}{\sum_{i=1}^{\infty} [A_i]} = \frac{c_t}{\sum_{i=1}^{\infty} K^{i-1} [A]^i} = \frac{1}{1 - K[A]} \quad (15)$$

By combining equations (6), (7) and (15), the degree of aggregation ϕ can be expressed in terms of DP_N . So DP_N can be calculated via equation (16):

$$1 - \phi = x_I = \frac{[A]}{c_t} = \frac{1}{(1 - K[A])^2} = DP_N^2 \quad (16)$$

Now DP_N is known as function of the temperature, the association constant at each temperature can be determined via equation (17). This equation is a combination of equations (11) and (15) and gives:

$$DP_N = \frac{1}{2} + \frac{1}{2} \sqrt{4Kc_t + 1} \quad (17)$$

Since it is more convenient to express equation (15) in Gd^{III} concentrations instead of disc concentrations. c_t , the total initial concentration of free discs will be replaced by C , the total initial concentration of Gd^{III} :

$$c_t = \frac{C}{3} \quad (18)$$

Thus $[A]$ used in equation (15) becomes:

$$[A] = \frac{1}{2} \frac{2 \frac{C}{3} K + 1 - \sqrt{4 \frac{C}{3} K + 1}}{\frac{C}{3} K^2} \quad (19)$$

Appendix C

The association constant (K) as function of the temperature

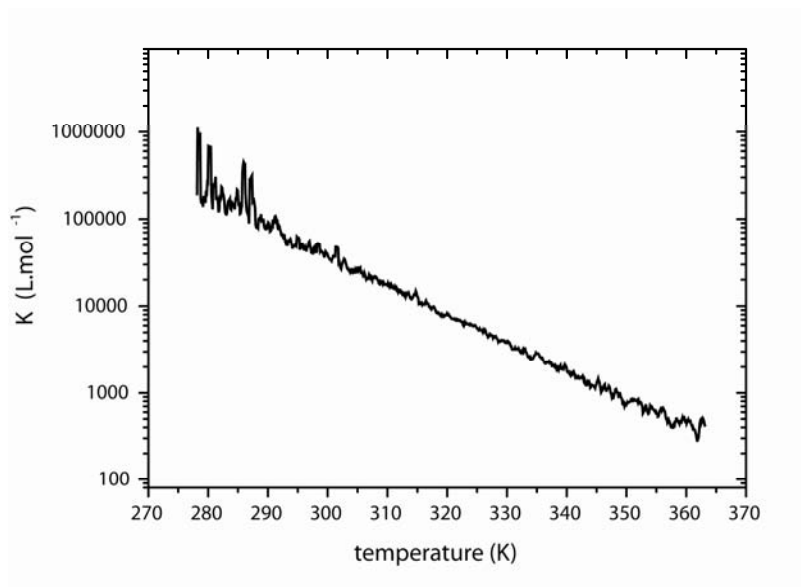


Figure A2. The association constant (K) as function of the temperature.

Appendix D

Derived models to fit the relaxivity data

Model 1

Model 1 assumes that there are two kinds of discs in solution—free discs (not aggregated) and discs within an aggregate—which display different ionic relaxivities. The total initial concentration of free discs c_t and the concentration of free discs $[A]$ are already derived in appendix B (equations (18) and (19)). The longitudinal ^1H relaxation rate can thus be written as:

$$R_1^{\text{obs}} - R_1^{\text{d}} = r_1^{\text{m}} \cdot 3[A] + r_1^{\text{a}} \cdot 3\left(\frac{C}{3} - [A]\right) \quad (20)$$

In which R_1^{obs} is the observed ^1H relaxation rate, R_1^{d} is the diamagnetic ^1H relaxation rate, r_1^{m} represents the ionic relaxivity of free discs, r_1^{a} gives the ionic relaxivity of discs within an aggregate and $(C/3 - [A])$ gives the concentration of discs within aggregates.

Model 2

Model 2 assumes that there are three kinds of discs in solution—free discs (not aggregated), aggregated discs with one neighbour (outer discs) and aggregated discs with two neighbours (inner discs)—, which display different ionic relaxivities. The longitudinal ^1H relaxation rate if expressed in Gd^{III} concentrations can then be written as:

$$R_1^{\text{obs}} - R_1^{\text{d}} = r_1^{\text{m}} \cdot 3[A] + r_1^{\text{out}} \cdot 3[A_{\text{out}}] + r_1^{\text{in}} \cdot 3[A_{\text{in}}] \quad (21)$$

In which r_1^{out} represent the ionic relaxivity of outer discs, $[A_{out}]$ the concentration of outer discs, r_1^{in} gives the ionic relaxivity of inner discs and $[A_{in}]$ gives the concentration of inner discs.

The concentration of outer discs $[A_{out}]$ can now be expressed in terms of the concentration of free discs $[A]$, since the concentration of aggregates, $c_p - [A]$ (for c_p see Appendix B equation (10)), is known:

$$c_p - [A] = \frac{K[A]^2}{1 - K[A]} \quad (22)$$

$$[A_{out}] = 2 \cdot (c_p - [A]) = \frac{2K[A]^2}{1 - K[A]} \quad (23)$$

The concentration of inner discs $[A_{in}]$ can now also be expressed in terms of the concentration of free discs $[A]$ (for c_t see Appendix B equation (9)):

$$[A_{in}] = c_t - [A] - [A_{out}] = \frac{K^2[A]^3}{(1 - K[A])^2} \quad (24)$$

Thus the final model can be written as:

$$R_1^{obs} - R_1^d = r_1^m \cdot 3[A] + \frac{r_1^{out} \cdot 6K[A]}{1 - K[A]} + \frac{r_1^{in} \cdot 3K^2[A]^3}{(1 - K[A])^2} \quad (25)$$

5.10 References and notes

- [1] S-P. Lin, J.J. Brown, *J. Magn. Res. Imaging* **2007**, *25*, 884–899.
- [2] S. Laurent, L. vander Elst, R.N. Muller, *Contrast Med. Mol. Imaging*, **2006**, *1* 128–137.
- [3] P. Caravan, J.J. Ellison, T.J. McMurry, R.B. Lauffer, *Chem. Rev.* **1999**, *99*, 2293–2352.
- [4] T. Barrett, H. Kobayashi, M. Brechbiel, P.L. Choyke, *Eur. J. Radiol.* **2006**, *60*, 353–366.
- [5] V. Jacques, J.F. Desreux, *Top. Curr. Chem.* **2002**, *221*, 123–164.
- [6] S. Langereis, Q.G. de Lussanet, M.H.P. van Genderen, W.H. Backes, E.W. Meijer, *Macromolecules* **2004**, *37*, 3084–3091.
- [7] P-J. Debouttière, S. Roux, F. Vocanson, C. Billotey, O. Beuf, A. Favre-Réguillon, S. Pellet-Rostaing, R. Lamartine, P. Perriat, O. Tillement, *Adv. Funct. Mater.* **2006**, *16*, 2330–2339.
- [8] J.M. Hooker, A. Datta, M. Botta, K.N. Raymond, M.B. Francis, *Nano Lett.* **2007**, *7*, 2207–2210.
- [9] B. Misselwitz, H. Schmitt-Willich, W. Ebert, T. Frenzel, H-J. Weinmann, *Magn. Reson. Mater. Phys., Biol. Med.* **2001**, *12*, 128–134.
- [10] F. Kiessling, M. Heilmann, T. Lammers, K. Ulbrich, V. Subr, P. Peschke, B. Waengler, W. Mier, H-H. Schrenk, M. Bock, L. Schad, W. Semmler, *Bioconjugate Chem.* **2006**, *17*, 42–51.
- [11] M. Spanoghe, D. Lanens, R. Dommissie, A. van der Linden, F. Alderweireldt, *Magn. Res. Imaging* **1992**, *10*, 913–917.
- [12] D.A. Fulton, E.M. Elemento, S. Aime, L. Chaabane, M. Botta, D. Parker, *Chem. Commun.* **2006**, 1064–1066.

- [13] R.B. Lauffer, D.J. Parmelee, S. Ouellet, R.P. Dolan, H. Sajiki, M. Scott, P.J. Bernard, E.M. Buchanan, K. Y. Ong, Z. Tyeklár, K.S. Midelfort, T.J. McMurry, R.C. Walovitch, *Acad. Radiol.* **1996**, *3*, 356–358.
- [14] S. Aime, L. Frullano, S. Geninatti Crich, *Angew. Chem.* **2002**, *114*, 1059–1061; *Angew. Chem., Int. Ed.* **2002**, *41*, 1017–1019.
- [15] P. Caravan, N.J. Cloutier, M.T. Greenfield, S.A. McDermid, S.U. Dunham, J.W.M. Bulte, J.D. Amedio Jr., R.J. Looby, R.M. Supkowski, W. DeW. Horrocks Jr., T.J. McMurry, R.B. Lauffer, *J. Am. Chem. Soc.* **2002**, *124*, 3152–3162.
- [16] J.B. Livramento, E. Tóth, A. Sour, A. Borel, A.E. Merbach, R. Ruloff, *Angew. Chem.* **2005**, *117*, 1504–1508; *Angew. Chem., Int. Ed.* **2005**, *44*, 1480–1484.
- [17] L. Prinzen, R.-J. J.H.M. Miserus, A. Dirksen, T.M. Hackeng, N. Deckers, N.J. Bitsch, R.T.A. Megens, K. Douma, J.W. Heemskerk, M.E. Kooi, P.M. Frederik, D.W. Slaaf, M.A.M.J. van Zandvoort, C.P.M. Reutelingsperger, *Nano Lett.* **2007**, *7*, 93–100.
- [18] V.S. Vexler, O. Clement, H. Schmitt-Willich, R.C. Brasch, *J. Magn. Res. Imaging* **1994**, *4*, 381–388.
- [19] T.S. Desser, L.D. Rubin, H.H. Muller, F. Qing, S. Khodor, G. Zanazzi, S.W. Young, D.L. Ladd, J.A. Wellons, K.E. Kellar, *J. Magn. Res. Imaging* **1994**, *4*, 467–472.
- [20] H.-J. Raatschen, R. Swain, D.M. Shames, Y. Fu, Z. Boyd, M.L. Zierhut, M.F. Wendland, B. Misselwitz, H.-J. Weinmann, K.-J. Wolf, R.C. Brasch, *Contrast Med. Mol. Imaging* **2006**, *1*, 113–120.
- [21] H.Y. Lee, H.W. Jee, S.M. Seo, B.K. Kwak, G. Khang, S.H. Cho, *Bioconjugate Chem.* **2006**, *17*, 700–706.
- [22] G.A.F. van Tilborg, W.J.M. Mulder, N. Deckers, G. Storm, C.P.M. Reutelingsperger, G.J. Strijkers, K. Nicolay, *Bioconjugate Chem.* **2006**, *17*, 741–749.
- [23] T.N. Parac-Vogt, K. Kimpe, S. Laurent, C. Piérart, L. vander Elst, R.N. Muller, K. Binnemans, *Eur. Biophys. J.* **2006**, *35*, 136–144.
- [24] M. Vaccaro, A. Accardo, D. Tesauero, G. Mangiapia, D. Löf, K. Schillén, O. Södermann, G. Morelli, L. Paduano, *Langmuir* **2006**, *22*, 6635–6643.
- [25] C. Gløgård, G. Stensrud, R. Hovland, S.L. Fossheim, J. Klaveness, *Int. J. Pharm.* **2002**, *233*, 131–140.
- [26] A. Accardo, D. Tesauero, G. Morelli, E. Gianolio, S. Aime, M. Vaccaro, G. Mangiapia, L. Paduano, K. Schillén, *J. Biol. Inorg. Chem.* **2007**, *12*, 267–276.
- [27] S.R. Bull, M.O. Guler, R.E. Bras, P.N. Venkatasubramanian, S.I. Stupp, T.J. Meade, *Bioconjugate Chem.* **2005**, *16*, 1343–1348.
- [28] A. Barge, G. Cravotto, B. Robaldo, E. Gianolio, S. Aime, *J. Incl. Phenom. Macrocycl. Chem.* **2007**, *57*, 489–495.
- [29] S. Langereis, H.-A.T. Kooistra, M.H.P. van Genderen, E.W. Meijer, *Org. Biomol. Chem.* **2004**, *2*, 1271–1273.
- [30] A. Dirksen, S. Langereis, B.F.M. de Waal, M.H.P. van Genderen, T.M. Hackeng, E.W. Meijer, *Chem. Commun.* **2005**, 2811–2813.
- [31] S. Torres, J.A. Martins, J.P. André, C.F.G.C. Geraldés, A.E. Merbach, E. Tóth, *Chem. Eur. J.* **2006**, *12*, 940–948.
- [32] G.M. Nicolle, E. Tóth, K.-P. Eiseniener, H.R. Mäcke, A.E. Merbach, *J. Biol. Inorg. Chem.* **2002**, *7*, 757–769.
- [33] A.R.A. Palmans, J.A.J.M. Vekemans, H. Fischer, R.A. Hikmet, E.W. Meijer, *Chem. Eur. J.* **1997**, *3*, 300–307.
- [34] L. Brunsveld, H. Zhang, M. Glasbeek, J.A.J.M. Vekemans, E.W. Meijer, *J. Am. Chem. Soc.* **2000**, *122*, 6175–6182.
- [35] L. Brunsveld, B.G.G. Lohmeijer, J.A.J.M. Vekemans, E.W. Meijer, *J. Incl. Phenom. Macrocycl. Chem.* **2001**, *41*, 61–64.

- [36] J.J. van Gorp, J.A.J.M. Vekemans, E.W. Meijer, *J. Am. Chem. Soc.* **2002**, *124*, 14759–14769.
- [37] K.P. van den Hout, R. Martín-Rapún, J.A.J.M. Vekemans, E.W. Meijer, *Chem. Eur. J.* **2007**, *13*, 8111–8123.
- [38] P.L. Anelli, F. Fedeli, O. Gazzotti, L. Lattuada, G. Lux, F. Rebasti, *Bioconjugate Chem.* **1999**, *10*, 137–140.
- [39] M.A. Williams, H. Rapoport, *J. Org. Chem.* **1993**, *58*, 1151–1158.
- [40] A. Barge, G. Cravotto, E. Gianolio, F. Fedeli, *Contrast Med. Mol. Imaging* **2006**, *1*, 184–188.
- [41] B.L. Gupta, *Talanta* **1974**, *21*, 683–684.
- [42] S. Langereis, Thesis: *Dendritic MRI contrast agents, synthetic strategies for targeting and multivalency*, Eindhoven University of Technology, Eindhoven (The Netherlands), **2005**.
- [43] R. Knorr, A. Trzeciak, W. Bannwarth, D. Gillessen, *Tetrahedron Lett.* **1989**, *30*, 1927–1930.
- [44] Enantiomeric excess of intermediate **5** was not determined with chiral HPLC.
- [45] M.M.J. Smulders, A.P.H.J. Schenning, E.W. Meijer, *J. Am. Chem. Soc.* **2007**, *130*, 606–611.
- [46] P. Jonkheijm, P. van der Schoot, A.P.H.J. Schenning, E.W. Meijer, *Science* **2006**, *313*, 80–83.
- [47] P. van der Schoot, In *Supramolecular polymers*; 2nd ed.; A. Ciferri, Ed. Taylor & Francis: London **2005**.
- [48] R.B. Martin, *Chem. Rev.* **1996**, *96*, 3043–3064.
- [49] G. Fleischer, *Polymer* **1985**, *26*, 1677–1682.
- [50] R. Raghavan, T.L. Maver, F.D. Blum, *Macromolecules* **1987**, *20*, 814–820.
- [51] A. Chen, D. Wu, C.S. Johnson Jr, *J. Am. Chem. Soc.* **1995**, *117*, 7965–7970.
- [52] A. Jerschow, N. Müller, *J. Magn. Reson.* **1997**, *125*, 372–375.
- [53] C.H. Cho, J. Urquidi, S. Singh, G. Wilse Robinson, *J. Phys. Chem. B* **1999**, *103*, 1991–1994.
- [54] G.G. Stokes, *Trans Cambridge Philos. Soc.* **1845**, *8*, 287.
- [55] M.M. Tirado, J. Garcia de la Torre, *J. Chem. Phys.* **1979**, *71*, 2581–2587.
- [56] This value is estimated from a plot in which the ionic relaxivity is plotted against the molecular weight for different generations of Gd^{III}-DTPA containing PPI dendrimers as described by S. Langereis^[6].
- [57] L.G. Longworth, *J. Phys. Chem.* **1960**, *64*, 1914–1917.
- [58] T.R. Nelson, S.M. Tung, *Magn. Res. Imaging* **1987**, *5*, 189–199.
- [59] P.A. Bottemly, T.H. Forster, R.E. Argersinger, L.M. Pfeifer, *Med. Phys.* **1984**, *11*, 425–448.

PEPTIDE DISCOTICS

Synthesis, self-assembly and application

Summary

Magnetic resonance imaging (MRI) is one of the most valuable non-invasive imaging techniques used in the medical world for early diagnosis of disease. This can in part be attributed to the recent development of MRI contrast agents. Most of the currently applied contrast agents are gadolinium(III) complexes of diethylenetriaminepentaacetic acid (Gd^{III} -DTPA). Properties that severely limit the utility of these low molecular weight contrast agents are their non-specificity, their low contrast efficiency and their fast renal excretion, which necessitates high dosages. In recent years, various strategies have been explored in order to improve the proton relaxivities of MRI contrast agents. Self-assembling contrast agents, such as paramagnetic micelles or liposomes, have recently gained attention due to their easily controlled properties and good pharmacological characteristics. An additional benefit of micelles is their dynamic nature, which allows combining the benefits of both low and high molecular weight contrast agents. Designing paramagnetic discotic amphiphiles might be a promising strategy for creating self-assembling contrast agents of a different shape and hence displaying different properties. Columnar self-assembling contrast agents based on discotic molecules may in the first place become very long, hence ensuring high local concentrations of gadolinium, and secondly, the discotic amphiphiles building up the columns are multivalent, which ensures higher local concentrations of contrast agent and opens possibilities for the use of asymmetric target-specific discotics. Moreover, the self-assembly of C_3 -symmetrical discotic molecules has been well-studied. In this thesis, a strategy towards new self-assembling contrast agents based on paramagnetic discotic amphiphiles has been developed and described. Peptide fragments are used as structuring elements because of their biocompatibility, hydrogen bonding properties and versatile nature.

In Chapter 1 a general introduction into the intriguing properties of self-assembling linear paramagnetic amphiphiles forming liposomal or micellar contrast agents is described. Furthermore, the self-assembling properties of C_3 -symmetrical discotics in apolar media as well as in water are addressed in this Chapter.

In Chapter 2, the synthesis of a new class of discotic molecules is presented. These molecules, which function as model compounds, consist of a 1,3,5-benzenetricarboxamide core extended with peptide fragments decorated with mesogenic groups incorporating hydrophobic tails. Several dipeptide fragments consisting of glycine, D-phenylalanine and/or L-phenylalanine and mono-peptide fragments, either L-alanine or L-phenylalanine, have been incorporated to be able to study the effects of increased hydrophobicity and extra opportunities for secondary interactions on the self-assembly properties. All discotic

molecules have been prepared via a convergent synthetic approach in combination with consecutive coupling of the desired amino acids. This synthetic strategy gave access to both the mono- and dipeptide discotics in high chemical and optical purities.

The self-assembly behaviour of these discotics in apolar media is discussed in Chapter 3. Two important properties investigated are the order within and the stability of the assemblies. It is indeed shown that the self-assembling properties of these discotic molecules can be tuned by modifying the peptides incorporated; the stability of the stacks significantly increases going from $\text{cr}(\text{GF})_3$, crA_3 , crF_3 , $\text{cr}(\text{FG})_3$, $\text{cr}(\text{Ff})_3 / \text{cr}(\text{fF})_3$ to $\text{cr}(\text{ff})_3 / \text{cr}(\text{FF})_3$. Single phenylalanine units were selected as the most suitable fragments for the preparation of amphiphilic peptide discotics capable of self-assembly in water owing to their stability and their synthetic accessibility.

In Chapter 4 the synthesis and self-assembling behaviour of an L-phenylalanine-based discotic bearing hydrophilic oligo(ethylene oxide) tails is described. Self-assembly of this discotic amphiphile was studied in solutions in chloroform and in water using multiple analytical techniques. Moreover, extra attention was paid to the size of the assemblies, which is shown to be unexpectedly small (nanometer range).

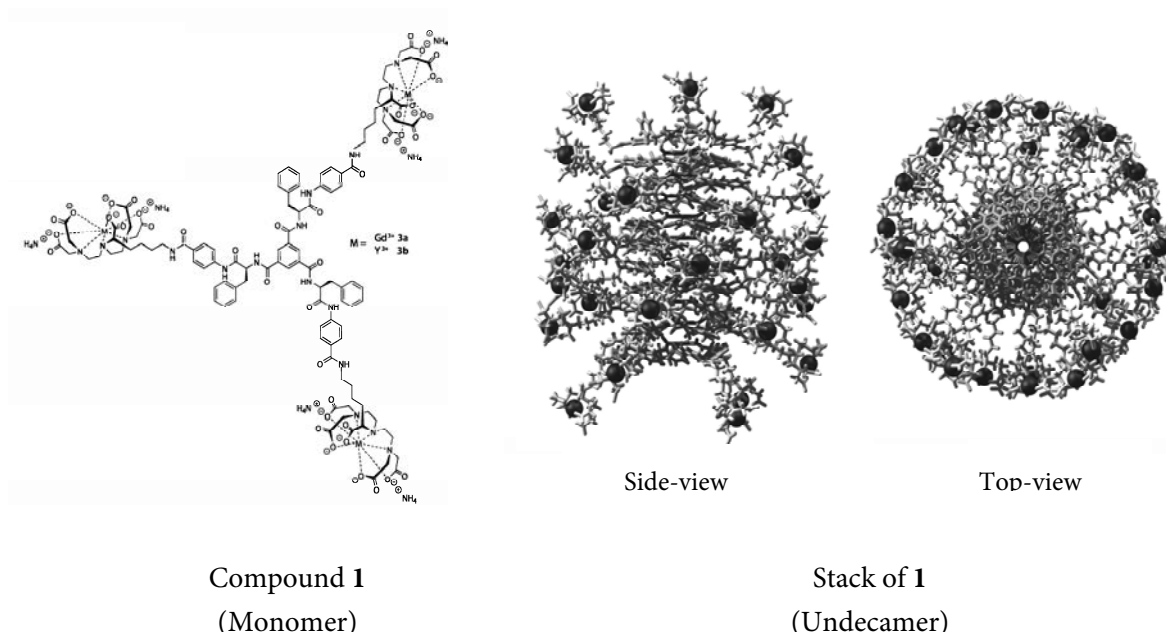


Figure S.1 Molecular structure of compound **1** and 3D-models of a stack of compound **1** (undecamer).

Going towards an application in MRI, in Chapter 5, the syntheses are described of three Gd^{III} -DTPA bearing peptide discotics, which differ in their opportunities for hydrogen bonding and/or π - π interaction. The self-assembly behaviour of these discotics has been studied in buffered aqueous solutions by CD spectroscopy in combination with longitudinal

relaxation time measurements. It has been established that Gd^{III}-DTPA discs with larger hydrophobic cores give rise to stronger stacking interactions and hence increased aggregate stabilities, higher ionic relaxivities and lower aggregation concentrations. Therefore, the largest Gd^{III}-DTPA disc **1** (Figure S.1) has been studied in more detail. A model, which distinguishes three types of discotic molecules has been derived to describe the relaxation time data. This model is shown to fit the relaxation time data pretty accurately and hence has been applied to calculate the ionic relaxivities of the molecularly dissolved discs and of the assemblies present in solution. Furthermore, ¹H-DOSY NMR measurements in combination with *cryo*TEM have been performed and show that the size of the assemblies is comparable to the size of the assemblies obtained for the phenylalanine-based discotics described in Chapter 4 (Figure S.1). Finally, the universality of our approach has been illustrated with the synthesis and characterization of a large disc in which the Gd^{III}-DTPA complexes are replaced by Gd^{III}-DOTAs. The relaxation time measurements of this Gd^{III}-DOTA disc indeed show that the obtained results are reproducible with a different type of ligand.

In this thesis a first step was made towards the use of paramagnetic discotic amphiphiles as self-assembling contrast agents for MRI. In the epilogue the author's personal opinion on the perspectives of the research is described. Hopefully, this thesis may contribute to the development of new target-specific, self-assembling contrast agents for MRI in the near future.

PEPTIDE DISCOTEN

Synthese, zelf-assemblage en applicatie

Samenvatting

Magnetic resonance imaging (MRI) is één van de meest belangrijke niet-invasieve beeldende technieken die toegepast wordt in de medische wereld om in een vroeg stadium diagnoses te stellen. Dit is mede te danken aan de recente ontwikkelingen op het gebied van MRI contrastmiddelen. In ziekenhuizen worden momenteel vooral gadoliniumcomplexen van diethyleentriaminepenta-azijnzuur (Gd^{III} -DTPA) als contrastmiddel gebruikt. Een nadeel van deze laagmoleculaire contrastmiddelen is de hoge dosis die vereist is vanwege hun specifieke verdeling in het lichaam, lage efficiëntie en snelle uitscheiding via de nieren. Het onderzoek heeft zich daarom de afgelopen jaren voornamelijk gericht op het ontwikkelen van efficiëntere contrastmiddelen. Tegenwoordig staan zelf-assemblerende contrastmiddelen, zoals paramagnetische lineaire amfifielen, die bolvormige aggregaten vormen (micellen en liposomen), veelvuldig in de belangstelling vanwege hun makkelijk te controleren en goede farmacologische eigenschappen. Verder hebben micellen een extra voordeel, namelijk, hun dynamische karakter, wat het mogelijk maakt om de voordelen van laag- en hoogmoleculaire contrastmiddelen te combineren. Het prepareren van paramagnetische schijfvormige amfifielen zou een veelbelovende strategie kunnen zijn om zelf-assemblerende contrastmiddelen te prepareren met andere dimensies en dus met andere eigenschappen. Cilindervormige contrastmiddelen gebaseerd op schijf-vormige moleculen (discoten) bezitten de mogelijkheid om heel lang te worden, wat kan leiden tot een hoge lokale concentratie aan gadolinium. Bovendien zijn de discoten, waaruit de cylinders opgebouwd zijn, multivalent. Ook dit resulteert in een hogere lokale concentratie aan gadolinium en biedt de mogelijkheid tot het gebruik van asymmetrische target-specifieke discoten. Daar komt bij dat het zelf-assemblage gedrag van C_3 -symmetrische discoten grondig onderzocht is. In dit proefschrift is een nieuwe strategie voor het verkrijgen van zelf-assemblerende contrastmiddelen gebaseerd op schijfvormige peptiden ontwikkeld en beschreven. Peptiden zijn gebruikt als structurerend element vanwege hun biocompatibiliteit, diversiteit en waterbrugvormende eigenschappen.

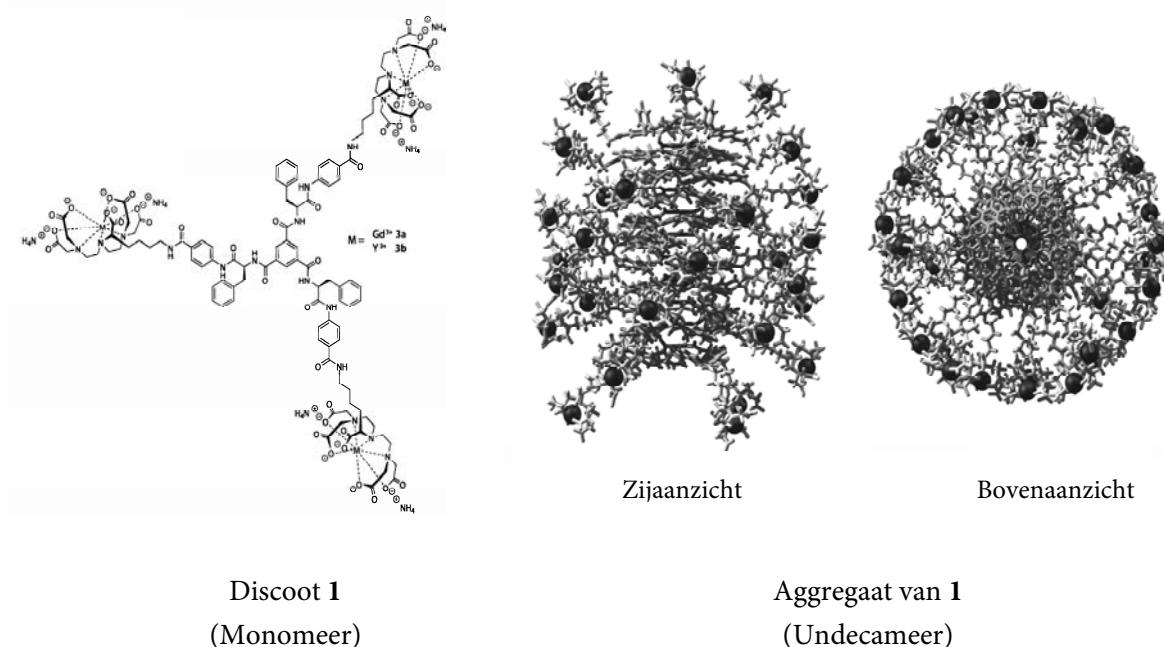
In Hoofdstuk 1 wordt een algemene inleiding omtrent de intrigerende eigenschappen van zelf-assemblerende lineaire paramagnetische amfifielen beschreven. Tevens worden de zelf-assemblerende eigenschappen van C_3 -symmetrische discoten in apolaire oplosmiddelen en in water besproken.

In Hoofdstuk 2 wordt de synthese van een nieuwe klasse van schijfvormige moleculen gepresenteerd. Deze modelstructuren bestaan uit een 1,3,5-benzeentricarboxamide centrum verlengd met peptidefragmenten die gekoppeld zijn aan mesogene groepen met hydrofobe staarten. Dipeptide fragmenten bestaande uit glycine, D-fenylalanine en/of L-fenylalanine en

mono-peptide fragmenten bestaande uit óf L-alanine óf L-fenylalanine zijn ingebouwd, zodat het effect van een toenemende hydrofobiciteit en een extra mogelijkheid voor de vorming van secundaire interacties op het zelf-assemblage gedrag bestudeerd kan worden. De moleculen zijn vervaardigd via een convergente syntheseroute waarbij de aminozuren één-voor-één ingebouwd zijn. Met behulp van deze methode kunnen alle peptidediscoten optisch zuiver en in hoge opbrengst verkregen worden.

Het zelf-assemblage gedrag van deze modelstructuren in apolaire oplosmiddelen is beschreven in Hoofdstuk 3. Twee belangrijke eigenschappen die bestudeerd zijn, zijn de orde aanwezig in én de stabiliteit van de aggregaten. Hierbij is gevonden dat de zelf-assemblage van deze moleculen bijgestuurd kan worden door het peptidefragment te wijzigen. De stabiliteit van de aggregaten neemt significant toe van $cr(GF)_3$, crA_3 , crF_3 , $cr(FG)_3$, $cr(Ff)_3$ / $cr(ff)_3$ naar $cr(ff)_3$ / $cr(FF)_3$. Vanwege de stabiliteit en de synthetische toegankelijkheid van de discoten waarbij phenylalanines zijn ingebouwd, is de phenylalanine eenheid geselecteerd om ingebouwd te worden in schijfvormige amfifielen met hydrofiele poly(ethyleenoxide) staarten.

In Hoofdstuk 4 is de synthese en het zelf-assemblage gedrag van een schijfvormig peptide amfifiel beschreven. Het zelf-assemblage gedrag is bestudeerd met verschillende analytische technieken in chloroform en in water. Tevens is de grootte van de aggregaten in water bepaald. De discot aggregereert in beide oplosmiddelen en het is vastgesteld dat de aggregaten in water enkele nanometers lang zijn.



Figuur S.1 Moleculaire structuur van product 1 en 3D-modellen van een aggregaat van 1 (undecameer).

Voor een toepassing in MRI is, in Hoofdstuk 5, de synthese van drie Gd^{III}-DTPA gelabelde discoten, die verschillen in hun mogelijkheid tot waterstofbrugvorming en π - π interactie, behandeld. Het zelf-assemblage gedrag van deze moleculen in een gebufferde oplossing is onderzocht met CD spectroscopie en longitudinale relaxiviteitsmetingen. Hierbij is gevonden dat schijven met een grotere hydrofobe kern sterker aggregeren en hogere ionische relaxiviteiten vertonen. Om deze reden is de grote Gd^{III}-DTPA discoot **1** (Figuur S.1) in meer detail bestudeerd. Er is een model afgeleid dat onderscheid maakt tussen drie type schijven om de relaxiviteitsdata te beschrijven. Dit model beschrijft de experimentele data vrij nauwkeurig en is daarom toegepast om de ionische relaxiviteiten van moleculair opgeloste schijven en aggregaten te berekenen. Daarnaast zijn ¹H-DOSY NMR en cryoTEM metingen uitgevoerd om de grootte van de paramagnetische aggregaten te bepalen. De grootte bleek vergelijkbaar met de grootte van de aggregaten beschreven in Hoofdstuk 4 (Figuur S.1). Tenslotte, is een discoot gesynthetiseerd en gekarakteriseerd waarbij de Gd^{III}-DTPAs zijn vervangen door Gd^{III}-DOTAs om zo de universeelheid van deze benadering te benadrukken. De relaxiviteitsmetingen laten inderdaad zien dat de data gereproduceerd kunnen worden met een discoot met een ander type ligand.

In dit proefschrift is een eerste stap gemaakt in de richting van het gebruik van paramagnetische discoten als zelf-assemblerende contrastmiddelen voor MRI. In de epiloog geeft de auteur haar persoonlijke visie over de toekomst van dit onderzoek. Hopelijk kan dit proefschrift bijdragen aan de ontwikkeling van efficiëntere target-specifieke zelf-assemblerende contrastmiddelen voor MRI.

Curriculum Vitae



Kelly van den Hout werd geboren op 19 oktober 1979 te Drunen. Na haar VWO-opleiding aan het d'Oultremontcollege te Drunen begon zij aan de studie Scheikundige Technologie aan de Technische Universiteit Eindhoven. Tijdens haar studie liep zij 4 maanden stage bij DSM Pharmaceuticals te Venlo. De studie werd in 2003 afgerond met een onderzoek naar multifunctionele contrastmiddelen voor MRI. Aansluitend trad zij in dienst van de Technische Universiteit Eindhoven als promovenda binnen de capaciteitsgroep Macromoleculaire en Organische Chemie van de faculteit Scheikundige Technologie. Onder leiding van prof.dr. E.W. Meijer, dr. J.A.J.M. Vekemans en dr.ir. M.H.P. van Genderen werkte zij tot en met juni 2008 aan haar promotieonderzoek. De belangrijkste resultaten hiervan staan beschreven in dit proefschrift. Vanaf 1 januari 2008 is de auteur gestart met de éénjarige eerstegraads lerarenopleiding scheikunde aan de Eindhoven School of Education.

Kelly van den Hout was born in Drunen, the Netherlands, on October 19, 1979. After secondary education at the d' Oultremontcollege in Drunen, she started studying Chemical Engineering at the Eindhoven University of Technology. During her master, a traineeship of 4 months was performed at DSM Pharmaceuticals in Venlo. The master degree was obtained in 2003 with an investigation into multi-functional contrast agents for MRI. From December 2003 to June 2008 she worked as a PhD student at the Eindhoven University of Technology in the laboratory of Macromolecular and Organic Chemistry at the department of Chemistry and Chemical Engineering. Under the supervision of prof. dr. E.W. Meijer, dr. J.A.J.M. Vekemans and dr.ir. M.H.P. van Genderen she worked on self-assembling discotic molecules with the aim to design new supramolecular contrast agents for MRI. The most important results of the research are described in this thesis. As of Januari 2008 the author started a one-year master programme in Chemistry Education, which will lead to a first degree teacher qualification in chemistry, at the Eindhoven School of Education.

Dankwoord

Na vier jaar hard werken is het einde van een plezierige en leerzame promotieperiode bij SMO in zicht. Graag maak ik dan ook van de gelegenheid gebruik om iedereen te bedanken die heeft bijgedragen aan de totstandkoming van dit proefschrift. Er zijn een aantal mensen die ik in het bijzonder wil bedanken.

Allereerst wil ik mijn promotor Bert Meijer bedanken. Bert, jouw enthousiasme en jouw geloof in mij als onderzoeker hebben ervoor gezorgd dat ik vier jaar geleden besloot om te gaan promoveren. Een beslissing waar ik zeker geen spijt van heb! Met evenveel vertrouwen heb je me nu de mogelijkheid gegeven om tijdens mijn promotie aan de lerarenopleiding te beginnen, waar ik je ook zeer dankbaar voor ben. Daarnaast zou ik Jef Vekemans en Marcel van Genderen graag willen bedanken voor de waardevolle discussies, opbouwende kritiek en razendsnelle correcties van de vele manuscripten; ik had me geen betere copromotoren kunnen wensen. Jef, jouw passie voor de organische synthese is zeker op mij overgeslagen en ik zal er alles aan doen om dit weer verder door te geven aan mijn eigen leerlingen. Marcel, jouw gestructureerdheid en vakdidactische kwaliteiten zijn een voorbeeld voor mij. Net zo'n goede docent worden als jij is dan ook mijn streven.

Dank aan prof. K. Nicolay en prof. J. van Esch voor het plaatsnemen in mijn kerncommissie en het corrigeren van mijn manuscript. I would like to thank Dr. J. Hartgerink for reading the manuscript and participating in my committee.

Ook wil ik dr. Sander Langereis bedanken voor zijn deelname aan de promotiecommissie. Sander, jouw promotieonderzoek naar dendritische MRI contrastmiddelen is een ware inspiratiebron voor mij geweest. Bedankt voor alles wat ik van je geleerd heb, het corrigeren van hoofdstuk 5 en de ICP metingen die je bij Philips voor mij uit hebt laten voeren.

Als promovenda heb ik de eer gehad om een aantal studenten te begeleiden. Leandra, bedankt voor jouw bijdrage aan het initiële onderzoek en heel veel succes met het afronden van je promotie. Rob Kleijnen, je wist je de synthese heel erg snel eigen te maken, wat ik heel erg knap vind. De opleiding scheikundige technologie zul je ongetwijfeld met een mooi resultaat afronden. Harald Albers, dankzij jouw labmotto "niet brommen, maar kolommen", heb je heel wat complexe structuren gesynthetiseerd, waarvan de meeste zijn opgenomen in hoofdstuk 5. Ik ben je hier erg dankbaar voor en wens je heel veel succes met je eigen promotieonderzoek bij het NKI in Amsterdam. Luc Starmans, de relaxiviteitsmetingen die jij op het einde van mijn promotie hebt uitgevoerd, hebben zeker tot nieuwe inzichten geleid, bedankt hiervoor.

Maarten Smulders bedankt voor alle hulp met de CD metingen, de nuttige discussies over de CD data en natuurlijk de hulp met de modellen. Tom de Greef en Thomas Hermans

ben ik zeer erkentelijk voor de hulp met de ^1H -DOSY NMR metingen. Tom, jouw bijdrage aan de modellen voor de relaxiviteitsmetingen heb ik ook erg op prijs gesteld. Rafael Martín-Rapún, thanks for all the XRD measurements you performed for me and the usefull discussions we had about the results. I wish you all the best in Spain. Nicole Papen-Botterhuis en Philippe Leclere, bedankt voor de moeite die jullie hebben genomen om AFM voor mij te meten. Nico Sommerdijk, Paul Bomans en Matthijn Vos wil ik bedanken voor de *cryo*TEM metingen en Otto van Asselen voor de hulp bij de IR metingen in oplossing. Bas de Waal, hartstikke bedankt voor de syntheses die je voor mij hebt uitgevoerd. Dankzij jou heb ik me niet hoeven verdiepen in de opzuivering van ethyleenoxide derivaten (zie hoofdsuk 4). SyMO-Chem BV. in de persoon van Henk Keizer, wil ik bedanken voor het verstrekken van het DOTA ligand. Joost van Dongen, Ralf Bovee en Xianwen Lou, bedankt voor de ondersteuning bij de vele analyses. Lou, I am very proud on the article we published in the journal of mass spectrometry. Koen Pieterse, je bent niet alleen een uitstekend grafisch ontwerper van covers en proefschriften (ik ben apetrots op onze Chemistry cover), ook het simulatiewerk van jou en Michel Debertrand heeft ons erg geholpen. Gustav Strijkers en Erik Sanders, bedankt voor alle hulp en waardevolle discussies op het gebied van de relaxiviteitsmetingen. Het secretariaat, bestaande uit Hanneke Veldhoen, Joke Rediker, Ingrid Dirckx, Carine van der Vaart en Angela Jones bedankt voor al jullie hulp. Hans Damen, ben ik dankbaar voor het regelen van alle chemicaliën waarvan ik veelvuldig gebruik heb gemaakt. Henk Eding, bedankt voor het uitvoeren van de vele element analyses, je gezelligheid en de thee die altijd voor me klaar stond.

Aangezien ik heel wat tijd op het lab heb doorgebracht wil ik ook al mijn labgenoten van lab 2 bedanken voor de gezellige tijd! Ook wil ik mijn kamergenoten van STO4.43 Nicole, Edith en Tristan en 'oud'-kamergenoten Patricia, Hinke en Tobias bedanken voor de steun en gezelligheid van de afgelopen jaren. Verder wil ik Eva, Linda, Hinke, Patricia, Nicole, Jolanda, Ingrid, Sagitta, Daniela, Maarten, Michel, Martin, Arjan, Frank en Dirk bedanken voor de gezamenlijke lunches, fruitjes, volleybalweekenden en andere uitstapjes.

Mieke, Elleke, Carla, Esther, Lian, Astrid, Femke, Sofie en Ellen, ik heb altijd veel plezier aan onze volleybalwedstrijden en weekendjes weg beleefd en ik hoop dan ook dat we ons plan om weer samen te gaan volleyballen daadwerkelijk zullen oppakken.

Ive, Micheal, Susanne, Martijn, Katriene, Tamara, Jon-Sjo, Betty, Rob, Kim, Mark, Ramona en Kjeld, bedankt voor al jullie steun de afgelopen tijd. Ik hoop dat onze vriendschap nog vele jaren mag duren.

Voor mijn paranimfen, Jolanda Spiering en Nicole Papen-Botterhuis, schieten woorden tekort. We hebben in de afgelopen jaren zoveel mooie, maar ook moeilijke

momenten met elkaar gedeeld. Vandaar dat ik heel erg blij ben dat jullie mijn paranimfen willen zijn. Ik hoop dat we nog heel erg lang bevriend zullen blijven.

Tenslotte wil ik mijn familie bedanken voor hun steun en vertrouwen. Tjibbe, Willemien, Rinske, Idso, Kars, Mieke en Annemieke, jullie gezin is vanaf onze eerste kennismaking een tweede 'thuis' voor mij (dit bleek ook wel weer uit de vele uurtjes die ik al werkend aan de Landmeerse loop 13 heb doorgebracht), bedankt hiervoor. Geert, je bent een hartstikke lieve broer waar ik erg trots op ben. Pap en mam, de afgelopen maanden hebben jullie me nog meer geholpen dan jullie altijd al deden en dat zal ik nooit vergeten. Dankzij jullie ben ik uitgegroeid tot wat ik nu ben en en daar ben ik jullie erg dankbaar voor. Sjoerd, de laatste regels van mijn dankwoord zijn voor jou. Ik heb tijdens het schrijven van mijn proefschrift veel van je gevraagd, maar je moet weten (al leek het soms niet altijd zo), je bent het mooiste wat me ooit is overkomen. Ik hou van jou!

A handwritten signature in black ink that reads "Kelly". The signature is written in a cursive style with a long, sweeping tail on the letter 'y'.

